Design, synthesis and exploration of P-chiral phosphoramidites: Implementations in asymmetric conjugate additions to cycloalkenyl ketones

Martín Fernández Pascual

Somerville College

University of Oxford

A thesis submitted for the degree of Doctor of Philosophy Michaelmas 2025

In loving memory of

Gonzalo Gómez Cepa

"Esta epístola inútil y palabrera ya existe en uno de los treinta volúmenes de los cinco anaqueles de uno de los incontables hexágonos, y también su refutación."

Jorge Luis Borges,

La Biblioteca de Babel

Declaration

This thesis presents the research conducted in the Chemistry Research Laboratory, University of Oxford, from October 2020 to January 2025, under the guidance of Prof. Stephen P. Fletcher. The work described herein is my own, unless explicitly acknowledged otherwise, and has not been submitted for a degree at this or any other university.

Martín Fernández Pascual

January 2025

Abstract

This thesis explores the development and application of stereoselective and diastereoselective methodologies for synthesizing complex chiral molecules using asymmetric catalysis. Chapter 1 introduces the importance of chirality in organic synthesis, highlighting key strategies for achieving enantiomerically enriched compounds and the design principles of privileged ligands in asymmetric catalysis. Chapter 2 focuses on asymmetric conjugate additions (ACAs) to cycloalkenyl ketones, detailing the discovery, optimization, and scope of a copper-catalyzed ACA reaction utilizing alkylzirconocene nucleophiles. This methodology offers a stereodivergent approach to access 1,2-disubstituted cyclic frameworks with high enantioselectivities. Chapter 3 investigates the ligand space of P-stereogenic phosphoramidites, exploring modifications to the BINOL backbone and amine substituents to enhance the diastereoselectivity and performance of ligands in the ACA of challenging substrates. Finally, Chapter 4 develops novel diastereoselective strategies for synthesizing the P-stereogenic phosphoramidite ligand **L$_{22S}$**, crucial for achieving high enantioselectivities in exocyclic ACA systems. Discussion of both the challenges encountered and the promising outcomes is included.

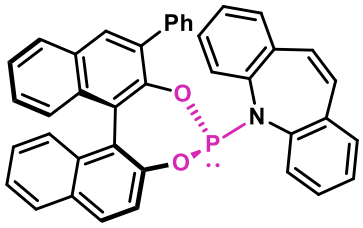

L$_{22S}$

Acknowledgement

Nothing worthwhile is ever possible without the help and involvement of numerous people, and this thesis is no exception. While I cannot mention everyone, I would like to express my gratitude to those who made the greatest contributions, both within and beyond Oxford.

First and foremost, I extend my heartfelt appreciation to my DPhil supervisors, Prof. Stephen P. Fletcher and Dr. Mireia Sidera Portela. They provided me with the opportunity to pursue this exciting project and have supported me throughout my studies with patience, motivation, enthusiasm, and knowledge. Their guidance, combined with the freedom they granted me to explore my interests, has been invaluable. I simply could not have asked for better supervisors for my DPhil programme.

My appreciation also goes to all the members of the Fletcher Group at the Chemistry Research Laboratory, where I spent four rewarding years. This dissertation has been enriched by their academic discussions, kindness, and friendship, which created a joyful and stimulating environment. I am especially grateful to Dr. David Egea Arrebola, Dr. Steven Webster, Matilda Royce Joyce, Dr. Michael B. G. Howlett, Dr. Laura Cunningham, Oliver Williams, and Dr. Lazlo Balasz for their support and collaboration.

A special acknowledgment is due to Dr. Sourabh Mishra for his guidance and encouragement at the start of my journey, which greatly influenced the direction of this work. I would also like to express my gratitude to Dr. Alexandre Brethome, whose initial contributions laid the foundation for this research.

In this incomplete list of acknowledgments, I cannot fail to include the names of my dear friends Nilgoun Bahar, Alexandra Bisia, Sofia Bustamante, Aleksandra Furmanek, Juan Losada, Carlos Outeiral, Julia Salafranca Gomez and Tytus Wilam for their companionship and the memorable moments we shared during my time in Oxford.

I cannot close without saying how grateful I am to my family, especially my father, mother, and sister for their unwavering patience, support, and encouragement throughout this journey.

List of Abbreviations

Ac . . . . . Acetyl or acetate

ACA . . . . . .Asymmetric Conjugate Addition

acac . . . . . .Acetylacetone

AH . . . . . .Asymmetric Hydrogenation

APCI . . . . .Atmospheric pressure chemical ionisation

aq . . . . . Aqueous

Ar . . . . . Aryl

BINAP . . . 2,2'-bis(diphenylphosphino)-1,1'-binaphthyl

BINOL . . . 1,1'-bi-2-napthol

Bn . . . . . Benzyl

Boc . . . . . tert-butyloxycarbonyl

br . . . . . .Broad (NMR, IR)

Bz . . . . . Benzoyl

c . . . . . .Concentration

ca. . . . . circa (approximately)

cld. . . . . .Calculated

COSY . . . . .Correlation spectroscopy

d . . . . . Doublet (NMR)

DCM . . . . . Dichloromethane

DFT . . . . . .Density functional theory

DIBAL-H . Diisobutylaluminium hydride

DMAP 4-dimethylaminopyridine

DMF . . . . . N,N-dimethylformamide

DMSO . . . .Dimethyl sulfoxide

DoE . . . . . .Design of Experiment

dr. . . . . Diasteromeric ratio

DuPhos . . 1,2-Bis[(2S,5S)-2,5-dimethylphospholano]benzene

ee . . . . . .Enantiomeric excess

equiv. . . . .Equivalent(s)

ESI . . . . . .Electrospray ionisation

Et . . . . . .Ethyl

FG . . . . . Functional group

g . . . . . .Gram(s)

GC . . . . . Gas chromatography

h . . . . . .Hour(s)

HRMS . . . .High resolution mass spectrometry

HSQC . . . . Heteronuclear single quantum correlation

HMBC . . . .Heteronuclear multiple bond connectivity

Hz . . . . . Hertz

IR . . . . . Infra-Red

J . . . . . .Coupling constant in Hz

LS . . . . . Ligand Space

M . . . . . .Molar/molarity

m . . . . . .Multiplet (NMR)

Me . . . . . .Methyl

m.p. . . . . .Melting point

n.d. . . . . Not determined

NHC . . . . . N-heterocyclic carbene

NMR . . . . .Nuclear magnetic resonance

o/n. . . . . .overnight

Ph . . . . . Phenyl

q . . . . . Quartet (NMR)

R . . . . . Any group

rac . . . . . .Racemic

rr. . . . . Regiomeric ratio

s . . . . . Singlet (NMR)

sat. . . . . saturated

SFC . . . . . Supercritical fluid chromatography

sp . . . . . Orbital hybridisation: 1:1 p:s character

sp^2 . . . . . Orbital hybridisation: 2:1 p:s character

sp^3 . . . . . Orbital hybridisation: 3:1 p:s character

t . . . . . .Triplet (NMR)

TADDOL. . .α,α,α',α'-tetraaryl-2,2-disubstituted 1,3-dioxolane-4,5-dimethanol

TBS . . . . . *tert*-butyldimethylsilyl

temp. . . . . .Temperature

TFA . . . . . Trifluoromethanesulfonate

THF . . . . . Tetrahydrofuran

TLC . . . . . .Thin layer chromatography

TMS. . . . . .Trimethylsilyl

Ts . . . . . Tosyl

TS. . . . . .Transition state

UV . . . . . .Ultraviolet

wt% . . . . . .Percentage by weight

δ . . . . . Chemical shift (NMR)

Table of Contents

"The universe then—at least our universe—or at the very least our section of our universe—is electronically left-handed, and that may have had an interesting effect on the development of life" – Isaac Asimov

Chapter 1: Introduction

Index

1.1 A brief introduction to asymmetric chemistry

1.1.1 Asymmetry is just another name for life

The search for symmetry is deeply human.[1] At a first glance, symmetry seems omnipresent: humans and most animals possess paired features—eyes, ears, hands—divided equally along the body's midline.[2,3] From architecture, to monuments to formal gardens, much of what we create reflects this intrinsic desire for balance.[4] We often regard symmetry as a hallmark of perfection, simplicity, and aesthetic appeal. Aristotle is known to have said:[5]

> *"The chief forms of beauty are order and symmetry and definiteness, which the mathematical sciences demonstrate in a special degree."*

Yet, almost paradoxically, even though symmetry is in part inspired by nature, nature itself is fundamentally asymmetric. On a visible human scale, this is evident in phenomena like the coiling of most snail shells, which typically spiral clockwise (dextral).[6] Asymmetry becomes even more pronounced at the microscopic level, with DNA and RNA exhibiting a consistent right-handed helical twist.[7] This principle extends to much larger scales; for instance, most planets and stars in the Milky Way rotate in alignment with the galaxy's overall spin. Even in what we perceive as symmetry, hidden asymmetry often lies beneath.[8] Consider our hands: while they appear similar, they are non-superimposable mirror images.[9] This "handedness," or chirality—a term derived from the Greek word *cheir,* meaning "hand"—is a recurring motif in nature, spanning all scales of existence.

The concept of handedness in nature has been recognized since antiquity, but it was not formally applied to chemistry until the 19th century. In 1848, Louis Pasteur made a groundbreaking discovery by separating the enantiomers of tartaric acid based on their differing optical rotations, establishing the foundation of stereochemistry.[10] It was Lord Kelvin, however, who first used the term "chirality" in 1884:

> *"I call any geometrical figure, or group of points, 'chiral', and say that it has chirality if its image in a plane mirror, ideally realized, cannot be brought to coincide with itself."* [11]

This definition highlighted the intrinsic asymmetry found in many molecules.

Understanding chirality is crucial in fields such as pharmacology, where enantiomers can exhibit drastically different biological activities.[12] The tragic case of thalidomide, a therapeutic drug for pregnant women, is one where enantiomers interconvert *in situ*. While one enantiomer was therapeutically effective the other caused severe birth defects. This example underscores the critical importance of enantioselectivity and how different enantiomers can have completely different effects on our body.[13-15] Thus, the development of methods to control stereochemistry, particularly through asymmetric catalysis, has become a cornerstone of modern synthetic chemistry, enabling the efficient production of enantiomerically pure compounds with minimal waste.[16-19]

Strategies for Accessing Enantiomerically Enriched Compounds

There are three primary strategies to access enantiomerically pure compounds (Figure 1.1): extraction from the chiral pool, racemic mixture resolution, and asymmetric synthesis.[19] While the first approach relies on naturally occurring chiral compounds, it is limited by availability and cost (Figure 1.1 A). In the figure depiction, the amount of chiral compound obtained is heavily restricted by its abundance in nature. These chiral pools are often scarce and the extraction process is costly.

Racemic resolution, as seen in Figure 1.1 B, involves separating enantiomers from a 50:50 mixture in high selectivity. This methodology can be effective but inherently wastes half of the product unless the unwanted enantiomer is recycled, a downside to this strategy.

In contrast, asymmetric catalysis offers a more direct and sustainable solution by converting achiral substrates into chiral products using sub-stoichiometric amounts of chiral catalysts (Figure 1.1 C). This strategy not only minimizes waste but also provides high enantioselectivities and yields. Landmark contributions by William S. Knowles, Ryōji Noyori, and K. Barry Sharpless in developing asymmetric hydrogenation and oxidation methodologies—recognized by the 2001 Nobel Prize in Chemistry—underscore the transformative power of asymmetric catalysis in the synthesis of enantiopure compounds.[20]

Asymmetric catalysis operates on the principle of creating a chiral environment around the substrate, typically using a chiral ligand-metal complex. The effectiveness of a chiral catalyst is determined by its ability to differentiate between the prochiral faces of a substrate, thereby favouring the formation of one enantiomer over the other. This

enantioinduction is governed by subtle steric and electronic interactions between the catalyst and the substrate, which can be fine-tuned by modifying the ligand structure. [21]

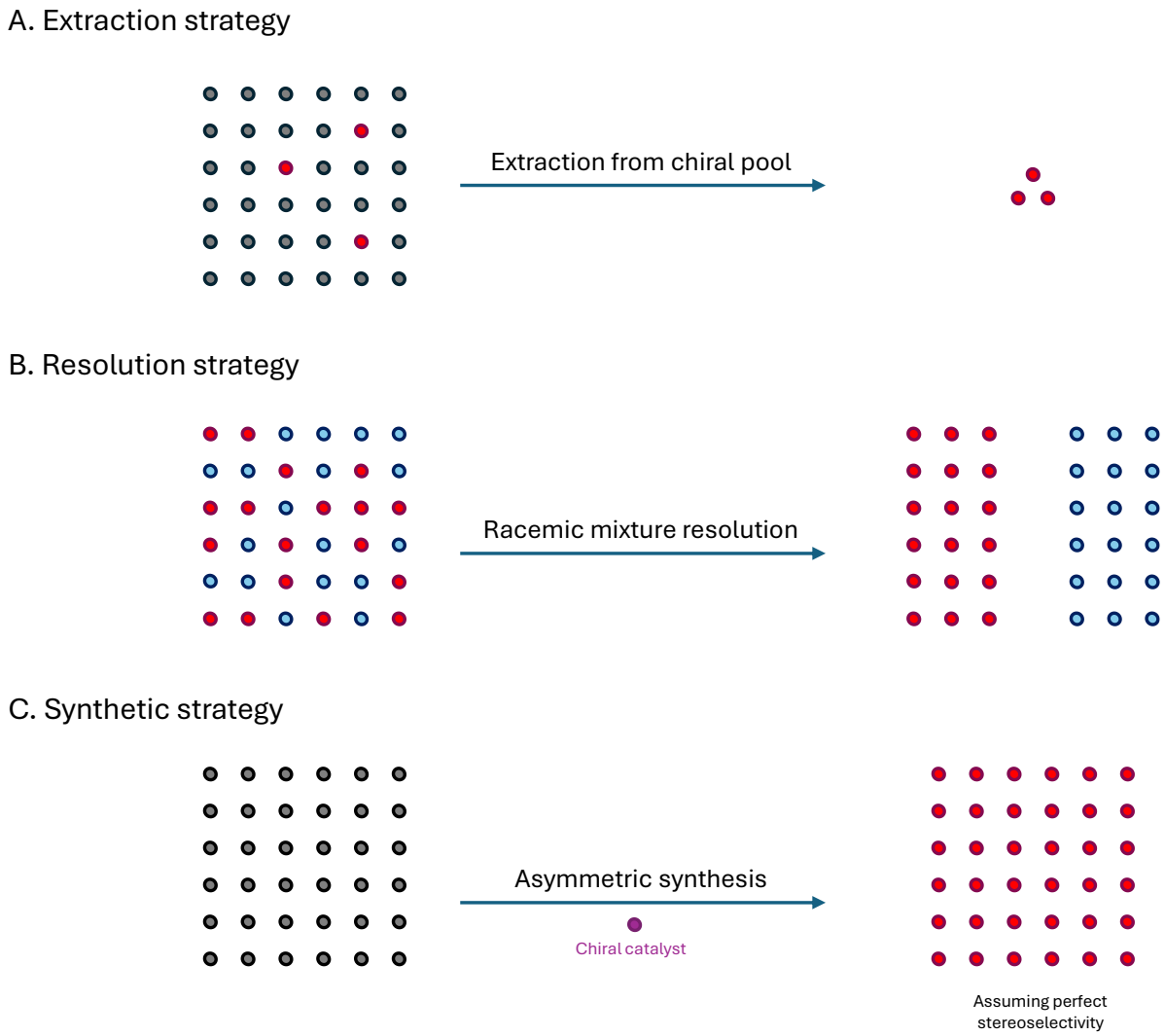

Figure 1.1: Different strategies to obtain enantiomerically enriched products (displayed in red and blue). Non-chiral molecules displayed in grey. **A** extraction from chiral pool strategy **B**. Racemic mixture resolution to separate both enantiomers **C**. Asymmetric synthesis, often necessitating a chiral catalyst to induce asymmetry.

The design of an efficient chiral catalyst involves balancing several key factors: substrate compatibility, high turnover frequency, and enantioselectivity.[22] Additionally, catalyst stability, ease of preparation, and the potential for recycling are crucial considerations for practical applications. These criteria have led to the concept of "privileged ligands"—chiral scaffolds that provide high enantioselectivity across a broad range of substrates and reactions.[23-26] Examples include BINAP, a bidentate phosphine ligand, and its derivatives, which have found use in numerous transition-metal-catalysed asymmetric transformations.[23,24]

1.1.2 Ligand space and design in asymmetric catalysis

The success of asymmetric catalysis largely depends on the development and optimization of ligands that can control the stereochemistry of the reaction environment. Designing effective ligands involves navigating a vast "ligand space"—a conceptual framework that encompasses the structural and electronic diversity of ligands available for catalyst design.[22] The aim is to explore this space efficiently to find ligands that yield high enantioselectivity, and activity for a wide range of substrates. By systematically modifying ligand structures, chemists can tailor the steric and electronic properties of the catalytic environment to suit specific reactions, allowing for broad application and optimization across numerous enantioselective transformations.[22]

Defining ligand space

The concept of ligand space refers to the range of possible ligands defined by their structural and electronic variations (Figure 1.2, shown for three ligand families). Each modification of a ligand, whether it be the length of a substituent chain or the introduction of a new functional group, occupies a unique point in this chemical space, altering the ligand's interaction with the metal centre and, consequently, the substrate.[22,27,28]

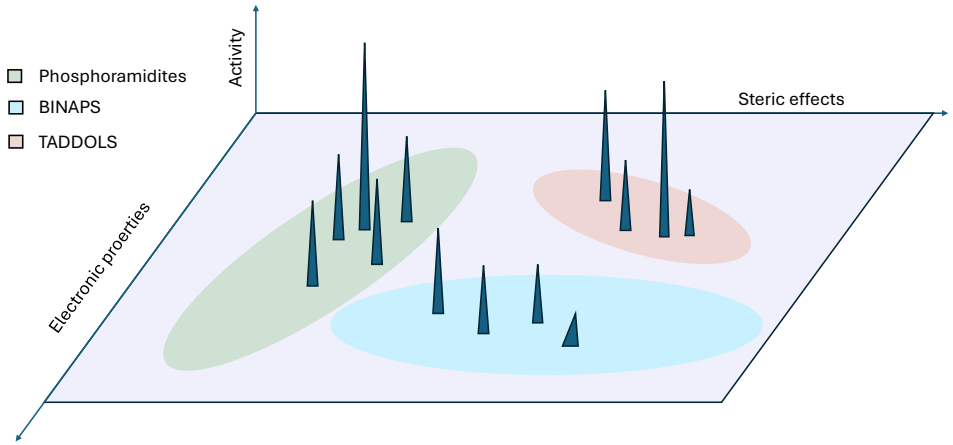

Figure 1.2: showcasing a simple two-dimensional Ligand Space where ligand 'steric effects' occupy one axis and their 'electronic properties' occupy the other. Peaks represent the specific ligands that are responsible for product. The hight of the peaks represents the activity of said ligand in the researched reaction. Regions represent different ligand groups. In green: Phosphoramidites, in red: TADDOLs and in blue: BINAPs.

In the concept of ligand space, different 'locations' represent distinct ligands, some of which may exhibit high activity for specific systems. Various ligand families, such as BINAPs, TADDOLs, and phosphoramidites, occupy unique regions or 'subspaces' within

this space, reflecting their functional characteristics. For instance, two phosphoramidites are more likely to behave similarly in a catalytic system than a phosphoramidite and a TADDOL. While the ligand space shown in Figure 1.2 provides a simplified representation, ligand spaces in most systems are inherently multidimensional. This added complexity can make exploration challenging but also enriches the landscape, offering a myriad of untapped opportunities for discovery.

The ligand space can be explored systematically by varying core scaffolds, substituents, donor groups, and symmetry elements. This exploration is critical in designing catalysts that not only achieve high enantioselectivities but also operate under mild conditions, exhibit stability, and minimize by-product formation. [22,28,30]

1.1.3 Privileged ligands and their role in ligand space

Privileged ligands are those that have been shown to consistently deliver high enantioselectivities across a variety of catalytic reactions (Figure 1.3). These ligands serve as benchmarks in catalyst design, providing reliable starting points for developing new catalytic systems.[22,30,31] Aside from their noteworthy selectivity, Privileged ligands are often regarded as a paragon due to their high compatibility, high TOF, ease of preparation, recycling potential and stability.

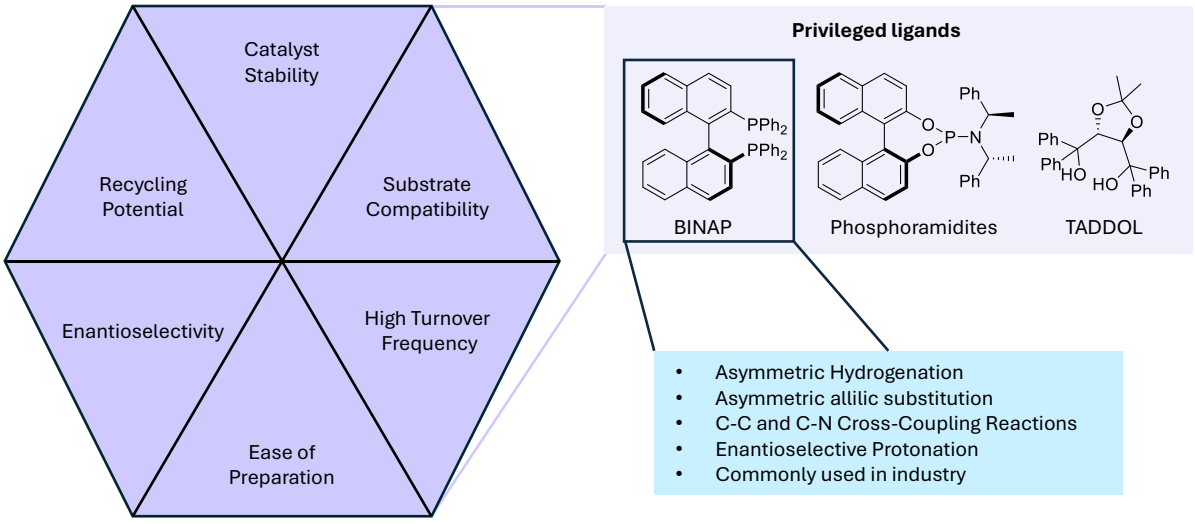

Figure 1.3: The essential characteristics of privileged ligands such as BINAPs, Phosphoramidites and TADDOLs. Further indulging on some of the reaction types and uses of BINAP as a privileged ligand.

Their ability to be applied in different metal-catalysed transformations makes them ideal for exploring ligand space since small structural modifications can yield broad changes in

reactivity and selectivity. Notable examples include BINAP (2,2'-bis(diphenylphosphino)-1,1'-binaphthyl), which has been employed in asymmetric hydrogenations,[32,33] Suzuki couplings,[34] and C–C bond-forming reactions;[34-37] and the Josiphos family, which has been extensively used in asymmetric hydroformylations[38] and allylic alkylations.[39]

Phosphoramidites, another class of privileged ligands, are renowned for their modular design and ease of modification.[40] Built on a flexible BINOL or biphenol backbone, phosphoramidites feature a P—N framework that can be systematically altered to optimize steric and electronic properties. This makes them a powerful tool for exploring large regions of ligand space with minimal synthetic effort. Their effectiveness has been demonstrated in various metal-catalysed transformations, such as rhodium-catalysed hydrogenations[41,42] and copper-catalysed conjugate additions[42-47].

Examples of privileged ligands in asymmetric catalysis

Numerous privileged ligands have been successfully applied in a variety of enantioselective transformations, demonstrating the versatility of well-designed ligands:

1. **BINAP**: Widely used in enantioselective hydrogenations and cross-couplings, BINAP's rigid structure and axial chirality provide excellent stereochemical control, making it a staple ligand in asymmetric reactions.[48,49]

2. **Josiphos**: This family of ligands is renowned for its application in asymmetric hydroformylation, producing branched aldehydes with high selectivity and enantiopurity. Josiphos ligands have also been applied in hydrogenations and C–N bond formations.[38,50,51]

3. **DuPHOS Ligands**: Featuring a phospholane backbone, DuPHOS ligands have been optimized for high enantioselectivities in hydroboration and hydrogenation reactions. Their rigid structure and unique electronic properties make them effective in controlling stereochemistry even in challenging substrates.[52,53]

4. **Phosphoramidites**: Phosphoramidites remain a quintessential example of modular ligands that explore a wide ligand space due to their ease of modification. Their application spans copper-catalyzed conjugate additions and allylic substitutions, where precise control over steric and electronic parameters is crucial.[54-59]

1.1.4 Strategies for exploring ligand space

Efficiently navigating ligand space requires both rational design and high-throughput screening approaches. One strategy involves focusing on core scaffold variations. For instance, BINAP, due to its rigid C_2-symmetric structure, has been extensively modified to yield a variety of analogues with different steric and electronic properties.[22] Similarly, the DuPHOS ligand class, featuring a phospholane backbone, has been tuned to enhance catalytic performance in different reactions, such as alkene hydrogenation.[52,60] This last ligand is even partly responsible for the first practical synthesis of (*R*) and (*S*) Warfarin.[61]

Another strategy is to incorporate combinatorial chemistry techniques, which allow for the rapid generation and testing of diverse ligand libraries.[30] By systematically varying substituents on known privileged scaffolds, chemists can map out regions of ligand space that optimize catalytic properties for specific transformations. This approach was successfully employed with hybrid bidentate ligands, such as phosphine-phosphoramidite hybrids, which demonstrated superior performance in asymmetric hydroformylation reactions due to their enhanced ability to stabilize metal centres in various oxidation states.

Design principles for effective ligands

Designing effective ligands requires a delicate balance between steric bulk and electronic properties, as well as consideration of the overall geometric arrangement around the metal centre. The use of chiral ligands that create well-defined asymmetric environments is key to inducing high enantioselectivity.[22] For example, in C_2-symmetric ligands like BINAP or SEGPHOS, the spatial arrangement of substituents is rigidly controlled, minimizing conformational flexibility and enhancing the ligand's ability to direct substrate orientation and reaction pathway.[22,62]

Another crucial factor is electronic tuning, which involves altering the ligand's electron-donating or withdrawing capacity to stabilize specific metal oxidation states or intermediates. Phosphine ligands, such as those in the DuPHOS or Josiphos families, have been modified with electron-donating groups to facilitate reductive elimination steps, thereby improving yields and selectivity in C–C bond-forming reactions.[63-65]

Steric effects are equally important and are often adjusted through substituent modifications.[65] Bulky groups near the metal centre can prevent undesired side reactions

by blocking specific coordination sites, as seen in bulky phosphites used for selective olefin hydroformylation.[66] Such modifications can also influence the approach angle of substrates, thereby affecting regio- and enantioselectivity in reactions like allylic alkylation[67] and hydroboration.[68]

An exemplary case of extensive ligand design is demonstrated by the Buchwald group, which has made significant contributions over the past two decades. They have developed a series of highly specialized dialkylbiaryl phosphine ligands with remarkable success. By systematically modifying the electronic properties surrounding the phosphorus atom, they have optimized these ligands for complex palladium-catalyzed transformations (Figure 1.4). Notably, ligands within this library are tailored to specific reaction types. For example, XPhos has proven highly effective in palladium-catalyzed amination reactions of aryl sulfonates, while SPhos has been particularly successful in Suzuki-Miyaura couplings involving heteroaryl substrates and other traditionally challenging reaction partners.

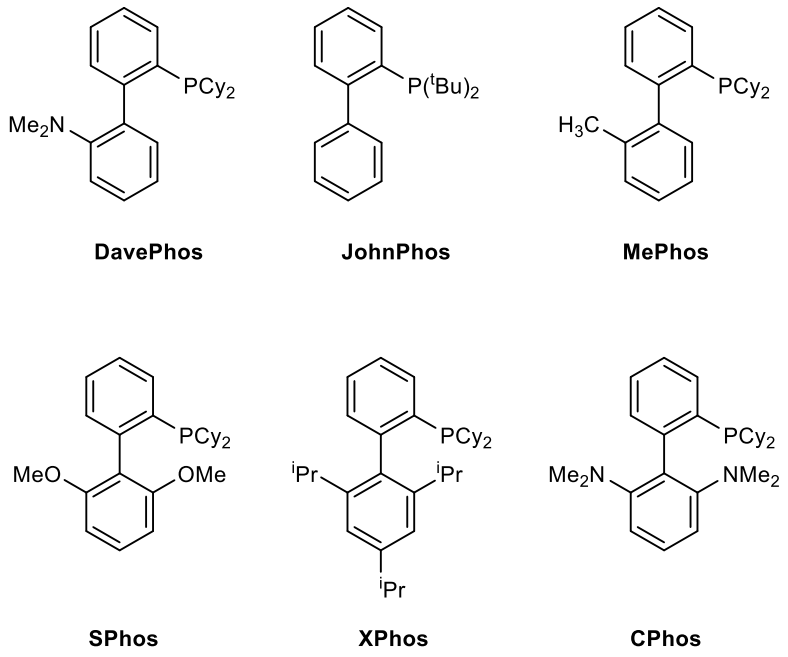

Figure 1.4: Buchwald ligand library with varying electronic and steric properties.

The discovery of new privileged ligands for sophisticated and underexplored transformations is increasingly essential. Expanding the ligand space can enhance our understanding of both straightforward asymmetric processes and more complex

transformations, enabling diverse and valuable outcomes. A notable example is stereodivergent reactions, where the development of highly selective ligands is particularly critical.

1.2 Introduction to stereodivergent catalysis

Stereodivergent catalysis is a strategy in asymmetric synthesis where a single catalytic system enables the selective formation of multiple stereoisomers of a product from the same set of starting materials (Figure 1.5). This type of catalysis has emerged as a powerful approach in the realm of asymmetric synthesis, allowing for the systematic construction of multiple stereocentres with complete control over both absolute and relative stereochemistry.

The ability to access all stereoisomers of a molecule from the same set of starting materials, merely by altering the catalyst or reaction conditions, is particularly advantageous for creating complex molecules with contiguous stereocentres.[69-71] This capability addresses a fundamental challenge in synthetic chemistry: efficiently generating stereochemical diversity in a single transformation without iterative synthetic steps. The significance of stereodivergent catalysis is underlined by its role in synthesizing biologically active molecules and natural products,[72] where subtle changes in stereochemistry can drastically alter biological activity.

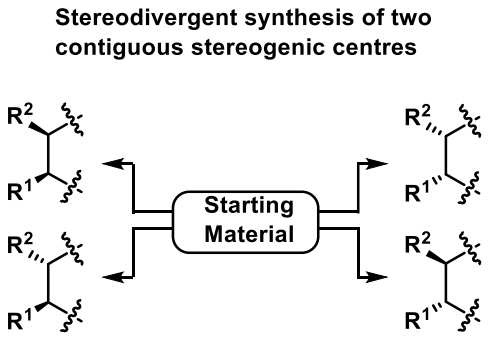

Figure 1.5: Stating the basis of stereodivergent synthesis of two contigious stereocentres. A single starting material can, under different conditions result in 4 different products (*S,S; S,R; R,S or R,R*).

Complexity arising from contiguous stereocentres

The addition of contiguous stereocentres to a molecular scaffold exponentially increases the complexity of the system, leading to a rapid escalation in the number of possible stereoisomers.[73] According to the Le Bel–van't Hoff rule, a molecule with *n* stereocentres

can have up to 2^n stereoisomers if all centres are non-equivalent and each stereocentre can adopt either of two configurations.[74-76]

This complexity is magnified in molecules with multiple contiguous stereocentres, such as in natural products, where achieving precise stereocontrol is paramount. Most complex natural products contain multiple stereocentres (Figure 1.6). Taxol, a particular tough example, contains 11 stereocentres which summate to 2048 (2^{11}) different possible stereoisomers. The stereodivergent synthesis of such natural products illustrates the challenges associated with setting multiple stereocentres, especially when absolute and relative configurations are not easily determined.[72]

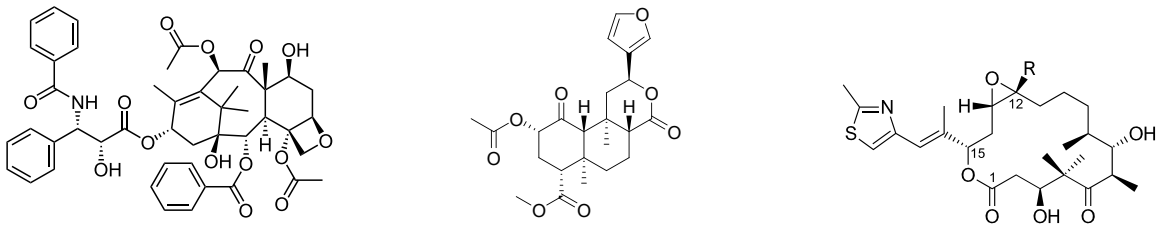

Taxol
11 stereocentres

Salvinorin A
7 stereocentres

Epothilone
7 stereocentres

Figure 1.6: Showing natural products containing large number of stereocentres.

Stereodivergent catalysis: concepts and strategies

Stereodivergent catalysis refers to the ability to selectively form multiple stereoisomers from a common set of starting materials using catalyst variations. Two key forms of stereodivergence are enantiodivergence and diastereodivergence, where the catalyst dictates not just the absolute configuration (enantiomers) but also the relative arrangement (diastereomers) of newly formed stereocentres.[70] A fully stereodivergent catalytic system ideally allows access to all stereoisomers by using the same substrates under identical reaction conditions, differing only by the nature of the catalysts used.[73]

One of the most efficient strategies for achieving stereodivergence involves dual-catalysis, wherein two distinct chiral catalysts simultaneously control the configuration of two stereocentres (Figure 1.7).[72] For example, the Carreira group demonstrated the α-

allylation of branched aldehydes using two independent chiral catalysts—an iridium-based catalyst for the allylic alcohol and a chiral amine catalyst for the aldehyde—resulting in full control over the two stereocentres formed.[72] This approach, termed "stereodivergent dual catalysis", enables systematic access to all possible stereoisomers (*R,S*; *R,R; S,S; S,R*) by simply switching between the enantiomers of the catalysts involved.

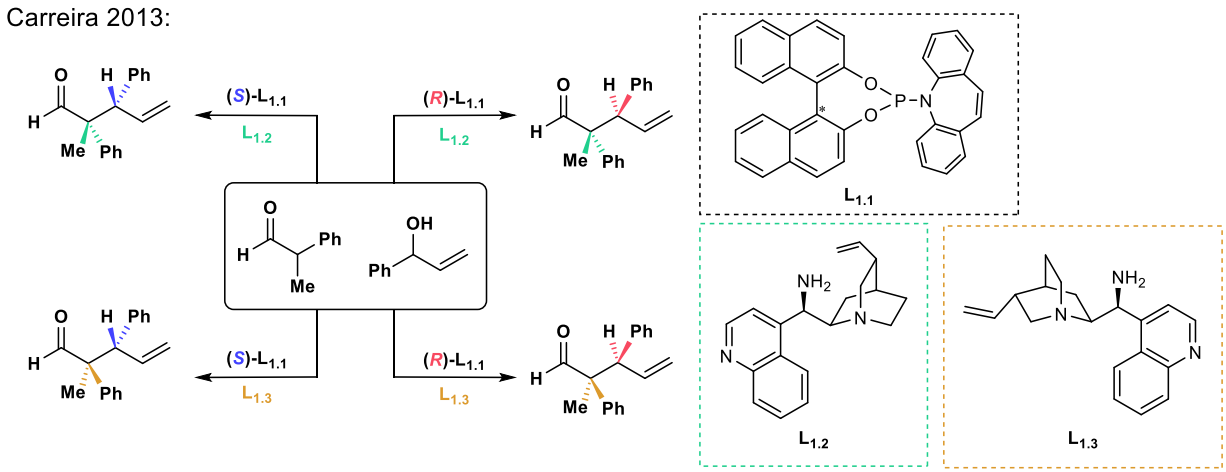

Figure 1.7: Example of stereodivergent with dual-catalysis yielding all four diastereoisomers (*R,S*; *R,R; S,S; S,R;* from left to right) depending on the catalyst used (either *R* or *S* $L_{1.1}$ and either $L_{1.2}$ or $L_{1.3}$). Colour is used to connect a stereocenter configuration to a specific ligand.[72]

Advantages in the synthesis of complex molecules

The major advantage of stereodivergent catalysis in the synthesis of complex molecules is its efficiency and sustainability. Traditional stereoselective methods often require multiple synthetic routes to access different stereoisomers, making the overall process time-consuming and resource-intensive. In contrast, stereodivergent catalysis minimizes synthetic efforts by providing access to all stereoisomers via a single pathway.[72,77] This efficiency is particularly relevant in the context of diversity-oriented synthesis (DOS) and library construction, where generating a wide array of stereoisomers is desirable for exploring structure-activity relationships (SAR).[71,78-80]

For instance, Ding and Hall (2013) illustrated how stereodivergent synthesis could simplify the preparation of all four stereoisomers of mefloquine, a compound with distinct pharmacological profiles for each stereoisomer.[81] By using a stereodivergent dual-catalytic approach, they bypassed the need for separate synthetic routes, achieving a streamlined and atom-economical process.

Controlling stereochemistry

Achieving stereodivergence in catalysis requires careful consideration of catalyst design and reaction environments. For reactions involving multiple contiguous stereocentres, catalysts must exert independent control over each stereogenic element. This is particularly challenging when inherent substrate biases or steric hindrances favour one stereoisomer over another.[82] Strategies to overcome these biases include employing dual-catalyst systems, modifying the reaction environment, or using cooperative catalysis where two catalysts function in tandem without mutual deactivation.[83,84]

Advances in ligand design and stereodivergent catalysis continue to reshape asymmetric synthesis, offering powerful tools to create complex, stereochemically rich molecules. These developments open pathways to explore new reactions, deepen our understanding of stereocontrol, and push the boundaries of what synthetic chemistry can achieve.

1.3 Thesis outline:

This thesis delves into the exploration of a new subclass of ligands with potential applications in asymmetric catalysis. We explore their ligand space, synthetic accessibility, and suitability for broader use in asymmetric catalysis. The findings aim to support the development of new tools for stereoselective transformation.

In **Chapter 2**, a Cu(I) asymmetric conjugate addition (ACA) to cycloalkenyl ketones is presented over a wide range of substrates. We present this as a stereodivergent synthesis of 1,2-disubstituted cyclic carbon cores. This reaction builds upon the research presented by Dr. Alexandre Brethome (in his thesis, Chapter 4) and follows the methodology of ACA often presented by our group. We utilize a new sub-class of P-chiral phosphoramidite ligands in order to obtain the desired yields and selectivities. Finally, we elucidate the source of stereodivergence by exploring chair conformations and their relative energies. We attempt to find other similar reactions for the ligand to do.

In **Chapter 3**, we explore the ligand space of this underexplored ligand subclass. We aim to find a library of P-chiral ligands with high diastereomeric ratios with high activity on the tested ACA. We opt for a "*ceteris paribus*" modification approach, modifying the BINOL and amine region one at a time. We delve into what attributes of each region of the phosphoramidite can give rise to higher diastereomeric ratios.

In **Chapter 4**, we explore on diastereoselective syntheses of a specific P-chiral ligand, which otherwise must be obtained through crystallisation from a 1:1 diastereomeric mixture. We touch upon the challenges in working with fragile P(III) substrates and explore different promising although partially-unsuccessful strategies that can give rise to diastereoselectivity in P-chiral phosphoramidites.

1.4 References:

1. Aristotle, *On the Heavens (De Caelo)*, Book II, Chapter 4, translated by J. L. Stocks, *The Internet Classics Archive*. Available at: classics.mit.edu. (accessed 03/04/2025).
2. A. Zee, *Fearful Symmetry: The Search for Beauty in Modern Physics*, Princeton University Press, Princeton, 2007.
3. I. Stewart, *Why Beauty Is Truth: A History of Symmetry*, Paperback ed., Harper Perennial, New York, 2008.
4. Vitruvius, *De architectura (The Ten Books on Architecture)*, translated by M. H. Morgan, Harvard University Press, Cambridge, 1914.
5. Aristotle, *Metaphysics*, Book XIII, 1078b.
6. M. Schilthuizen, A. Davison, *Naturwissenschaften*, 2005, **92**, 504–515.
7. A. Guijarro, M. Yus, *The Origin of Chirality in the Molecules of Life: A Revision from Awareness to the Current Theories and Perspectives of this Unsolved Problem,* Royal Society of Chemistry, Cambridge, 2008.
8. M. Gardner, *The Ambidextrous Universe*, Pelican Books, London, 1964.
9. J. P. Riehl, *Mirror-Image Asymmetry: An Introduction to the Origin and Consequences of Chirality*, Wiley, New Jersey, 2010.
10. L. Pasteur, *C. R. Acad. Sci. Paris*, 1848, **26**, 535–538.
11. W. Thomson (Baron Kelvin), *The Molecular Tactics of a Crystal*, Clarendon Press, Oxford, 1894, p. 27.
12. S. W. Smith, *Toxicol. Sci.*, 2009, **110**, 4–30.
13. C. Blakemore, S. Jennett, *The Oxford Companion to the Body*, Oxford University Press, Oxford, 2001.
14. M. T. Miller, *Trans. Am. Ophthalmol. Soc.*, 1991, **LXXXIX**, 623–673.
15. I. Fleming, A. Barbero, D. Walter, *Chem. Rev.*, 1997, **97**, 2063–2192.
16. P. R. Savoie, C. N. von Hahmann, A. Penger, Z. Wei, J. T. Welch, *Org. Biomol. Chem.*, 2018, **16**, 3151–3159.
17. T. Kwok, O. Hoff, R. J. Armstrong, T. J. Donohoe, *Chem. Eur. J.*, 2020, **26**, 12912–12926.
18. A. V. Karnik, M. Hasan, *Stereochemistry: A Three-Dimensional Insight*, 2021, Chapter 1, Elsevier, Amsterdam, pp. 3–23.

19. R. E. Gawley, J. Aube, *Principles of Asymmetric Synthesis*, Elsevier, Amsterdam, 2012, Chapter 1, pp. 1–63.
20. *The Nobel Prize in Chemistry 2001*, NobelPrize.org, Nobel Prize Outreach AB, 2001. Available at: https://www.nobelprize.org/ (accessed 2024-06-10).
21. B. M. Trost, D. L. Van Vranken, C. Bingel, *J. Am. Chem. Soc.*, 1992, **114**, 9327–9343.
22. R. Ardkhean, S. P. Fletcher, R. S. Paton, in *New Directions in the Modeling of Organometallic Reactions*, A. Lledós, G. Ujaque (eds.), Springer, Cham, 2020, *Topics in Organometallic Chemistry*, **67**, pp. 153–189.
23. Q.-L. Zhou, *Privileged Chiral Ligands and Catalysts*, Wiley-VCH Verlag GmbH & Co. KGaA, Weinheim, 2011.
24. C. Nájera, J. M. Sansano, *Chem. Rec.*, 2016, **16**, 2430–2448.
25. J. F. Teichert, B. L. Feringa, *Angew. Chem. Int. Ed. Engl.*, 2010, **49**, 2486–2528.
26. M. Žabka, L. Naviri, R. M. Gschwind, *Angew. Chem. Int. Ed.*, 2021, **60**, 25832–25838.
27. S. Ma, Y. Cao, Y.-F. Shi, C. Shang, L. He, Z.-P. Liu, *Chem. Sci.*, 2024, **15**, 13359–13368.
28. A. Brethomé, *A Physical-Organic Approach to Asymmetric Catalysis: Design and Synthesis of Chiral Ligands Using Multivariate Modelling*, Doctoral Thesis, University of Oxford, 2019, Chapter 1.
29. D. J. Durand, N. Fey, *Chem. Rev.*, 2019, **119**, 6561–6594.
30. J. Wassenaar, J. N. H. Reek, *Org. Biomol. Chem.*, 2011, **9**, 1704.
31. J. Mas-Roselló, A. G. Herraiz, B. Audic, A. Laverny, N. Cramer, *Angew. Chem. Int. Ed. Engl.*, 2021, **60**, 13198–13224.
32. A. Miyashita, A. Yasuda, H. Takaya, K. Toriumi, T. Ito, T. Souchi, R. Noyori, *J. Am. Chem. Soc.*, 1980, **102**, 7932.
33. R. Noyori, *Angew. Chem. Int. Ed.*, 2002, **41**, 2008–2022.
34. P. Schäfer, T. Palacin, M. Sidera, S. P. Fletcher, *Nat. Commun.*, 2017, **8**, 15762.
35. T. V. RajanBabu, *Synlett*, 2009, **6**, 853–885.
36. R. Noyori, H. Takaya, *Acc. Chem. Res.*, 1990, **23**, 345–350.
37. S. Akutagawa, *Appl. Catal. A: Gen.*, 1995, **128**, 171–207.
38. H.-U. Blaser, W. Brieden, B. Pugin, F. Spindler, M. Studer, A. Togni, *Top. Catal.*, 2002, **19**, 3–16.

39. A. Togni, C. Breutel, A. Schnyder, F. Spindler, H. Landert, A. Tijani, *J. Am. Chem. Soc.*, 1994, **116**, 4062–4066.
40. B. L. Feringa, *Acc. Chem. Res.*, 2000, **33**, 346–353.
41. M. van den Berg, A. J. Minnaard, R. M. Haak, M. Leeman, E. P. Schudde, A. Meetsma, B. L. Feringa, A. H. M. de Vries, C. E. P. Maljaars, C. E. Willans, D. Hyett, J. A. F. Boogers, H. J. W. Henderickx, J. G. de Vries, *Chem. Eur. J.*, 2003, **9**, 308–323.
42. Y. Fu, X.-X. Guo, S.-F. Zhu, A.-G. Hu, J.-H. Xie, Q.-L. Zhou, *J. Org. Chem.*, 2004, **69**, 4648–4655.
43. R. M. Maksymowicz, P. M. C. Roth, S. P. Fletcher, *Nat. Chem.*, 2012, **4**, 649–654.
44. P. M. C. Roth, M. Sidera, R. M. Maksymowicz, S. P. Fletcher, *Nat. Protoc.*, 2014, **9**, 104–111.
45. M. Vuagnoux-d'Augustin, A. Alexakis, *Chem. Eur. J.*, 2007, **13**, 9647–9662.
46. S. Ng, C. Howshall, T. N. Ho, B. K. Mai, Y. Zhou, C. Qin, K. Z. Tee, P. Liu, F. Romiti, A. H. Hoveyda, *Science*, 2024, **386**, 167–175.
47. J. F. Teichert, B. L. Feringa, *Chem. Commun.*, 2011, **47**, 2679–2681.
48. C. Hawner, D. Müller, L. Gremaud, A. Felouat, S. Woodward, A. Alexakis, *Angew. Chem. Int. Ed. Engl.*, 2010, **49**, 7769–7772.
49. J. P. Wolfe, S. L. Buchwald, *J. Org. Chem.*, 2000, **65**, 1144–1157.
50. H. U. Blaser, B. Pugin, F. Spindler, *Helv. Chim. Acta*, 2021, **104**, e2000192.
51. R. Silva Villatoro, J. R. Belfield, H. D. Arman, L. W. Hernandez, E. M. Simmons, Z. J. Garlets, S. R. Wisniewski, J. R. Coombs, D. E. Frantz, *Organometallics*, 2023, **42**, 3164–3172.
52. M. J. Burk, *J. Am. Chem. Soc.*, 1991, **113**, 8518–8519.
53. R. S. Hoerrner, D. Askin, R. P. Volante, P. J. Reider, *Tetrahedron Lett.*, 1998, **39**, 3455–3458.
54. K. Tissot-Croset, D. Polet, A. Alexakis, *Angew. Chem. Int. Ed. Engl.*, 2004, **43**, 2426–2428.
55. A. Alexakis, N. Krause, S. Woodward, in *Copper-Catalyzed Asymmetric Synthesis*, 2014, pp. 33–68.
56. S. Zou, Z. Zhao, G. Yang, H. Huang, *Nat. Commun.*, 2024, **15**, 10477.
57. K. Biswas, O. Prieto, P. J. Goldsmith, S. Woodward, *Angew. Chem. Int. Ed. Engl.*, 2005, **44**, 2232–2234.

58. P. Perlmutter, *Conjugate Addition Reactions in Organic Synthesis*, Pergamon, Oxford, 1992.
59. C. A. Falciola, K. Tissot-Croset, A. Alexakis, *Angew. Chem. Int. Ed. Engl.*, 2006, **45**, 5995–5998.
60. M. J. Burk, *Acc. Chem. Res.*, 2000, **33**, 363–372.
61. A. Robinson, H.-Y. Li, J. Feaster, *Tetrahedron Lett.*, 1996, **37**, 8321–8324.
62. A. Pfaltz, W. J. Drury III, B. M. Trost, *Proc. Natl. Acad. Sci. U.S.A.*, 2004, **101**, 5723–5726.
63. H. Frauenrath, D. Brethauer, S. Reim, M. Maurer, G. Raabe, *Angew. Chem. Int. Ed. Engl.*, 2001, **40**, 177–179.
64. C. Shan, X. Liu, X. Luo, Y. Lan, *Sci. Rep.*, 2024, **14**, 24031.
65. S. J. Webster, L. B. Balázs, F. W. Goetzke, V. Stojalnikova, K. Liu, K. E. Christensen, H. W. Mackenzie, S. P. Fletcher, *J. Am. Chem. Soc.*, 2024, **146**, 24708–24715.
66. A. A. Dabbawala, H. C. Bajaj, R. V. Jasra, *J. Mol. Catal. A: Chem.*, 2009, **302**, 97–106.
67. E. Rideau, S. P. Fletcher, *Beilstein J. Org. Chem.*, 2015, **11**, 2435–2443.
68. H. Iwamoto, T. Imamoto, H. Ito, *Nat. Commun.*, 2018, **9**, 2290.
69. S. Krautwald, E. M. Carreira, *J. Am. Chem. Soc.*, 2017, **139**, 5627–5639.
70. I. P. Beletskaya, C. Nájera, M. Yus, *Chem. Rev.*, 2018, **118**, 5080–5200.
71. D. Moser, T. A. Schmidt, C. Sparr, *J. Am. Chem. Soc. Au*, 2023, **3**, 2612–2630.
72. S. Krautwald, D. Sarlah, M. A. Schafroth, E. M. Carreira, *Science*, 2013, **340**, 1065–1068.
73. P. Li, E. Zheng, G. Li, Y. Luo, X. Huo, S. Ma, W. Zhang, *Science*, 2024, **385**, 972–979.
74. E. L. Eliel, S. H. Wilen, L. Mander, *Stereochemistry of Organic Compounds*, Wiley, New York, 1994.
75. *Bulletin de la Société Chimique de Paris*, 1874, **22**, 337–347.
76. *Archives Néerlandaises des Sciences Exactes et Naturelles*, 1875, **9**, 445–454.
77. X. Yang, C. Yuan, S. Ge, *Chem.*, 2023, **9**, 198–215.
78. Y. Hu, J.-Y. Huang, R.-J. Yan, Z.-C. Chen, Q. Ouyang, W. Du, Y.-C. Chen, *Chem. Sci.*, 2023, **14**, 1896–1901.
79. L. Massaro, J. Zheng, C. Margarita, P. G. Andersson, *Chem. Soc. Rev.*, 2020, **49**, 2504–2522.
80. M. A. Schafroth, G. Zuccarello, S. Krautwald, D. Sarlah, E. M. Carreira, *Angew. Chem.*, 2014, **126**, 14118–14121.

81. J. Ding, D. G. Hall, *Angew. Chem. Int. Ed.*, 2013, **52**, 8069–8073.
82. S. Doobary, A. J. D. Lacey, S. G. Sweeting, S. B. Coppock, H. P. Caldora, D. L. Poole, A. J. J. Lennox, *Nat. Chem.*, 2024, **16**, 1647–1655.
83. B. Kim, H. Lee, I. Song, S. Y. Lee, *Chem. Soc. Rev.*, 2025, **54**, 715-741
84. Y. Wang, J. Feng, E.-Q. Li, Z. Jia, T.-P. Loh, *Org. Biomol. Chem.*, 2024, **22**, 37–54.

Chapter 2:

Asymmetric conjugate additions on cycloalkenyl ketones

2.1. Starting the cycle, a brief glance of cyclohexane, and 1,2- substituted variants.

Unlike its aromatic counterpart, benzene, which is naturally sourced, cyclohexane had not been found in nature in the late 19th century and it was instead synthesised chemically.[1,2] Initial attempts to synthesise cyclohexane began in 1867, but it wasn't until 1894 that it was successfully isolated by Adolf von Baeyer.[3-8] While benzene is a planar hexagonal molecule with angles of 120° and sp^2 hybridized carbons, the cyclohexane carbon core has an sp^3 hybridized skeleton, and adopts a low-energy "chair-shaped" conformer, which renders the bond angles at 109.5°.[9,10] This conformation possesses two different environments of hydrogen atoms named axial (ax.) and equatorial (eq.). Axial hydrogens point directly up or down, perpendicular to the ring plane, while equatorial hydrogens extend roughly parallel to the ring plane. This ring conformation is subject to change; the ring is known to 'flip,' swapping the previously axial hydrogens into equatorial positions and vice versa (Figure 2.1a). The energy required to go from one chair conformer to another in unsubstituted cyclohexane is approximately 43 $kJ \cdot mol^{-1}$ with the molecule transversing through multiple higher energy conformations (half-chair, twist-boat and boat) before getting to the other chair conformer.[9,11] In the case of cyclohexane, both chair conformations are indistinguishable from each other. However, this is not the case for most substituted cyclohexanes.

Chemists developed A-values to estimate the steric bulk of substituents in the axial position, measured in kcal/mol, with 0 kcal/mol set for equatorial positions. These values indicate the energy cost of axial placement, aiding in predicting the preferred conformation of substituted cyclohexane molecules. This empirical index is especially useful for understanding conformational preference in multi-substituted cyclohexane rings. Generally, larger substituents prefer equatorial positions, minimizing steric clash and reducing the energy the molecule.[12]

Elucidating the preferred conformation becomes more complicated when considering non-equal substituents, diverse ring sizes, and cycles containing heteroatoms. In general, larger substituents prefer to occupy equatorial positions due to minimized steric hindrance and A values can help identify the preferred conformation. Thus, in substituted

cyclohexanes, the equilibrium will usually favour the chair conformation in which the bulkier group adopts an equatorial position/lower overall A-values.

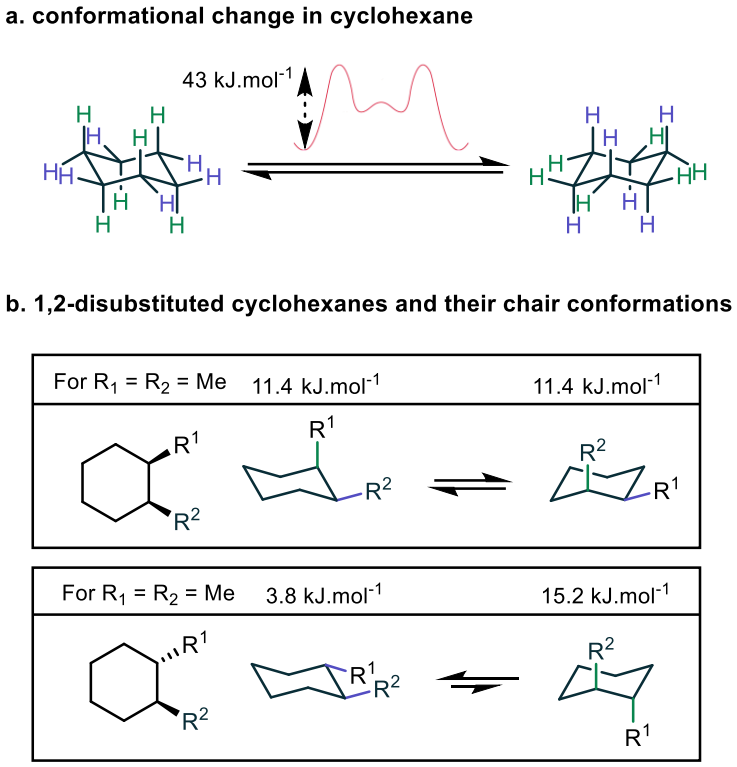

Figure 2.1: a. (Left) Chair conformer of cyclohexane showing equatorial hydrogens (blue) axial hydrogens (green). Axial and equatorial positions can be swapped via chair flipping. **b**. Chair conformations of *cis* (top) and *trans* (bottom) 1,2- disubstituted cyclohexanes. Given energies are for 1,2-dimethyl cyclohexane.

For 1,2-disubstituted cyclohexanes, the spatial arrangement of the substituents affects the molecule's stability. These compounds can be either *cis* or *trans*–isomers. In the *cis* configuration, both substituents adopt either an axial-equatorial or equatorial-axial arrangement in the two chair conformations. The two conformations are similarly stable, as each has one substituent in an energetically favourable equatorial position and one in the less stable axial position, resulting in a total strain energy of around ~11.4 kJ·mol^{-1} for the di-methyl cyclohexane example (Figure 2.1b).

In contrast, for *trans*–1,2-disubstituted cyclohexanes, one chair conformation has both substituents in the equatorial positions (di-equatorial), making it more stable, while the other conformation places both substituents in axial positions (di-axial), which significantly increases steric clash due to four 1,3-diaxial interactions (15.2 kJ.mol^{-1} when R_1=R_2= Me). As a result, the di-equatorial conformation is favoured, reducing steric interactions and overall strain (3.8 kJ.mol^{-1}).[13-15]

Methods capable of controlling the stereochemistry of multiple stereogenic centres, so that a specific isomer within a diastereomeric or enantiomeric set can be selectively formed, are highly valuable. Such approaches are particularly powerful when different stereoisomers can be targeted simply by modifying a single reaction parameter, allowing rapid and flexible access to any stereoisomer of interest. These principles are especially significant for 1,2-disubstituted cyclic systems, which are abundantly in nature and are gaining increasing prominence in the pharmaceutical industry due to their structural complexity (Figure 2). Moreover, the ability to simultaneously generate contiguous stereocentres enhances molecular diversity and biological relevance, making them attractive scaffolds for drug development. The use of dual catalytic systems within a single reaction to independently control distinct stereogenic elements is a noteworthy strategy, enabling stereodivergent synthesis of contiguous cyclic stereocentres and stereoisomer selection through precise reaction condition optimization. These carbon cores are notoriously difficult to synthesise asymmetrically. In the literature, a few routes have gained prominence in the synthesis of these types of molecules.

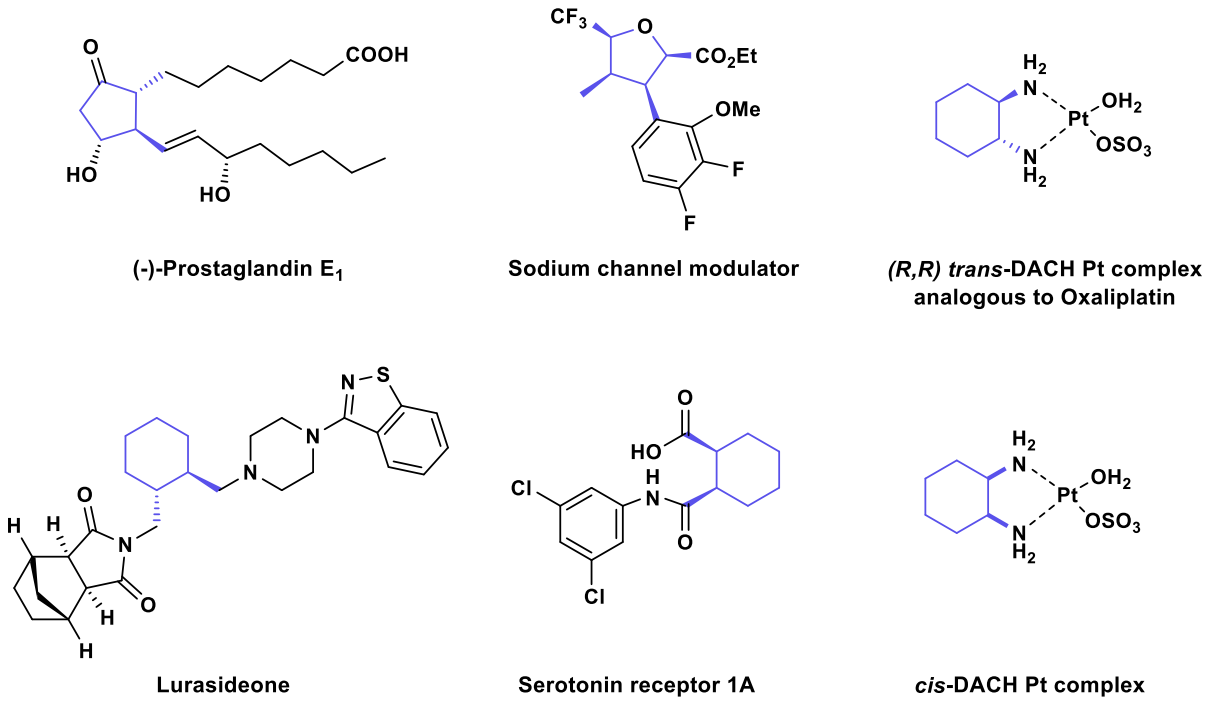

Figure 2.2: Examples of multi-substituted cyclic cores baring contiguous stereocentres in nature and industry.

Both cyclic diastereomers often present different biological activities. The difference is evident when the *trans*– and *cis*–diastereomers of 1,2-diaminocyclohexane (DACH) platinum complexes are compared. The *trans*– diastereomer is analogous to an active

form of Oxaliplatin and it shows high anti-tumour properties.[16,17] On the other hand, the *cis*–DACH Pt complex shows a much poorer activity. Different ligands added to the complexes can massively affect these relative activities.[17]

2.2. Asymmetric hydrogenation, an approach to contiguous stereocentres and 1,2-disubstituted cyclic cores

Asymmetric Hydrogenation, (AH) recognized with the 2001 Chemistry Nobel Prize,[18] has become a crucial strategy for producing complex carbon cores structures both in academia and industry. Recent progress in this field has enabled selective reductions of various important prochiral substrates, such as oximes, minimally differentiated dialkyl ketimines, in-situ formed imines, and isomeric mixtures of enones.[19, 20]

The reduction of aromatic molecules has emerged as a leading approach to synthesise substituted all-*cis* cyclohexanes through single-face hydrogenation of polysubstituted arenes.[21] This strategy allows for the diastereoselective formation of complex structures, including multi-fluorinated cyclohexanes and piperidines, and allows the asymmetric reduction of six-membered ring-containing bicyclic compounds.[22-30] While these methods have been largely restricted to six-membered rings, the reduction of heteroaromatic cores has been utilized to access a variety of ring sizes, demonstrating the versatility of this transformation.[31,32]

In this context, the work by the Glorius, O'Hagen and Marks showcases the remarkable power of hydrogenations in organic synthesis.[33-37] Drawing a parallel to the industrial synthesis of cyclohexane via hydrogenation of benzene, this chemistry has been applied to a wide array of aromatic molecules to form their cyclic hydrocarbon analogues (Figure 2.3).

Despite these advancements, challenges remain in the enantioselective reduction of certain fundamental substitution patterns. It is important to note that hydrogenations on aromatic systems are usually not performed enantioselectively, which is a major limitation of this approach. Additionally, not all diastereomers are obtainable through this process; typically, only same-faced substituted aromatics are produced, albeit with very high diastereomeric ratios.

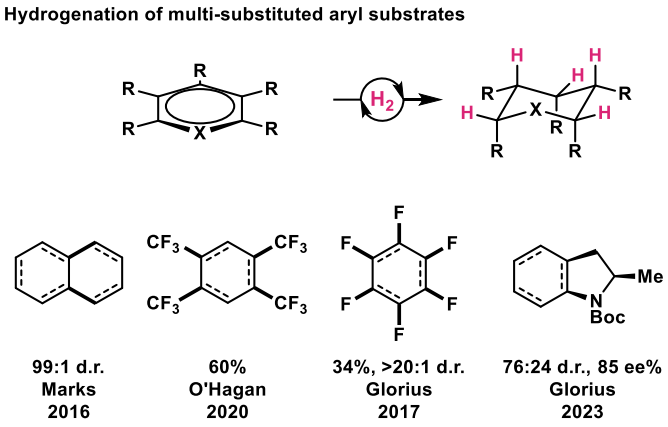

Figure 2.3: Previous work on hydrogenation of multi-substituted substrates.

Asymmetric hydrogenation (AH) has seen significant advancements, but its application to complex systems, particularly tetra-substituted and cyclic olefins, remains highly challenging. Most successful AH methods rely on strongly activating groups or specific substitution patterns (Figure 2.4). For instance, inactivated tri-alkyl substituted olefins (**4a**) usually exhibit low reactivity due to the lack of a coordinating group. Tetra-substituted olefins (**4b**) often require electron-rich substituents for high selectivity. In cyclic systems (**4c**), the stereospecificity of AH typically results in *cis*–diastereomers, making access to *trans*–1,2-disubstitued scaffolds extremely difficult. Several groups have expanded the scope of these AHs strategies (Figure 2.5).

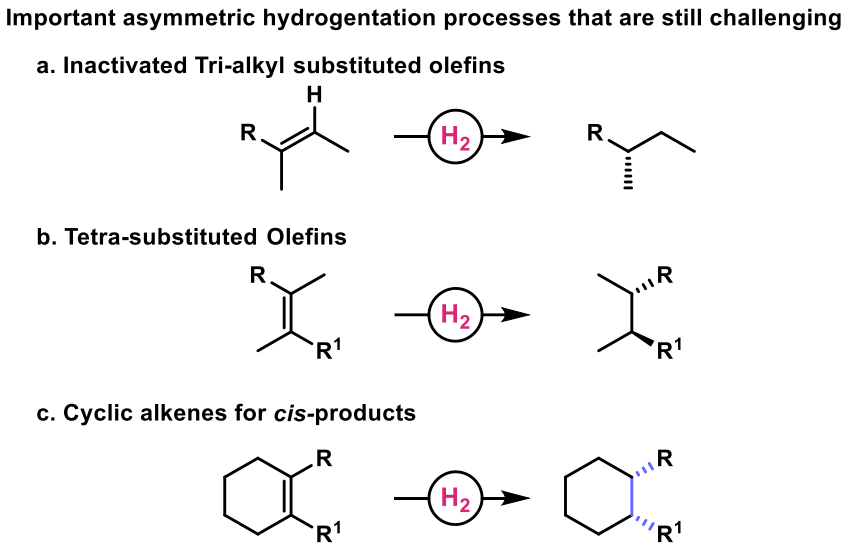

Figure 2.4: Challenging AH reactions. *a*. Inactivated trialkyl substituted olefins. *b*. Tetrasubstituted Olefins. *c*. Cyclic alkenes for *cis*–products.

The Pfaltz group has addressed several key challenges in AH, particularly in systems where the lack of activating groups traditionally limited their reactivity. Their iridium-

catalysed methods have shown high efficiency and selectivity in hydrogenating tri-alkyl substituted olefins with excellent enantiomeric excesses (*ee*), even for unfunctionalized substrates (92% *ee*), which broadens the scope of AH by bypassing their reliance on coordinating functional groups (Figure 2.5a).[38]

Even though some success has been seen on linear tetra-substituted olefines, obtaining high yields and selectivities, they once again necessitate activating groups such as multiple adjacent aryl groups.[39]

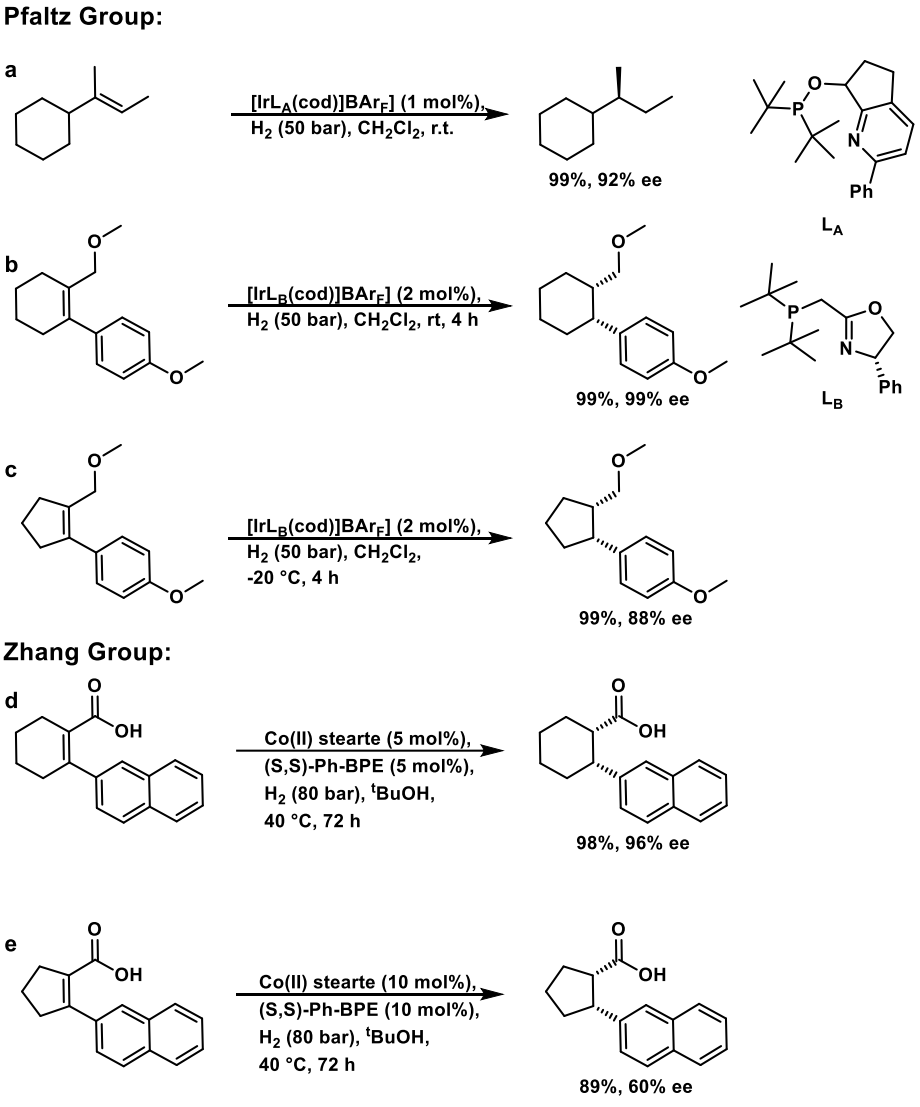

Figure 2.5: Advancements on Asymmetric hydrogenations of tri- and tetra substituted olefins.[38-42]

The Pfaltz group attempted to tackle the sterically demanding tetra-substituted olefin system. While they achieved outstanding results for linear and six-membered ring substrates (Figure 2.5b, 99% ee), a drop in enantioselectivity was observed for five-

membered rings (Figure 2.5c, 88% ee).[40] This drop was attributed to steric congestion around the reaction centre and geometric constraints in five-membered systems. The pentacyclic hydrogenation had also to be conducted at sub-zero conditions, something that might prove problematic for industrial adaptation. The stereoselectivity that arise from the hydrogenation was restricted to forming *cis*–diastereomers, highlighting the inherent stereochemical limitations of cyclic substrates in AH. Furthermore, this subset of substrates requires the presence of multiple activating groups (ether groups and aryls). Further work by this group has succeeded with five-membered rings but often depends on activating groups, limiting the methodology's scope.[41]

Similarly, the Zhang group made notable advances using cobalt as an alternative to expensive noble metals, providing a cost-effective solution for AH in tetrasubstituted olefins achieving good results in six-membered ring systems (96% ee); results comparable to iridium-based methods.[42] The stereochemical outcome was again restricted to the *cis*–diastereomer, and when applied to five-membered rings, the enantioselectivity dropped (60% ee). This decrease reflects similar limitations to those observed in Pfaltz's work, where the small ring size led to increased steric hindrance and reduced catalytic selectivity. Similarly, the cobalt system also required activating groups, such as a carboxylic acid moiety on one side and an aromatic group on the other.

Hoffmann-La Roche has developed an efficient method for the AH of cyclic tetra-substituted olefins, achieving excellent enantioselectivity (95% ee) using a Ru-catalyst system (Figure 2.6).[43] However, the process still suffers from most of the downsides seen previously, i.e. the necessity for activating groups and the limitation to the *cis* 1,2-disubstituted cyclic core. Despite all of this, the high selectivity and yield make it an appealing process for industry, particularly for synthesizing 1,2-disubstituted cyclic molecules with well-defined stereochemistry. The widespread applicability of this method underscores the industrial interest in refining AH for such complex substrates.

In contrast, Vertex Pharmaceuticals Ltd. approach for synthesizing tetra-substituted tetrahydrofurans, crucial intermediates for sodium channel modulators, highlights a major lack of general, asymmetric strategies.[44] Due to the lack of effective AH approaches for their systems, they resort to non-asymmetric hydrogenation. This process leads to a racemic mixture of *syn*-diastereomers (Figure 2.6), impacting the overall yield and relying on costly separation methods like preparative supercritical fluid chromatography

(SFC) to obtain the desired enantiomer. Such examples emphasize the need for continued development in this field to reduce reliance on post-reaction separation and achieve enantioenriched outcomes directly.

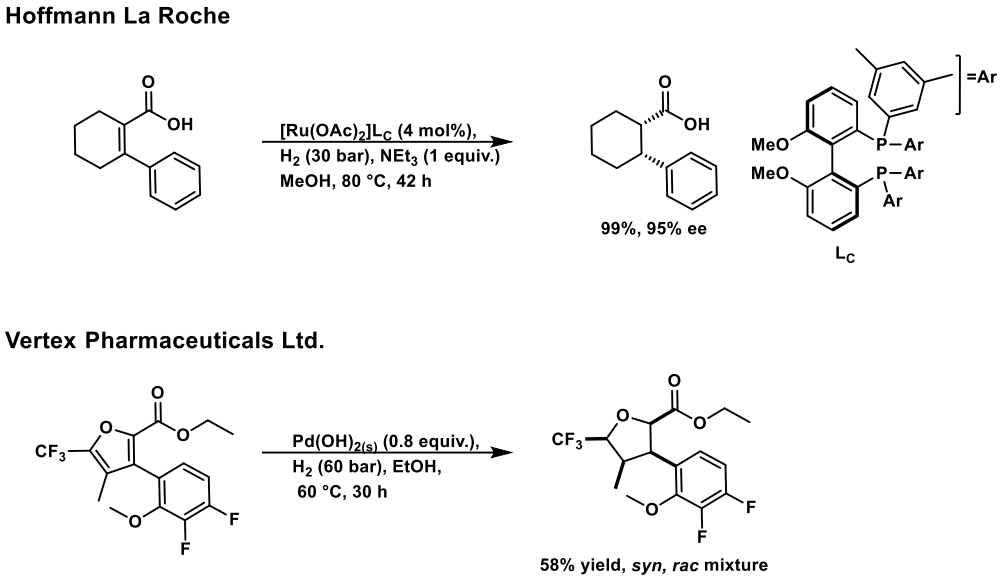

Figure 2.6: Uses and development of AH and its current limitations.

2.3. Asymmetric conjugate additions, an alternative

Asymmetric conjugate addition (ACA) has become a cornerstone in organic synthesis,[45] giving chemists a powerful toolbox for constructing carbon–carbon bonds with high stereocontrol. Since its development in the late 20th century, ACA has been instrumental in the synthesis of complex molecules, including natural products, pharmaceuticals, and agrochemicals (Figure 2.7).[46-48] The ability to form chiral centres enantioselectively while creating a new sp^3-sp^3 C-C bond has made ACA an indispensable reaction in modern synthetic strategies.

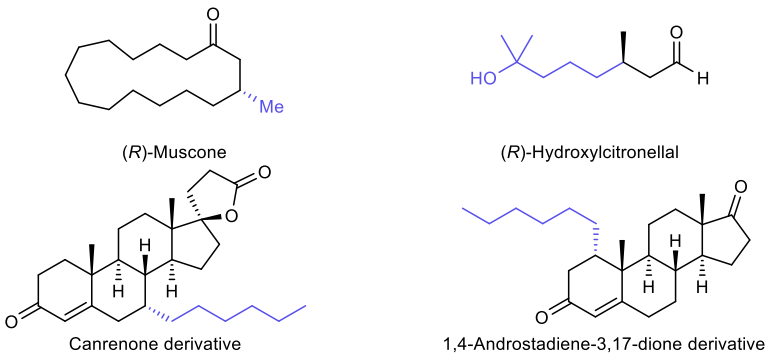

Figure 2.7: Examples of natural products or natural product derivatives prepared by ACA of cyclic/linear substrates. In blue, the fragment added via ACA.

Early advancements in ACA focused predominantly on cyclic α,β-unsaturated carbonyl compounds. The inherent rigidity and defined geometry of cyclic enones, such as cyclohexenone and cyclopentenone, provide a favourable environment for achieving high enantioselectivity. Copper-catalysed ACA reactions with these substrates have been extensively studied, utilizing various organometallic nucleophiles like organozinc, organoaluminum, and Grignard reagents (Figure 2.8a).[49-51] Chiral ligands, particularly phosphoramidites, have played a crucial role in these transformations, facilitating the formation of products with excellent enantiomeric excess.

Building upon the successes with cyclic substrates, research efforts expanded to include linear, acyclic α,β-unsaturated carbonyl compounds. Acyclic enones present additional challenges due to their increased conformational flexibility and the possibility of s-*cis*/s-*trans*–isomerization, which can impact both reactivity and selectivity. Despite these challenges, significant progress has been made in developing effective ACA protocols for acyclic and complex cyclic substrates.[52,53]

One of the limitations in ACA of cyclic and linear substrates is the use of highly reactive organometallic reagents, which can pose practical and safety concerns. These reagents often require strict anhydrous conditions and sub-zero temperatures to prevent side reactions and to maintain high selectivity. Such conditions can be challenging to implement on an industrial scale and may limit the functional group compatibility of the substrates, restricting the reactions scope.

To address these issues, alternative reagents have been explored. The use of softer alkylzirconium nucleophiles, generated *in situ* from alkenes and the Schwartz reagent (zirconocene hydrochloride), has emerged as a promising strategy. Alkenes are abundant, readily available, and can be transformed into alkylzirconium intermediates under mild conditions. The Fletcher group has extensively studied the copper-catalysed ACA of these alkylzirconocenes to both cyclic and acyclic enones, achieving high yields and enantioselectivities (Figure 2.8b).[54,55]

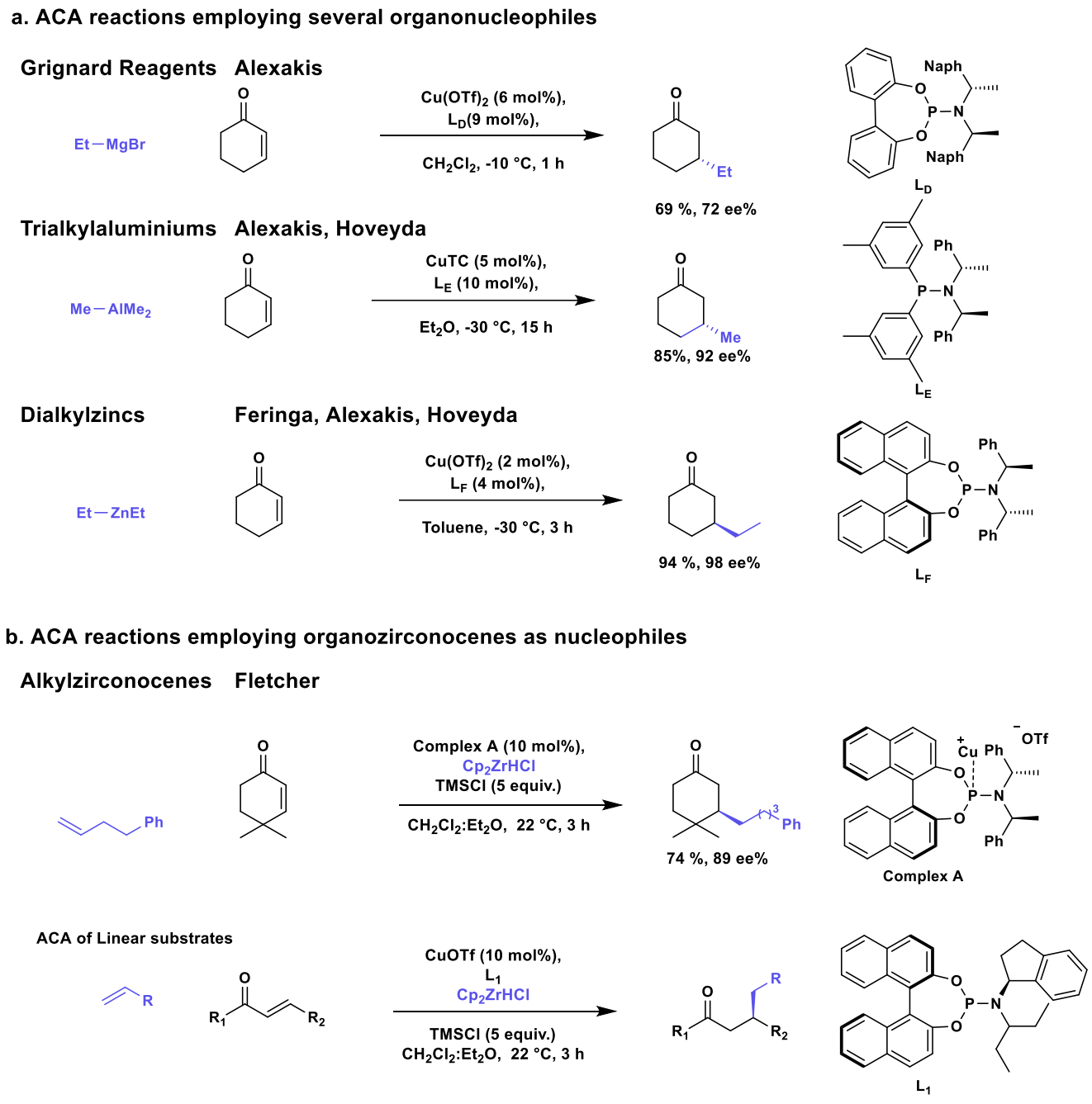

Figure 2.8: a. ACA of cyclic and acyclic substrates utilizing several organometallic nucleophiles. **b**. ACA of cyclic and linear substrates using organozirconium developed in the Fletcher group.

The advantages of using alkylzirconium reagents include improved functional group tolerance and the avoidance of reactive organometallic reagents. This approach has enabled the synthesis of products bearing sensitive functionalities and has facilitated the formation of tertiary and quaternary stereocentres. The methodology has expanded the scope of ACA, making it more accessible and practical for a wider range of substrates.[56]

Despite these advancements, certain classes of substrates remain challenging for ACA reactions. One such substrate class are exocyclic α,β-unsaturated carbonyls. These molecules characterised by an endocyclic C-C double bond attached to an exocyclic carbonyl group, introduce unique conformations that can complicate the traditional ACA process (Figure 2.9).

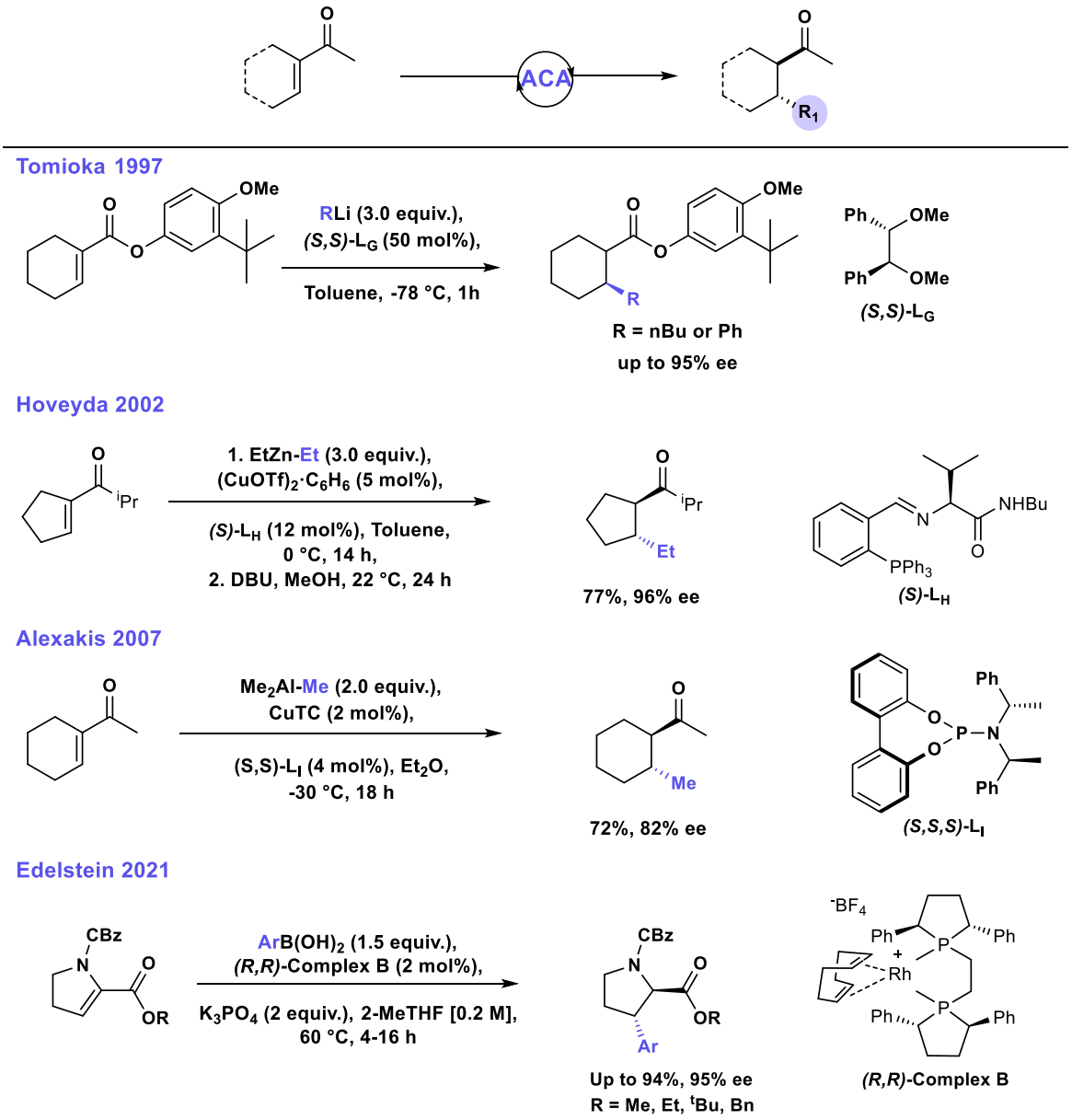

Figure 2.9: ACA of alkylmetals to exocyclic α,β-unsaturated carbonyls.

The Tomioka group made a significant contribution in 1997 by showcasing the ACA of organolithium reagents to BHA (2,6-di-*tert*-butyl-4-methoxyphenyl) enoate.[57] The high yields and enantioselectivities were greatly limited to the use of phenyllithium and n-

butyllithium reagents (>80% yield, >90% ee). Copper-catalysed conjugate additions of alkylmetals to exocyclic α,β-unsaturated carbonyl compounds have been previously reported, but, to the best of our knowledge, asymmetric variants of these reactions have been seldom described.

In 2002, the Hoveyda group reported an ACA methodology for five-membered exocyclic enones, achieving excellent results (up to 77% yield, 96% ee).[58] However, this procedure is unsuitable for six-membered ring substrates, and the ligand used must be modified to improve performance for challenging substrates.

In 2007, the Alexakis group successfully reported the ACA of alkylaluminum reagents to a 6-membered ring exocyclic enone, achieving high yields and enantioselectivities (>90% yield, >80% ee) exclusively with trimethylaluminum.[59]

An extensive methodology was recently developed by the Edelstein group in 2021, achieving high enantioselectivities and yields; however, the transformation's success is limited to the addition of aryl groups to protected 2,3-dihydro-*1H*-pyrrole esters.[60]

2.4. Project goals

Building on the success of the Cu/Zr system in achieving enantioselectivity with phosphoramidite ligands, we were curious whether modular modifications to these ligands could also promote high enantio- and diastereoselectivities in exocyclic systems.

This project aims to investigate a Cu-catalysed ACA of exocyclic systems, which could serve as a strategic approach to accessing 1,2-disubstituted cyclic frameworks. Our objective is to broaden the methodology to a generalized scope, encompassing various alkenes, exocyclic enones, ring sizes, and heterocycles. Additionally, we plan to assess the scalability of the reaction and extend the methodology to related systems (Figure 2.10).

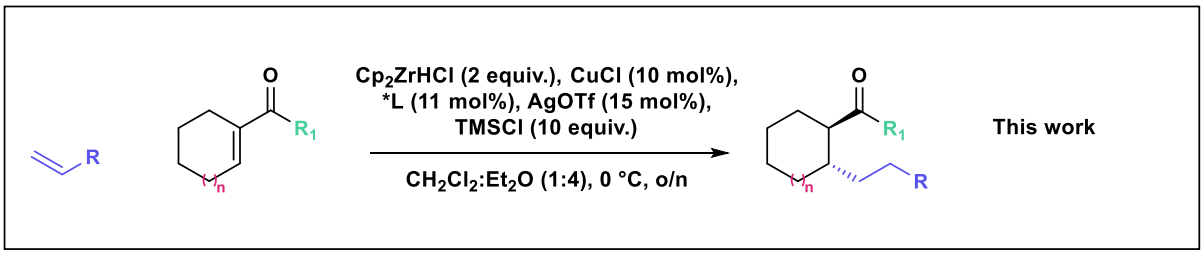

Figure 2.10: Towards a general procedure for synthesis of 1,2- substituted cyclic cores enantioselectively.

2.5. Reaction discovery and Optimisation:

2.5.1 Initial Electrophile Screening

Preliminary work on reaction optimization and initial ligand screening was undertaken by ***Dr. Alexandre Brethome****, a former member of our research group.*[61]

The organozirconocene nucleophile (**1a'**) was generated *in situ* by mixing 4-phenyl-1-butene (**1a**) with the Schwartz reagent (Cp_2ZrHCl) in dichloromethane. This hydrozirconation step forms the organozirconocene intermediate, which acts as the nucleophile in the subsequent conjugate additions.

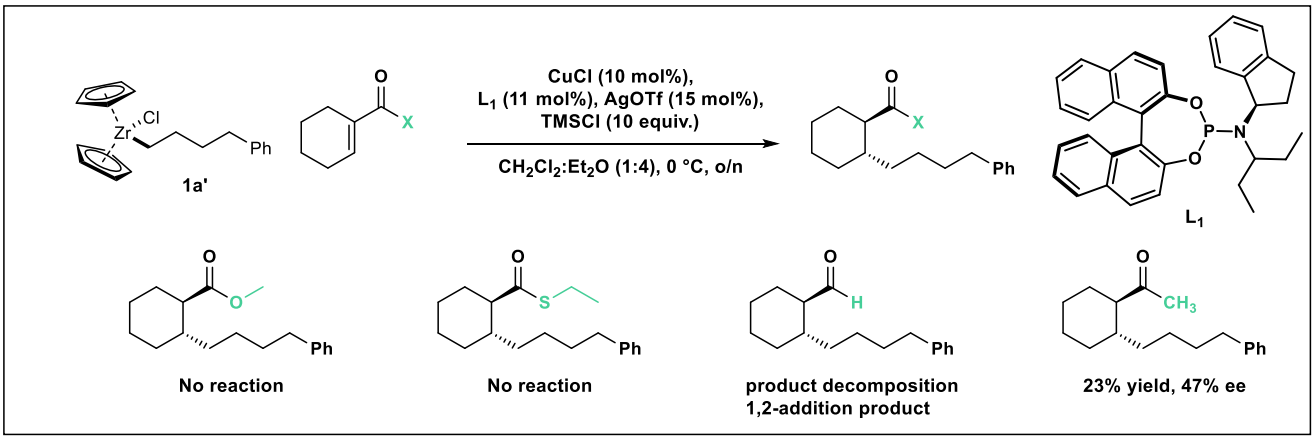

Figure 2.11: Testing the reactivity of different enone types.

The organozirconocene was then reacted with various electrophilic substrates in the presence of copper(I) triflate and a chiral, non-racemic ligand (Figure 2.11). The aim was to promote the addition to elusive exocyclic enones.

We explored the reactivity of several exocyclic substrates, including α,β-unsaturated thioesters, esters, ketones, and aldehydes. Among these, only the ketone and aldehyde substrates exhibited any reactivity. While we could observe conjugate addition product while using the ketone, the use of aldehyde as starting material mostly led to undesired 1,2-addition product and other undetermined side products.

2.5.2 Initial condition optimisation

Initial optimization efforts focused on the reaction between 4-phenyl-1-butene (**1a**) and 1-acetyl-1-cyclohexene (**2a**), an enone selected for its structural simplicity and commercial availability.

Starting reaction conditions yielded a moderate 23% of the desired product, with an enantiomeric excess of –47%. To overcome this, we systematically optimized five reaction parameters: Equivalents of Schwartz reagent, alkene-Schwartz ratio, copper-silver ratio, copper source and TMSCl equivalents (Figure 2.12), aiming to improve both yield and selectivity.

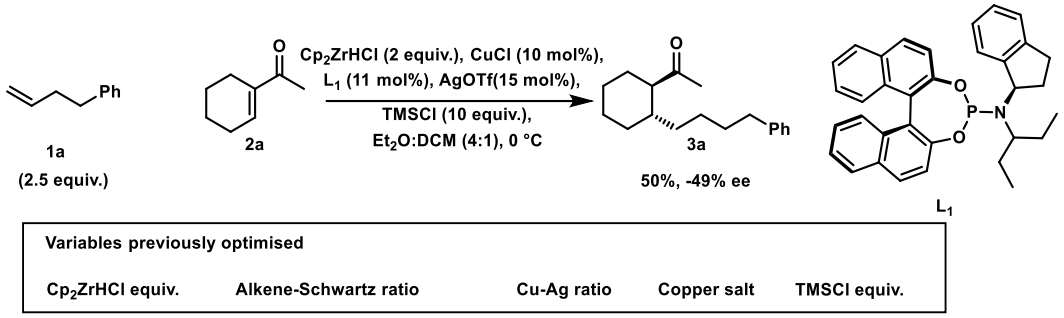

Figure 2.12: Starting conditions of the exocyclic ACA.

Even after extensive optimization, the improvements were only marginal. The best conditions achieved a yield of 50% with an ee of –49%.[61] Further modifications to the solvent system and reaction temperature did not yield significant enhancements in either reactivity or selectivity at this stage.

2.5.3. Initial ligand scope

Following the initial optimization of reaction conditions, efforts were directed towards identifying an effective ligand to enhance yield and enantioselectivity. The preliminary ligand screening, conducted by Dr. Brethome, focused primarily on the amine modification of common phosphoramidite ligands, evaluating a selection from our in-house database. Since synthesizing new ligands was deemed unnecessary if known ligands achieved desirable results, we prioritized established ligands known to exhibit high activity (Figure 2.13).

Ligand **L2**, classified as a 'privileged' ligand in the context of asymmetric catalysis,[62,63] and the commercially available **L3** have both been reported to induce high enantioselectivity (~90% ee) in the copper-catalysed addition of cyclic enones.[51, 64]

However, initial tests using **L2**, **L3**, and **L1**—an iteratively optimized ligand for sterically demanding substrates—resulted in poor outcomes, with **L1** yielding only 50% of the desired product and 49% ee. Most ligands tested in this initial screen (**L1**–**L5**) produced yields and enantioselectivities below 50%, underscoring the need for further ligand screening. **L6**, a structural variant of **L1**, exhibited only slightly improved results with a moderate yield of 44% and an ee of 56%. The first breakthrough came with ligand **L7**, which provided an enhanced yield of 77% while maintaining a moderate ee of 47%.

Structurally, **L7** is a phosphoramidite derivative featuring a dibenzazepine moiety. This ligand has been typically employed in asymmetric catalysis with precious metals such as iridium and rhodium.[65-67] Despite its widespread use in those systems, **L7** has rarely been explored in copper-catalysed asymmetric reactions, with only one prior report demonstrating poor selectivity.[67] However, due to its high reactivity on this system, we were encouraged to perform structural modifications on **L7**.

A series of structural modifications were made to optimize the amine groups in both **L6** (**L8**–**L11**) and **L7** (**L12**–**L20**). These modifications aimed to explore the ligand's steric and electronic properties to see which properties enhanced the performance in the reaction. However, most modifications yielded only slight improvements. The best outcome was observed with **L13**, achieving a modest 60% ee, indicating limited potential for these structural variations. Despite the results, the screening revealed the critical role of the dibenzazepine moiety in **L7**'s enantioselectivity. Removal of the amine double bond (**L17**) caused a drastic drop in reactivity, reducing the yield from 77% to 30%. Similarly, breaking the seven-membered ring structure (**L16**, **L18**–**L20**) resulted in a substantial decline in enantioselectivity (~10% ee). These findings underscored the necessity of preserving the core dibenzazepine structure, as any disruption severely compromised the ligand's ability to induce asymmetry.

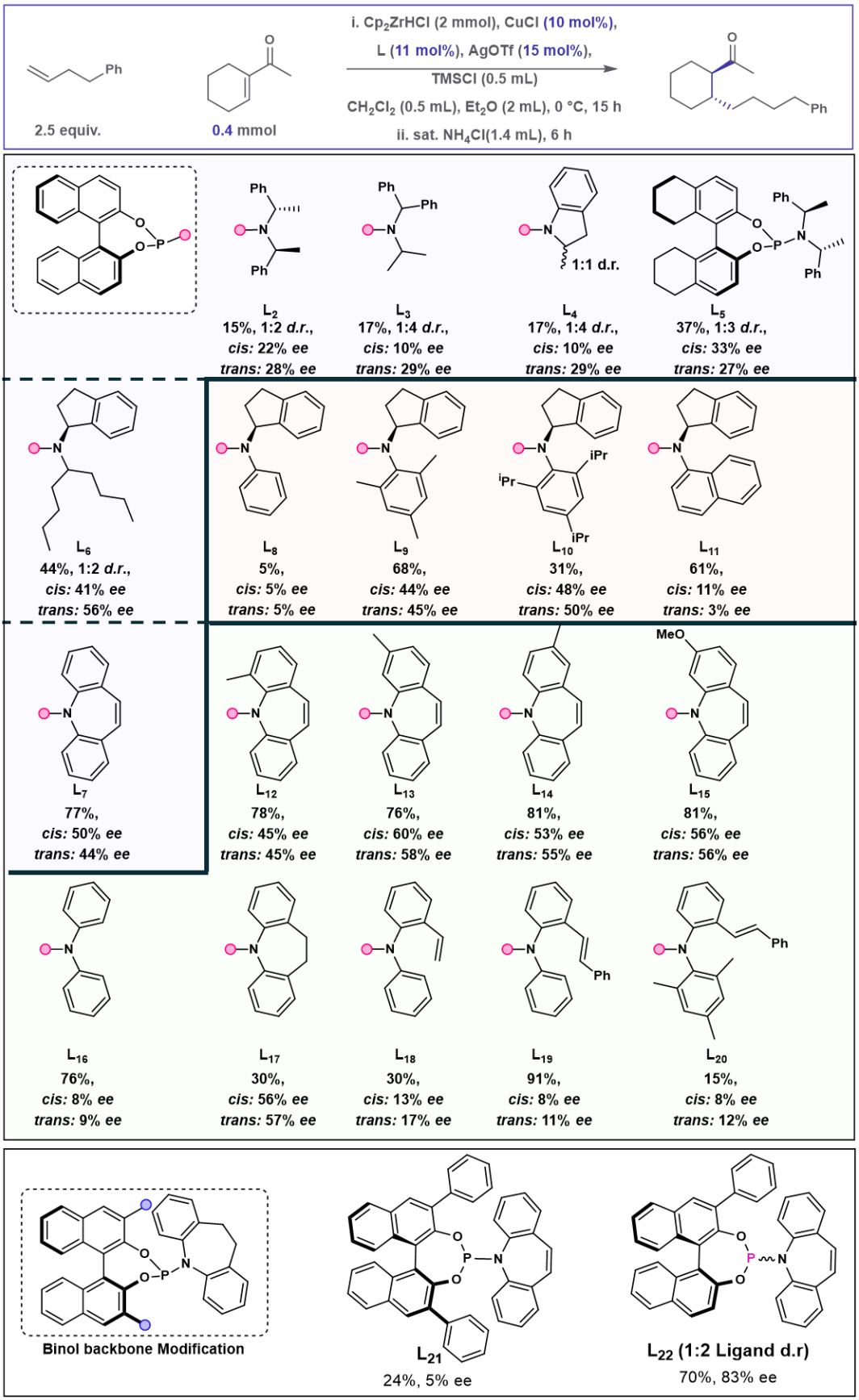

Figure 2.13: Initial ligand scope showing amine and BINOL backbone modifications.

Given the limited success in modifying the amine component, attention shifted towards modifying the BINOL backbone while retaining the dibenzazepine moiety. The initial modification involved incorporating two phenyl groups at the BINOL moiety (**L21**), maintaining the C_2-symmetry of the ligand. However, this alteration led to a nearly complete erosion of catalytic performance (24% yield, 5% ee), highlighting the critical influence of the BINOL backbone's structure on the reaction.

In contrast, breaking the C_2-symmetry through mono-substitution at the BINOL backbone (**L22**) resulted in a significant breakthrough (70%, 83% ee). This phosphoramidite is itself obtained as a mixture of two diastereomers, each with a stable P-stereogenic centre (Figure 2.13). The introduction of asymmetry in the BINOL backbone proved crucial for tuning the ligand's properties.

We hypothesised that the presence of the P-stereogenic centre contributed to the enhanced enantioselectivity. From this point forward, **L22** became our lead ligand, and further efforts focused on understanding the effect of the ligand diastereomeric ratio on the reaction performance.

2.6. Effect of Lligand dr on the reaction.

We hypothesized that **L22**, as a mixture of diastereomers, likely consists of an optimal ligand, highly selective and reactive, and a sub-optimal ligand with lower efficiency. Attempts to separate these diastereomers through standard chromatographic methods proved challenging, yielding column fractions with varying, albeit low diastereomeric ratios. To overcome this, with assistance from Vertex Pharmaceuticals, we employed preparative supercritical fluid chromatography (SFC) to isolate the two diastereomers (**L22R** and **L22S**) in high diastereomeric purity (>20:1 dr).

The stereochemistry and spatial arrangement of ligand **L22S** were confirmed through single-crystal X-ray crystallography (Figure 2.14). This analysis provided insight into the distinct configurations arising from the P-stereogenic centre. In **L22S** (*S*,S_P), the phosphorus lone pair orients away from the phenyl group, creating a chiral pocket that is conducive to copper coordination. Notably, the benzodiazepine double bond aligns approximately with the stereogenic phosphorus atom, suggesting its potential

involvement in stabilizing the ligand-copper interaction. In contrast, the less active diastereomer, **L22R** (*S,RP*), is hypothesized to adopt a conformation where the benzodiazepine double bond points toward the phenyl group, restricting the spatial accommodation of copper. These structural distinctions between diastereomers likely influence ligand binding energies and reactivity, emphasizing the importance of the chiral environment around the metal centre. The structural insights provided by Figure 2.14 thus highlight a clear correlation between stereochemistry, spatial arrangement, and the ligand's catalytic activity.

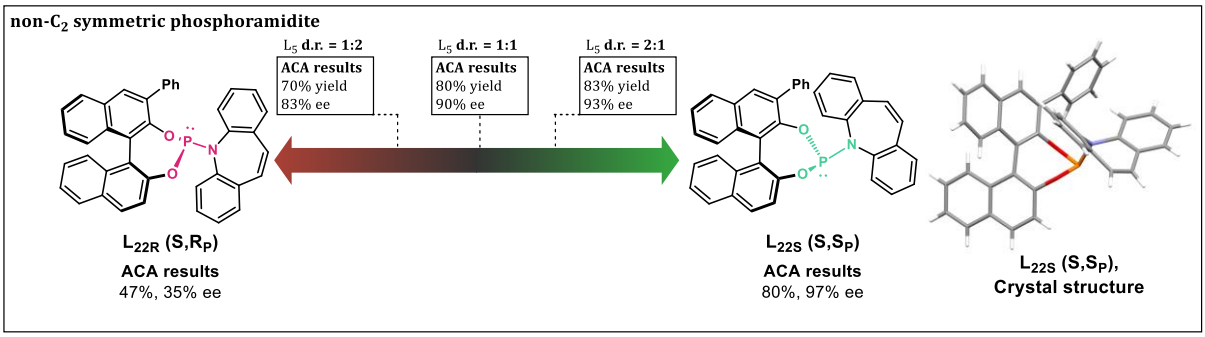

Figure 2.14: Showcasing the diverse selectivity between both **L22** diastereomers on the ACA of exocyclic substrates. On the right, crystal structure of **L22S**.

Upon testing, the *S,RP* diastereomer (**L22R**) showed poor performance with a 40% yield and 35% ee, while the *S,SP* diastereomer (**L22S**) exhibited excellent reactivity, achieving 82% yield and 97% ee. These stark differences suggested that the overall reaction outcome is strongly influenced by the ratio of the two diastereomers present in the mixture. We developed a simple kinetic model (Figure 2.15) to explore this relationship, assuming each copper atom binds to a single ligand without non-linear (cooperative) binding effects.

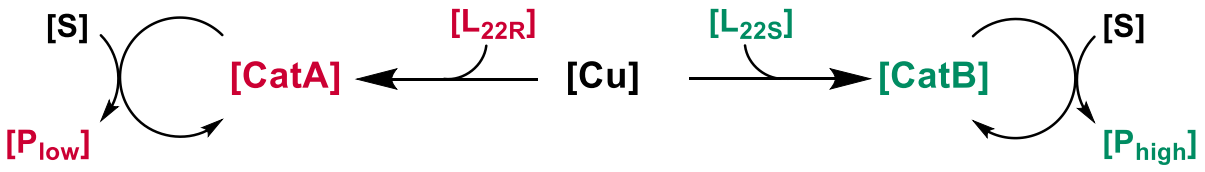

Figure 2.15: Simple kinetic system for a catalytic reaction with ligand competition. Showing concentrations of: Substrate (S), free copper(I) (Cu), low selectivity ligand (**L22R**), high selectivity ligand (**L22S**), metal complexed to L_{22S} (CatA), metal complexed to L_{22R} (CatB), low ee product (P_{low}), and high ee product (P_{high}).

According to the model, the diastereomeric ratio (dr) of **L22** directly impacts the enantioselectivity of the product. When both ligands are present simultaneously, they compete, each forming distinct copper-ligand complexes that operate with different rates and selectivities. By systematically varying the dr of **L22** and mapping the resulting enantioselectivity (ee) of the product, we observed a positive non-linear effect: the ee of the product consistently exceeded what would be expected from a simple linear relationship between the dr of **L22** and product ee. (Graph 2.1) This phenomenon indicates that the more selective diastereomer (**L22S**) not only directs higher enantioselectivity but also has a faster reaction rate.

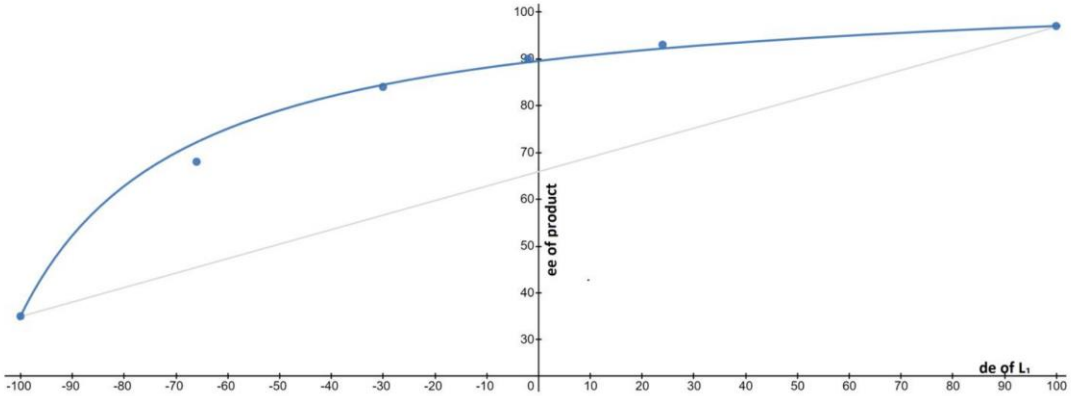

Graph 2.1: The effect of the de (**L22**) on the product ee where negative diastereomeric excess (de) represents higher proportions of **L22R**, the poorly selective ligand. Data were obtained experimentally from ^{31}P NMR of the ligand post purification (ligand de) and from the ACA reaction using different **L22** (*SP:RP*) ligand ratios (product ee). In grey, expected linear relationship between de (**L22**) and product ee.

Given the pronounced effect of the ligand's diastereomeric ratio on the product's enantiomeric excess—ranging from 35% to 97%—it became essential to obtain virtually pure **L22S**. Here, we detail the crystallization approach used to isolate the more selective diastereomer. Attempts at a diastereoselective synthesis of **L22S** are discussed separately in Chapter 4.

2.7. Diastereomeric crystallization of $\mathbf{L_{22}}$

The desired ligand, $\mathbf{L_{22}}$, is synthesised via the phosphoramidation of phenyl BINOL and *5H*-dibenz[b,f]azepine. This reaction unavoidably produces a 1:1 mixture of diastereomers, $\mathbf{L_{22S}}$ and $\mathbf{L_{22R}}$ (Figure 2.16). Extensive optimization efforts—including variations in temperature (from 40 °C to –20 °C), concentration (0.1 to 1 M), and solvent choice (DCM, THF, Et_2O, $CHCl_3$)—failed to improve the diastereomeric ratio.

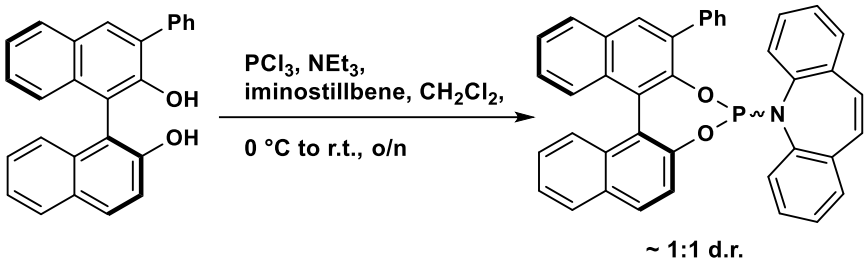

Figure 2.16: Phosphoramidation reaction yielding a diastereomeric mixture.

Although preparative supercritical fluid chromatography can efficiently separate these molecules, it is not accessible in most laboratories. We sought to develop an accessible methodology to obtain these valuable P-chiral ligand diastereoselectively.

Working with these ligands in solution is notoriously challenging due to their high sensitivity to oxygen, acids, silica, and light. Column chromatography is unsuitable for purifying phosphoramidites— not only must the process be rapid to prevent ligand oxidation, but $\mathbf{L_{22S}}$ also oxidizes faster than $\mathbf{L_{22R}}$ on the column, decreasing the diastereomeric ratio over time. Attempts to separate the ligands using preparative thin-layer chromatography (prep-TLC) were also unsuccessful.

We initiated a solvent system exploration by conducting a trituration study of $\mathbf{L_{22}}$ in various solvents. After stirring the ligand with each solvent for 30 minutes, the solution was analysed by ^{31}P NMR spectroscopy to determine the diastereomeric ratio of the dissolved ligand. Solvent systems that fully dissolved the ligand were deemed unsuitable, while those yielding blank, or significantly weak ^{31}P NMR signals were discarded. Among all solvents tested, acetonitrile showed the most pronounced effect, enriching the diastereomeric ratio to 10:1 in favour of $\mathbf{L_{22S}}$. Interestingly, this result was inconsistent; when a purified sample of $\mathbf{L_{22}}$ was treated similarly, acetonitrile did not produce the same level of enrichment, resulting in mediocre outcomes (~1.5:1). The diastereoselective

trituration appears effective only on the crude reaction mixture, which contains high levels of *5H*-dibenz[b,f]azepine and triethylamine hydrochloride in addition to the diastereomers.

Following the phosphoramidation reaction, the crude mixture was concentrated, triturated with acetonitrile, stirred for 30 minutes, and then filtered. The filtrate predominantly contained triethylamine hydrochloride and **L22R**, with notably low levels of *5H*-dibenz[b,f]azepine and **L22S**. The filtered liquid contained *5H*-dibenz[b,f]azepine and exhibited an increased diastereomeric ratio favouring **L22S** (3:1) (Figure 2.17).

It is important to note that although these results are promising, they are not consistently reproducible; the increase in diastereomeric ratio can vary, sometimes being as low as 1.5:1. The enriched filtrate was concentrated and passed through a short silica gel plug. Finally, a slow-diffusion crystallization was performed on the enriched mixture to selectively crystallize the desired ligand (Figure 2.17). This overall process may require sequential crystallizations and can be time-consuming and low yielding. However, when scaled up, it can yield considerable amounts (up to 1.2 grams after sequential crystallisations) of **L22S** with excellent selectivity (dr > 20:1).

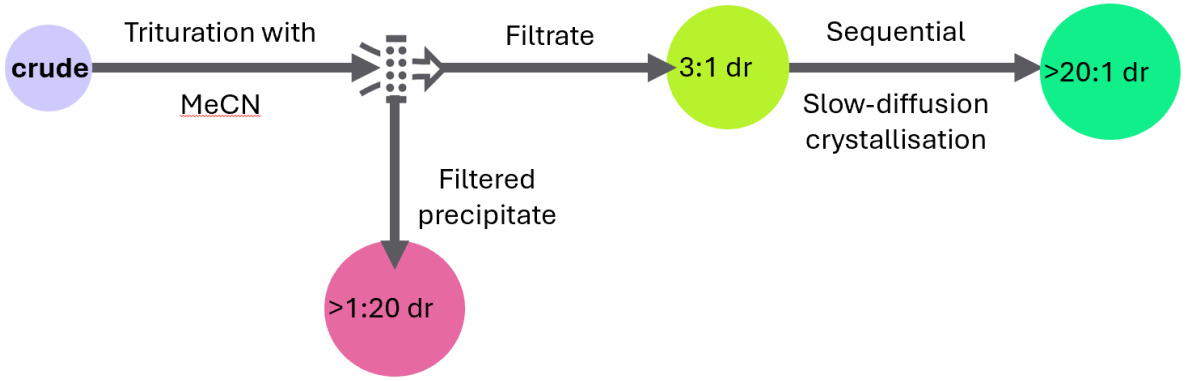

Figure 2.17: Flow-chart following on the standard diastereoselective enrichment process for **L22S**.

2.8. Engineering the ACA diastereomeric ratio

The addition of alkylzirconocenes to exocyclic enones presents a valuable strategy for constructing two adjacent stereocentres in a single synthetic step.[68] However, achieving precise stereocontrol at the α-position relative to the carbonyl group has been challenging. This difficulty stems from the deprotection of the trimethylsilyl enol intermediate, which often leads to poor and inconsistent diastereomeric ratios—typically around 1:2 favouring the *cis*–isomer. The instability of the enol intermediate leads to the formation of similar proportions of *cis*– and *trans*–isomers, complicating diastereoselectivity. Achieving high diastereomeric ratios is crucial for establishing this approach as a reliable stereodivergent strategy.

To address this issue, we explored some post-reaction epimerization strategies using a product initially isolated with a diastereomeric ratio (dr) of 1:1.4 favouring the *cis*–isomer (Figure 2.18). Acidic conditions proved ineffective in altering the diastereomeric ratio. In contrast, base-mediated epimerization in a protic solvent at 50 °C using an excess of several bases improved selectivity, achieving a dr of 1:15 favouring the *trans*–isomer while preserving enantiomeric purity. Despite this improvement, the requirement for an additional epimerization step reduced the practicality of the approach.

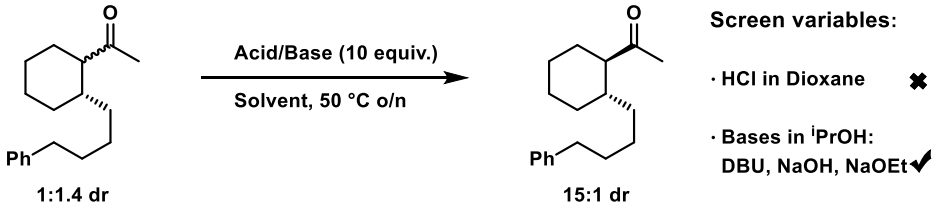

Figure 2.18: Acid and base methodologies to attempt epimerization.

Further investigations suggested that the unpredictability in diastereoselectivity could be influenced by variations in the quenching procedure (Figure 2.19). Introducing a saturated solution of ammonium chloride to the crude reaction mixture and extending the stirring time to six hours dramatically shifted the diastereomeric ratio to 1:18, favouring the *trans*–isomer. (Quenching Method A) This outcome is attributed to the in-situ generation of hydrochloric acid (HCl) from the reaction between NH_4Cl and excess trimethylsilyl chloride (TMSCl), which catalyses the equilibration toward the thermodynamically preferred *trans*–product. Conversely, when the reaction mixture was quenched without NH_4Cl and stirred briefly at room temperature (Quenching Method B),

the *cis*–isomer was favoured with a dr of 4:1, indicating that the stereochemical outcome can be directly manipulated by adjusting the quenching conditions. (Figure 2.19).

Further insights into the elucidation of the quenching mechanism for this stereodivergent procedure are provided later in this chapter (Section 2.10: Conformational Analysis of 1,2-Substituted Quenching Methods).

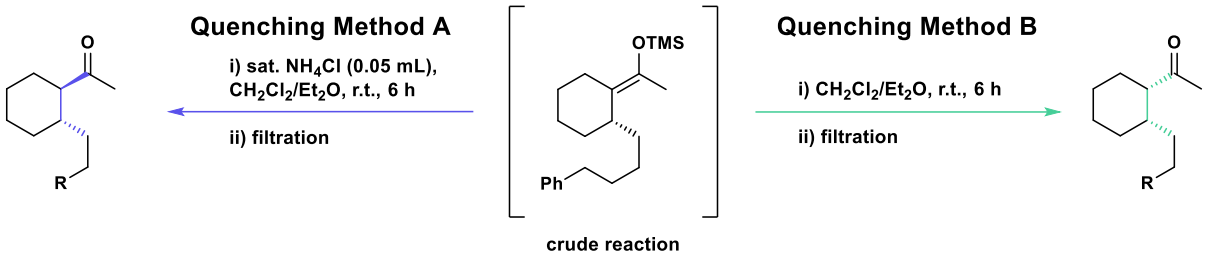

Figure 2.19: Quenching protocol reflects on product diastereomeric ratioof the ACA reaction.

2.9. Scope of the reaction

2.9.1 Nucleophile scope

We have developed two distinct quenching protocols that enable precise control over the stereochemistry of asymmetric catalytic addition (ACA) products derived from the reaction of electrophile **3a** with various nucleophiles (Figure 2.20). By simply modifying the work-up procedure, we can selectively obtain either the *trans* (**4a**–**f** and **4k**) or the *cis* (**4g**–**j** and **4l**) isomers. Quenching the reaction mixture with ammonium chloride (NH_4Cl) consistently favoured the formation of the *trans*–isomer, achieving diastereomeric ratios of up to 18:1. In contrast, filtration of the crude reaction mixture through a silica gel plug followed by concentration favoured the *cis*–isomer. While the diastereoselectivity varied with each individual substrate, the ability to selectively isolate either stereoisomer by altering the quenching conditions showcases the versatility and practical utility of this methodology, especially when combined with the high enantioselectivity observed in these reactions.

We tested a wide range of alkenyl nucleophiles with electrophile **3a** and consistently achieved high enantioselectivities ranging from 94% to 98% ee, along with moderate to

high yields of 47% to 90%. Notably, the results were consistent even with nucleophiles containing halides (**4d**, **4e**, and **4j**) and protected alcohols (**4c** and **4i**). The tolerance of such functional groups is particularly valuable, as they provide versatile handles for further chemical elaboration.

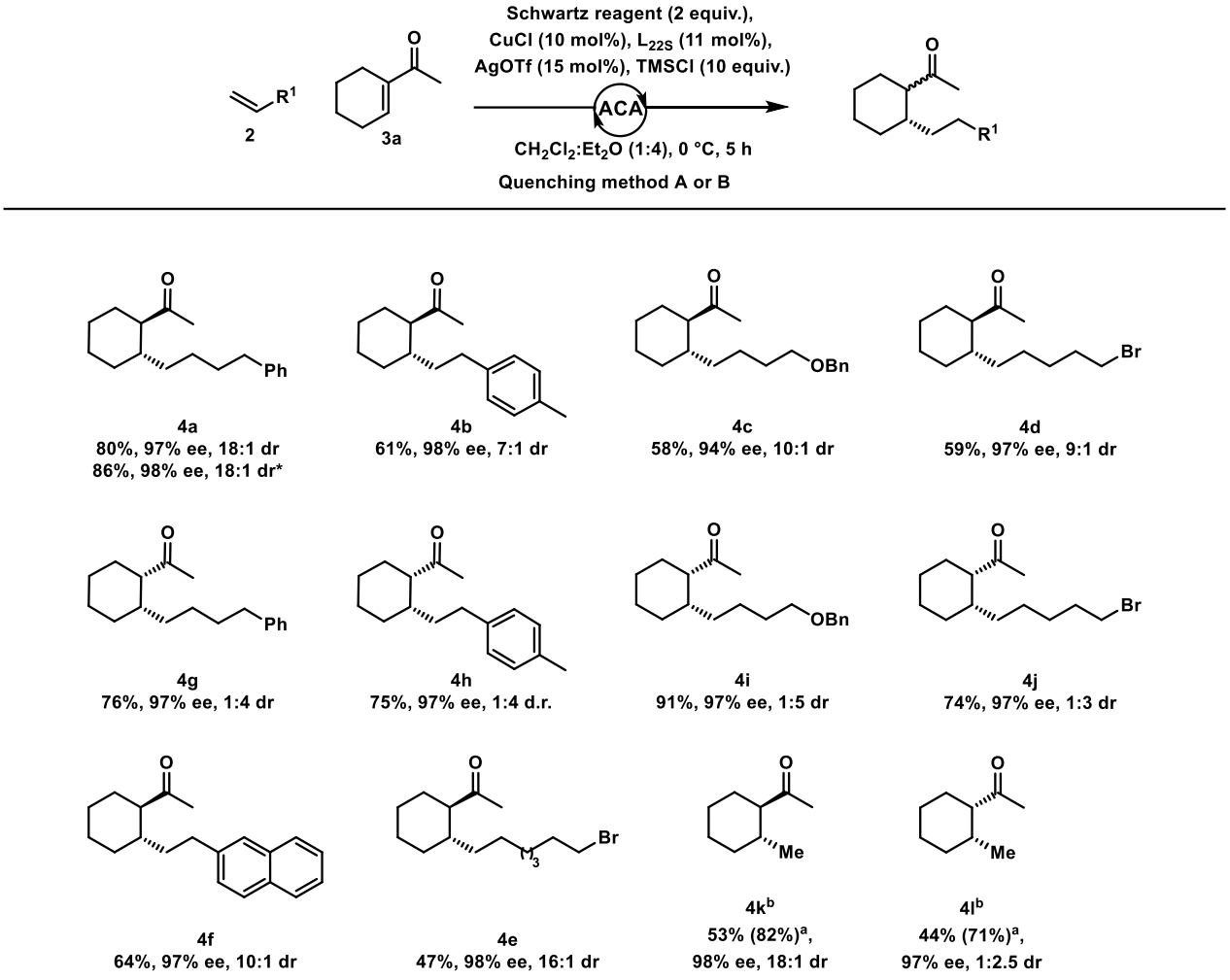

Figure 2.20: Reaction nucleophile substrate scope. Enone **3a** (0.4 mmol, 1 equiv.), alkene (2.5 equiv.), Cp_2ZrHCl (2 equiv.), CuCl (10 mol%), **L22s** (11 mol%), AgOTf (15 mol%), TMSCl (10 equiv.). [a]yield determined by NMR spectroscopy. [b]$Cp_2ZrMeCl$ (2 equiv.) was utilized instead of alkane/Cp_2ZrHCl. Enantioselectivity of these examples measured via GC. *Gram scale reaction: **3a** (5.66 mmol, 1 equiv.), **2a** (2.5 equiv.), Cp_2ZrHCl (2 equiv.), CuCl (5 mol%), **L22s** (5.5 mol%), AgOTf (7.5 mol%), TMSCl (5 equiv.). **Gram scale reaction 1% Catalyst loading: **3a** (5.66 mmol, 1 equiv.), **2a** (2.5 equiv.), Cp_2ZrHCl (2 equiv.), CuCl (1 mol%), **L22s** (1.1 mol%), AgOTf (1.5 mol%), TMSCl (5 equiv.). All reported examples show isolated yield, enantioselectivity measured via Chiral SFC and diastereomeric ratio measured via Chiral SFC.

Traditional Schwartz reagents, such as Cp_2ZrHCl, typically require alkenes to generate nucleophilic intermediates, with the simplest example being ethylene, which results in

ethyl group insertion. This limitation makes the selective insertion of a methyl group unattainable with standard Schwartz reagents, limiting its use in natural product and drug synthesis, where precise methylation is often crucial.[69] By substituting Cp_2ZrHCl with $Cp_2ZrMeCl$, we successfully achieved direct and asymmetric insertion of a methyl group, (**4k** and **4l**).

To examine the synthetic utility and scalability of the reaction, we performed an experiment on a gram scale and decreased the catalyst loading to 5 mol%. The reaction yielded 1.25 grams of product **3a** in 85% yield and 98% ee, indicating that the reaction can be run on a preparative scale without significant loss of efficiency or enantioselectivity. We further attempted to reduce the catalyst loading to 1% CuCl, but in this case, the yield suffered a significant decrease (~60% yield), although the enantioselectivity remained high (97% ee). Further insight into the reaction mechanism could help us further decrease the catalyst loading without sacrificing yield.

2.9.2 Enone scope:

We further extended our investigation of ACA reactions to encompass various cyclic alkenes activated by exocyclic ketones, exploring substrates with different ring sizes—ranging from five- to eight-membered rings—and ketone substituents such as methyl (Me), phenyl (Ph), *n*-butyl (*n*-Bu), and benzyl (CH_2Ph) (Figure 2.21).

The addition to a five-membered ring substrate proceeded smoothly, yielding the *trans*–product **4m** with a diastereomeric ratio (dr) of approximately 26:1 in favour of the *trans*–isomer, a 69% yield, and an excellent enantioselectivity of 97% ee. Accessing these systems is notoriously challenging for both ACA and Asymmetric Hydrogenations. Our methodology thus offers a unique advantage in synthesizing the *trans*–isomer of cyclopentanes.

In contrast, attempts to synthesise the *cis*–isomer (**4s**) from the same five-membered ring substrate resulted in a 1:1 mixture of **4s** and **4m**, although similar enantioselectivities (97% ee) and reactivity (65% yield) were observed. These results reflect the inherent differences in the relative energies of the stereoisomers in five-membered rings compared to six-membered rings. The decreased diastereoselectivity when targeting the *cis*–isomer suggests that the steric hindrance and conformational preferences in smaller

rings significantly impact the stereochemical outcome, making selective synthesis more challenging.

We also examined the formation of seven- (**4t**) and eight-membered ring (**4u**) products, which proceeded with high yields (~74%) and very high enantioselectivities (>95% ee). These results illustrate a clear dependence of the diastereomeric ratio on ring size. Using our procedures, five- and six-membered rings favour the formation of the *trans*–product with better selectivity, while seven- and eight-membered rings preferentially yield the *cis*–isomers. Indeed, we were unable to produce seven- and eight–membered ring products with diastereomeric ratios favouring the *trans*–isomer.

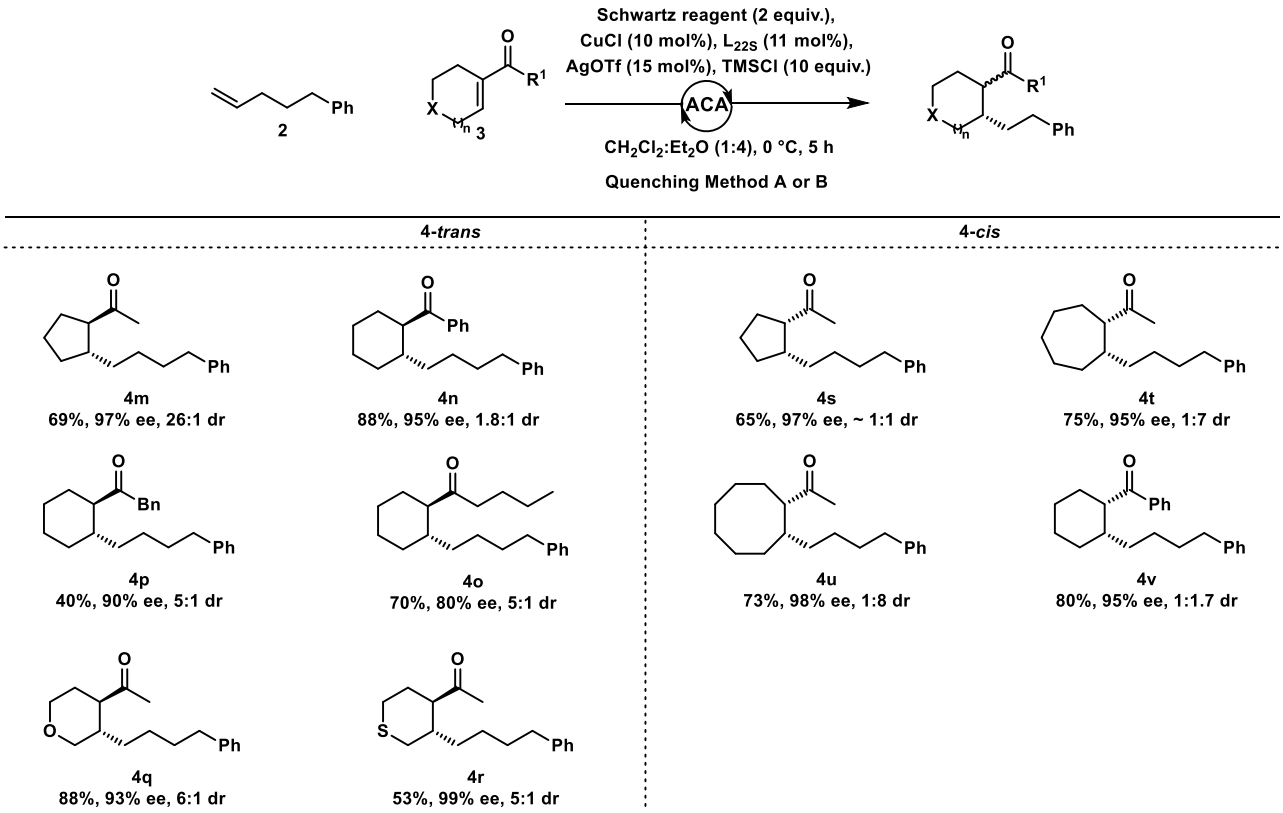

Figure 2.21: Reaction electrophile substrate scope. Enone (0.4 mmol, 1 equiv.), alkene **2a** (2.5 equiv.), Cp_2ZrHCl (2 equiv.), CuCl (10 mol%), **L22S** (11 mol%), AgOTf (15 mol%), TMSCl (10 equiv). All reported examples show isolated yield, enantioselectivity measured via Chiral SFC and diastereomeric ratio measured via Chiral SFC.

Modification of the non-cyclic ketone's substituent was also explored. A phenyl substituent (leading to products **4n** and **4v**) gave high yields (88%) and enantioselectivity (95% ee), but the diastereomeric ratios were reduced when synthesizing either the *trans*–isomer **4n** (1.8:1 dr) or the *cis*–isomer **4v** (1:1.7 dr). A

benzyl substituent (**4p**) resulted in good stereoselectivity (5:1 dr, 95% ee) but with a lower yield number. An *n*-butyl ketone (substrate **3o**) afforded a product with 80% ee. These results indicate that different ketone substituents are compatible with the reaction to some extent. While they may not provide optimal diastereoselectivity or yield in every case, the enantioselectivity is often conserved.

The use of heterocyclic enones was also briefly investigated. The oxygen-containing heterocycle (product **4q**) and the sulfur-containing heterocycle (**4r**) were each formed with good yields and high enantioselectivity (up to 99% ee). The ability to perform this chemistry on heterocyclic systems presents a significant advantage, as such motifs—particularly oxygen-containing rings—are prevalent in natural products like sugars. This may open the possibility of emulating and creating sugar-inspired molecules in future studies, enhancing the synthetic utility of our approach. An analogous tosylate-protected nitrogen-containing enone was tested but no reactivity was observed. Exploring alternative protecting groups could mitigate this issue, potentially expanding the scope of the reaction to include nitrogen-containing heterocycles, which are common in biologically active compounds.

While limitations exist, our work provides a versatile and efficient approach for constructing complex molecular architectures with precise stereochemical control.

2.10. Conformational effects on diastereoselectivity: Quenching methods

Analysing 6-membered rings

The ability to choose one diastereoisomer or another by simply utilizing a different quenching procedure gives great versatility to this procedure.

These results can be rationalized by examining the conformational preferences of the diastereomers involved. During the reaction, the enol intermediate initially forms with a β-stereocentre determined by the configuration of the chiral ligand. We believe that in this initial state, the R group would populate an axial position in the ring. The basis of this claim is the amount of steric interactions that an equatorially placed R group would have with the enol group (Figure 2.22). The formation of the α-stereocentre is governed by the direction of protonation, which is sensitive to the steric and electronic environment. In

the 6-membered ring exocyclic enone system, steric hindrance restricts the conformational flexibility of the intermediate, resulting in distinct energy minima.

This hypothesis is based not on computational studies but on A-values for structurally similar molecules. These values portrayed are derived from experimental data such as calorimetric data (ΔH_f, ΔH_c) and A-values.[12,70,71] A-values for an alkyl (Et) and an acetyl group were used to calculate energies for all chair conformations.

The stereochemical outcome is further dictated by the energy differences between the possible transition states during protonation. Under kinetic control (Quenching Method B), the rigid enone ring directs the substituent into an axial position, favouring the formation of the *cis*–isomer due to a lower activation energy (ΔG_k). Interestingly, there might be a second effect that might promote the formation of the *cis*–isomer over the *trans*. Because the R group is fixed in the axial position, protonation would lead to either the axial-axial (*trans*) or axial-equatorial (*cis*) conformations. When comparing these two meta-stable minima, the *cis*–product is of lower energy.

This difference in energy (ΔG_M) can favour formation of the *cis*–product, provided the system does not have enough energy to get to the lower energy conformations. The energy required to get to these conformations for 6 membered rings is about 43 kJ.mol^{-1} (for cyclohexane).

In contrast, thermodynamic conditions in Quenching Method A induces epimerization, placing the reaction under thermodynamic control. This change possibly gives the system enough energy to overcome chair conformational changes, arriving at the eq-eq and eq-ax lower energy conformations. This shift favours the *trans*–isomer, (ΔG_T) which adopts a lower-energy conformation with substituents in equatorial positions, thereby minimizing destabilizing 1,3-diaxial and gauche interactions.[9]

The discrepancy in diastereomeric ratios between the two protocols can be explained by considering the energy barriers associated with each transition state and product. When quenching conditions promote thermodynamic control (Method A), the energy difference between the conformations ($\Delta G_T \sim 5$ kJ.mol^{-1}) provides a driving force favouring the *trans*–product. Even though this is an apparently small energy difference, it would constitute to a dr of almost 10:1 assuming a simple Boltzmann distribution of two interconverting species.

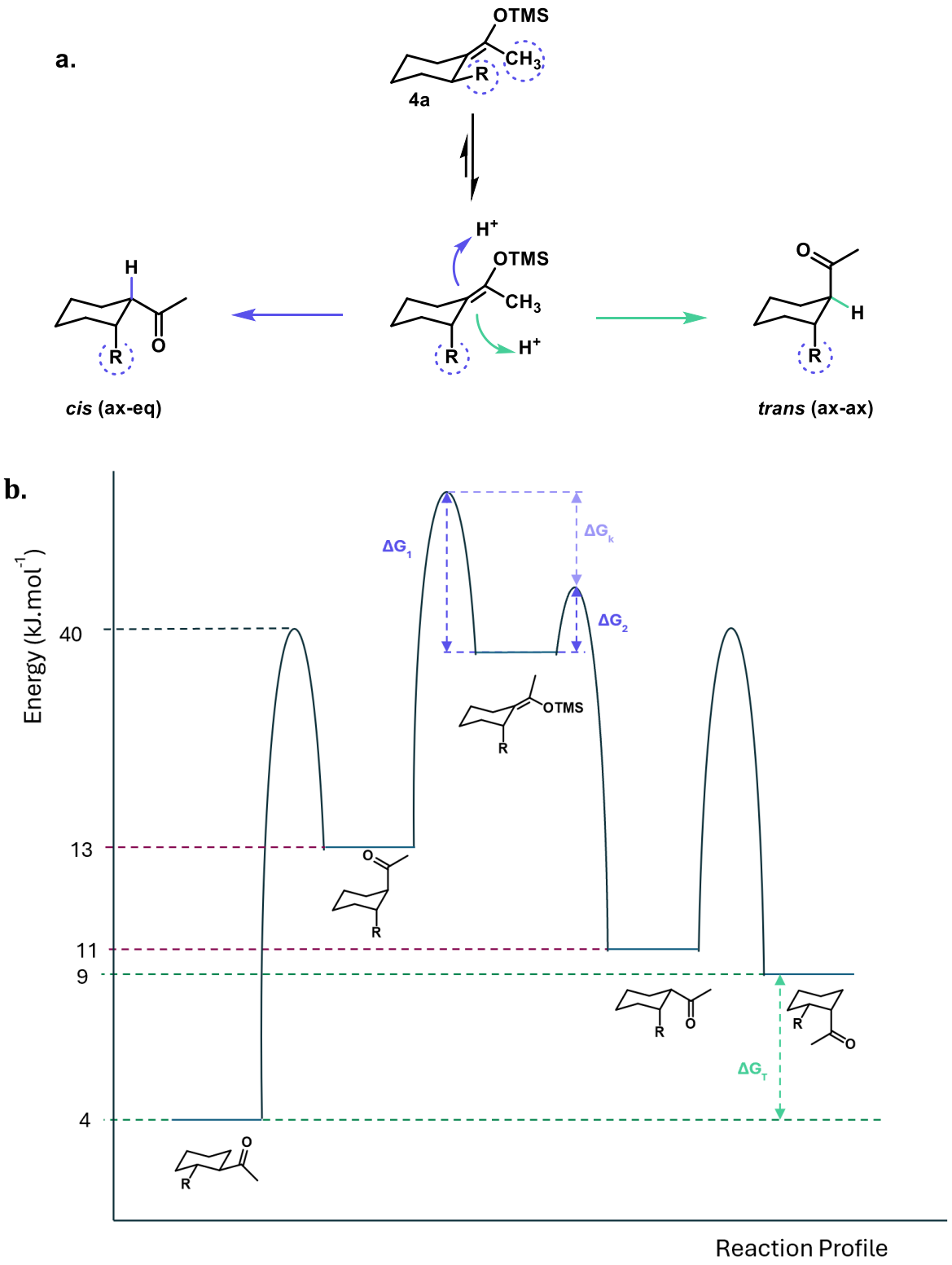

Figure 2.22: Conformational analysis of **4a'**. **a.** Differential protonation lead to unique conformations. **b.** Reaction profile for **4a'**. Energies estimated by utilising A-values of COMe and ethyl groups, values remaining comparatively to 1,2-dimethyl cyclohexane estimates. Transition energy level estimated on chair flip energy for cyclohexane (43 kJ.mol[1]). ΔG_1 = Transition energy required to go from **4a'** to **4a** (*trans*). ΔG_2 = Transition energy required to go from **4a'** to **4a** (*cis*). ΔG_T = Thermodynamic Free energy, ΔG_M = Meta-stable Free energy, ΔG_K = Kinetic Free energy.

Conversely, under kinetic control (Method B), the smaller energy barrier difference (ΔG_k) results in a weaker preference for the *cis*–isomer and lower diastereomeric ratios. Taking into consideration the possibility of 'meta-stable' states (ax-ax vs ax-eq) also appears to follow the observed results as the difference in energy is smaller in comparison ($\Delta G_T > \Delta G_M$).

Analysing 5-membered rings:

The conformational behaviour of 5-membered rings deviates significantly from that of 6-membered rings due to the smaller ring size and increased strain. These systems typically adopt two primary conformations: the "envelope" and the "half-chair".[72] The envelope conformation is slightly more stable, but both exist at relatively similar energy levels. This close energy proximity, coupled with the non-planar nature of 5-membered rings, results in substituents lacking fixed axial or equatorial positions. Instead, the ring undergoes a process called pseudorotation, where each carbon can sequentially move out of the plane, altering substituent orientations. This dynamic flexibility increases the steric interactions between adjacent substituents, particularly at the 1,2-positions, as the ring's rigidity prevents these interactions from being fully alleviated through conformational adjustments.

As a result, the difference in energy barriers for 1,2-substituent interactions (ΔG_k) is often lower than in 6-membered rings, while the inherent difference in thermodynamic energies (ΔG_T) is increased to the previous example ($\sim$7 kJ·mol^{-1}).[70] This unique conformational profile eliminates the distinct axial/equatorial preference seen in 6-membered rings, rendering the traditional model of *cis*/*trans*–selectivity based on these positions invalid. This effect thus invalidates the possibility of higher energy meta-stable states seen on 6 membered rings; an effect that hinted to *cis*–diastereomeric preference. Consequently, the energy diagram (Figure 2.23) is simplified, with the thermodynamic product distribution heavily favouring the *trans*–isomer, while kinetic control leads to a weak preference for the *cis*–isomer.

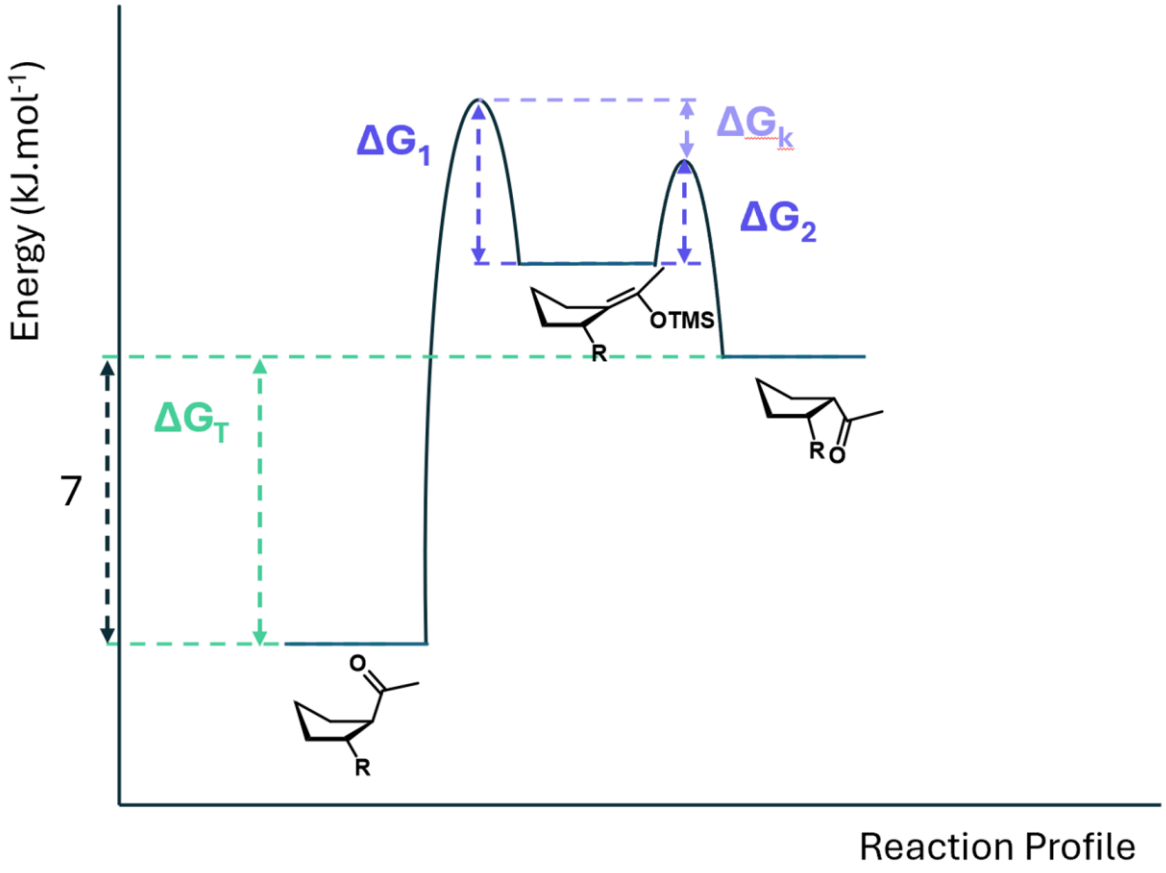

Figure 2.23: Reaction profile for a 5-membered ring system. Energies estimated using values of 1,2-dimethyl cyclopentane. ΔG_T = Thermodynamic Free energy, ΔG_K = Kinetic Free energy.

Analysing 7- and 8-membered rings:

In contrast, 7- and 8-membered rings exhibit much greater flexibility due to their increased ring size, leading to a multitude of possible conformations (e.g., crown, boat-chair, tub, boat-boat, and various twisted forms).[73] This increased conformational freedom reduces the steric strain between substituents at the 1,2-positions, resulting in a smaller energy difference between *cis*– and *trans*–isomers compared to 5- and 6-membered rings. For example, in 1,2-dimethyl cycloheptane, the reported *cis*/*trans* energy difference is only ~3 kJ·mol^{-1} (±1 kJ·mol^{-1}), considerably lower than the values observed in its smaller ring equivalents (~7.6 kJ·mol^{-1} for 6-membered and ~7.2 kJ·mol^{-1} for 5-membered systems).

However, this increased flexibility complicates the mapping of conformational energy diagrams and makes predicting reactivity and selectivity challenging. For 8-membered

rings, data is even scarcer, and conclusions are often circumstantial due to the lack of a comprehensive energy profile. Although experimental evidence suggests a preference for the *cis*–isomer under both kinetic and thermodynamic conditions, this observation cannot draw strong conclusions. The low energy differences and complex conformational landscape of these larger rings require further investigation to develop a robust understanding of their stereoselectivity.

2.11. Testing further enones:

As previously described, α,β-unstaturated ketones are suitable for the exocyclic ACA (unlike, esters, thioesters, and aldehydes). We decided to explore two diverse classes of enones. Firstly, we were keen on testing the reactivity on 'pseudo' exocyclic enones, such as 3-methyl-3-penten-2-one. This compound has an α-substituent next to the ketone and is structurally similar to the exocyclic system (Figure 2.24), and to the best of our knowledge, these pseudo exocyclic substrates are greatly underreported as ACA substrates. These molecules would, similarly to exocyclic substrates, yield two contiguous stereocentres in one single step and, similarly we could tune the quenching method to yield one or the other diastereomer.

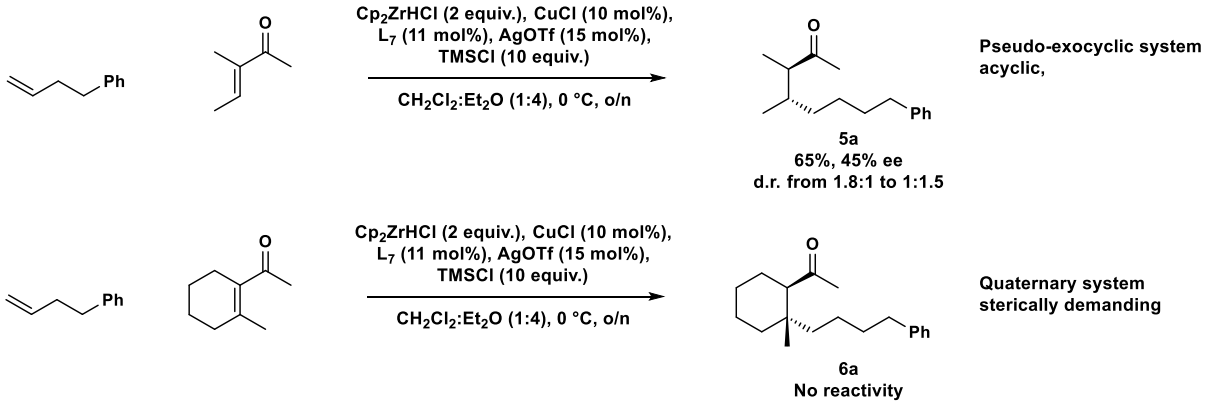

Figure 2.24: Potential complicated enone substrates.

The second type of related substrate we would want to test is to make products containing stereo-defined all-carbon quaternary centres out of a tetrasubstituted exocyclic enone (2-methyl-1-acetyl-1-cyclohexene). Molecules with quaternary stereogenic centres are often coveted in asymmetric chemistry, not only for the significant challenges they present in synthesis but also for their potential synthetic utility. Nature and the pharmaceutical industry are filled with a myriad of examples of chiral quaternary carbons which are notoriously challenging to make.

Initially we attempted to make the product **6a** by using the standard ACA conditions that had worked well for the exocyclic scope. This resulted in no observable yield. Tougher conditions were then attempted: higher nucleophile equivalents, different Alkene-schwartz ratios, a range of temperatures and different counter anions were tested. Unfortunately, no improvement was made (Figure 2.25).

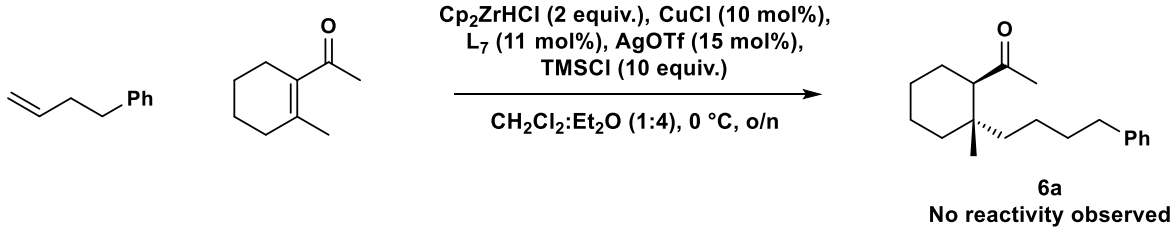

Variables tested

Cp_2ZrHCl equiv.	Alkene-schwartz ratio	Concentration	Silver salt	Temperature
2.0	1.25:1	0.133 M	AgOTf	room temp.
10.0	1.25:1	0.11 M	AgOTf	room temp.
2.0	3:1	0.133 M	AgOTf	room temp.
2.0	1.25:1	0.133 M	$AgNTf_2$	room temp.
2.0	1.25:1	0.133 M	AgOTf	40 °C

Figure 2.25: Attempted optimisation of conditions for quaternary product exocyclic ACA.

We then shifted our efforts towards the pseudo exocyclic substrate. Utilizing the standard ACA conditions used for the exocyclic product, we were able to obtain very positive results (Figure 2.26). The initial results showed up to 90% yield and 93% ee when using **L**$_{22S}$. Unfortunately, the displayed diastereoselectivity was very low for either, *cis*– and *trans*–products (1.8:1 and 1:1.5 respectively). A detailed investigation by Oliver Williams[74] (previous group member) goes in depth on the ACA of these pseudo-exocyclic systems. He attempted to test several different copper sources, solvent systems and some ligands.[74] A more extensive ligand screen is further described on Chapter 3.

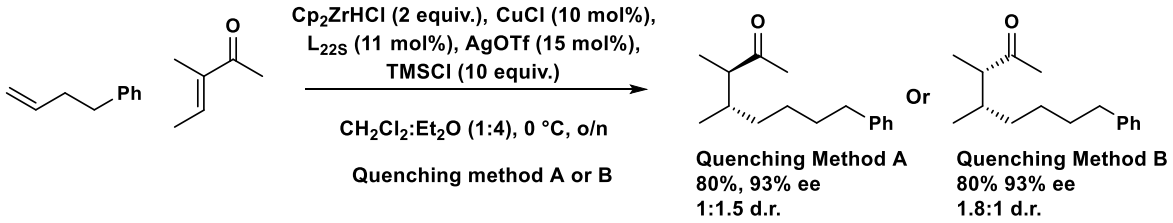

Figure 2.26: ACA of pseudo exocyclic enones using **L**$_{22S}$ and previously optimised conditions.

We believe that the reason for the observed low dr is based on the lack of rigidity on the carbon core (Figure 2.27). Unlike typical exocyclic substrates, which have fewer degrees

of freedom, this linear substrate allows for single-bond rotation. This rotation can possibly lower the difference between both protonation transition states. This is due to the existence of a more delocalised steric factor; the R group (and the β-methyl group) can rotate, reducing their bulk effect and effectively lowering the dr obtained when favouring the kinetic product. These high degrees of freedom also affect discrimination towards the thermodynamic product (Figure 2.27). Furthermore, both *cis*– and *trans*–products can rotate freely to minimise their energies. This results in energetically similar molecules, as seen from their Newman projections, and diminishes the thermodynamic drive towards one particular diastereomer ($\Delta G_T \sim 0$).

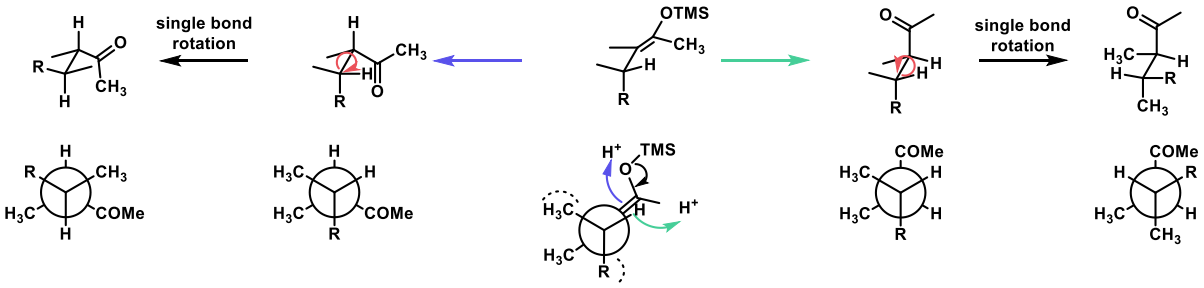

Figure 2.27: Conformations of the pseudo-exocyclic product, leading to either diastereomers.

2.12. Conclusion and future work

In this study, we developed a versatile ACA methodology for the efficient synthesis of 1,2-disubstituted cyclic molecules, achieving high enantioselectivity and diastereoselectivity. By optimizing reaction conditions and ligand selection—particularly through the identification and isolation of the P-chiral ligand **L22S**—we demonstrated precise control over the stereochemical outcomes of ACA products. The use of two distinct quenching protocols allows for the selective formation of either the *cis*– or *trans*–isomers for some cyclic systems, enhancing the practical utility of this approach. The methodology is compatible with a wide range of nucleophiles and electrophiles, including various ring sizes and heterocyclic systems, and achieved the challenging synthesis of *trans*–1,2-disubstituted cyclopentanes with high enantioselectivity. Despite these successes, some challenges remain to extend the methodology to substrates leading to all-carbon quaternary stereocentres and nitrogen-containing heterocycles.

Future work should focus on overcoming these limitations by exploring alternative protecting groups, reaction conditions, nucleophiles, and ligand designs. In the future, we aim to broaden the utility of this methodology for synthesizing complex molecules relevant to pharmaceuticals and natural products. Furthermore, attempting to understand the mechanism and the different conformations that give rise to different diastereomers is essential. Computational techniques such as DFT could aid us in this task, allowing us to better understand these systems.

2.13. References

1. E. W. Warnhoff, *J. Chem. Educ.*, 1996, **73**, 494–496.
2. A. Baeyer, *Liebigs Ann. Chem.*, 1894, **278**, 88–116.
3. M. Berthelot, *Bull. Soc. Chim. Fr.*, 1867, **7**, 53–65.
4. M. Berthelot, *Bull. Soc. Chim. Fr.*, 1868, **9**, 8–31.
5. A. Baeyer, *Ann. Chem. Pharm.*, 1870, **155**, 266–281.
6. V. V. Markovnikov, *Chem. Centralbl.*, 1890, **61**, 242–243.
7. W. H. Perkin Jr., *Ber. Dtsch. Chem. Ges.*, 1894, **27**, 216–217.
8. E. Haworth and W. H. Perkin Jr., *J. Chem. Soc. Trans.*, 1894, **65**, 591–602.
9. J. Keeler and P. Wothers, in *Chemical Structure and Reactivity: An Integrated Approach*, Oxford University Press, Oxford, 2014, pp. 524–534.
10. H. Sachse, *Z. Phys. Chem.*, 1892, **10**, 203–241.
11. A. L. Anet and A. J. R. Bourn, *J. Am. Chem. Soc.*, 1967, **89**, 760–768.
12. E. L. Eliel, S. H. Wilen, and L. N. Mander, *Stereochemistry of Organic Compounds*, Wiley, New York, 1994, pp. 696–705.
13. D. H. R. Barton, *Experientia*, 1950, **6**, 316–320.
14. G. Gill, D. M. Pawar, and E. A. Noe, *J. Org. Chem.*, 2005, **70**, 10726–10731.
15. M. B. Smith and J. March, in *March's Advanced Organic Chemistry: Reactions, Mechanisms, and Structure*, 7th ed., John Wiley & Sons, New Jersey, 2013, pp. 122–192.
16. J. Graham, M. Muhsin, and P. Kirkpatrick, *Nat. Rev. Drug Discov.*, 2004, **3**, 11–12.
17. Z. H. Siddik, S. Al-Baker, T. L. Burditt et al., *J. Cancer Res. Clin. Oncol.*, 1993, **120**, 12–16.
18. *The Nobel Prize in Chemistry 2001*. NobelPrize.org, Nobel Prize Outreach AB, 2001.
19. V. Ratovelomanana-Vidal and P. Phansavath, Eds., *Asymmetric Hydrogenation and Transfer Hydrogenation*, Wiley-VCH, Weinheim, 2021.
20. J. M. Brown, in *Comprehensive Asymmetric Catalysis*, E. N. Jacobsen, A. Pfaltz, and H. Yamamoto, Eds., Springer, Berlin, 1999, vol. I, chap. 5.1.
21. Y. Li, H. Shi, and G. Yin, *Nat. Rev. Chem.*, 2024, **8**, 535–550.
22. M. P. Wiesenfeldt, Z. Nairoukh, W. Li, and F. Glorius, *Science*, 2017, **357**, 908–912.
23. S. Yuan et al., *Nat. Commun.*, 2020, **11**, 621.
24. B. Sahoo et al., *Chem. Sci.*, 2018, **9**, 8134–8141.
25. A. Kaithal et al., *J. Am. Chem. Soc.*, 2023, **145**, 4109–4118.

26. L. Lückemeier, M. Pierau, and F. Glorius, *Chem. Soc. Rev.*, 2023, **52**, 4996–5012.
27. A. Kaithal et al., *Angew. Chem. Int. Ed.*, 2022, **61**, e202206687.
28. T. Wagener, L. Lückemeier, C. G. Daniliuc, and F. Glorius, *Angew. Chem. Int. Ed.*, 2021, **60**, 6425–6429.
29. T. Wagener et al., *ACS Catal.*, 2020, **10**, 12052–12057.
30. D. Moock et al., *ACS Catal.*, 2020, **10**, 6309–6317.
31. D.-S. Wang et al., *J. Am. Chem. Soc.*, 2011, **133**, 8866–8869.
32. F. Zhang, H. S. Sasmal, C. G. Daniliuc, and F. Glorius, *J. Am. Chem. Soc.*, 2023, **145**, 15695–15701.
33. S. Urban, B. Beiring, N. Ortega, D. Paul, and F. Glorius, *J. Am. Chem. Soc.*, 2012, **134**, 15241–15244.
34. Z. Nairoukh, M. Wollenburg, C. Schlepphorst, K. Bergander, and F. Glorius, *Nat. Chem.*, 2019, **11**, 264–270.
35. D. Moock, T. Wagener, T. Hu, T. Gallagher, and F. Glorius, *Angew. Chem. Int. Ed.*, 2021, **60**, 13677–13681.
36. C. Yu et al., *Angew. Chem. Int. Ed.*, 2020, **59**, 19905–19909.
37. M. M. Stalzer et al., *Angew. Chem. Int. Ed.*, 2016, **55**, 5263–5267.
38. *S. Bell, B. Wüstenberg, S. Kaiser, F. Menges, T. Netscher, and A. Pfaltz, Science, 2006, **311**, 642–644.*
39. R. Bigler et al., *Angew. Chem. Int. Ed.*, 2020, **59**, 2844–2849.
40. A. Schumacher, M. G. Schrems, and A. Pfaltz, *Chem. – Eur. J.*, 2011, **17**, 13502–13509.
41. M. G. Schrems, E. Neumann, and A. Pfaltz, *Angew. Chem. Int. Ed.*, 2007, **46**, 8274–8276.
42. X. Du, Y. Xiao, Y. Yang, Y.-N. Duan, F. Li, Q. Hu, L. W. Chung, G.-Q. Chen, and X. Zhang, *Angew. Chem. Int. Ed.*, 2021, **60**, 11384–11390.
43. S. Bachmann, M. Scalone, and P. Schnider, U.S. Patent US2007/232653, 2007.
44. S. Durrant, N. Ahmad, E.M. Beck, L. Carvalho Meireles, E.I. Chudyk, G. Etxebarria Jardi, B. Galan, S.S. Hadida Ruah, D.J. Hurley, R.M. Knegtel, T.D. Neubert, J.L. Pinder, J. Pontillo, R. Pullin, Y. Schmidt, D.M. Shaw, S. Skerratt, D. Stamos, S.A. Thomson, A.N. Virani and C. Wray, World Patent WO2021/113627, 2021.
45. J. Clayton, N. Greece's, and S. Warren, *Organic Chemistry*, 2nd ed., Oxford University Press, Oxford, 2012, chap. 22.

46. A. Alexakis, N. Krause, and S. Woodward, Eds., *Copper-Catalyzed Asymmetric Synthesis*, Wiley-VCH, Weinheim, 2014, vol. I, chap. 2–3.
47. A. Alexakis, J. E. Bäckvall, N. Krause, O. Pamies, and M. Dieguez, *Chem. Rev.*, 2008, **108**, 2796.
48. S. R. Harutyunyan, T. den Hartog, K. Geurts, A. J. Minnaard, and B. L. Feringa, *Chem. Rev.*, 2008, **108**, 2824.
49. L. Palais and A. Alexakis, *Tetrahedron: Asymm.*, 2009, **20**, 2866–2870.
50. A. Alexakis, V. Albrow, K. Biswas, M. d'Augustin, O. Prieto, and S. Woodward, *Chem. Commun.*, 2005, **2843**–2845.
51. B. L. Feringa, M. Pineschi, L. A. Arnold, R. Imbos, and A. H. M. de Vries, *Angew. Chem. Int. Ed. Engl.*, 1997, **36**, 2620–2623.
52. J. Cesati, J. de Armas, and A. H. Hoveyda, *J. Am. Chem. Soc.*, 2004, **126**, 96–101.
53. S. Ng, C. Howshall, T.N. Ho, B.K. Mai, Y. Zhou, C. Qin, K.Z. Tee, P. Liu, F. Romiti and A.H. Hoveyda, *Science*, 2024, **386**, 167–175.
54. R. Maksymowicz, P. M. C. Roth, and S. P. Fletcher, *Nat. Chem.*, 2012, **4**, 649–654.
55. A. V. Brethomé, R. S. Paton, and S. P. Fletcher, *ACS Catal.*, 2019, **9**, 7179–7187.
56. P. M. C. Roth, M. Sidera, R. M. Maksymowicz, and S. P. Fletcher, *Nat. Protoc.*, 2014, **9**, 104–111.
57. Y. Asano, A. Iida, and K. Tomioka, *Tetrahedron Lett.*, 1997, **38**, 8973–8976.
58. S. J. Degrado, H. Mizutani, A. H. Hoveyda, *J. Am. Chem. Soc.*, 2002, **124**, 13362–13363.
59. M. Vuagnoux-d'Augustin and A. Alexakis, *Chem. – Eur. J.*, 2007, **13**, 9647–9662.
60. E. K. Edelstein, D. A. Rankic, C. C. Dudley, S. E. McMinn, and D. A. Adpressa, *ACS Catal.*, 2021, **11**, 743–749.
61. A. Brethomé, *A Physical-Organic Approach to Asymmetric Catalysis: Design and Synthesis of Chiral Ligands Using Multivariate Modelling*, Doctoral Thesis, University of Oxford, 2019.
62. J. F. Teichert and B. L. Feringa, *Angew. Chem. Int. Ed.*, 2010, **49**, 2486–2528.
63. M. Žabka, L. Naviri, and R. M. Gschwind, *Angew. Chem. Int. Ed.*, 2021, **60**, 25832–25838.
64. E. E. Maciver, R. M. Maksymowicz, N. Wilkinson, P. M. C. Roth, and S. P. Fletcher, *Org. Lett.*, 2014, **16**, 3288–3291.

65. C. Defieber, M. A. Ariger, P. Moriel, and E. M. Carreira, *Angew. Chem. Int. Ed.*, 2007, **46**, 3139–3143.
66. J. Y. Hamilton, D. Sarlah, and E. M. Carreira, *J. Am. Chem. Soc.*, 2013, **135**, 994–997.
67. E. Drinkel, A. Briceño, and R. Dorta, *Organometallics*, 2010, **29**, 2503–2514.
68. H. E. Zimmerman, *J. Org. Chem.*, 1955, **20**, 549–557.
69. K. Garrec and S. P. Fletcher, *Org. Lett.*, 2016, **18**, 3814–381.
70. W. H. Johnson, E. J. Prosen, and F. D. Rossini, *J. Res. NBS*, 1949, **42**, 251–255. 5
71. N. L. Allinger and N. A. Pamphilis, *J. Org. Chem.*, 1973, **38**, 316–319. 7
72. A. V. Karnik and M. Hasan, in *Stereochemistry*, Elsevier Inc., 2021, pp. 301–302.
73. A. V. Karnik and M. Hasan, in *Stereochemistry*, Elsevier Inc., 2021, pp. 302–304.
74. O. Williams, (2024). *Asymmetric Conjugate Additions to Exocyclic Thioesters and Related Substrates*. Honour School of Chemistry Part II Thesis, University of Oxford.

Chapter 3:

Exploration of the P-stereogenic phosphoramidite ligand space

3.1. Exploring ligand space

Ligands play a paramount role in catalysis, particularly regarding reactivity and selectivity. The absence of an ideal ligand often results in poor reactivity and the formation of racemic products, which are undesirable in asymmetric synthesis. In contrast, the use of an optimal ligand can lead to significant improvements, achieving high levels of enantioinduction and yields.[1-4] This dramatic effect underscores the critical importance of ligand selection in catalytic processes.

To identify the optimal ligand, several approaches are utilized. Most commonly, these begin with a systematic screening of ligands, varying one parameter at a time (*ceteris paribus)* to understand the effect of each individual modification on the ligand's effectiveness.[4,5] This unidimensional approach allows chemists to easily estimate the impact of specific structural features on the catalytic outcome. In addition to this simple approach, many groups have employed more complex multi-variable strategies such as Quantitative Structure-Selectivity Relationship (QSSR), which alongside the use of computational models, increase the power of the screen.[6-15] These models help predict how changes in ligand structure might influence the selectivity and reactivity of the catalyst, thereby streamlining the search for the optimal ligand. The advantage of QSSR and multi-variable methods is clear as it allows a more complete view of the studied ligand space. However, the amount of data required often increases exponentially with increasing complex systems.[7-11]

This integrated approach has been previously employed in our group to identify an optimal phosphoramidite for the asymmetric conjugate addition (ACA) of linear enones (Figure 3.1).[15] *Dr. Alex Brethome* began his search with a standard ligand screening to find a potential lead, focusing specifically on modifications to the amine moiety of the phosphoramidite ligands. The amine component is known to significantly influence both the electronic and steric properties of the ligand, which in turn would affect the catalytic activity.[16]

After discovering a promising candidate, **L23**, which provided (71% ee) on the ACA, Dr. Brethome proceeded to test the effect of changing several structural parameters within the amine groups R^1 and R^2. He examined the impact of chirality at the R^1 position by testing both *S* and *R* stereocenters, as well as varying the ring sizes between five- and six-

membered rings to assess steric effects. These modifications aimed to understand how the spatial arrangement of atoms around the nitrogen could influence the chiral environment of the catalyst.

For the aliphatic group R^2, he explored a range of modifications, including different open-chain hydrocarbons and cyclic carbon rings. By altering R^2, he could evaluate how steric hindrance from different substituents affected the overall selectivity and reactivity of the ligand. This thorough investigation allowed him to correlate specific structural features with catalytic performance.

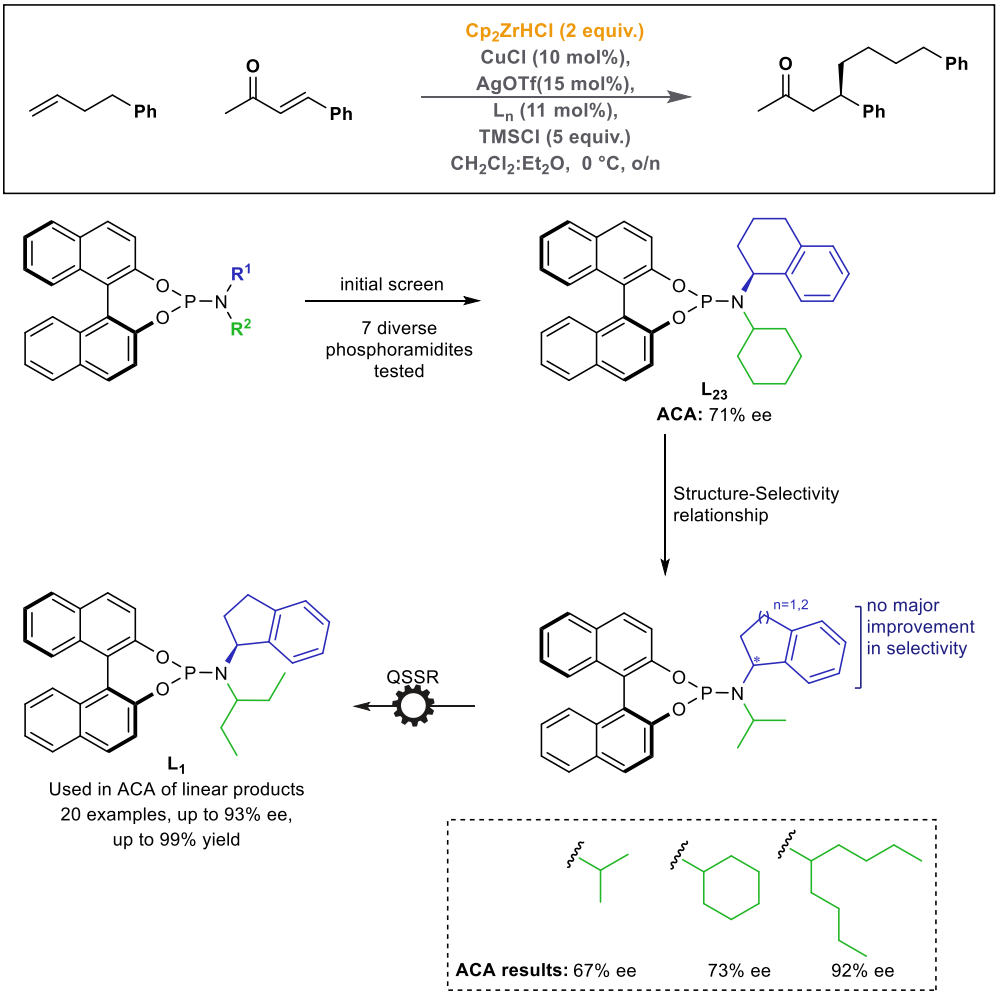

Figure 3.1: Demonstrating the applications of Ligand design for the ACA of linear enones.

After extensive testing, R^2 was identified as the main parameter responsible for influencing selectivity, with observed enantiomeric excesses varying significantly (from 67% to 92% ee) as different R^2 groups were employed. Recognizing this, Dr. Brethome focused his efforts on a methodical QSSR approach, varying only the R^2 parameter while

keeping all other variables constant. This systematic study eventually led to the discovery of the optimal ligand **L1**, which delivered impressive results, forming addition product Y in up to 92% yield and 91% ee.

3.2.Evolution of phosphoramidites

Non-substituted phosphoramidites

Over the past 25 years, phosphoramidite ligands have become instrumental in modern asymmetric catalysis, where their diverse structures facilitate fine control over reactivity and selectivity in various reactions. Traditionally, C_2-symmetric phosphoramidite ligands have been extensively studied and applied, achieving impressive results in numerous transformations across organic synthesis.[17-20] These ligands are particularly valued for their structural symmetry, which simplifies synthesis and purification. This simple structure aids in ligand space discovery, as a large range of these ligands can be produced quickly. Many research groups have successfully applied these ligands to achieve excellent enantioselectivities and yields in processes such as hydrogenation and allylic dearomatization.[21]

However, despite their widespread use, traditional C_2-symmetric phosphoramidites possess inherent limitations. The chiral environment created by these ligands is confined by their symmetrical structure, which can restrict the degree of enantioselective induction achievable in complex or challenging reactions.

Di-substituted phosphoramidites

To address these limitations, chemists have explored more flexible ligand spaces by designing di-substituted phosphoramidite ligands.[22-30] Unlike their symmetric counterparts, di-substituted phosphoramidites enable the introduction of additional modifiable groups, often providing more control over the steric and electronic environment surrounding the metal centre. These adjustments can lead to significant enhancements in enantioselectivity and yield, especially in reactions where traditional ligands fall short (Figure 3.2).[25-30]

Di-substituted phosphoramidites are increasingly utilized in synthesis, finding application across diverse reactions with a wide range of metals. As illustrated in Figure 3.2, these ligands have been successfully employed in various enantioselective

transformations, including gold-catalysed cycloadditions, iridium- and rhodium-catalysed hydrogenations, and palladium-catalysed allylic annulations, among others. Each example compares non-substituted phosphoramidites with their di-substituted counterparts, consistently highlighting the superior selectivities and yields achieved by the latter.

While there are instances where non-substituted phosphoramidites outperform their di-substituted analogues, the portrayed cases underscore the limitations of the simpler ligand design. Modifications to the BINOL backbone expand the available ligand space, presenting new opportunities to enhance reaction outcomes in challenging transformations.

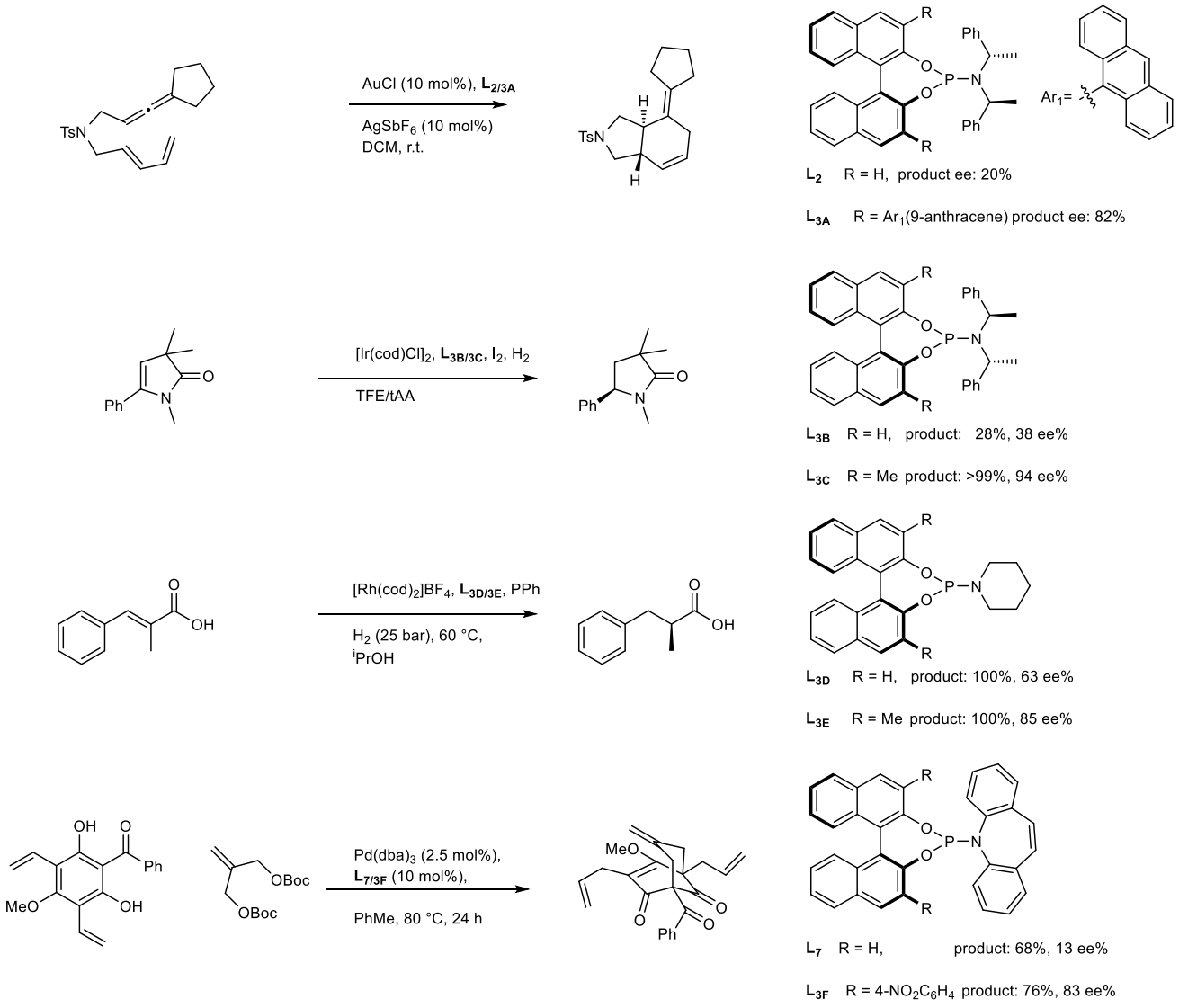

Figure 3.2: Showcasing limits of non-substituted phosphoramidites and how this limit can be overcome by di-substituted phosphoramidites.

Mono-substituted phosphoramidites

In addition to di-substituted ligands, mono-substituted phosphoramidites offer an even more expansive and flexible alternative ligand space, enabling the customization of multiple structural elements within a single ligand framework.[30,31] Mono-substituted ligands introduce stereogenicity at the phosphorus centre itself, which potentially allows for additional layers of configurational control. This unique feature, combined with the ability to vary both the amine and BINOL groups independently, creates a specialised chiral environment that can be optimized for complex transformations. In practical terms, this means that mono-substituted phosphoramidites can potentially outperform di-substituted and non-substituted phosphoramidites in reactions requiring highly specific chiral environments.

However, the exploration of these expanded ligand spaces is not without challenges. As the complexity of ligand design increases, so does the difficulty of synthesis. P-chiral phosphoramidites are considerably more labor-intensive to produce compared to their C_2-symmetric counterparts (Figure 3.3a). The synthesis of P-chiral ligands often requires non-commercially available, selectively mono-functionalized BINOL derivatives, alongside specific amine modifications. Furthermore, this process can not only be time-consuming but also prone to producing mixtures of diastereomers, which are often inseparable. These mixtures complicate reaction optimization, as the individual diastereomers can exhibit differing catalytic activities and selectivity, adding further complexity to the analysis and refinement of catalytic systems.

For all these reasons, there are only few examples of these phosphoramidites in the literature (Figure 3.3b).[31-35]

Despite these drawbacks, P-chiral phosphoramidites have proven indispensable for challenging reactions such as the ACA of exocyclic substrates (Chapter 2). In these cases, traditional C_2-symmetric and disubstituted phosphoramidites were confined to a selectivity ceiling. This is exemplified by ligand **L7**, which achieved only around 50% ee. This limitation suggests that there are inherent constraints in the chiral environment that C_2-symmetric ligands can provide for certain substrates.

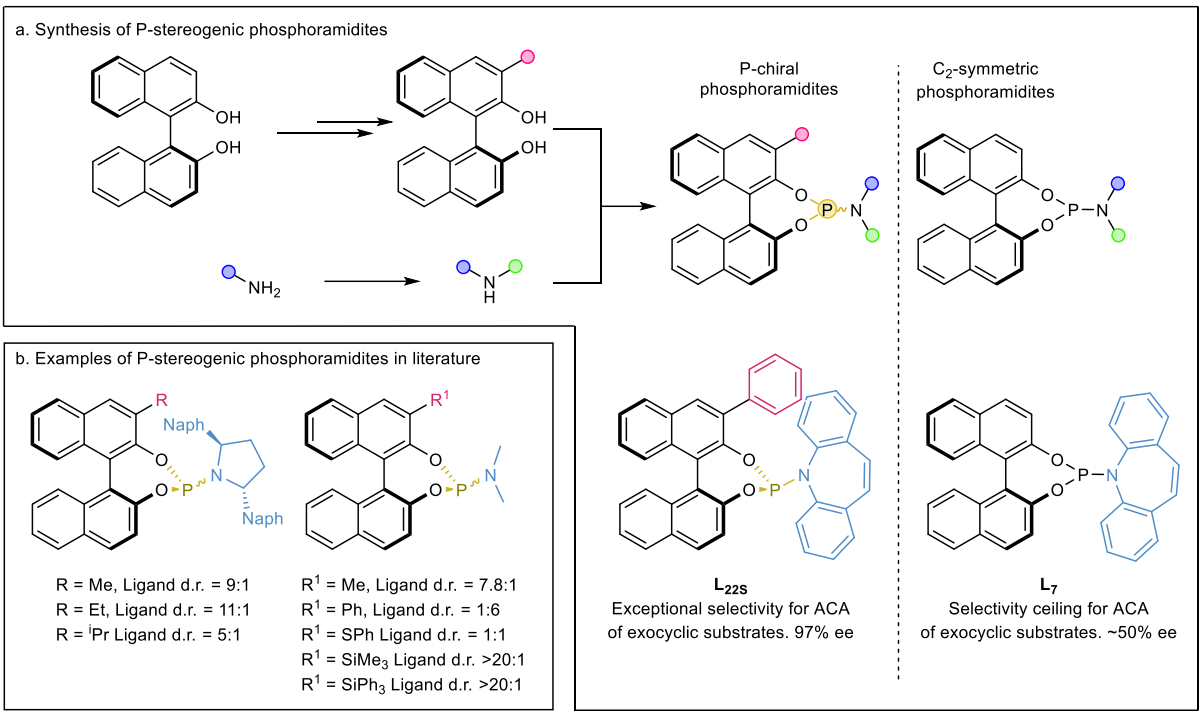

Figure 3.3: *a*. Showcasing the standard synthesis of P-chiral phosphoramidites and their comparative advantage over C_2-symmetric phosphoramidites on the ACA of Exocyclic substrates. *b*. examples of P-stereogenic phoshparamidites in literature and their respective obtained ligand dr.

In stark contrast, the P-chiral ligand variant **L22S** surpassed this limitation, achieving 97% ee. This result indicates that P-chiral ligands can create a more defined and effective chiral environment around the metal centre, which is crucial for inducing higher enantioselectivity. The success of **L22S** in this reaction highlights the untapped potential of P-chiral phosphoramidites in asymmetric catalysis.

3.3. Aims and goals

The main aim of the showcased research is to investigate the P-stereogenic phosphoramidite ligand space utilizing a unidimensional (*ceteris paribus*) approach to identify:

- Whether the enhanced selectivity with **L22S** is unique to this ligand or a general feature of P-chiral phosphoramidites. Understanding this could guide future ligand design, justifying the synthetic effort if P-chirality consistently improves selectivity in asymmetric synthesis.
- A relationship between structural parameters, such as BINOL groups or amine substituents, and the diastereomeric ratio of P-chiral phosphoramidites. Identifying this could enable diastereoselective synthesis, favouring the S,S_P diastereomer, which we believe is optimal for the studied ACA systems.

By accomplishing these goals, we would avoid the need for multiple time-consuming crystallizations that are otherwise required to isolate P-stereogenic phosphoramidites, such as **L22S** from a diastereomeric mixture. Additionally, we would eliminate the necessity to synthesise both diastereomers, effectively reducing the overall synthetic effort and resources required while increasing atom efficiency.

3.4. BINOL backbone modification:

We initiated our design campaign by synthesizing a structurally diverse range of mono-substituted BINOLs. To keep as many parameters constant as possible, we opted to use iminostilbene as the amine coupling partner due to its notable positive effects in the ACA reaction. Our strategy was to find a relationship between the R-group on the BINOL and the resulting diastereomeric ratio of the phosphoramidite ligands. Once this relationship was established, we aimed to exploit it to synthesise ligands with the desired configuration, ideally *S,S*$_P$. Diastereomeric ratios were measured by ^{31}P NMR of the ligand after purification via flash column chromatography.

To begin, we freely varied the R-group and observed the effect of these changes on the diastereomeric ratio of the ligand (Figure 3.4). Many of the added substituents showed little to no effect on the resulting diastereomeric ratio. For instance, planar aryl groups such as phenyl or naphthyl exhibited a modest tendency toward forming the *S,R*$_P$ diastereomer as the preferred diastereomer. This effect however was mild and lead to low diastereomeric rations (<1:2). A similar scenario was observed when halogens were introduced at position 3 of the BINOL moiety, resulting in very poor diastereomeric ratios with a slight preference for the *S,R*$_P$ configuration.

More noticeable changes in the diastereomeric ratio were observed when bulkier, sp^3-hybridized groups were employed at position 3 of the BINOL. Ligand **L$_{27}$**, featuring a semi-sp^3 BoroMIDA moiety, achieved a modest diastereomeric ratio of 2.3:1. Furthermore, substituents such as silanes—specifically trimethylsilyl (TMS) and triisopropylsilyl (TIPS) groups in ligands **L$_{28S}$** and **L$_{29S}$**, respectively—achieved high diastereoinduction by selectively forming only the *S,S*$_P$ diastereomer. This observation aligns with literature reports from the Reetz group, which has been active in synthesizing simple P-chiral phosphoramidites with silanes at position 3 of the BINOL. In similar ligands, they observed exclusive formation of the *S,S*$_P$ configuration.[31]

From this initial screening, we were able to discover some ligands that formed diastereoselectively and identify what appears to be a key factor leading to this selectivity: steric effects. The bulkiness of the substituent at position 3 seems to play a crucial role in directing the formation of a specific diastereomer. However, despite the high diastereomeric ratios achieved with the silane-substituted ligands, they are

considerably structurally different from the original phenyl ligand **L22S**. This structural disparity raised concerns that they might underperform in the ACA reaction due to potential differences in electronic properties or steric hindrance.

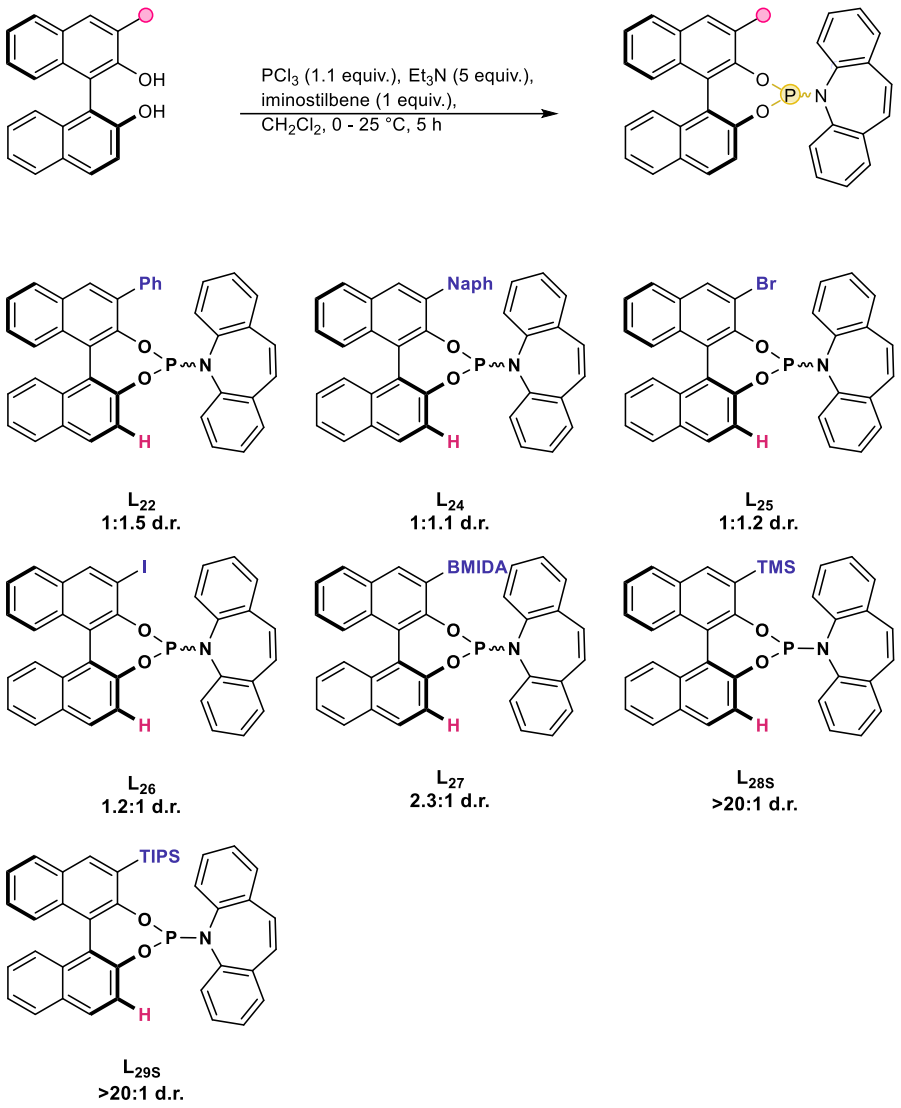

Figure 3.4: Initial modification of the BINOL backbone utilising a diverse range of groups. Diastereomeric ratio values relate to the P-chiral phosphoramidite product and was measured via ^{31}P NMR.

This realization prompted us to undertake a sequential screening focused on modifying the substituents on the phenyl ring. By doing so, we aimed to find a ligand that is both structurally similar to **L22S** and capable of being synthesised diastereoselectively. To avoid the appearance of rotamers that would further complicate these studies, we limited our search to simple symmetric *para*–, *meta*–, and *ortho*–substituted aryl groups.

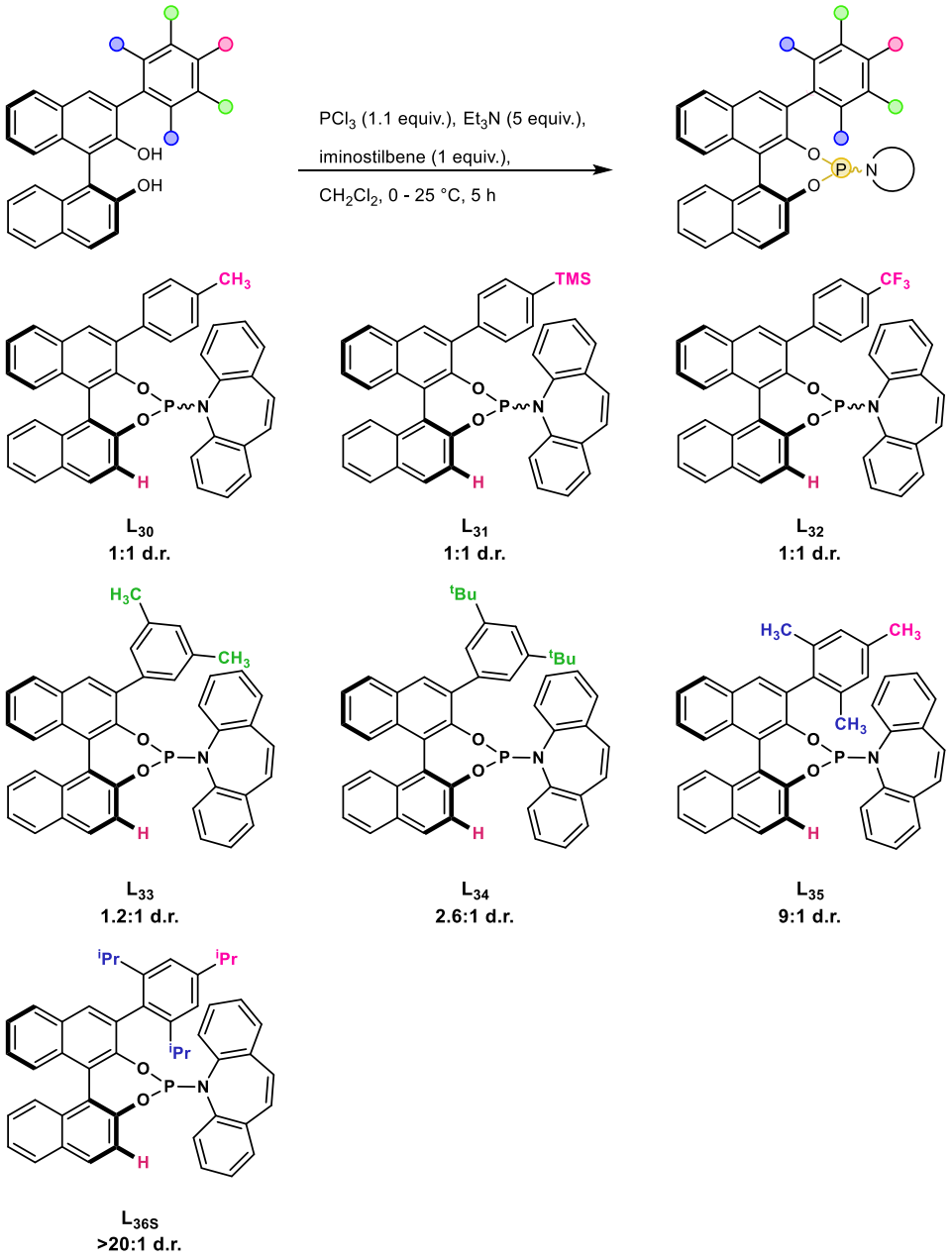

Figure 3.5: Structural modification of the aryl–BINOL backbone, testing the effect of *para*–, *meta*– and *ortho*– positions on the resulting diastereomeric ratio of the phosphoramidite.

As depicted in Figure 3.5, *para*–substituted aryls showed no observable effect on the diastereoselectivity of the final ligand (**L30**-**L32**). Even when employing bulky groups (**L31**) or electron-withdrawing groups (**L32**), the diastereomeric ratios remained unchanged. This observation suggests that neither electronic effects nor steric effects at the *para*–position significantly influence diastereoselectivity, possibly because of this position being too distant from the active site where the phosphoramidation reaction occurs.

Meta–substituted aryl groups began to show more promising results. Ligand **L33**, which contains 3,5-dimethyl groups on the aryl substituent, exhibited a weak preference for the *S,S*$_P$ configuration with a diastereomeric ratio of 1.2:1. Although this is not a substantial effect, it hints at the role of steric factors in this transformation. This diastereoinduction was further enhanced with bulkier *meta*–substituents, such as in the 3,5-di-*tert*-butyl variant ligand **L34**. In contrastwith *para*–substitutions, adding bulkier groups in the *meta*–positions resulted in increased diastereoinduction, achieving a ratio of 2.6:1.

Encouraged by these findings, we turned our attention to the *ortho*–positions to assess their effect on the diastereomeric ratio of the resulting ligands. We synthesised 2,4,6-trisubstituted aryl variants, testing both methyl and isopropyl groups.

To our delight, the *ortho*–substituted ligands performed even better than the *meta*–variants. The ligand with simple methyl groups at the *ortho*–positions (**L35**) achieved a notable diastereomeric ratio of 9:1. The bulkier isopropyl ligand variant (**L36S**) was synthesised effectively as a single diastereomer, achieving a diastereomeric ratio greater than 20:1. These results underscore the significant influence of steric hindrance at the *ortho*–positions in directing diastereoselectivity at phosphoramidation.

3.4.1 Steric considerations and their effect on dr

After all this testing, we concluded that steric factors predominantly influence the diastereomeric ratio of the resulting ligands. However, a few questions arose from this hypothesis. Firstly, how is it that notably large substituents, such as naphthyl and 4-TMS aryl groups, (**L24**, **L31**) yield a similar diastereomeric ratio as the significantly smaller halogen-substituted variants (**L25**, **L26**)? Secondly, why do some bulkier ligands, like **L34** (bearing two bulky *tert*-butyl substituents), exhibit a smaller effect on the diastereomeric ratio than ligands with arguably smaller substituents, such as **L28** and **L35**?

These disparities in behaviour prompted us to examine the structure of the BINOLs more closely. After much consideration, taking into account the substrates as multidimensional parameters, we believe to have found a plausible argument for the observed trend.

As illustrated in Figure 3.6, halogens have considerably less bulk volume than the one present in sp^3-hybridized substituents like silanes. This size difference is heavily supported by countless literature articles such as A-value comparisons.[36-39]

This sp^3 bulkiness might hinder interactions between the amine-phosphorus electrophile and the nearby hydroxyl group (O_A), thereby inducing a stereodifferenciating effect to the phosphoramidation reaction. Since smaller substituents such as halides have a lower steric factor, the chemical environment of O_A is likely to be similar to the other hydroxyl group, resulting in no stereo differentiation between either oxygen with respect to the electrophile, therefore resulting in low ligand drs.

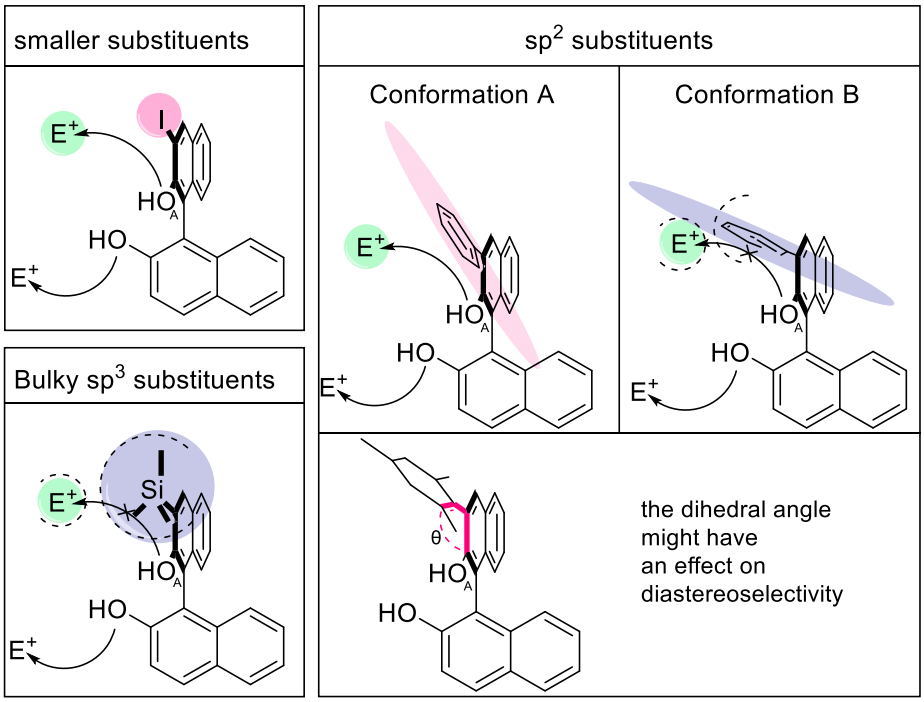

Figure 3.6: Suggested effect of R groups in diastereoselectivity, divided on three types: smaller substituents, Bulky sp^3 substituents and sp^2 substituents.

In the case of aryl-substituted BINOLs, this observation remains consistent. Due to the planar nature of the sp^2 ring system, the three-dimensionality of the aryl group is greatly dependent on the dihedral angle (θ) between the aryl substituent and the BINOL core. Small θ angles result in a more planar, two-dimensional structure (Conformation A), which might behave more like non-bulky groups. Conversely, the closer θ is to 90°, the more 'three-dimensional' the BINOL moiety behaves (Conformation B). This implies that the observed diastereoselectivity could be a function of the dihedral angle θ rather than merely the size of the aryl group.

More specifically, at higher dihedral angles (closer to 90°), the steric bulk of the substituents may block the electrophile (E^+) from approaching oxygen O_A, whereas at

lower dihedral angles (0-45°), the electrophile can approach O_A more easily, facilitating the reaction (Figure 3.6)

Steric and electronic effects in biaryl systems

The balance between steric and electronic effects is critical in determining the torsion angle of biaryl systems. Electronic effects, such as conjugation between the two aryl rings, stabilize biaryls at lower dihedral angles, typically close to 0°, because conjugation is maximized when the rings are planar. However, this planar conformation introduces steric clashes between *ortho*–hydrogens or other *ortho*–substituents, which destabilize the system due to their spatial proximity (Figure 3.7).

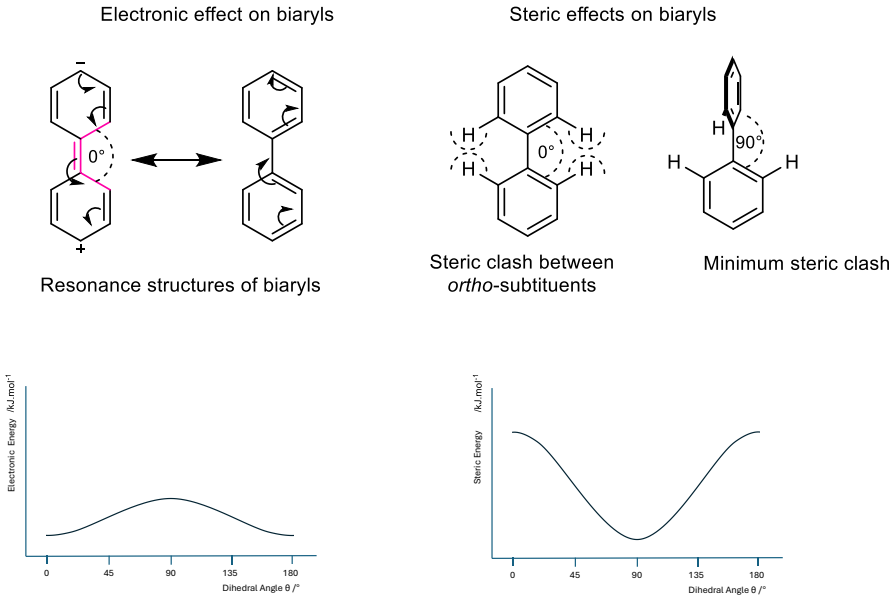

Figure 3.7: Steric and electronic considerations regarding conformation of biaryls.

On the other hand, steric effects between *ortho*–substituents are minimized when the biaryl adopts a near-perpendicular orientation (~90°), as this reduces the overlap between bulky groups on adjacent rings. These conflicting electronic and steric effects lead to a compromise: rather than adopting extreme values (0° or 90°), the dihedral angle of many biaryl systems settles around a middle point, typically close to 44°, where both steric and electronic energy costs are minimized.[40] This balance is observed across a wide range of substituted biaryls, and computational models consistently show this compromise as a preferred conformation (Figure 3.8a).[41,42]

For many aryls, the energy profile reveals two maxima: one at 90°, where conjugation is fully disrupted, and another near 0/180°, where steric clashes between *ortho*–hydrogens increase the conformational energy. The global minimum, however, is found at approximately 44°, where the two opposing forces—conjugation and steric hindrance—are balanced.[43-48] This is why, for example, in **L22S** the phenyl-phenyl (Ph-Ph) system, which should theoretically adopt a 44° torsion angle, does indeed show a dihedral angle of 45.4° (Figure 3.8b) as seen from the crystal structure, a result consistent with both experimental and computational expectations

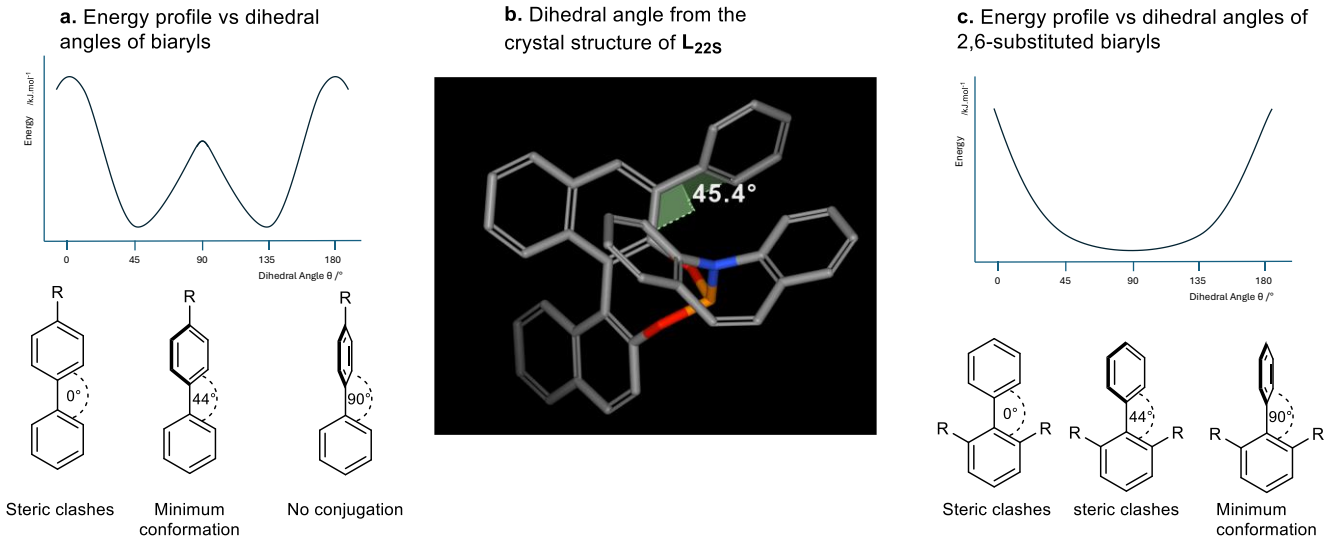

Figure 3.8: a. Different conformations adopted by biaryl systems. **b.** Crystal structure of **L22S** showcasing its biaryl dihedral angle. **c.** Different conformations adopted by 2,6-substituted biaryl systems.

Para–substituted biaryl systems generally follow this pattern since the *para*–substituent is too far from the biaryl bond to affect the torsion angle significantly. Likewise, Ph-2-naphthyl biaryls, where the steric effect remains moderate, also tend to adopt a similar conformation due to the same balancing of electronic and steric factors. The torsion angle in these cases remains close to 44°.[49,50]

In *meta*–substituted systems, steric effects are not typically strong enough to drastically alter the torsion angle. Although bulkier *meta*–substituents might influence the reaction outcome to some degree, they do not have as pronounced an impact on the biaryl conformation as *ortho*–substituents. Nonetheless, the role of *meta*–substituents on dihedral angles of biaryls remains less well understood.

Ortho–substitution: Stronger steric dominance

In *ortho*–substituted systems, steric effects dominate over conjugative stabilization, driving the dihedral angle closer to 90°. As Figure 3.8c shows, the steric interactions between bulky *ortho*–substituents greatly outweigh any stabilization offered by electronic conjugation. In these cases, the global minimum shifts towards 90°, as the energetic cost of maintaining a planar conformation is too high.[49,50]

This preference for a near-perpendicular orientation has significant implications for diastereoselectivity. In systems such as **L35** and **L36S**, the *ortho*–substituents probably force the torsion angle to ~90°, which potentially restricts the spatial accessibility of the electrophile to O_A. This steric locking might favour the selective formation of one diastereomer over the others, as the constrained conformation might induce a stereodifferenciation factor. To further support these arguments, detailed computational simulations should be employed.

3.4.2. Results of the exocyclic ACA reaction with P-chiral ligands

After synthesizing the P-chiral ligands with moderate to high diastereomeric ratios, we proceeded to test their efficacy in the exocyclic asymmetric conjugate addition (ACA) reaction. As shown in Figure 3.9, most of these ligands significantly underperformed, yielding poor enantioselectivities and low yields of the ACA product. Notably, the steric bulk that appeared crucial in enhancing the diastereoselectivity of the ligands appeared to be counterproductive in the ACA reaction itself.

This inverse relationship is particularly evident when comparing ligands such as **L35** and **L36S**, both of which are *ortho*–aryl substituted. The bulkier isopropyl variant suffered a considerable decrease in both yield and selectivity (30%, 35% ee) compared to its less bulky methyl counterpart (40%, 65% ee). In fact, while the selectivity of the methyl variant (**L35**) is moderately higher than that of C_2-symmetric ligands, the selectivity of ligand (**L36S**) is even worse than that of the commercially available ligand **L7**.

A similar trend is observed with the silane-substituted ligands. The trimethylsilyl (TMS) version exhibits good enantioselectivity (**L28S**, 83% ee) but results in a low yield. Conversely, the bulkier triisopropylsilyl (**L29S**) version performs poorly, presumably due to the increased steric hindrance, leading to low yields and reduced enantioinduction

levels (30% yield, 36% *ee*). This represents a considerable decline in selectivity between two structurally similar ligands.

Interestingly, even a ligand with a significantly lower diastereomeric ratio, such as the *meta*–substituted **L34**, achieves an enantioselectivity similar to that of the methyl *ortho*–substituted variant, despite its comparatively higher diastereomeric purity. This observation suggests that factors other than diastereomeric ratio may play a significant role in influencing the outcome of the ACA reaction.

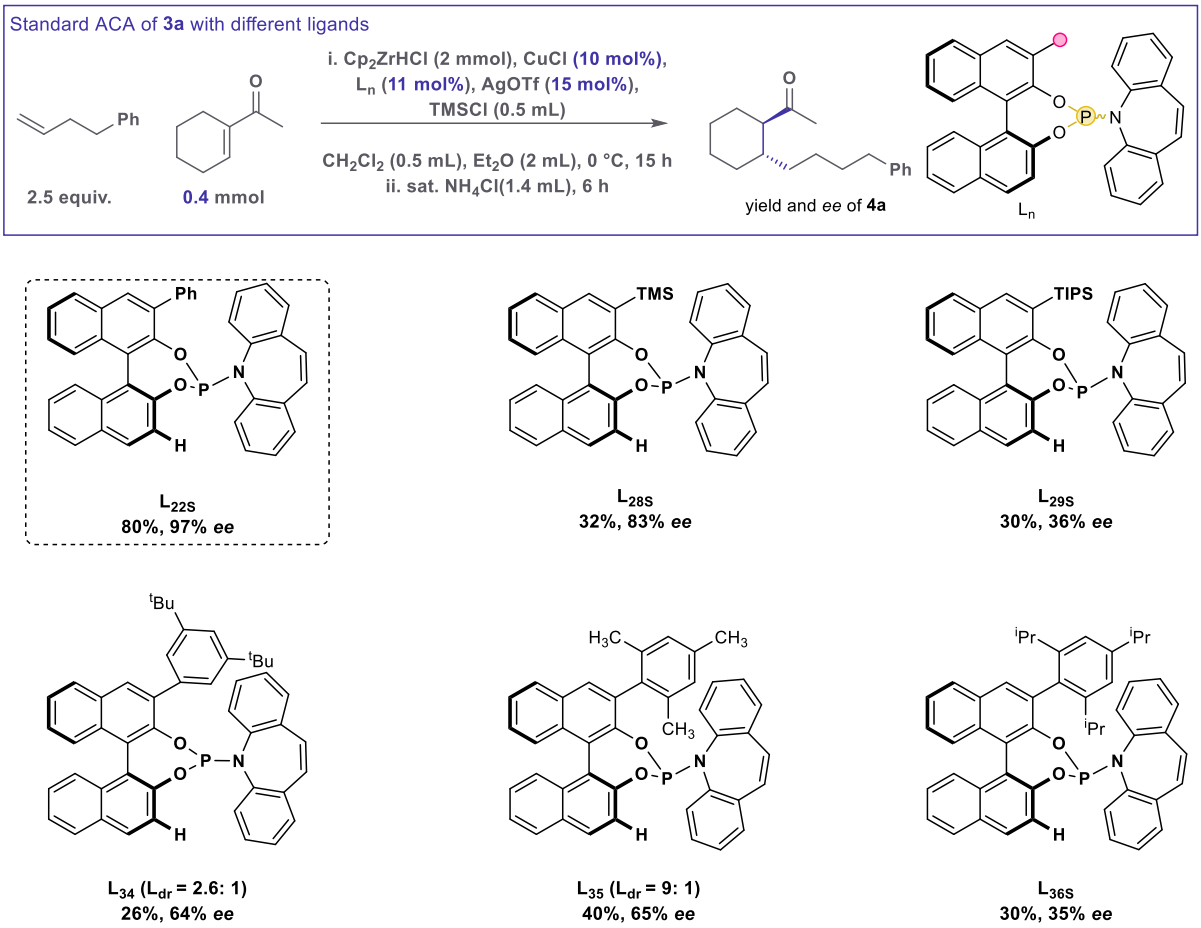

Figure 3.9: Testing BINOL backbone modified P-Chiral ligands on the ACA of exocyclic substrates.

Unfortunately, even though some ligands achieved moderately high enantioselectivities in the ACA reaction, they are notably lacklustre when compared to the *S,S*$_P$ phenyl ligand **L22S**, which delivers an 80% yield and 97% *ee*. Even using a 1:1 diastereomeric mixture of **L22** (containing equal amounts of **L22S** and **L22R**) yields a respectable 90% *ee* and 65% yield, a considerably better result than any obtained in this P-Chiral ligand screen. These

findings point out the exceptional performance of **L22S** and highlight the challenges in finding a suitable alternative.

This screening, although unsuccessful in identifying an alternative to **L22S**, provides valuable insights into the critical role of the phenyl group in the ligand's structure. It suggests that the presence of the phenyl group is essential and that modifications to it can significantly impact the ligand's performance in the ACA of exocyclic substrates. The data implies that while increasing steric bulk can enhance diastereoselectivity during ligand synthesis, it may adversely affect catalytic activity and enantioselectivity in the ACA reaction.

3.5. Amine modification of P-stereogenic phosphoramidites

Initial amine scope

Given that the BINOL modification screening did not produce any highly effective ligands for the exocyclic ACA, we shifted our focus to modifying the amine component instead. Different amines can potentially have a favourable effect on both the resulting diastereomeric ratio of the ligand and the enantioinduction level in the ACA of exocyclic enones. (Figure 3.10)

First, we began the amine screening by testing simple non-chiral moieties to determine if the increase in diastereomeric excess depends on amine chirality. In all experiments, the 3-phenyl BINOL substrate was kept constant, as it demonstrated superior activity in the ACA of exocyclic substrates compared to all other tested substituents (*ceteris paribus*). Unsurprisingly, small non-chiral amines such as dimethylamine and morpholine (**L37** and **L38**) showed no significant effect on the diastereomeric ratio. However, to our surprise, the diisopropyl variant (**L39**) demonstrated a significant improvement in the ligand ratio (3.8:1). This result suggests that neither chirality nor disparity between the two amine R-groups is necessary for high stereodifferentiation.

We were also intrigued by the synthesis of a ligand where the amine is composed of two different substituents or branches (**L40**): one is a methyl group, and the other, R^1, considerably bulkier (-$CHPh_2$). Interestingly, the observed dr (10:1) is higher than that of **L39**, where the ^{i}Pr groups are significantly less bulky than the R^1 group in **L40**.

After this initial test, we were encouraged to explore chiral amines, not only to assess their effect on the diastereomeric ratio of the ligand but also due to their potential to enhance selectivity in the ACA of exocyclic substrates. In this screening, we opted to keep the amine structure closely related to the diisopropyl amine, as its structure achieved good diastereomeric ratios. To our delight, all these chiral ligands achieved very high diastereomeric ratios. Aside from one ligand, which attained a respectable 10:1 ratio (**L_{41}**), all the chiral ligands (**L_{42} – L_{44}**) were synthesised diastereoselectively (>20:1 dr). Notably, ligands resembling those synthesised by the Feringa group—essentially the P-chiral versions of these 'privileged ligands'—were included. The C_2-symmetric versions have been used extensively in numerous reactions, including several ACAs performed by our group and others.[51-54] Although these "privileged" ligands have performed poorly in the ACA of exocyclic substrates, we hoped this modified version could potentially enhance their performance in the reaction.

After synthesizing this ligand library, we tested these ligands in the ACA reaction. We evaluated both the standard exocyclic ACA substrate (3-acetylcyclohexene) and a pseudo-exocyclic ACA substrate **3aa** (3-methyl-3-penten-2-one) forming molecules **4a** and **5a** respectively. For the regular exocyclic reaction, all these tested ligands were quite underwhelming. The simpler ligands with low diastereomeric ratios (**L_{37}**, **L_{38}**) provided no significant enantioinduction. Overall, the other tested ligands gave poor enantioselectivities and moderate yields.

Interestingly, while ligand **L_{43}** underperformed its non-C_2 symmetric version (as **L_{43}** showed to have no reactivity in the system), the other diastereomer (**L_{42}**) showed a comparatively enhanced reactivity (obtaining 41% *ee* compared to the achieved 22-28% *ee* from **L_2**). Finally, the bulkier **L_{44}** obtained a considerably poor yield and selectivity. Unfortunately, all the ligands in this library achieved no significant enantioinduction levels and better results are obtained with the commercially available **L_7**.

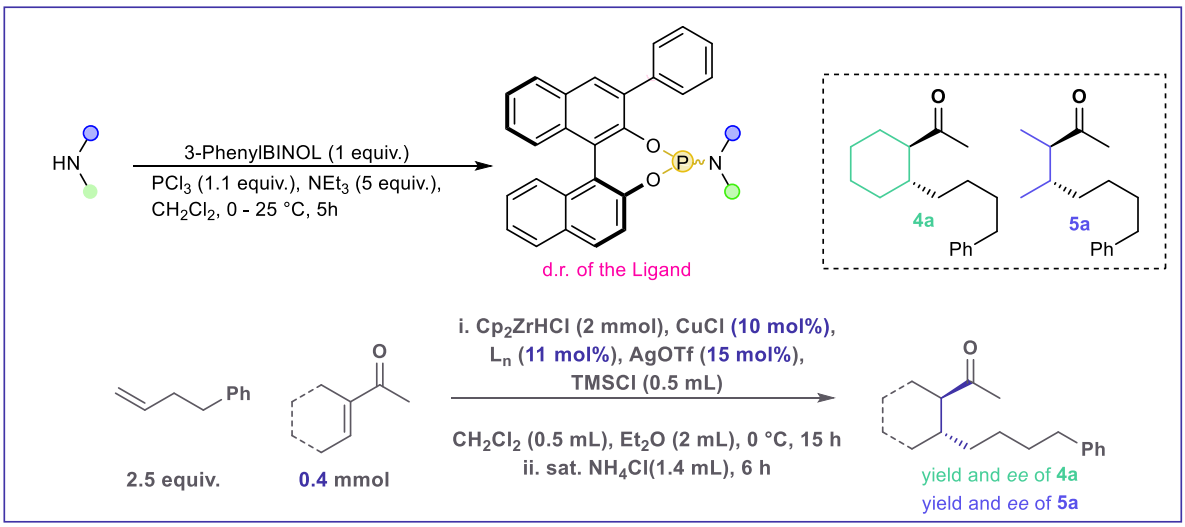

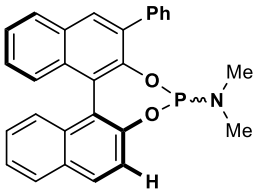

L_{37}
1:1.5 d.r.
N/A
N/A

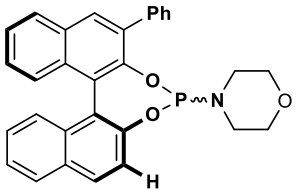

L_{38}
1:1.1 d.r.
46%, -3.6% *ee*
44%, 21% *ee*

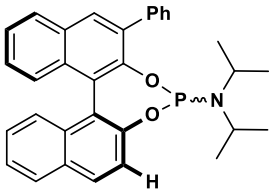

L_{39}
4:1 d.r.
48%, 35% *ee*
66%, 55% *ee*

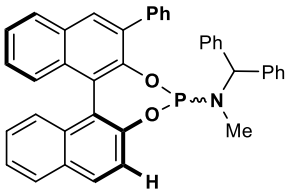

L_{40}
10:1 d.r.
40%, 25% *ee*
60%, 56% *ee*

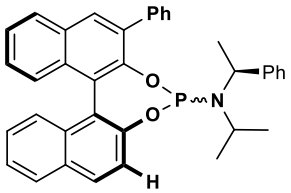

L_{41}
10:1 d.r.
30%, 34% *ee*
63%, 68% *ee*

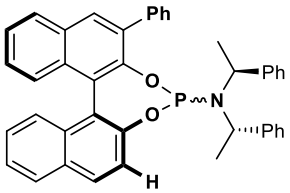

L_{42}
>20:1 d.r.
N/A
N/A

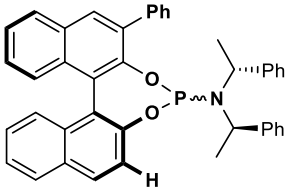

L_{43}
>20:1 d.r.
40%, 41% *ee*
65%, 73% *ee*

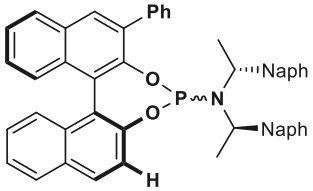

L_{44}
>20:1 d.r.
18%, 17% *ee*
33%, 45% *ee*

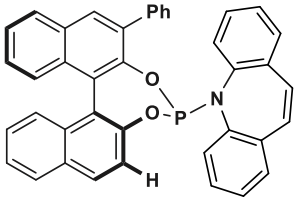

L_{22S}
>20:1 d.r.
80%, 97% *ee*
90%, 93% *ee*

Figure 3.10: Initial modification of the amine moiety utilising a diverse range of groups. Diastereomeric ratio values relate to the P-chiral phosphoramidite product and was measured via ^{31}P NMR. In green, results of the ACA of **3a**, yielding **4a**. In blue, results of the ACA of 3-methyl-3-penten-2-one, yielding **5a**. Results are compared to **L_{22S}** for the same reactions. Diastereomeric values for **5a** consistently poor (~1.5:1).

When testing the ACA on 3-methyl-3-penten-2-one, the results were markedly more promising. The trends observed were qualitatively similar: ligands with comparatively higher selectivity in one reaction remained higher in the other, and those with lower selectivity remained lower. Fortunately, the overall selectivity increased for every example. Most ligands, when tested on this substrate, achieved moderate selectivities. The best case in this screen was a ligand that provided moderate yields and selectivity (**L**$_{43}$, 65% yield, 73% ee). Even though, these results outperform the ones obtained by **L**$_7$ on similar systems (70%, 49% ee) they unfortunately are not comparable to the ones obtained by **L**$_{22S}$ on the same system (80, 93% ee).

Further amine scope

Inspired by our previous work on ligand design pioneered by Dr. Brethome, we decided to create a library of ligands similar to a previously successful ligand, **L**$_1$. This ligand had shown great success with linear substrates (>90% yield, 93% ee) and moderate success with the exocyclic ACA (50% ee) (Figure 3.11). Following a similar design strategy, we tested different ring sizes in the bicyclic region (five- and six-membered rings) and different chiral centres to find the structure-selectivity relationship in the system. For the other amine branch (showed in green) we tested various alkyl substituents—some withclosed rings and others with diverse carbon chain lengths. For all synthesised examples, the ligand diastereomeric excess was gratifyingly high (>20:1 dr). Once again, the two enone test substrates were evaluated for ACA reactivity.

In the standard exocyclic reactions, most results yielded poor to moderate yields and moderate selectivity. The change in the chiral centre of the amine seemed to have no significant effect on either the yield or enantioinduction levels (**L**$_{47}$ and **L**$_{48}$). However, it is noteworthy that these ligands showed a marginal improvement compared to their non-C_2 symmetric counterpart (**L**$_1$, 50%, 49% ee).

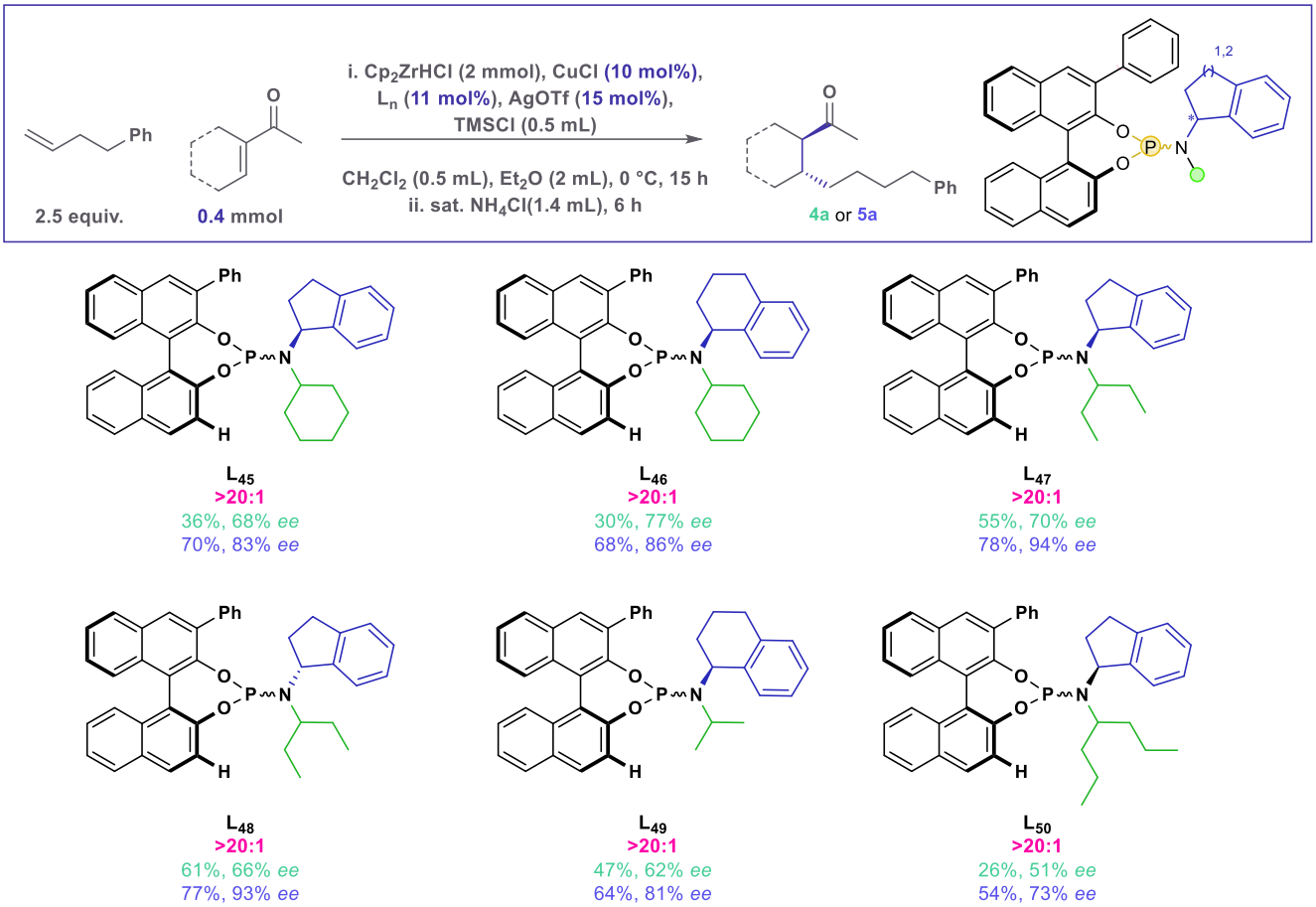

Figure 3.11: Structure-selectivity relationship of P-chiral phosphoramidites, testing out the different positions of the amine that works for linear substrates.

Altering the ring size of the bicyclic part of the amine had a more pronounced effect on both selectivity and reactivity. A six-membered ring favoured higher selectivity (**L46**, 30%, 77% ee) at the expense of lower reactivity compared to the five-membered ring version (**L45**, 36%, 68% ee). Lastly, we examined the effect of different alkyl chains. Long open-ended chains had an overall negative effect on both enantioinduction and reactivity (**L50** 26% yield, 51% ee). Small open-ended chains (**L49**) had a considerably positive effect on yields (from 30 to 47%) at the cost of selectivity, which was reduced from 77% to 62% ee. From this screening, the most selective ligand was obtained with large bicyclic rings and a closed six-membered alkyl chain, **L46**. Nevertheless, even though this result is better than most other obtained results across this ligand space, it still falls short of the results obtained by using **L22S**.

Finally, all these ligands were tested on the pseudo-exocyclic system (**5a**). Once again, most results remained qualitatively similar while achieving overall higher yields and selectivities with many examples in this ligand library obtaining high yields and

selectivities. Particularly, **L47** and **L48** achieved notable results (~77% yield, 93% ee) which are comparable to the results obtained by **L22S** on the same system. Just like in the standard exocyclic screen, changing the amine stereocentre did not gave a major change in selectivity or yield. A larger 6 membered bicycle ring (**L46**) gave marginally better selectivity at the cost of yield (compared to the 5 membered ring bicycle, **L45**), however it is important to note that this change is even less pronounced in this screen. Finally, long alkyl chains once again seem to negatively affect the ligands performance (**L50**).

Overall, this final screening has exhibited some success. The ligand space was further explored, and suitable candidates (**L47** and **L48**) have been found for a challenging ACA yielding **5a**, an alternative to **L22S** for the standard ACA to make **4a** is yet to be discovered.

3.6. Summary and future work:

Herein, we explored the ligand space of P-chiral phosphoramidites to enhance the asymmetric conjugate addition (ACA) of exocyclic enones. Given the extensive range of modifiable parameters, we employed a unidimensional approach (*ceteris paribus*) to isolate the effects of specific structural modifications.

Our investigations revealed that increasing the steric bulk at the BINOL backbone significantly improves diastereoselectivity during ligand synthesis. Ligands containing large sp^3 substituents, such as silanes (*e.g.* **L28S**, **L29S**), were obtained as single diastereomers, whereas ligands containing smaller groups exhibited unsatisfactory diastereomeric ratios. Additionally, variations in aryl substituents demonstrated notable effects: non-substituted and para–substituted aryl groups showed minimal influence, whereas ortho–substituted aryl groups (*e.g*. **L35**, **L36S**) led to markedly higher diastereoselectivity. This trend suggests that steric effects, rather than electronic contributions, play a dominant role in achieving high diastereomeric ratios.

Overall, the ability to synthesize these ligands without the need for laborious serial crystallizations significantly streamlines the synthetic methodology, as exemplified by ligands **L28S**, **L29S**, **L35**, and **L36S**.

Subsequent modifications to the amine component of the phosphoramidites also produced promising outcomes. Ligands incorporating amines with moderately bulky alkyl groups (*e.g*. isopropyl or larger) consistently resulted in high diastereomeric ratios, simplifying ligand synthesis by avoiding crystallization steps. For instance, ligands **L42**–**L50** were obtained as single diastereomers, reinforcing the importance of steric considerations in both the BINOL and amine components.

These findings establish a robust framework for the efficient exploration of this underexplored ligand space. Future ligand development could involve synthesizing ligands with novel amines or more complex BINOL backbone modifications, such as additional sp^3-alkyl groups or sterically demanding substituents. Notably, combining silane-modified BINOL scaffolds with diverse amine groups presents an opportunity to achieve high diastereoselectivity across a broader ligand set.

The performance of the synthesized ligands was evaluated in the ACA reactions yielding **4a** and **5a**. In the case of **4a**, none of the tested ligands outperformed the benchmark

ligand **L22S**, despite the synthetic advantages conferred by their high diastereomeric purity. The TMS-substituted ligand **L28S**, although displaying a modest enantiomeric excess (83% ee), did not achieve the desired conversion levels (32% yield). Further optimization—for example, pairing TMS-substituted BINOL backbones with alternative amines—may enhance performance to levels comparable to **L22S**.

Conversely, the ACA reaction yielding **5a** exhibited more favourable outcomes. Several ligands, particularly **L47** and **L48**, achieved enantioselectivities comparable to **L22S** (93% ee) while offering significant synthetic simplicity. These ligands were synthesized with exceptional diastereomeric ratios (>20:1), circumventing the bottleneck of sequential crystallization inherent to **L22S**. This highlights the potential of **L47** and **L48** as highly accessible and efficient alternatives for ACA reactions.

Key future directions involve further exploration of **L47** and **L48** to assess their broader applicability across diverse substrates and reaction types (Figure 3.12).

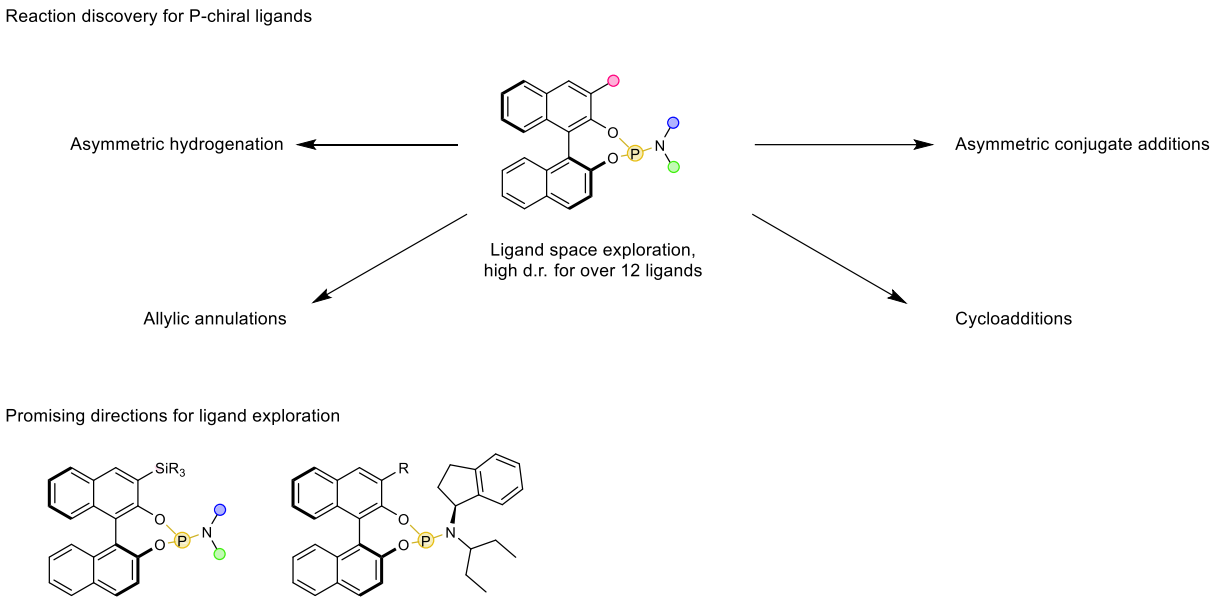

Figure 3.12: Reaction discovery and possible further directions on ligand exploration.

Moreover, applying the newly developed ligands to challenging ACA reactions and related transformations—particularly those that conventionally require disubstituted phosphoramidites—holds the potential to enhance performance across various systems. Notably, the reactions previously illustrated in Figure 3.2 present ideal candidates for evaluation. These transformations, known for their reliance on disubstituted

phosphoramidites, still leave room for improvement despite yielding promising outcomes. P-chiral ligands may offer improved results in these cases, particularly for challenging substrates which offer further opportunities for improvement.

Testing these ligands in other catalytic transformations, such as allylic substitutions or asymmetric hydrogenations, may further demonstrate their versatility. By establishing a systematic approach to ligand exploration, this work provides a foundation for advancing ligand design and reaction discovery. Overall, development of synthetically accessible P-chiral ligands with high diastereomeric purity opens new pathways for catalytic applications.

3.7. References:

1. J. Clayden, N. Greeves, and S. Warren, in *Organic Chemistry*, 2nd ed., Oxford University Press, Oxford, 2023, pp. 360–397.
2. V. K. Yadav, in *Steric and Stereoelectronic Effects in Organic Chemistry*, 2nd ed., Springer, Cham, Switzerland, 2021.
3. R. Ardkhean, S. P. Fletcher, and R. S. Paton, in *Ligand Design for Asymmetric Catalysis: Combining Mechanistic and Chemoinformatics Approaches*, Chapter 10, *New Directions in the Modeling of Organometallic Reactions*, Springer, Cham, Switzerland, 2020, pp. 153–190.
4. D. J. Durand and N. Fey, *Chem. Rev.*, 2019, **119**, 6561–6594.
5. P. M. C. Roth and S. P. Fletcher, *Org. Lett.*, 2015, **17**, 912–915.
6. C. Hansch, P. P. Maloney, T. Fujita, and R. M. Muir, *Nature*, 1962, **194**, 178–180.
7. J. B. van der Linden, E.-J. Ras, S. M. Hooijschuur, G. M. Klaus, N. T. Luchters, P. Dani, G. Verspui, A. A. Smith, E. W. P. Damen, B. McKay, and M. Hoogenraad, *QSAR Comb. Sci.*, 2005, **24**, 94–98.
8. S. Mazurek, T. R. Ward, and M. Novič, *Mol. Divers.*, 2007, **11**, 141–152.
9. A. Milo, A. J. Neel, F. D. Toste, and M. S. Sigman, *Science*, 2015, **347**, 737–743.
10. K. C. Harper, E. N. Bess, and M. S. Sigman, *Nat. Chem.*, 2012, **4**, 366–374.
11. M. S. Sigman, K. C. Harper, E. N. Bess, and A. Milo, *Acc. Chem. Res.*, 2016, **49**, 1292–1301.
12. R. Ardkhean, M. Mortimore, R. S. Paton, and S. P. Fletcher, *Chem. Sci.*, 2018, **9**, 2628–2632.
13. Q. Peng, F. Duarte, and R. S. Paton, *Chem. Soc. Rev.*, 2016, **45**, 6093–6107.
14. A. V. Brethomé, S. P. Fletcher, and R. S. Paton, *ACS Catal.*, 2019, **9**, 2313–2323.
15. A. V. Brethomé, R. S. Paton, and S. P. Fletcher, *ACS Catal.*, 2019, **9**, 7179–7187.
16. A. Brethomé, *A Physical-Organic Approach to Asymmetric Catalysis: Design and Synthesis of Chiral Ligands Using Multivariate Modelling*, Doctoral Thesis, University of Oxford, Wolfson College, Michaelmas 2019.
17. T. Hammerer, W. Leitner, and G. Franciò, *ChemCatChem*, 2015, **7**, 1583–1592.
18. T. M. Beck and B. Breit, *Angew. Chem. Int. Ed.*, 2017, **56**, 1903–1907.
19. J. F. Teichert and B. L. Feringa, *Angew. Chem. Int. Ed. Engl.*, 2010, **49**, 2486–2528.
20. A. H. M. De Vries, A. Meetsma, and B. L. Feringa, *Angew. Chem. Int. Ed.*, 1996, **35**, 2374–2376.

21. C.-X. Zhuo, C. Zheng, S.-L. You, *Acc. Chem. Res.* **2014**, *47*, 2558–2573.
22. C. Recsei and C. S. P. McErlean, *Tetrahedron*, 2012, **68**, 464–480.
23. Z. Chu, Z. Tang, K. Zhang, L. Wang, W. Li, H.-H. Wu, and J. Zhang, *Organometallics*, 2019, **38**, 4036–4042.
24. W. Zhao, T. Wang, R. Zhao, H. Xie, and L. Liu, *Tetrahedron: Asymmetry*, 2016, **27**, 157–162.
25. I. Alonso, B. Trillo, F. López, S. Montserrat, G. Ujaque, L. Castedo, A. Lledós, and J. L. Mascareñas, *J. Am. Chem. Soc.*, 2009, **131**, 13020–13030.
26. Z. Gao, J. Liu, H. Huang, H. Geng, and M. Chang, *Angew. Chem. Int. Ed.*, 2021, **60**, 27307–27311.
27. Q. Yuan, D. Liu, and W. Zhang, *Org. Lett.*, 2017, **19**, 1144–1147.
28. R.-D. Gao, L. Ding, C. Zheng, L.-X. Dai, and S.-L. You, *Org. Lett.*, 2018, **20**, 748–751.
29. R. Hoen, J. A. F. Boogers, H. Bernsmann, A. J. Minnaard, A. Meetsma, T. D. Tiemersma-Wegman, A. H. M. de Vries, J. G. de Vries, and B. L. Feringa, *Angew. Chem. Int. Ed.*, 2005, **44**, 4209–4212.
30. S. Li, Q. Chen, X. Xie, J. Yang, and J. Zhang, *Org. Lett.*, 2021, **23**, 7824–7828.
31. M. T. Reetz, J.-A. Ma, and R. Goddard, *Angew. Chem. Int. Ed.*, 2005, **44**, 412–415.
32. B. M. Trost, D. A. Bringley, and S. M. Silverman, *J. Am. Chem. Soc.*, 2011, **133**, 7664–7667.
33. K. N. Gavrilova, I. V. Chuchelkina, V. M. Trunina, I. D. Firsin, Y. P. Bityak, D. A. Fedorov, V. S. Zimarev, and N. S. Goulioukin, *Russ. J. Gen. Chem.*, 2022, **92**, 2612–2619.
34. K. N. Gavrilov, S. V. Zheglov, I. M. Novikov, I. V. Chuchelkin, V. K. Gavrilov, V. V. Lugovsky, and I. A. Zamilatskov, *Russ. Chem. Bull. Int. Ed.*, 2015, **64**, 1595–1601.
35. X. Xiong, T. Zheng, X. Wang, Y.-L. S. Tse, and Y.-Y. Yeung, *Chem*, 2020, **6**, 919–932.
36. B. Cordero, V. Gómez, A. E. Platero-Prats, M. Revés, J. Echeverría, E. Cremades, F. Barragán, and S. Alvarez, *Dalton Trans.*, 2008, **2832**–2838.
37. F. H. Allen, O. Kennard, D. G. Watson, L. Brammer, A. G. Orpen, and R. Taylor, *J. Chem. Soc., Perkin Trans. 2*, 1987, S1–S19.
38. J. R. Hwu and N. Wang, *Chem. Rev.*, 1989, **89**, 1599–1615.
39. P. Thangsan, T. Rukkijakan, B. Thanaussavadate, K. Yiamsawat, J. Sirijaraensre, K. P. Gable, and P. Chuawong, *Org. Biomol. Chem.*, 2023, **21**, 1501–1503.
40. J. C. Sancho-García and J. Cornil, *J. Chem. Theory Comput.*, 2005, **1**, 581–589.

41. M. K. Dahlgren, P. Schyman, J. Tirado-Rives, W. L. Jorgensen, *J. Chem. Inf. Model.* **2013**, *53*, 1191–1199.
42. S. Sitha, *Phys. Chem. Chem. Phys.* **2022**, *21*, 13110–13118.
43. A. Gamba, E. Rusconi, and M. Simonetta, *Tetrahedron*, 1969, **26**, 871–877.
44. A. Almenningen, S. J. Cyvin, O. Bastiansen, L. Fernholt, S. Samdal, and B. N. Cyvin, *J. Mol. Struct.*, 1985, **128**, 59–70.
45. M.-H. Hao, O. Haq, and I. Muegge, *J. Chem. Inf. Model.*, 2007, **47**, 2242–2252.
46. N. L. Allinger, in *Molecular Structure: Understanding Steric and Electronic Effects from Molecular Mechanics*, John Wiley & Sons, New Jersey, 2010, pp. 246.
47. A. R. Campanelli and A. Domenicano, *Struct. Chem.*, 2013, **24**, 867–876.
48. R. Zimmermann, C. Weickhardt, U. Boesl, and E. W. Schlag, *J. Mol. Struct.*, 1994, **327**, 81–97.
49. S. M. Gutiérrez Sanfeliciano and J. M. Schaus, *PLOS ONE*, 2018, **13**, 1–21.
50. N. L. Allinger, in *Molecular Structure: Understanding Steric and Electronic Effects from Molecular Mechanics*, John Wiley & Sons, New Jersey, 2010, pp. 43–47.
51. J. F. Teichert and B. L. Feringa, *Angew. Chem. Int. Ed.*, 2010, **49**, 2486–2528.
52. M. Žabka, L. Naviri, and R. M. Gschwind, *Angew. Chem. Int. Ed.*, 2021, **60**, 25832–25838.
53. R. Kučera, F. W. Goetzke, and S. P. Fletcher, *Org. Lett.*, 2020, **22**, 2991–2994.
54. R. Ardkhean, P. M. C. Roth, R. M. Maksymowicz, A. Curran, Q. Peng, R. S. Paton, and S.P. Fletcher, *ACS Catal.*, 2017, **7**, 6729–6737.

Chapter 4:

Diastereomeric synthesis strategies for the P-stereogenic ligand **L22s**

4.1 Phosphorous, a brief introduction

Phosphorus occupies a critical position in Group 15 of the periodic table, sharing the group with nitrogen, arsenic, antimony, and bismuth. Phosphorus, sitting below nitrogen, demonstrates properties that both parallel and deviate from its lighter counterpart.[1]

A key distinction between nitrogen and phosphorus lies in their respective barriers to inversion (Figure 4.1). Nitrogen compounds often exhibit lower inversion barriers, a characteristic tied to its smaller size, stronger orbital overlap (between nitrogen and other atoms), and more directional bonding. For example, the N–H bonds in ammonia are relatively short and strong due to efficient sp^3 hybridization, contributing to easier rotation around the nitrogen centre.

In contrast, in phosphine, phosphorus's larger atomic size leads to weaker orbital interactions and longer P–H bonds. Additionally, phosphorus often exhibits less pronounced hybridization, with its lone pair occupying a nearly pure 3p orbital rather than being fully integrated into sp^3 hybridized orbitals. This results in increased lone-pair repulsion and steric hindrance, raising the energy barrier for inversion in phosphine compared to ammonia. When compared, the frequency to inversion for PH_3 is 4000 times lower than for NH_3. Due to this difference in levels of hybridization, nitrogen and phosphorous compounds also have different angles. While nitrogen compounds, such as ammonia, exhibit angles closer to 107°, while phosphorous compounds, such as phosphine have lower angles (~93.5°).[2]

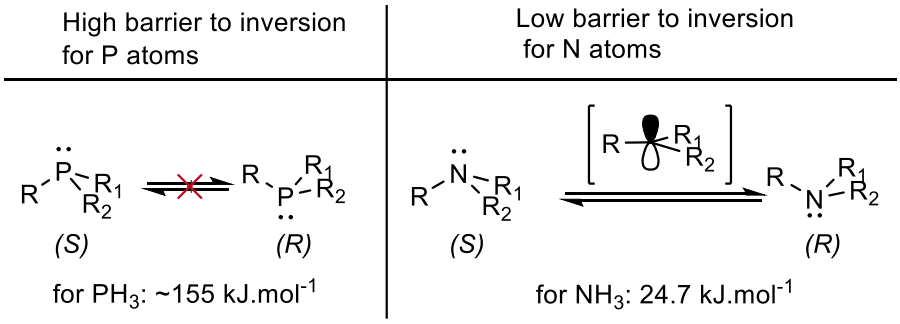

Figure 4.1: Difference between barriers of inversion of phosphines (left) and tertiary amines (right) showcasing the barriers to inversion of PH_3 and NH_3.

The high inversion barriers in phosphorus have significant stereochemical consequences. For compounds containing a P-stereocenter (P-chiral), the higher rotational barrier ensures configurational stability, making it possible to isolate enantiomers. These stereoisomers can be subject to high temperatures without any noticeable P-center inversion. Conversely, the low barrier to inversion in tertiary amines leads to rapid interconversion between configurations (even at room temperature), eventually leading to racemization of the N-centre.

4.2 Introduction to P-stereogenic compounds

P-stereogenic compounds are a specialized class of chiral molecules containing a stereogenic phosphorus atom, a feature that gives them unique structural and functional properties. The term "P-stereogenic" is more encompassing than "P-chiral," as it can also refer to achiral geometric isomers, such as phosphaalkenes, which display stereogenicity through different substituent configurations (*Z* and *E*). These compounds have gained prominence due to their versatility in catalysis,[3,4] materials science,[5,6] agrochemistry,[7] and pharmaceuticals.[8] The growing interest in these compounds can be attributed to their ability to act as chiral ligands, catalysts, and biologically active molecules.[9]

Pioneering Work

The field of P-stereogenic compounds was first significantly advanced by Knowles and Horner, who explored the use of chiral phosphines in catalytic hydrogenations in the 1960s and 1970s (Figure 4.2).[10,11] This work laid the foundation for using P-stereogenic ligands in a wide range of metal-catalysed asymmetric reactions and lead to Knowles earning part of the 2001 Nobel prize in chemistry, for its work in asymmetric hydrogenations.[12] The phosphine enantiomer (**L4A**) was successfully obtained via fractional crystallisation of the racemic mixture.[13] Since these discoveries, research has expanded to develop structurally diverse P-stereogenic ligands (Figure 4.3), which have become standard in the toolkit of asymmetric synthesis.

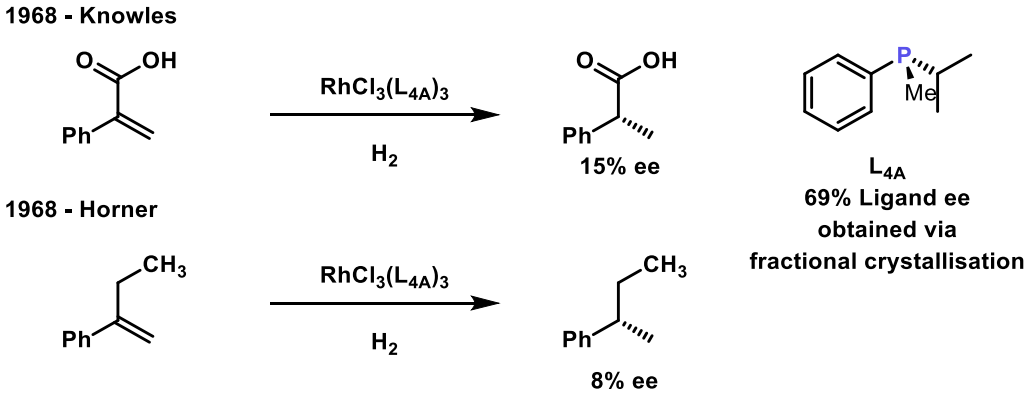

Figure 4.2: First instances of P-chiral ligands in Asymmetric Hydrogenation.

P-chiral compounds are present in medicines and natural compounds, with Phosmidosine and Remdesivir (Figure 4.3A) as representatives of each class. Phosmidosine is a naturally occurring compound originally isolated from a strain of Streptomyces bacteria. Recently, it has been of interest due to its potential anticancer and antiproliferative abilities.[14,15]

Remdesivir, on the other hand, is a broad-spectrum antiviral medication which had gained prominence during the COVID-19 pandemic as one of the first treatments to be authorized for emergency use in hospitalized patients. While studies showed mixed results,[16] it had achieved some success in certain patients, underscoring the drug as a significant tool in antiviral therapy.[17]

P-stereogenic ligands in catalysis

Following Knowles' and Horner's seminal work, P-stereogenic phosphines have become widely used as chiral ligands in asymmetric catalysis (Figure 4.3B). Their stereogenic phosphorus centre allows for fine-tuning of the electronic and specially the steric environment around the metal catalyst, thereby enhancing enantioselectivity. One notable example is the use of DIPAMP, a P-stereogenic ligand that was critical in the first large-scale industrial synthesis of L-DOPA.[18,19] Other examples include trichickenfootphos and SIP. Both ligands, containing a considerably different structure are effective for very distinct reactions. While trichickenfootphos has been used successfully in Asymmetric Hydrogenation,[20] SIP has found great success in [2+2+2] intramolecular cycloadditons.[21]

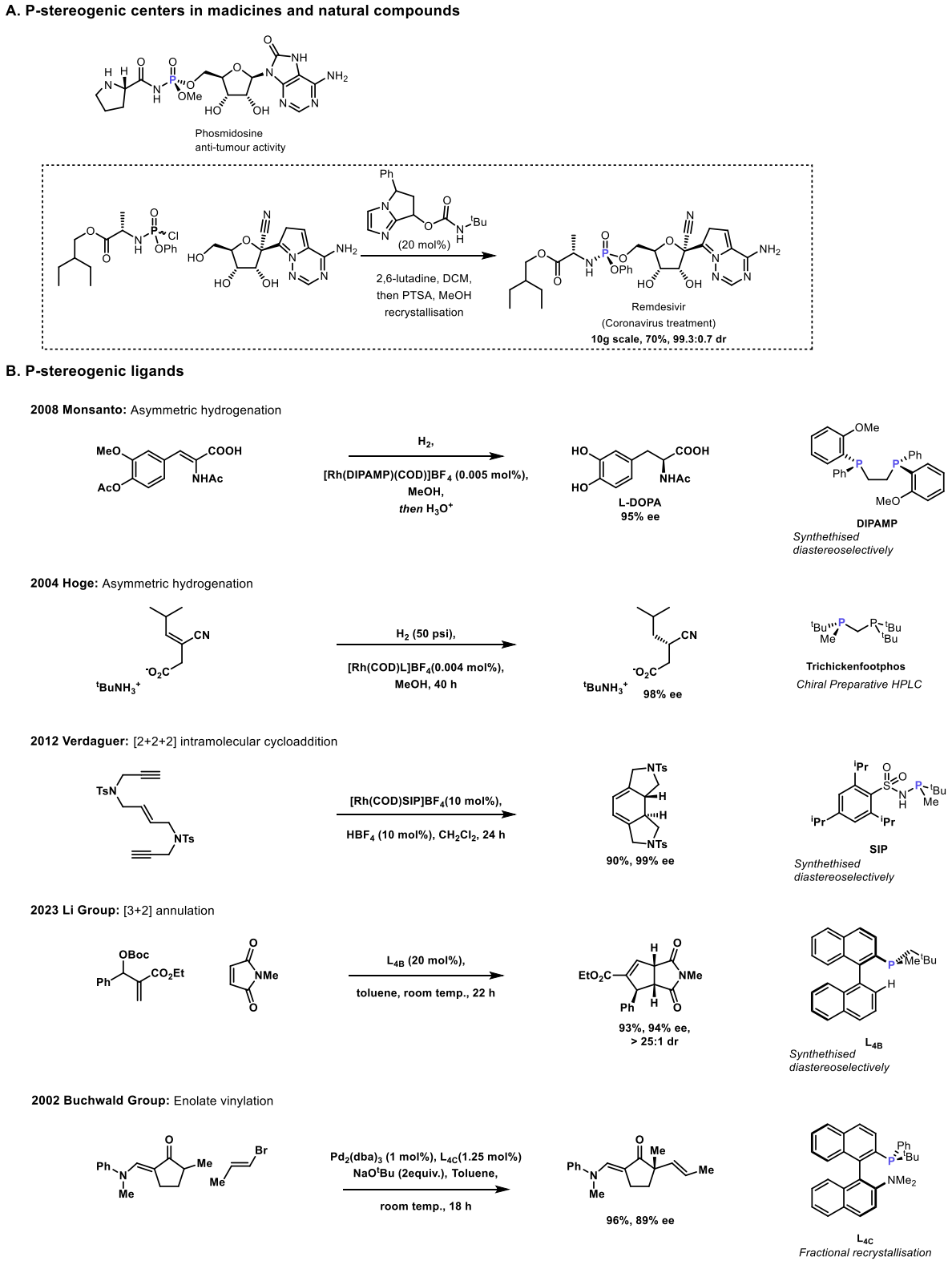

Figure 4.3: Different molecules containing P-stereogenic centres **A**. Natural products and drugs. **B**. Ligands and their uses in asymmetric catalysis.

P-stereogenic ligands such as those synthesised by the Buchwald and the Li Group feature both axial- and P-chirality and have been successfully applied in enolate vinylation[22] and [3+2] annulation,[23] respectively. These ligands often exhibit high enantioselectivities and

broad substrate scope, making them valuable tools in both academic and industrial settings.[24]

The stereoselective synthesis of P-stereogenic compounds is challenging due to the need for precise control over the configuration at the phosphorus centre. Traditional methods have relied on resolving racemic mixtures or using chiral auxiliaries.

For example, camphor and *trans*-(+)-limonene oxide have been employed as chiral auxiliaries to introduce stereogenicity at phosphorus. However, these methods often suffer from low atom economy, require extensive purification steps, and of course limit the overall yield to 50% in the case where only one of the two isomers is desired. Many of the portrayed ligands have been successfully resolved via fractional crystallisation (**L4A**, **L4C**)[13,22] or separated via preparative HPLC (Trichickenfootphos).[20]

In recent years, catalytic asymmetric strategies have gained traction due to their ability to produce enantiomerically enriched P-stereogenic compounds more efficiently.[25,26] Organocatalysis, has shown promise in dynamic kinetic resolutions and desymmetrisation reactions.[27]

For example, N-heterocyclic carbene (NHC)-catalysed desymmetrisation of bisphenol phosphine oxides has been used to generate P-stereogenic phosphinates with excellent enantioselectivity. This desymmetrisation strategy is often used to synthetise a precursor to DIPAMP.[28]

Other strategies successfully apply dynamic kinetic resolution (DKR) to obtain P-chiral products from a racemic mixture. This transformation is employed in the synthesis of Remdesivir (Figure 4.3a) and the structurally similar molecule Uprifosbuvir.[24,29]

In tandem with those methodologies, transition-metal catalysis also plays a central role in the synthesis of P-stereogenic molecules. The use of palladium and nickel catalysts for enantioselective C–P bond formation has enabled the creation of P-stereogenic phosphines and phosphine oxides with high diastereo- and enantioselectivities. Notably, palladium-catalysed C–P cross-coupling reactions have been employed by the Feringa group in 2022 to transfer axial chirality from a BINOL auxiliary to the phosphorus centre, achieving excellent stereocontrol (Figure 4.4).[30]

Alternatively, in 2018 Cramer successfully designed an iridium catalysed C-H arylation reactions where a non-chiral P(V) species can be transformed into a P-chiral compound, achieving high levels of both point and axial chirality with one single step.[31]

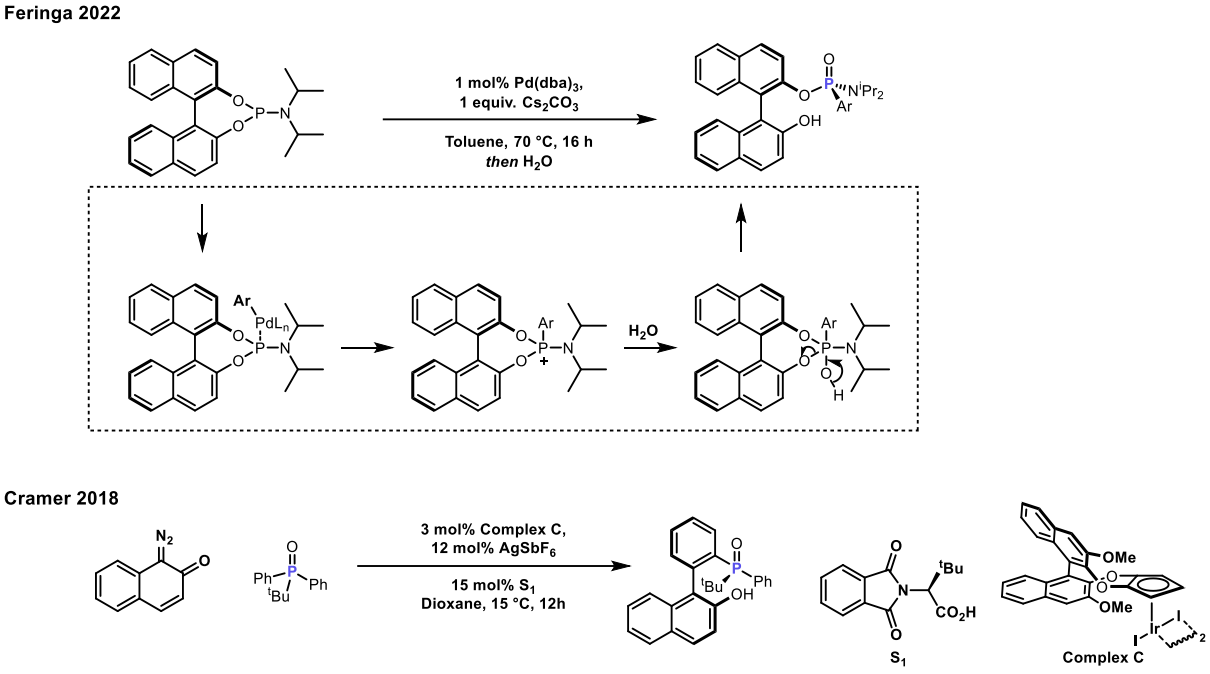

Figure 4.4: Advances in enantioselecive and disatereoselective synthesis of P-stereogenic small molecules.

P-chiral phosphoramidites

As discussed in previous chapters, the synthesis of enantioenriched molecules is a cornerstone of modern organic chemistry and lately, P-chiral ligands have played a pivotal role in this pursuit. Among these, phosphoramidites, which have been recognized for their versatility and ease of modification, stand out as promising candidates. Phosphoramidites are compounds defined by featuring a trivalent phosphorus atom bonded to an amino group (–NR_2), and two alkoxy groups (–OR), typically represented as P(OR)(NR_2)(OR'). These compounds are often synthesized via a phosphoramidation reaction. A transformation which involves the coupling of a secondary amine to a di-alcohol (typically a BINOL) by utilizing a highly electrophilic phosphorous species.

Over the past 15 years, P-chiral phosphoramidites have emerged as a distinct subclass, with limited but notable examples demonstrating their potential in challenging asymmetric reactions such as hydrogenations and conjugate additions (ACAs).[32,33]

While phosphoramidites are useful ligands across various transformations, their unique structure introduces limitations. Unlike P-chiral phosphines and phosphine oxides, which benefit from relatively straightforward oxidation and reduction between P(III) and P(V) states, phosphoramidites lack this advantage.[34-36] The reduction of phosphoramidites from P(V) to P(III) often results in their complete destruction due to harsh reaction conditions. This instability likely stems from the weaker P–N bond compared to the more robust P–C bonds, making phosphoramidites particularly susceptible to degradation under certain conditions.

The Feringa group has demonstrated the vulnerability of phosphoramidites in a diastereoselective reaction (Figure 4.4). Here, mild conditions akin to those in a Suzuki-Miyaura coupling, combined with the presence of water, led to complete oxidation of the P(III) phosphoramidite compound.[30] Such sensitivity poses a significant obstacle to the discovery and development of P-chiral phosphoramidites via stereoselective transformations. Despite these challenges, limited examples exist in literature where groups have developed these ligands for a range of challenging asymmetric reactions.

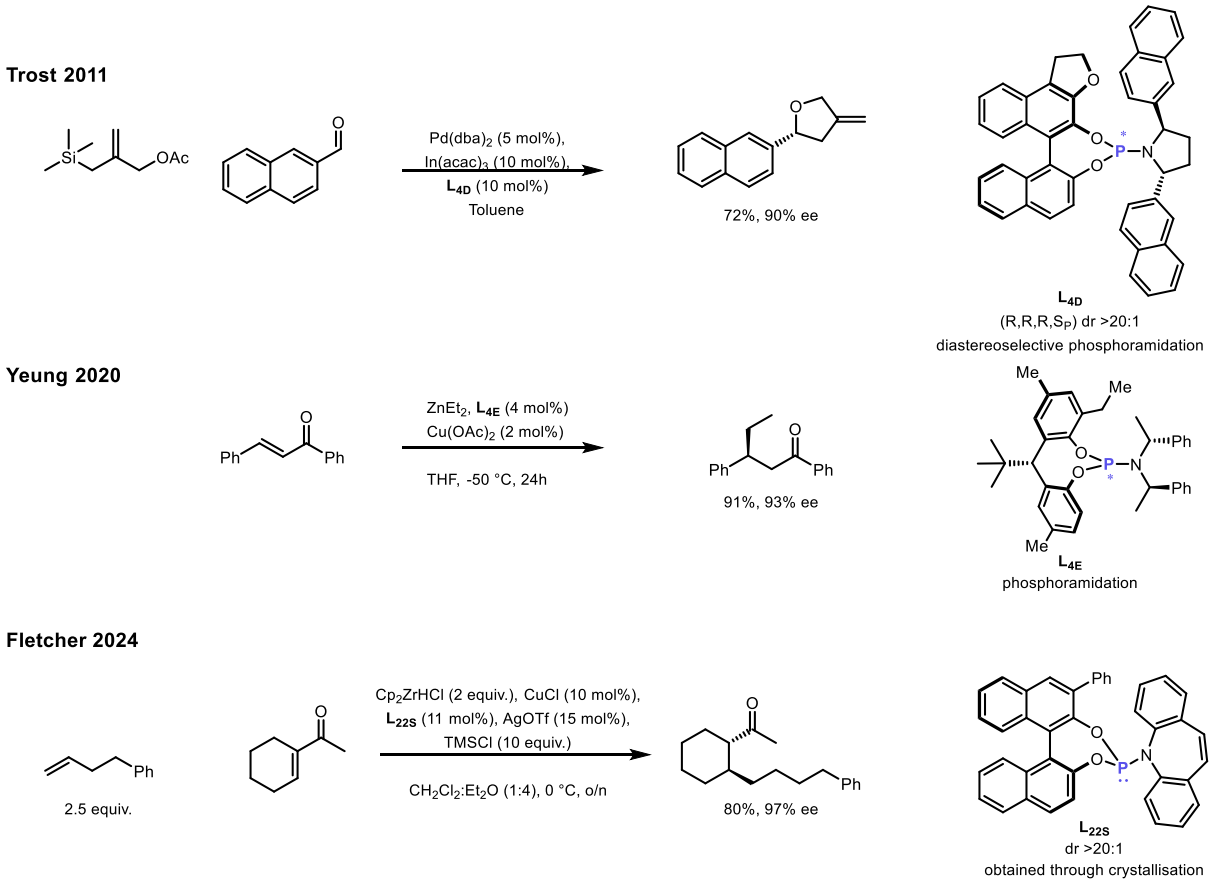

Figure 4.5: Uses of P-stereogenic phoshporamidites in asymmetric catalysis.

As seen on Figure 4.5, in 2001, the Trost group developed a palladium-catalyzed [3+2] cycloaddition of trimethylenemethane (TMM) with aldehydes. This transformation represents a direct and efficient route to chiral tetrahydrofurans, structures prevalent in both natural and synthetic compounds.[37,38] Central to this process is the employment of a P-chiral phosphoramidite ligand, synthesized diastereoselectively through phosphoramidation (*R,R,R,S*$_P$, dr >20:1). Under optimized conditions, the reaction affords the desired cycloadduct in 72% yield with an enantiomeric excess of 90%.[37]

Another example, reported by the Yeung group, highlights an ACA targeting a challenging linear substrate (Figure 4.5). This Cu(I)-catalyzed process relies on $ZnEt_2$ as a nucleophilic reagent and a P-chiral phosphoramidite ligand. Notably, the ligand in this example is also synthesized via phosphoramidation, though the diastereomeric ratio (dr) of the process is unspecified. The reaction proceeds delivering the product in 91% yield and 93% ee.[39]

Another example, contributed by the Fletcher group, focuses on the ACA of exocyclic α,β-unsaturated ketones. As discussed in Chapter 2, these are particularly challenging substrates. The reaction employs a Zr/Cu(I) catalyst system and a P-chiral phosphoramidite ligand. Unlike the ligands in the previous examples, the ligand high diastereomeric purity (>20:1 dr) is achieved through fractional crystallization, allowing for the selective isolation of the active diastereomer. The product of the ACA is obtained in 80% yield and 97% ee.

Unfortunately, crystallisation as a strategy to obtain P-chiral phosphoramidites has its downsides. Unlike in diastereselective processes, **L$_{22S}$** is initially obtained as a 1:1 mixture of diastereomers, from which it then must be purified. This process has low atom economy as one diastereomer (*S,R*$_P$) is poorly selective in the reaction (35 ee%). Furthermore, the crystallisation process can be unreliable, time-consuming and low yielding.

4.3 Project objectives:

The aim of this chapter is to develop a diastereoselective strategy for the P-chiral phosphoramidite ligand **L22S**. This ligand is crucial for the asymmetric conjugate addition of exocyclic substrates but presents significant challenges in its synthesis. Current methods, such as crystallization and preparative SFC, are inefficient, time-consuming, and exhibit low atom economy.

4.4. Diastereoselective approaches

4.4.1. Strategy I: Substituted BINOLs followed by cross-couplings

Previous work by Reetz et al. successfully demonstrated that mono-substituted/P-chiral phosphoramidites can be prepared diastereospecifically.[40] They achieved these results by utilizing a trimethylsilyl (TMS)-substituted BINOL component in the phosphoramidation step (Figure 4.6A). Comparatively, as shown in Chapter 2, a similar phosphoramidation utilizing phenyl substituted BINOLs yields a 1:1 mixture of **L22** (Figure 4.6B).

We hypothesized that steric effects played a key role in this outcome, as the TMS group is significantly bulkier in three dimensions compared to the flat, planar structure of an sp^2 phenyl ring. This bulkiness would create greater steric hindrance around one of the hydroxyl groups of BINOL, particularly during phosphoramidation. As a result, the electrophile is less likely to approach the hydroxyl group shielded by the TMS group, favoring reaction at the non-covered hydroxyl group. This selective interaction minimizes steric clashes between the substituent at the 3-position and the electrophilic phosphorus atom, thereby influencing diastereoselectivity. This hypothesis is followed by extensive ligand screenings and insights on biaryl conformations (Chapter 3).

With this rationale, we strategized that by introducing bulky, yet labile or easily converted substituents to the BINOL framework, we could manipulate the diastereomeric ratio (dr) obtained after phosphoramidation. The resultant phosphoramidite could then undergo a transformation, such as a cross-coupling reaction with a phenyl substrate, yielding **L22S** while preserving the previously achieved diastereomeric ratio (Figure 4.6C).

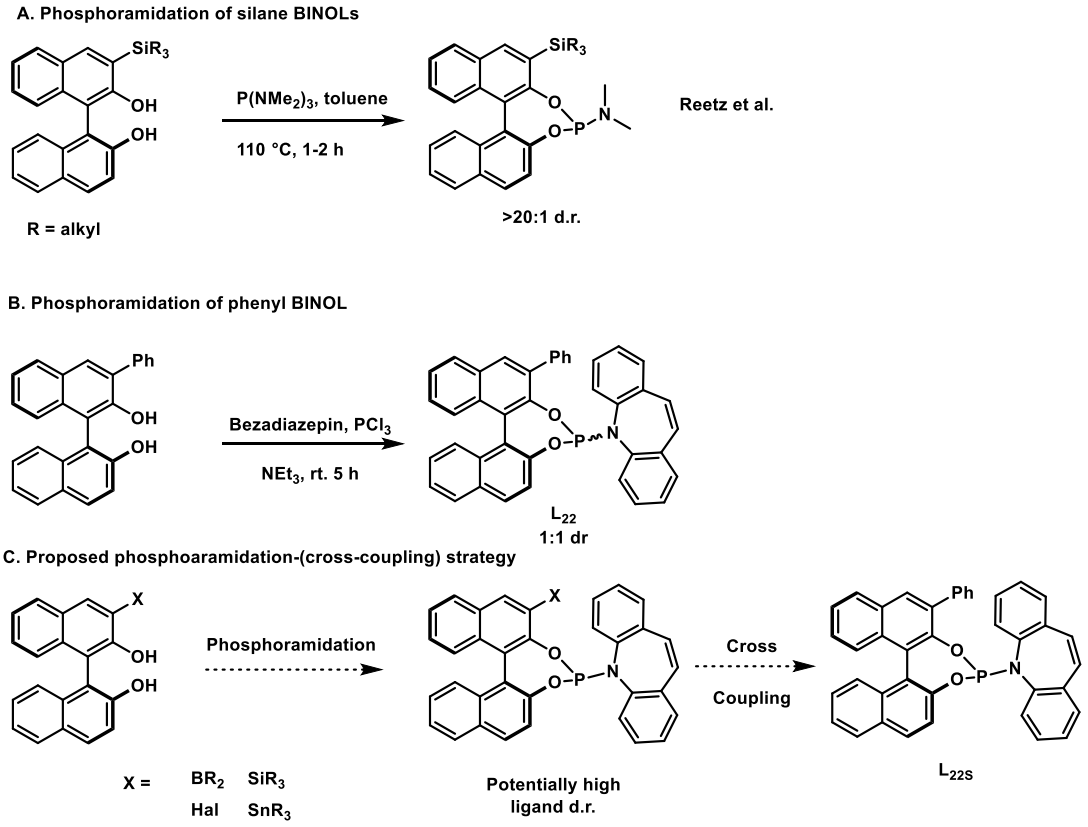

Figure 4.6: A. Example shown by the Reetz group, obtaining silane phosphoramidites in high dr. **B**. Standard phosphoramidation forming **L22** with a low dr. **C**. Strategy involving phosphoramidation on substituted BINOLs followed by cross-coupling, aiming to get **L22S** at a high diastereomeric ratio.

1.Utilizing the Suzuki-Miyaura cross-coupling reaction:

A traditional Suzuki-Miyaura cross coupling forms a C-C (sp^2-sp^2) bond out of two substituents, one containing a halogen, the other, a boronic acid or ester.[41-43] We attempted to explore both options, synthesising: 1. a 3-halogen-BINOL, which would react with phenylboronic acid. And 2. A set of boronic acid/ester substituted BINOLs, which would react with iodo-benzene.

Halogen-substituted BINOLs

The first ligands synthesized were halogen-substituted P-chiral phosphoramidites, primarily because halogenated BINOLs were already explored as intermediates to phenyl-substituted BINOLs. Both bromine- and iodine-substituted P-chiral ligands were obtained without major complications. However, as previously discussed in Chapter 3, these ligands were not synthesized with exceptional diastereomeric ratios. Both

exhibited a poor dr of 1:1.1, slightly favouring the undesired diastereomer (Figure 4.7). Since halogens are not very bulky, it stands to reason that the diastereomeric ratio of the ligand remained largely unaffected. Since the diastereomeric ratio of these ligands is not any better than **L22** we chose not to proceed with the cross-coupling reaction.

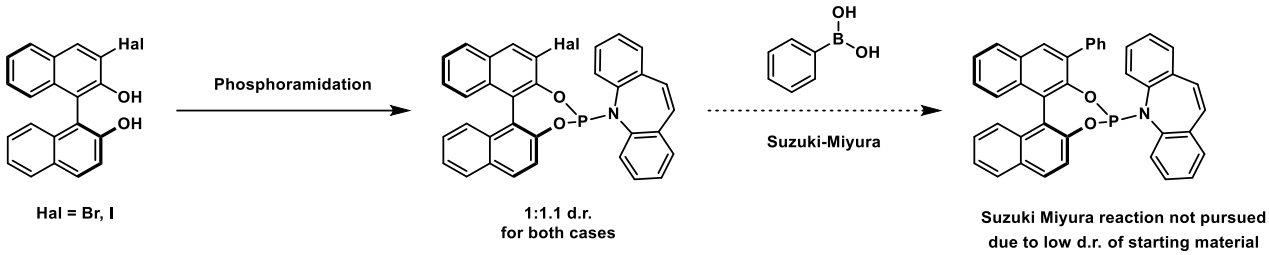

Figure 4.7: Attempting the phosphoramidation/cross-coupling strategy on mono-halogenated BINOLs.

Borane-substituted BINOLs

The synthesis of borane-substituted BINOLs was initially simple and straightforward. These molecules were synthesized via lithium-borylation of MOM-protected BINOL, yielding various boron-containing groups such as boronic acids, boronic pinacol esters, and boronic MIDA esters. Unfortunately, during the removal of the MOM protecting groups from the BINOL, the pinacol ester moiety was cleaved, resulting in the formation of mono-boronic acid BINOLs (Figure 4.8).

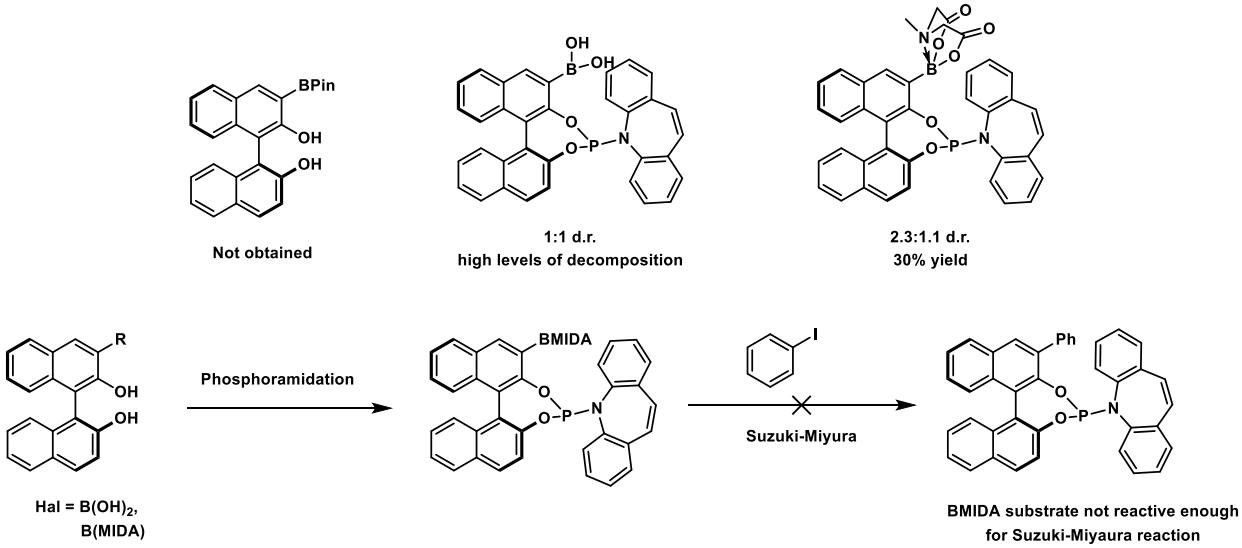

Figure 4.8: Attempting the phosphoramidation/cross-coupling strategy with monoborylated BINOLs.

After phosphoramidation, the diastereomeric ratio of the boronic acid phosphoramidite was unimpressive, and the yields were considerably low (~1:1 dr, 20% yield). Interestingly, the BMIDA ester phosphoramidite did achieve a favourable, albeit modest, diastereoselectivity toward the desired diastereomer, with a dr of approximately 2.3:1. Nevertheless, this phsohporamidite was not reactive enough to achieve a Suzuki-Miyaura transformation under mild conditions.

2. Silane substituted BINOLs

Aside from the vastly explored Suzuki-Miyaura reaction, there are other numerous cross-coupling reactions that have seen great success in literature. The Negishi, Murahashi and Kumada cross couplings are some examples of sp^2-sp^2 reactions that could be employed in a simple catalytic system.[44-46] Unfortunately, all these reactions necessitate reactive and often unstable groups that would likely interact negatively in the phosphoramidation stage (aryl zincs, aryl lithiums, and Grignards respectively).

Instead of these reactions we considered using a Hiyama cross-coupling approach. The advantage of this reaction is that it works under considerably mild conditions when employing silane esters, notoriously bulky groups.[47-49] We hoped that this would induce diastereoselectivity as it was previously seen in literature.

The synthesis of simple BINOL-silane derivatives was straightforward. Common silanes such as trimethylsilyl (TMS) and triisopropylsilyl (TIPS) groups were introduced into the BINOL framework via lithium-silylation of MOM-protected BINOL (Figure 4.9). These groups were sufficiently robust to remain attached to the BINOL after MOM deprotection. Subsequent phosphoramidation successfully yielded only the desired diastereomer, akin to the results obtained by the Reetz group.[40]

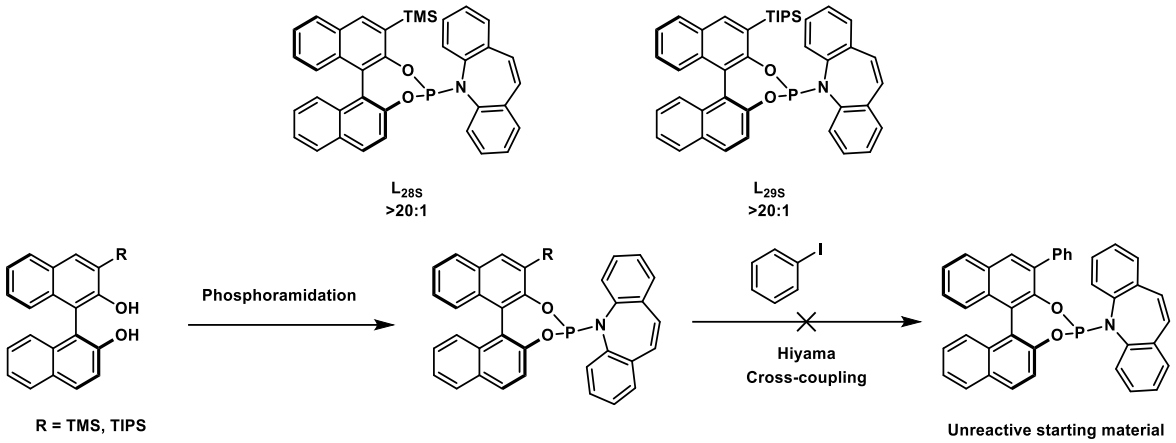

Figure 4.9: Attempting the phosphoramidation/cross-coupling strategy with mono-silene BINOLs.

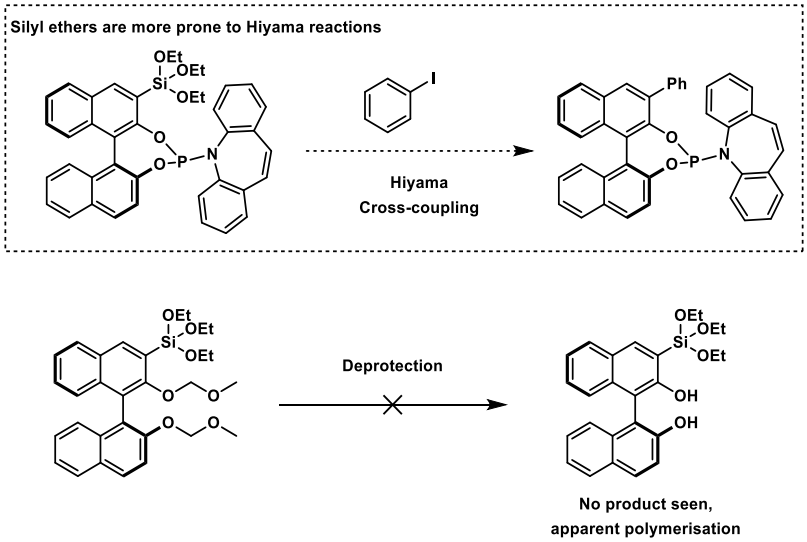

Figure 4.10: Attempting the strategy with silene ether BINOLs.

Unfortunately, these silane-substituted phosphoramidites were not reactive to mild Hiyama cross-coupling conditions to yield **L22S** (Figure 4.9 bottom). Harsh conditions were required—such as the use of fluoride salts and high temperatures—and the phosphoramidite degraded under such conditions. Attempts were made to synthesize more reactive groups, such as silyl ethers (e.g., triethoxysilane), which could react under milder Hiyama conditions (Figure 4.10)[50]. However, the synthesis proved challenging, as

the silane tended to polymerize when subjected to the mono-functionalisation conditions required for the MOM-protected BINOL.

3. Stannane substituted BINOLs

The final group tested was stannane-substituted BINOLs, chosen for their well-known lability in undergoing Stille cross-coupling reactions and their sp^3-hybridized bulkiness, which even surpasses that of silanes (Figure 4.11).[51,52] The addition of chlorotributyltin to a MOM-protected BINOL was straightforward, yielding the desired stannane in good yields. Unfortunately, the stannane moiety was unstable during the deprotection of the MOM groups. Several other protecting groups were tested—such as TBS, TMS, and benzyl groups—to preserve the tin-aryl bond, but to no avail. The stannane was unstable even under mild acidic conditions, such as diluted acetic acid. In some cases, these conditions would remove the stannane while leaving the hydroxyl protecting group intact. This instability, coupled with the practical complications associated with using organotin compounds, rendered this strategy unattractive.

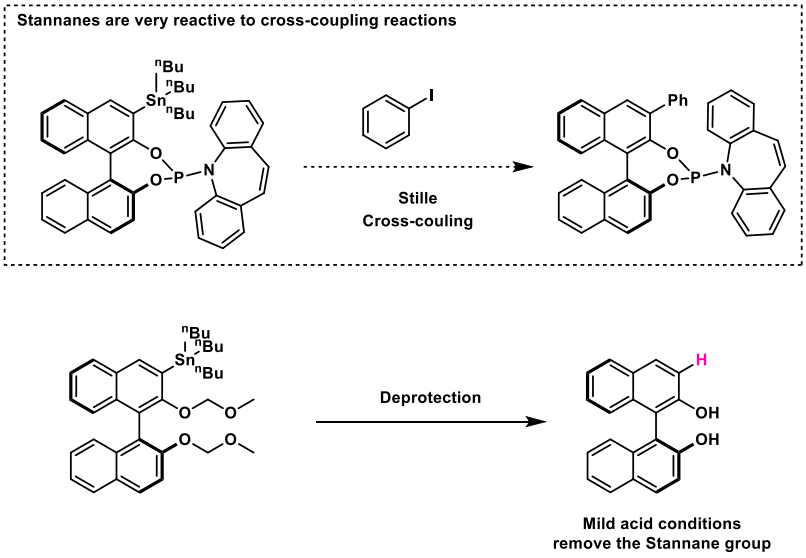

Figure 4.11: Attempting the strategy with mono-stannane substituted BINOLs.

Although these strategies were unsuccessful in producing **L22S** diastereoselectively, they did yield other useful ligands that have the potential to achieve high enantioinduction and reactivity in other transformations (See Chapter 3). Moreover, the silane-substituted examples are particularly interesting from an academic perspective, as they appear to generate exclusively the desired diastereomer of the ligand.

4.4.2. Strategy II: P-chirality as an auxiliary

With our initial strategy amiss, an alternative approach was attempted. We based this new approach in stereodifferentiation and the use of a P-handle.

Di-substituted phosphoramidites such as **L_{21}** (Figure 4.12A) are not P-chiral, unlike mono-substituted phosphoramidites. This is because the phosphorous atom in di-substituted phosphoramidites is always close to the same functional group type (phenyl). Thus, a C_2-rotation symmetry present in the molecule prevents the existence of P-chirality. This symmetry group is broken for mono-substituted phosphoramidites such as **L_{22S}** and **L_{22R}** since the groups are always different (Ph group compared to hydrogen). The orientation of the phosphorus atom is critical, as it defines the formation of a distinct P-stereocentre. This phenomenon is similarly observed in all di-substituted phosphoramidites bearing two different substituents (R_1 and R_2). It is key to note that even in simple same-group di-substituted phosphoramidites, which are not P-chiral, the two groups (R_1) will be in a different environment (Figure 4.12B). The (non-chiral) P atom would be pointing to one group (green R_1), subjecting it to a different environment to the other R_1 group (blue). These R_1 groups are diastereotopic and could allow for stereodifferentiation. Furthermore, due to the high ability of phosphorous molecules as ligands, the phosphorous pro-stereogenic centre in the molecule might act itself as an 'intrinsic auxiliary', coordinating with catalysts and thus directing the reactivity towards one specific site.

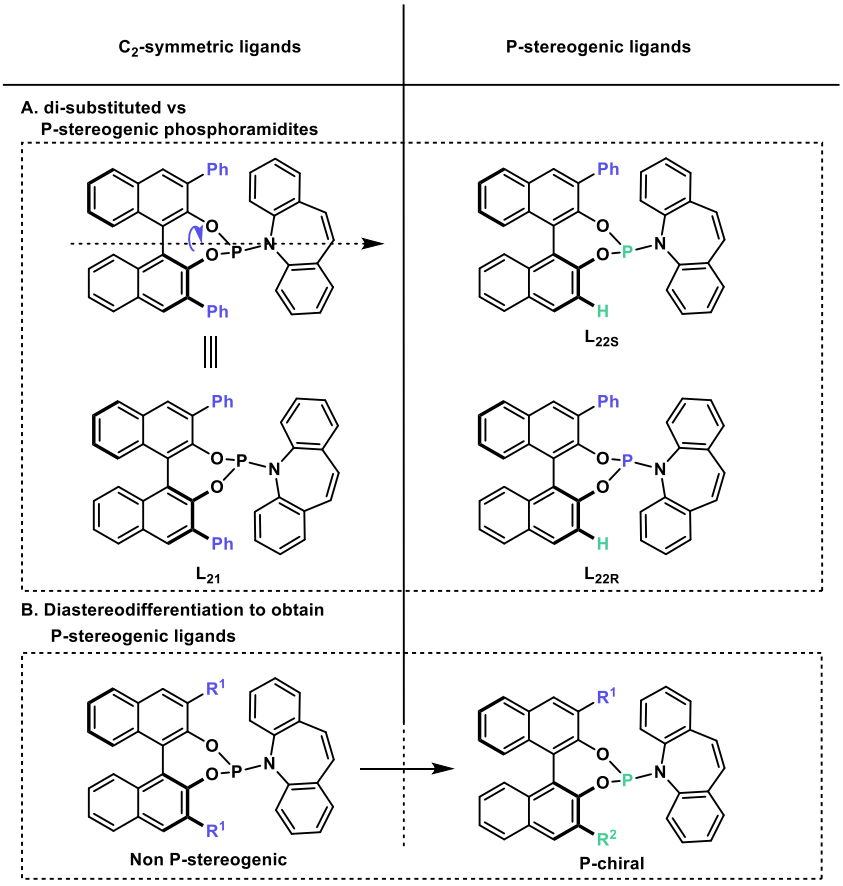

Figure 4.12: A. Showcasing the difference between C_2-symmetric phosphoramidities, such as **L21** (Left) and P-stereogenic phosphoramidites, such **L22S** and **L22R** (right). **B**. Possible translation from C_2-symmetric phosphoramidites to P-stereogenic phosphoramidites via reactive **R1** group.

We decided to adapt this strategy by synthesizing the di-halogenated phosphoramidite **L51**. The synthesis of this ligand was much more straightforward than its P-chiral counterpart. Firstly, due to it being di-functionalised, there is no possibility of over -functionalising the BINOL backbone at the beginning to the ligand synthesis. This is often a concern when making the mono-substituted BINOL variants. Secondly, due to it containing no P-stereocentre, we avoid the existence of diastereomers.

We hoped that because of this P-intrinsic auxiliary one iodine (blue) would behave differently when undergoing a chemical transformation, compared to the other (green) (Figure 4.13). We wanted to take advantage of this ability to generate the desired di-substituted diastereomer (*S,S*$_P$) and then remove the remaining halogen to obtain the desired mono-phenylated ligand **L22S**. We planned to do this by employing the Suzuki-Miyaura cross coupling reaction to insert a phenyl moiety diastereoselectively, forming **L52** in high diasteromeric ratio (Figure 4.13). This molecule, would then be subjected to a

de-halogenation reaction, removing the remaining halogen and resulting in **L22**, conserving a high diastereomeric ratio.

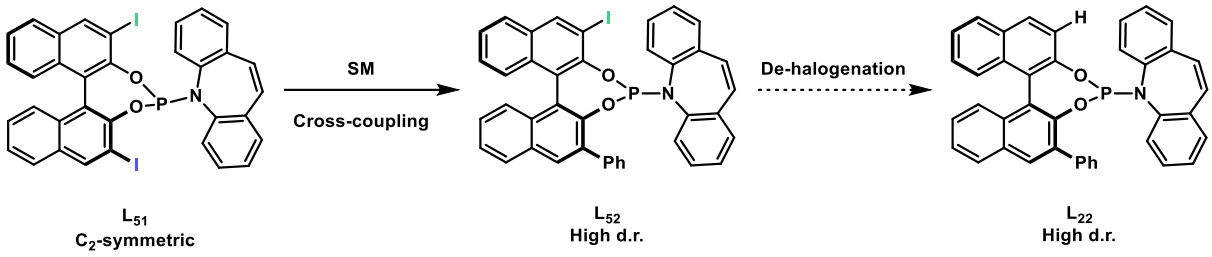

Figure 4.13: Alternative strategy involving Suzuki-Miyaura of a diastereotopic ligand **L51** following dehalogenation.

Optimisation for Suzuki-Miyaura conditions:

We attempted to find optimal conditions for the Suzuki-Miyaura reaction, in most cases obtaining unsatisfactory reactivity (Figure 4.14). We focused on testing different bases, palladium salts, ligands, boronic acid/pinacol ester, solvents and temperatures. Many cases seemed to give complete or partial decomposition of the phosphoramidite. Some other results, particularly the ones with low concentrations of base, seem to lead to a quick oxidation of the ligand.

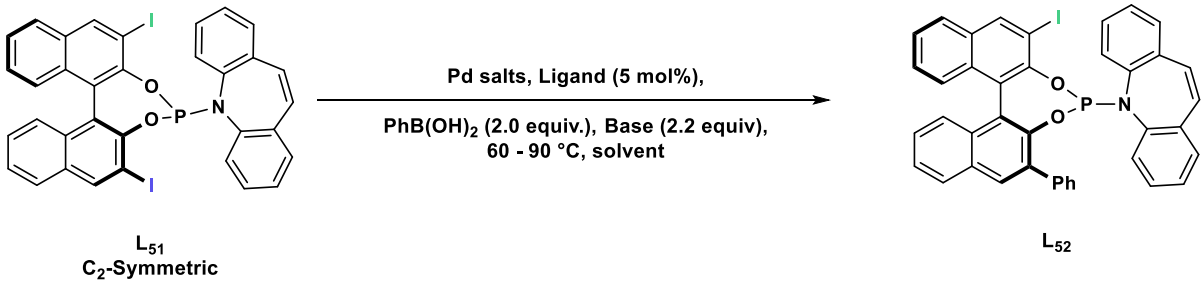

Figure 4.14: Suzuki-Miyaura of a diastereotopic ligand **L51**.

We were delighted with these results obtained by utilizing the PEPPSI catalyst, even though this ligand obtained no better diastereoselectivity than any other catalyst or methodology, it was responsible for a considerable increase in the yield obtained (61%). Its key to note that, to our delight, only one diastereomer was formed in all procedures and only traces of the di-phenylated **L21** was observed (<5%).

After obtaining this P-stereogenic product in high diastereomeric ratios we followed the synthetic process by employing a radical catalysed dehalogenation. This transformation

was efficient and had no major complications (Figure 4.15). We were able to conserve the high diastereoselectivity of **L52** when forming **L22**. Unfortunately, the stereomeric configuration of this ligand is S,R_P. This process, albeit successfully synthesising P-chiral phosphoramidites diastereoselectively, had yielded **L22R** instead of the sought out **L22S**.

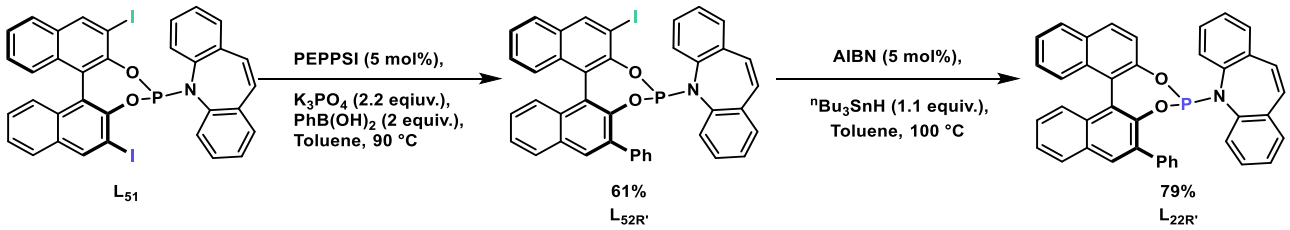

Figure 4.15: SM-Dehalogenation procedure yielding **L22R** diastereoselectively.

Even though this was not the result we were hoping for, it proved that the strategy is capable of very high diastereoselectivities and inspired us to apply a tuned strategy to achieve the desired **L22S**.

Proposed mechanism for the diastereoselective Suzuki-Miyaura:

The suggested Suzuki-Miyaura catalytic cycle (Figure 4.16) features a dihalogenated phoshporamidite bearing a pro-stereogenic phosphorus atom that serves as a stereodirecting handle, influencing the selectivity of the reaction between two different halogens, (X^1, X^2). The cycle would begin when a palladium(0) species coordinates to the phosphorus atom, positioning the metal centre near the X^1 halogen. This spatial proximity potentially promotes selective oxidative addition into the C-X^1 bond, generating a palladium(II) complex.

The phosphorus atom's interaction with the Pd centre could prevent oxidative addition at the spatially separated X^2 halogen. In the next step, transmetalation with phenylboronic acid would occur, replacing the X^1 halogen with a phenyl group from the boron compound, forming a new C-Pd bond. Following transmetalation, reductive elimination would then proceed efficiently, coupling the two organic groups to form the desired C-C bond.

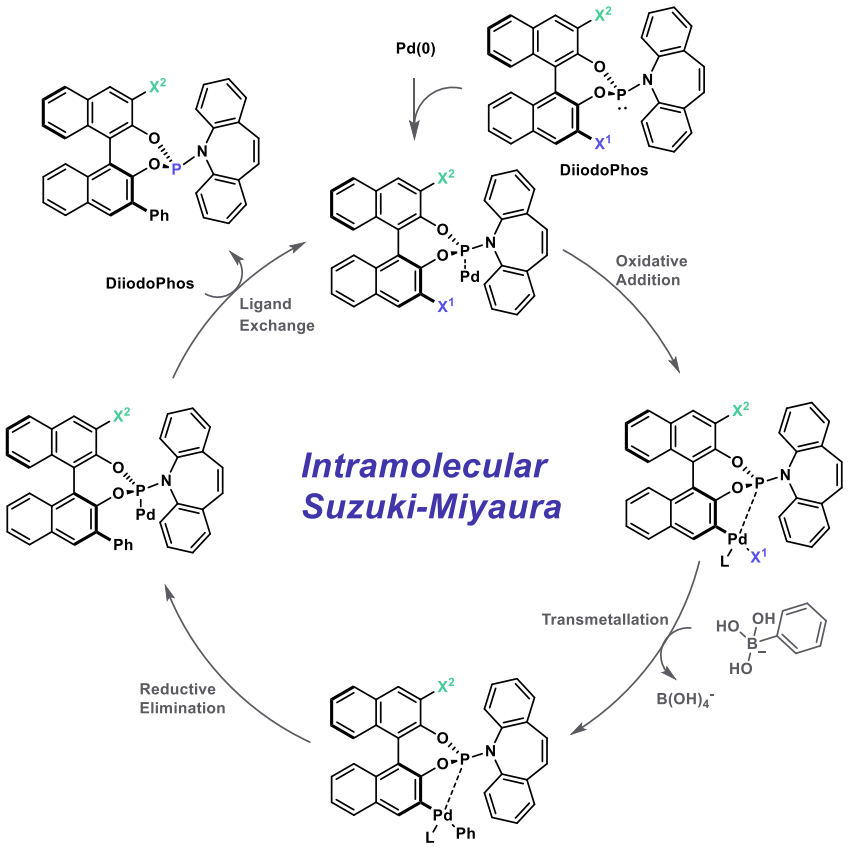

Figure 4.16: Proposed Intramolecular Suzuki-Miyaura reaction mechanism utilizing the Phosphorous as a P-handle that brings the palladium to one of the halogens (X^1) promoting oxidative addition while leaving the other one (X^2) unchanged.

The final step in this proposed mechanism regenerates the palladium(0) species, releasing the P-stereogenic ligand and the cycle restarts. Due to the stereodirecting influence of the phosphorus centre, the reaction would occur almost exclusively at the X^1 halogen, leading to a high degree of regioselectivity even in the presence of a competing X^2 halogen. Notably, this specific configuration will lead to the S,R_P diasteromer (**L_{22R}**) after dehalogenation, as the phenyl group has been added on the position the phosphorous lone pair was pointing to. This mechanism could help explain the observed stereodifferentiation, and, more importantly, can inspire us to tune the strategy for the S,S_P diastereomer.

Dehalogenation-cross-coupling strategy:

Inspired by the highl stereodifferentiation seen, we attempted to modify the procedure in order to produce the desired diastereomer **L_{22S}** (Figure 4.17). We believed that if the R^1 group was more liable than R^2, we could begin the process with a dehalogenation reaction. This would change R^1 to a hydrogen instead of a Phenyl group, leading to the

desired configuration (*S,S*$_P$). Afterwards, we could then attempt a cross-coupling transformation in order to produce **L$_{22S}$**. This procedure should be able to have a high level of diastereoselectivity, similar to the previously described stereodifferentiation strategy.

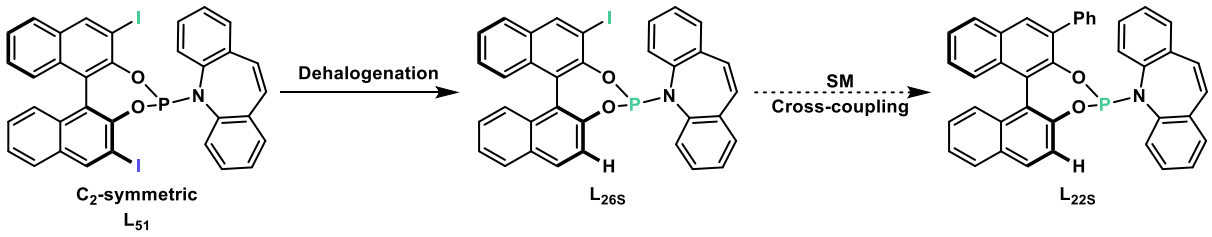

Figure 4.17: Alternative strategy composed by stereoselective dehalogenation of **L$_{51}$** to form **L$_{26S}$** followed by Suzuki-Miyaura to obtain **L$_{22S}$**.

Unlike the previously studied Suzuki-Miyaura reaction on this type of systems, the selectivity of dehalogenations were not consistently high (Table 1). Highly reactive radical systems (entry 1) leaded to low diastereomeric ratios of **L$_{26}$** (1:1 dr) and leaded to a large amount of overreacted product (**L$_7$**). Dehalogenation reactions involving hydrogen gas (entries 2,3) produced low conversions and leaded to no noticeable diastereoselectivities of **L$_{26}$** (1:1 dr). Interestingly, harsher hydrogenations with protic solvents such as MeOH lead to complete hydrogenation of the amine-backbone's double bond, resulting in **L$_{53}$** (entry 4). Methods that required homogeneous catalysis and used hydrogen as a de-halogenation agent (entries 5,6) were completely unreactive in the system. Interestingly, employing magnesium turnings, with the hope that the metal will attach to the phosphoramidite via oxidative addition followed by quenching with a protic source (H_2O) did result in **L$_{26}$** with some favourable diastereoselectivity, albeit, modest (1.6:1). Furthermore, the yield was considerably poor and some decomposition/oxidation was observed.

Fortunately, we were able to achieve high levels of **L$_{26}$** in high diastereomeric excess via a palladium catalysed de-halogenation utilizing silanes as the hydrogen source. Furthermore, the resulting phosphoramidite was obtained mostly pure, with high diastereoselectivity, and the desired configuration (*S,S*$_P$). Only 5-10% of **L$_7$** was obtained as an inseparable impurity.

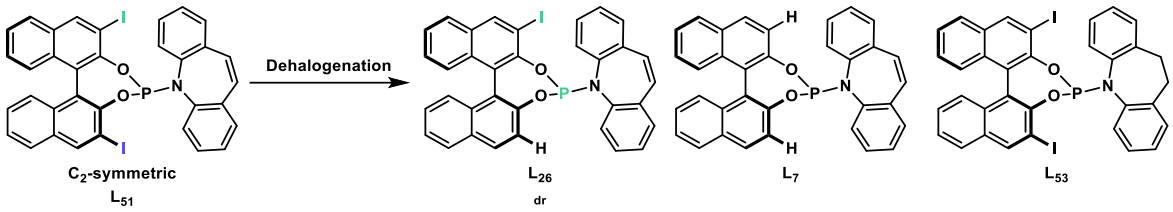

Entry	Catalyst/ reagent	Solvent	Hydrogen source	L26 yield /(%)	L26 (dr)	L7 /(%)	L53 /(%)
1	AIBN	Toluene	$^{n}Bu_3SnH$	30	1:1	50	ND
2	Pd/C	THF	H_2	<5	1.1:1	ND	ND
3	Pd/C	EtOAc	H_2	<5	1.2:1	ND	ND
4	Pd/C	MeOH	H_2	ND	N/A	ND	70
5	$Pd(OAc)_2$, bases	THF	H_2	ND	N/A	ND	ND
6	$[RhCl(PPh_3)]$	THF	H_2	ND	N/A	ND	ND
7	Mg(s)	THF	H_2O	25	1.6:1	ND	ND
8	$Pd(OAc)_2$, H_2O	THF	Et_3SiH	80	20:1	5 - 10	ND

Table 1: Different dehalogenation conditions showcasing different products and diastereoselectivities.

Exploiting the P-handle to obtain S,S$_P$ P-chiral phosphoramidities

Following the same principles observed in the Suzuki-Miyaura mechanism, we suggest that a similar P-handle effect is portrayed in the dehalogenation reaction of dihalogenated phosphoramidites when using palladium acetate as a catalyst (Figure 4.18). Inspired by the current mechanistic understanding of palladium dehalogenations,[53,54,55] we suggest the following diastereoselective mechanism:

The halogen X^1, is once again liable compared to X^2 due to the P-stereogenic moiety. During these conditions however, X^1 is exchanged to a hydrogen atom. The result is a diastereoselective synthesis for P-chiral phosphoramidites that does result in the desired S,S$_P$ configuration.

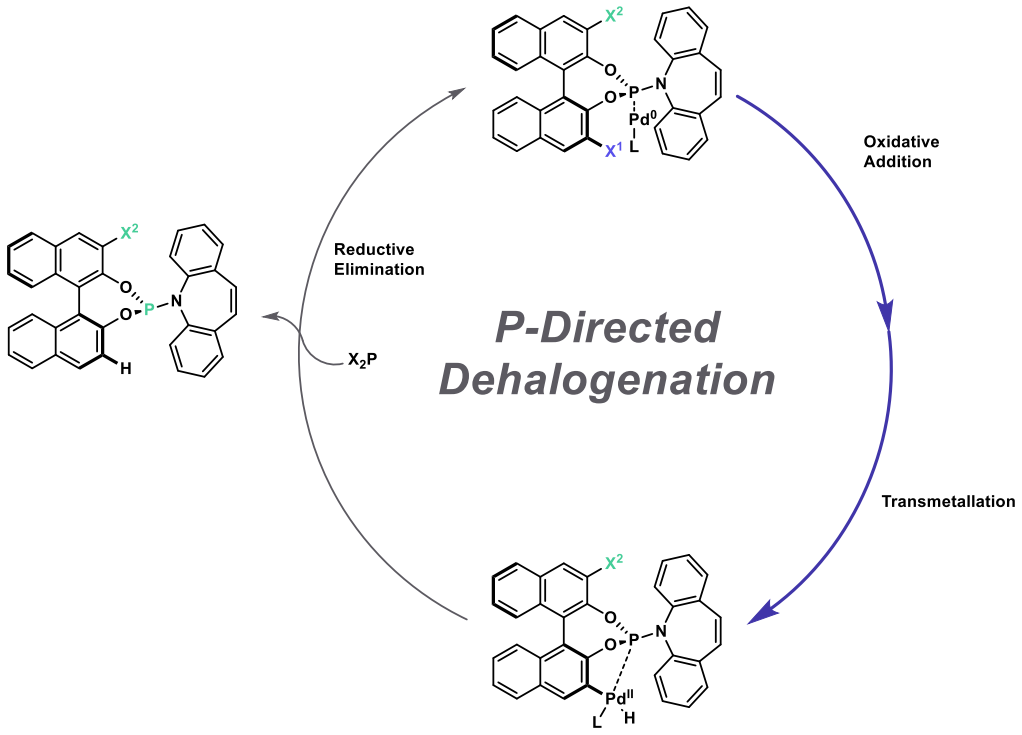

Figure 4.18: Proposed P-Directed Dehalogenation reaction mechanism. Utilizing the Phosphorous as a P-handle that brings the palladium to one of the halogens (X^1) promoting oxidative addition while leaving the other one (X^2) unchanged.

Fortunately, we were able to form **L26S** with high diastereoselectivity and minimal amount of impurities. We tested this ligand on the ACA reaction to test its selectivity on the reaction. We were able to obtain considerably good results (47% yield, 82% ee) with this ligand, albeit less impressive than when utilizing **L22S**. This once again underscores the importance of making **L22S** diastereoselectively. Fortunately, we believed than a simple Suzuki-Miyaura should be able to modify **L26S** into **L22S** without affecting the diasteromeric ratio.

Nevertheless, this did not happen to be the case. Even when attempting several different conditions (temperature, bases, palladium sources, solvents) the phosphoramidite was unstable and tended to either oxidize at the P centre or to decompose. We presume this is due to the palladium binding to the phosphorous atom (which, in this case is nowhere near the halogen). The palladium can then promote hydrolysis or oxidation breaking the phosphoramidite in a similar way to the reaction previously described by the Feringa group (Figure 4.19).[30]

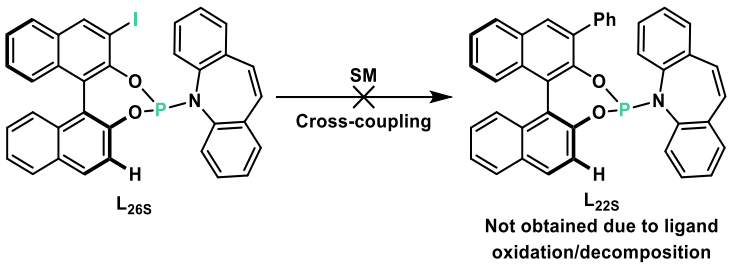

L_{26S} L_{22S}
Not obtained due to ligand oxidation/decomposition

Figure 4.19: Suzuki-Miyaura of $\mathbf{L_{26}}$ to obtain $\mathbf{L_{22S}}$ was deemed unsuitable due to decomposition/oxidation.

This roadblock once again shows the great complications on working on these fragile systems and unfortunately forced us to forfeit our attempts on diastereoselective synthesis.

4.5 Summary and future work

In this chapter, we explored two main strategies to synthesize the P-chiral phosphoramidite ligand $\mathbf{L_{22S}}$, which we have shown in Chapter 2 induces high levels of selectivity and yields in ACA to exocyclic compounds The first strategy involved using substituted BINOLs with labile groups that could be replaced with a phenyl group after diasteroselective phosphoramidation, in order to form $\mathbf{L_{22S}}$. While some of these substituents yielded phosphoramidites with high diastereomeric ratios, their lack of desired reactivity prevented effective conversion to $\mathbf{L_{22S}}$.

The second strategy focused on utilizing a stereodirecting phosphorus center as an intrinsic auxiliary to influence selectivity during cross-coupling or C-I reduction reactions. This approach successfully generated high diastereoselectivity for $\mathbf{L_{22R}}$, but ultimately failed for $\mathbf{L_{22S}}$ due to the high sensitivity of the phosphoramidite system, which was prone to decomposition and oxidation. Despite these challenges, we successfully synthesized $\mathbf{L_{22R}}$ and $\mathbf{L_{26S}}$ with high diastereoselectivity.

Future research could focus on leveraging other cross-coupling reactions, such as Stille, Negishi, or Kumada couplings, to attempt the synthesis of $\mathbf{L_{22S}}$ from $\mathbf{L_{26S}}$. These reactions may provide alternative pathways that are less prone to decomposition and oxidation, potentially overcoming the challenges faced with the previous methods. Additionally, exploring the application of $\mathbf{L_{22R}}$ and $\mathbf{L_{26S}}$ in reaction discovery could be highly rewarding. These ligands occupy a unique place in the ligand space and could potentially give rise to

new asymmetric transformations, expanding the toolkit available to organic chemists in both academic and industrial settings.

4.6 References:

1. R. B. Jordan, in *Principles of Inorganic Chemistry*, Springer, Cham, Switzerland, 2024, pp. 661–738.
2. N. N. Greenwood and A. Earnshaw, *Chemistry of the Elements*, 2nd ed., Butterworth-Heinemann, Oxford, 1997, pp. 473–546.
3. R. Martin and S. L. Buchwald, *Acc. Chem. Res.*, 2008, **41**, 1461–1473.
4. D. Parmar, E. Sugiono, S. Raja and M. Rueping, *Chem. Rev.*, 2014, **114**, 9047–9153.
5. M. Stolar and T. Baumgartner, *Chem. – Asian J.*, 2014, **9**, 1212–1225.
6. G. E. Oosterom, J. N. H. Reek, P. C. J. Kamer and P. W. N. M. van Leuwen, *Angew. Chem., Int. Ed.*, 2001, **40**, 1828–1849.
7. M. Kazemi, A. M. Tahmasbi, R. Valizadeh, A. A. Naserian and A. Soni, *Agric. Sci. Res. J.*, 2012, **2**, 512–522.
8. H. Seto, in *Comprehensive Natural Products Chemistry*, ed. O. Meth-Cohn, D. Barton, K. Nakanishi, Elsevier, 1999, vol. 1, pp. 865-880.
9. M. Dutartre, J. Bayardon, and S. Juge, *Chem. Soc. Rev.*, 2016, **45**, 5771–5794.
10. W. S. Knowles and M. J. Sabacky, *Chem. Commun.*, 1968, **1445**–1446.
11. L. Horner, H. Siegel, and H. Büthe, *Angew. Chem. Int. Ed.*, 1968, **7**, 942.
12. *The Nobel Prize in Chemistry 2001*. NobelPrize.org. Nobel Prize Outreach AB 2001. Mon. 4 Sept 2024.
13. O. Korpiun and K. Mislow, *J. Am. Chem. Soc.*, 1967, **89**, 4784.
14. J. J. Petkowski, W. Bains, and S. Seager, *Molecules*, 2019, **24**, 1–66.
15. T. Moriguchi, N. Asai, K. Okada, K. Seio, T. Sasaki, and M. Sekine, *J. Org. Chem.*, 2002, **67**, 3290–3300.
16. Y. Wang, D. Zhang, G. Du, R. Du, J. Zhao, Y. Jin, S. Fu, L. Gao, Z. Cheng, Q. Lu, Y. Hu, G. Luo, K. Wang, Y. Lu, H. Li, S. Wang, S. Ruan, C. Yang, C. Mei, Y. Wang, D. Ding, F. Wu, X. Tang, X. Ye, Y. Ye, B. Liu, J. Yang, W. Yin, A. Wang, G. Fan, F. Zhou, Z. Liu, X. Gu, J. Xu, L. Shang, Y. Zhang, L. Cao, T. Guo, Y. Wan, H. Qin, Y. Jiang, T. Jaki, F. G. Hayden, P. W. Horby, B. Cao, and C. Wang, *Lancet*, 2020, **395**, 1569–1578.
17. J. H. Beigel, K. M. Tomashek, L. E. Dodd, A. K. Mehta, B. S. Zingman, A. C. Kalil, E. Hohmann, H. Y. Chu, A. Luetkemeyer, S. Kline, D. Lopez de Castilla, R. W. Finberg, K. Dierberg, V. Tapson, L. Hsieh, T. F. Patterson, R. Paredes, D. A. Sweeney, W. R. Short, G. Touloumi, D. C. Lye, N. Ohmagari, M. Oh, G. M. Ruiz-Palacios, T. Benfield,

G. Fätkenheuer, M. G. Kortepeter, R. L. Atmar, C. B. Creech, J. Lundgren, A. G. Babiker, S. Pett, J. D. Neaton, T. H. Burgess, T. Bonnett, M. Green, M. Makowski, A. Osinusi, S. Nayak, and H. C. Lane, for the ACTT-1 Study Group Members, *N. Engl. J. Med.*, 2020, **383**, 1813–1826.

18. B. D. Vineyard, W. S. Knowles, M. J. Sabacky, G. L. Bachman, and D. J. Weinkauff, *J. Am. Chem. Soc.*, 1977, **99**, 5946–5952.
19. W. S. Knowles, *Acc. Chem. Res.*, 1983, **16**, 106–112.
20. G. Hoge, H.-P. Wu, W. S. Kissel, D. A. Pflum, D. J. Greene, and J. Bao, *J. Am. Chem. Soc.*, 2004, **126**, 5966–5967.
21. T. León, M. Parera, A. Roglans, A. Riera, and X. Verdaguer, *Angew. Chem. Int. Ed.*, 2012, **51**, 6951–6955.
22. T. Hamada and S. L. Buchwald, *Org. Lett.*, 2002, **4**, 999–1001.
23. L. Pang, Z. Huang, Q. Sun, G. Li, J. Liu, B. Li, C. Ma, J. Guo, C. Yao, J. Yu, and Q. Li, *Nat. Commun.*, 2023, **14**, 4437.
24. J. Liu, H. Chen, M. Wang, W. He, and J.-L. Yan, *Front. Chem.*, 2023, **11**, 1–7.
25. O.I. Kolodiazhnyi, *Recent Advances in Asymmetric Synthesis of P-Stereogenic Phosphorus Compounds*, in *Phosphorus Chemistry I* (Ed.: J. L. Montchamp), Springer, Cham, Switzerland, 2014, vol. 360, pp. 161–236.
26. R. Beaud, R. J. Phipps, M. J. Gaunt, *J. Am. Chem. Soc.*, 2016, **138**, 13183–13186.
27. J. S. Harvey, V. Gouverneur, *Chem. Commun.*, 2010, **46**, 7477–7485.
28. Z. Huang, X. Huang, B. Li, C. Mou, S. Yang, B.-A. Song, et al., *J. Am. Chem. Soc.*, 2016, **138**, 7524–7527.
29. V. Gannedi, B. K. Villuri, S. N. Reddy, C.-C. Ku, C.-H. Wong, and S.-C. Hung, *J. Org. Chem.*, 2021, **86**, 4977–4985.
30. A. Mondal, N. O. Thiel, R. Dorel, and B. L. Feringa, *Nat. Catal.*, 2022, **5**, 10–19.
31. Y.-S. Jang, Ł. Woźniak, J. Pedroni, and N. Cramer, *Angew. Chem. Int. Ed.*, 2018, **57**, 12901–12905.
32. A. Alexakis, N. Krause, and S. Woodward, Eds., *Copper-Catalyzed Asymmetric Synthesis*, Wiley-VCH, Weinheim, 2014, chap. 2–3.
33. A. J. Minnaard, B. L. Feringa, L. Lefort, and J. G. de Vries, *Acc. Chem. Res.*, 2007, **40**, 1267–1277.
34. D. Hérault, D. H. Nguyen, D. Nuel, and G. Buono, *Chem. Soc. Rev.*, 2015, **44**, 2508–2528.

35. Ł. Kapuśniak, P. N. Plessow, D. Trzybiński, K. Woźniak, P. Hofmann, and P. I. Jolly, *Organometallics*, 2021, **40**, 693–701.
36. L. I. Simándi, in *Catalytic Activation of Dioxygen by Metal Complexes*, 1st ed., Springer, Dordrecht, 1992, pp. 363–370.
37. B. M. Trost, D. A. Bringley, and S. M. Silverman, *J. Am. Chem. Soc.*, 2011, **133**, 7664–7667.
38. B. M. Trost and G. Mata, *Angew. Chem. Int. Ed.*, 2018, **57**, 12333–12337.
39. X. Xiong, T. Zheng, X. Wang, Y.-L. S. Tse, and Y.-Y. Yeung, *Chem*, 2020, **6**, 919–932.
40. M. T. Reetz, J.-A. Ma, and R. Goddard, *Angew. Chem. Int. Ed.*, 2005, **44**, 412–415.
41. R. Martin and S. L. Buchwald, *Acc. Chem. Res.*, 2008, **41**, 1461–1473.
42. N. Miyaura, K. Yamada, and A. Suzuki, *Tetrahedron Lett.*, 1979, **20**, 3437–3440.
43. S. Lai, N. Takaesu, W. X. Lin, and D. M. Perrin, *Tetrahedron Lett.*, 2021, **74**, 153147.
44. A. O. King, N. Okukado, and E. Negishi, *J. Chem. Soc., Chem. Commun.*, 1977, **19**, 683–684.
45. K. Tamao, K. Sumitani, and M. Kumada, *J. Am. Chem. Soc.*, 1972, **94**, 4374–4376.
46. S. Murahashi, M. Yamamura, K. Yanagisawa, N. Mita, and K. Kondo, *J. Org. Chem.*, 1979, **44**, 2408–2417.
47. Y. Hatanaka and T. Hiyama, *J. Org. Chem.*, 1988, **53**, 918–920.
48. B. Török, C. Schäfer, and A. Kokel, in *Heterogeneous Catalysis in Sustainable Synthesis*, Elsevier, Amsterdam, 2021, pp. 379–440.
49. S.-N. Chen, W.-Y. Wu, F.-Y. Tsai, *Tetrahedron*, 2008, **64**, 8164–8168.
50. F. Foubelo, C. Nájera, and M. Yus, *J. Chem. Soc. Jpn.*, 2016, **16**, 2521–2533.
51. C. Cordovilla, C. Bartolomé, J. M. Martínez-Ilarduya, and P. Espinet, *ACS Catal.*, 2015, **5**, 3040–3053.
52. J. K. Stille, *Angew. Chem. Int. Ed. Engl.*, 1986, **25**, 508–524.
53. G. M. Noonan, B. R. Hayter, A. D. Campbell, T. W. Gorman, B. E. Partridge, G. M. Lamont, *Tetrahedron Lett.*, 2013, **54**, 4518–4521.
54. J. Moon, S. Lee, *J. Organomet. Chem.*, 2009, **694**, 473–477.
55. M. R. Hurst, L. N. Zakharov, A. K. Cook, *Chem. Sci.*, 2021, **12**, 13045–13060.
56. R. Ardkhean, S. P. Fletcher, and R. S. Paton, in *Ligand Design for Asymmetric Catalysis: Combining Mechanistic and Chemoinformatics Approaches*, Chapter 10, *New Directions in the Modelling of Organometallic Reactions*, Springer, Cham, Switzerland, 2020, pp. 153–190.

57. J. Wassenaar and J. N. H. Reek, *Org. Biomol. Chem.*, 2011, **9**, 1704–1713.
58. C. H. Heathcock, C. T. White, J. J. Morrison, and D. VanDerveer, *J. Org. Chem.*, 1981, **46**, 1296–1309.

Chapter 5:

Experimental section

5.1 General information

All procedures were conducted in flame-dried flasks, under an inert argon atmosphere, in anhydrous conditions and with continuous magnetic stirring, unless stated otherwise. Reaction temperatures of 0 °C were maintained using ice-water baths, with periodic ice replenishment and insulation for overnight stirring. Light-sensitive reactions were protected with aluminum foil. Heating was achieved using DrySyn heating blocks.

Analytical thin-layer chromatography (TLC) was performed on silica gel-coated glass plates (TLC Silica gel 60 RP-18 F_{254}s). Visualization employed UV light (254 nm) aqueous basic potassium permanganate ($KMnO_4$) stains, as detailed in the general methods. Flash column chromatography utilized VWR (40–63 μm) or Sigma Aldrich silica gel, while SCX column chromatography was performed with Isolute® flash SCX-2 columns from Biotage.

Nuclear Magnetic Resonance (NMR) spectroscopy was performed at room temperature. ^{1}H and ^{13}C NMR spectra were recorded on Bruker AVIII HD 400 spectrometers (400/101 MHz). Chemical shifts (δ) are reported in parts per million (ppm) relative to the residual solvent peak, with coupling constants (*J*) in Hertz (Hz) and signal multiplicities described as singlet (s), doublet (d), triplet (t), quartet (q), multiplet (m), or apparent (app.) combinations thereof. Coupling constants (*J*) were reported to one decimal place (Hz), and chemical shifts were noted to two decimal places (^{1}H NMR) or one decimal place (^{13}C, ^{19}F, and ^{31}P NMR). HSQC, COSY, and HMBC experiments supported spectral assignments.

Chiral separations using supercritical fluid chromatography (SFC) were conducted on a Waters Acquity UPC2 system with Waters Empower software, utilizing Chiralpak® columns (150 × 3 mm, 3 μm particle size). HPLC-grade solvents were sourced from Fisher Scientific, Sigma Aldrich, or Rathburn. Chiral GC measurements were conducted on a HP6890 (H_2 as vector gas) GC with the stated column in the characterisation.

Infrared (IR) spectra were recorded using a Bruker Tensor 27 FTIR spectrometer with a PIKE Miracle ATR accessory, using solid samples or thin films for liquids ($CHCl_3$). IR data is reported in wavenumbers (cm^{-1}).

High Resolution Mass Spectra were carried out by internal service at the University of Oxford. Electron spray ionisation (ESI) was recorded on a Fisons Platform II. Calculated masses for expected ions came from addition of naturally abundant isotopes.

Optical rotations ($[\alpha]^{25}_{D}$, in deg.mL.g^{-1}.dm^{-1}) were measured using a Schmidt Haensch Unipol L2000 polarimeter with a 1 dm path-length cell, using the sodium D line (589 nm). Sample concentrations (*c*) are reported in g/100 mL. Temperatures are given in °C.

5.2 Chemicals:

Commercially available reagents and ligands were purchased from Acros Organics, Alfa Aesar, Fisher Scientific, Fluorochem, Sigma Aldrich and Strem Chemicals and unless otherwise stated were used without further purification.

Dry solvents were collected fresh from an mBraun SPS–800 solvent purification system after having passed 2 through anhydrous alumina columns. Deuterated solvents were purchased from Sigma Aldrich. Anhydrous MeOH and other solvents were used as purchased. Preformed ligand-copper complexes were filtered under argon through polytetrafluoroethylene (PTFE) syringe filters (25 mm, 0.2 μm) from Fisher Scientific

The 99.99% purity CuCl was from Alfa Aesar and was used without any further purification. Dry Trimethylsilyl chloride (TMSCl) under inert atmosphere was used without further purification from Sigma-Aldrich. PCl_3 from Sigma-Aldrich was freshly distilled every time before use.

5.3 General procedures:

5.3.1 ACA procedures

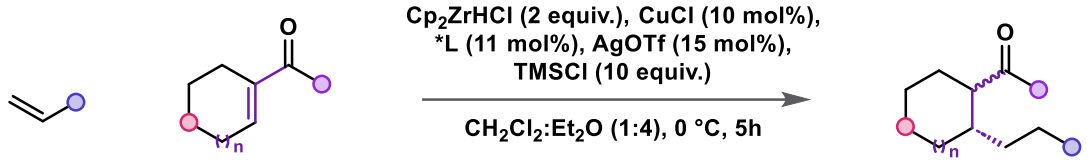

General procedure A (for racemic products):

In a 5 mL flame-dried round bottom flask was added CuCl (8.0 mg, 0.080 mmol, 0.20 eq.). The flask was purged (3 × argon/vacuum), covered with aluminium foil to protect it from the light and dry Et_2O (2.0 mL) was then added under an argon atmosphere. In the meantime, Cp_2ZrHCl (206 mg, 0.80 mmol, 2.0 eq.) was added to a 10 mL flame-dried round bottom flask, purged (3 × argon/vacuum), and covered with aluminium foil to protect it from the light. Addition of dry CH_2Cl_2 (0.5 mL) under an argon atmosphere forms a milky solution. The olefin (1.00 mmol, 2.5 eq.) was immediately added. After stirring for 15 min, the resulting yellow clear olefin solution was manually swirled in order to remove the traces of Schwartz reagent on the inside walls of the flask and stirring was continued. After stirring the foiled flask containing CuCl for 30 min, AgOTf (31 mg, 0.090 mmol, 0.30 eq.) was added, and the grey – brown cloudy solution was stirred for 15 min. The mixture was then transferred over (using a syringe filter) to the yellow clear solution. To the resulting black mixture, was added the unsaturated ketone (0.4 mmol, 1.0 eq.) and TMSCl (0.5 mL, 3.9 mmol, 10 eq.). Stirring was continued for 5 h. Reaction was quenched and purified by following General procedure C or D, depending on the desired diastereoisomer.

General procedure B (for enantiopure products):

In a 5 mL flame-dried round bottom flask was added CuCl (4.0 mg, 0.040 mmol, 0.10 eq.) and *(S)*-**L22S** (25.7 mg, 0.044 mmol, 0.11 eq.). The flask was purged (3 × argon/vacuum), covered with aluminium foil to protect it from the light and dry Et_2O (2.0 mL) was then added under an argon atmosphere. The resulting colourless clear solution was stirred for 1 h at room temperature. In the meantime, Cp_2ZrHCl (206 mg, 0.80 mmol, 2.0 eq.) was added to a 10 mL flame-dried round bottom flask, purged (3 × argon/vacuum), and

covered with aluminium foil to protect it from the light. Addition of dry CH_2Cl_2 (0.5 mL) under an argon atmosphere formed a milky solution. The olefin (1.00 mmol, 2.5 eq.) was immediately added. After stirring for 15 min, the resulting yellow clear solution was manually swirled in order to remove the traces of Schwartz reagent on the inside walls of the flask and stirring was continued. After stirring the foiled flask containing CuCl for 1 h, AgOTf (15.5 mg, 0.060 mmol, 0.15 eq.) was added, and the grey-brown cloudy solution was stirred for 15 min. The suspension was taken up with a syringe and transferred over (passing through a syringe filter) to the yellow clear solution. The resulting black mixture was then cooled to 0 °C and stirred for a further 5 min before the ketone (0.40 mmol, 1.0 eq.) and then TMSCl (0.5 mL, 3.9 mmol, 10 eq.) were added dropwise via syringe. Stirring at 0 °C was continued for 5 h. The reaction was quenched and purified following General procedures C or D, depending on the desired diastereoisomer.

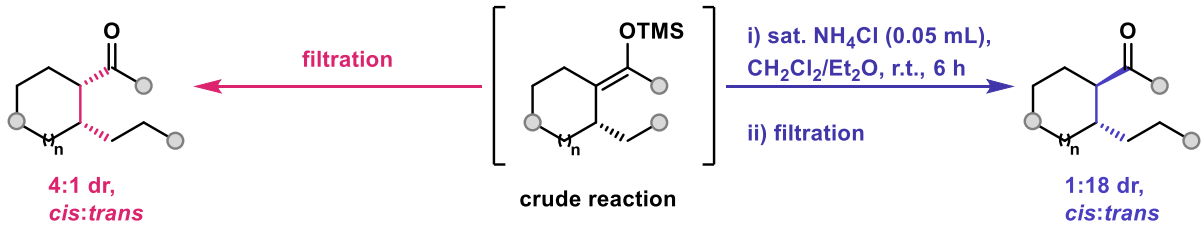

General procedure C (Quenching for trans diastereoselectivity)

The crude mixture from general procedure A was quenched by the addition of aqueous NH_4Cl (1 M, ca 0.1 mL) and stirring was continued for 5 h at room temperature. The mixture was concentrated under reduced pressure then diluted with hexane (ca 10 mL), filtered and concentrated again under reduced pressure. The crude mixture was purified by flash column chromatography (hexane:EtOAc, 97:3, SiO_2) to afford the desired products as a mixture of *cis*- and *trans*-diastereoisomers.

General procedure D (Quenching for cis diasteroselectivity)

The mixture was filtered, concentrated under reduced pressure then diluted with hexane (ca 10 mL), filtered and concentrated again under reduced pressure. The crude mixture was purified by flash column chromatography (hexane:EtOAc, 97:3, SiO_2) to afford the desired products as a mixture of *cis*- and *trans*-diastereoisomers.

5.3.2 Preparation of enones:

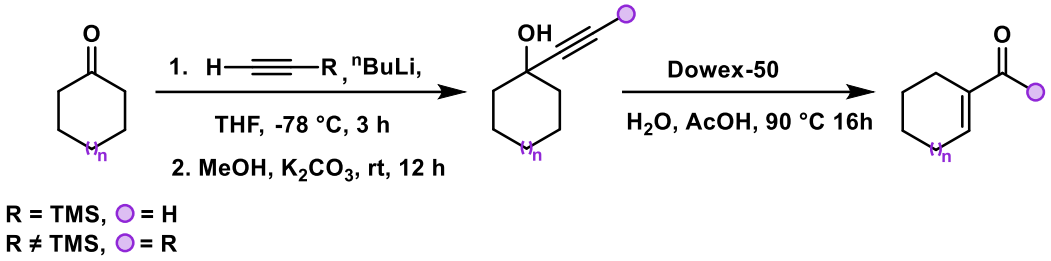

General procedure E:

According to modified procedures,[1] alkyne (8.0 mmol, 1.6 eq.) was added in THF (10 mL) and cooled to -78 °C. ^{n}BuLi (2.4 mL, 6.0 mmol, 1.2 eq) was added dropwise over 5 minutes and the mixture was stirred for 30 minutes. The cyclic ketone (5.0 mmol, 1.0 eq.) was then added and the solution was stirred for 3 hours at room temperature. The reaction was quenched with aqueous NH_4Cl (sat.) and extracted with EtOAc and dried with Na_2SO_4, concentrated under vacuum. The crude mixture was dissolved in MeOH (15 mL), K_2CO_3 (1.76 g, 12.6 mmol) was added and the mixture was stirred at room temperature for 12 hours. The reaction was concentrated under vacuum to remove MeOH. The reaction was dissolved in water and extracted with EtOAc. The organic phase was washed with water, brine dried with Na_2SO_4 and concentrated under vacuum. The alcohol was isolated after flash column chromatography.

General procedure F:

According to a modified procedure,[2] the alcohol was dissolved in AcOH (5 mL) and water (0.5 mL). Resin Dowex-50 (320 mg) was added and the mixture was heated to 90 °C for 16 h. The mixture was cooled down to room temperature, filtered and quenched by small additions of $NaHCO_3$ until effervescence stops. The mixture was extracted with EtOAc three times. The organic fractions were combined, washed with water, brine, dried with Na_2SO_4 and concentrated under vacuum. The enone was isolated after flash column chromatography.

5.3.3 Preparation of phosphoramidites

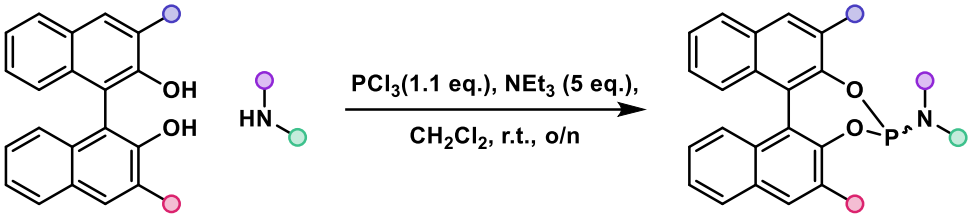

General procedure G

According to a procedure reported by our group,[3] triethylamine (5.0 eq.) was added dropwise to a stirred solution cooled at 0 °C of freshly distilled PCl_3 (1.1 eq.) in CH_2Cl_2 (0.1 M). The amine (1.0 eq.) was added in one portion and the solution was left to warm up to room temperature. After 3 h of stirring, the BINOL (1.0 eq.) was added to the reaction and the subsequent mixture was stirred for 16 h. The mixture was concentrated under vacuum to afford a yellow residue. The phosphoramidite was obtained as a foamy colourless solid after flash column chromatography. Care was taken to minimise the exposure of the phosphoramidite to light and air. To limit phosphoramidite decomposition, triethylamine (1%) was incorporated into the solvent system, and the column chromatography was run rapidly. Re-crystallization purification varies for specific examples.

5.4 Characterization of compounds

5.4.1 Copper-catalysed asymmetric conjugate addition products

1-((*1R,2S*)-2-(4-phenylbutyl)cyclohexyl)ethan-1-one (4a)

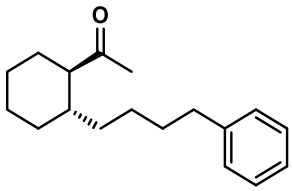

The title compound was obtained following General procedure B using 1-(cyclohex-1-en-1-yl)ethan-1-one (50 μL, 0.4 mmol, 1.0 eq.) and but-3-en-1-ylbenzene (150 μL, 1.0 mmol, 2.5 eq.).

The crude was treated following General procedure C and purified by flash column chromatography (hexane:EtOAc, 97:3, SiO_2) to afford 1-((*1R,2S*)-2-(4-phenylbutyl)cyclohexyl)ethan-1-one (82.7 mg, 0.320 mmol, 80%, 18:1 dr) as a mixture of diastereoisomers. The product was obtained as a pale-yellow oil.

^{1}H NMR (400 MHz, CDCl3) δ 7.23 – 7.15 (m, 2H), 7.14 – 7.03 (m, 3H), 2.58 – 2.42 (m, 2H), 2.11 – 2.06 (m, 1H), 2.03 (s, 3H), 1.83 – 1.59 (m, 4H), 1.59 – 1.41 (m, 3H), 1.40 – 1.24 (m, 1H), 1.24 – 1.09 (m, 5H), 1.05 – 0.88 (m, 1H), 0.86 – 0.72 (m, 1H).

^{13}C NMR (101 MHz, $CDCl_3$) δ 213.4, 142.8, 128.5 (2C), 128.3(2C), 125.7, 58.0, 38.5, 36.0, 34.8, 31.7, 30.9, 29.9, 29.2, 26.2, 25.9 (2C).

$[\alpha]_D^{25}$: –21.6 (*c* 1.0, $CHCl_3$).

IR: 3021, 2932, 1702, 1454 cm^{-1}.

MS: *m/z* calculated for $C_{18}H_{25}O^-$ $[M-H]^-$ = 257.1911; found = 257.1910.

SFC analysis indicated an enantiomeric excess of 97% [Chiralpak® IG-3; 1500 psi, 30 °C, flow: 1.5 mL/min; 1.0% to 30.0% MeOH in 5 min; λ = 218 nm; major enantiomer (*1R,2S*), t_R = 3.34 min; minor enantiomer (*1S,2R*), t_R = 4.89 min].

1-((*1R,2S*)-2-(4-methylphenethyl)cyclohexyl)ethan-1-one (4b)

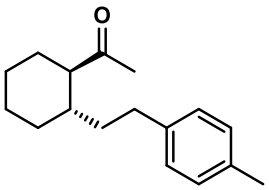

The title compound was obtained following General procedure B using 1-(cyclohex-1-en-1-yl)ethan-1-one (50 μL, 0.4 mmol, 1.0 eq.) and 1-methylstyrene (132 μL, 1.0 mmol, 2.5 eq.).

The crude was treated following General procedure C and purified by flash column chromatography (hexane:EtOAc, 97:3, SiO_2) to afford 1-((*1R,2S*)-2-(4-methylphenethyl)cyclohexyl)ethan-1-one (59.6 mg, 0.244 mmol, 61%, 7:1 dr) as a mixture of diastereoisomers. The product was obtained as a pale-yellow oil.

^{1}H NMR (400 MHz, $CDCl_3$) δ 7.09 – 7.03 (m, 4H), 2.68 – 2.64 (m, 1H), 2.48 – 2.44 (m, 1H), 2.32 (s, 3H), 2.23 – 2.22 (m,1H), 2.07 (s, 3H), 2.03 – 1.99 (m 1H), 1.87 – 1.50 (m, 5H), 1.43 – 1.16 (m, 4H), 1.08 – 0.89 (m, 1H).

^{13}C NMR (101 MHz, $CDCl_3$) δ 213.1, 139.5, 135.2 (2C), 129.1 (2C), 128.3, 57.9, 38.1, 37.0, 32.5, 30.8, 29.8, 29.0, 25.8 (2C), 21.1.

$[\alpha]_D^{25}$: –30.0 (*c* 1.0, $CHCl_3$).

IR: 3018, 2932, 2858, 1703 cm^{-1}.

MS: *m/z* calculated for $C_{17}H_{25}O^+$ $[M+H]^+$ = 245.1900; found = 245.1918.

SFC analysis indicated an enantiomeric excess of 98% [Chiralpak® IG-3; 1500 psi, 30 °C, flow: 1.5 mL/min; 1.0% to 30.0% MeOH in 5 min; λ = 218 nm; major enantiomer (*1R,2S*), t_R = 3.20 min; minor enantiomer (*1S,2R*), t_R = 3.56 min].

1-((*1R,2S*)-2-(4-(benzyloxy)butyl)cyclohexyl)ethan-1-one (4c)

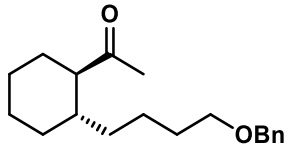

The title compound was obtained following General procedure B using 1-(cyclohex-1-en-1-yl)ethan-1-one (50 μL, 0.4 mmol, 1.0 eq.) and ((but-3-en-1-yloxy)methyl)benzene (162 μL, 1.0 mmol, 2.5 eq.).

The crude was treated following General procedure C and purified by flash column chromatography (hexane:EtOAc, 97:3, SiO_2) to afford afford 1-((*1R,2S*)-2-(4-(benzyloxy)butyl)cyclohexyl)ethan-1-one (66.9 mg, 0.232 mmol, 58%, 10:1 dr) as a mixture of diastereoisomers. The product was obtained as a pale-yellow oil.

^{1}H NMR (400 MHz, $CDCl_3$) δ 7.26 (d, *J* = 3.5 Hz, 4H), 7.23 – 7.17 (m, 1H), 4.42 (s, 2H), 3.37 (t, *J* = 6.4 Hz, 2H), 2.20 – 2.06 (m, 1H), 2.04 (s, 3H), 1.82 – 1.80 (m, 1H), 1.77 – 1.61 (m, 4H), 1.59 – 1.31 (m, 2H), 1.30 – 1.07 (m, 5H), 1.06 – 0.94 (m, 1H), 0.84 – 0.79 (m, 2H).

^{13}C NMR (101 MHz, $CDCl_3$) δ 213.3, 138.8, 128.4 (2C), 127.7 (2C), 127.5, 72.9, 70.4, 57.9, 38.4, 34.7, 30.8, 30.0, 29.8, 29.1, 25.8, 25.8, 23.2.

$[\alpha]_D^{25}$: –18.1 (*c* 1.0, $CHCl_3$).

IR: 3018, 2936, 2860, 1703 cm^{-1}.

MS: *m/z* calculated for $C_{19}H_{28}O_2Na^+$ $[M+Na]^+$ = 311.1982; found = 311.1988.

SFC analysis indicated an enantiomeric excess of 94% [Chiralpak® IG-3; 1500 psi, 30 °C, flow: 1.5 mL/min; 1.0% to 30.0% MeOH in 5 min; λ = 218 nm; major enantiomer (*1R,2S*), t_R = 4.00 min; minor enantiomer (*1S,2R*), t_R = 4.51 min].

1-((*1R,2S*)-2-(5-bromopentyl)cyclohexyl)ethan-1-one (4d)

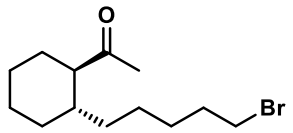

The title compound was obtained following General procedure B using 1-(cyclohex-1-en-1-yl)ethan-1-one (50 μL, 0.4 mmol, 1.0 eq.) and 5-bromoheptene (118.5 μL, 1.0 mmol, 2.5 eq.).

The crude was treated following General procedure C and purified by flash column chromatography (hexane:EtOAc, 97:3, SiO_2) to afford afford 1-((*1R,2S*)-2-(5-bromopentyl)cyclohexyl)ethan-1-one (65.0 mg, 0.236 mmol, 59%, 9:1 dr) as a mixture of diastereoisomers. The product was obtained as a pale-yellow oil.

^{1}H NMR (400 MHz, $CDCl_3$) δ 3.36 (t, *J* = 6.8 Hz, 2H), 2.21 – 2.11 (m, 1H), 2.10 (s, 3H), 1.90 – 1.64 (m, 6H), 1.64 – 1.49 (m, 1H), 1.42 – 1.28 (m, 3H), 1.28 – 1.13 (m, 5H), 1.08 – 0.94 (m, 1H), 0.88 – 0.84 (m, 1H).

^{13}C NMR (101 MHz, $CDCl_3$) δ 213.2, 57.9, 38.3, 34.7, 33.9, 32.8, 30.8, 29.9, 29.2, 28.4, 25.9, 25.8, 25.7.

$[\alpha]_D^{25}$: –24.0 (*c* 1.0, $CHCl_3$).

IR: 3053, 3017, 2932, 1702 cm^{-1}.

MS: *m/z* calculated for $C_{13}H_{24}O[^{79}Br]^+$ $[M+H]^+$ = 275.1005; found = 275.1011.

SFC analysis indicated an enantiomeric excess of 97% [Chiralpak® IG-3; 1500 psi, 30 °C, flow: 1.5 mL/min; 1.0% to 30.0% MeOH in 5 min; λ = 218 nm; major enantiomer (*1R,2S*), t_R = 3.88 min; minor enantiomer (*1S,2R*), t_R = 4.16 min].

1-((*1R,2R*)-2-(7-bromoheptyl)cyclohexyl)ethan-1-one (4e)

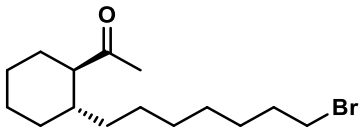

The title compound was obtained following General procedure B using 1-(cyclohex-1-en-1-yl)ethan-1-one (50 μL, 0.4 mmol, 1.0 eq.) and 7-bromoheptene (152.2 μL, 1.0 mmol, 2.5 eq.).

The crude was treated following General procedure C and purified by flash column chromatography (hexane:EtOAc, 97:3, SiO_2) to afford afford 1-((*1R,2R*)-2-(7-bromoheptyl)cyclohexyl)ethan-1-one (57.0 mg, 0.188 mmol, 47%, 16:1 dr) as a mixture of diastereoisomers. The product was obtained as a pale-yellow oil.

^{1}H NMR (500 MHz, $CDCl_3$) δ 3.39 (t, *J* = 6.9 Hz, 2H), 2.18 – 2.14 (m, 1H), 2.12 (s, 3H), 1.93 – 1.67 (m, 6H), 1.67 – 1.52 (m, 1H), 1.43 – 1.36 (m, 2H), 1.35 – 1.12 (m, 10H), 1.07 – 0.87 (m, 2H).

^{13}C NMR (126 MHz, $CDCl_3$) δ 213.5, 58.0, 38.5, 34.9, 34.1, 32.9, 30.9, 29.9, 29.7, 29.2, 28.8, 28.2, 26.4, 25.9 (2C).

$[\alpha]_D^{25}$: –17.6 (*c* 1.0, $CHCl_3$).

IR: 2932, 2857, 1702, 1448 cm^{-1}.

MS: *m/z* calculated for $C_{15}H_{28}O[^{79}Br]^+$ $[M+H]^+$ = 303.1318; found = 303.1324.

SFC analysis indicated an enantiomeric excess of 98% [Chiralpak® IG-3; 1500 psi, 30 °C, flow: 1.5 mL/min; 1.0% to 30.0% MeOH in 5 min; λ = 218 nm; major enantiomer (*1R,2R*), t_R = 3.36 min; minor enantiomer (*1S,2S*), t_R = 4.03 min].

1-((*1R,2S*)-2-(2-(naphthalen-2-yl)ethyl)cyclohexyl)ethan-1-one (4f)

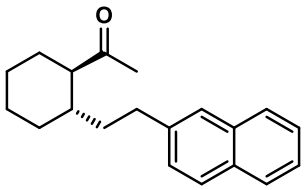

The title compound was obtained following General procedure B using 1-(cyclohex-1-en-1-yl)ethan-1-one (50 μL, 0.4 mmol, 1.0 eq.) and 2-vinylnaphthalene (154.2 mg, 1.0 mmol, 2.5 eq.).

The crude was treated following General procedure C and purified by flash column chromatography (hexane:EtOAc, 97:3, SiO_2) to afford 1-((*1R,2S*)-2-(2-(naphthalen-2-yl)ethyl)cyclohexyl)ethan-1-one (71.8 mg, 0.256 mmol, 64%, 10:1 dr) as a mixture of diastereoisomers. The product was obtained as a pale-yellow oil.

^{1}H NMR (500 MHz, $CDCl_3$) δ 7.87 – 7.74 (m, 3H), 7.62 – 7.58 (m, 1H), 7.47 – 7.40 (m, 2H), 7.31 – 7.29 (m, 1H), 2.88 – 2.86 (m, 1H), 2.69 – 2.67 (m, 1H), 2.33 – 2.17 (m, 1H), 2.08 – 2.04 (m, 4H), 1.87 – 1.77 (m, 2H), 1.74 – 1.65 (m, 3H), 1.52 – 1.39 (m, 1H), 1.33 – 1.21 (m, 3H), 1.10 – 0.97 (m, 1H).

^{13}C NMR (126 MHz, $CDCl_3$) δ 213.1, 140.1, 133.7, 132.0, 128.0, 127.7, 127.5, 127.4, 126.3, 126.0, 125.2, 57.9, 38.1, 36.7, 33.1, 30.8, 29.8, 29.0, 25.8 (2C).

$[\alpha]_D^{25}$: –18.0 (*c* 1.0, $CHCl_3$).

IR: 2932, 2858, 1704, 1601 cm^{-1}.

MS: *m/z* calculated for $C_{20}H_{24}ONa^+$ $[M+Na]^+$ = 303.1719; found = 303.1709.

SFC analysis indicated an enantiomeric excess of 97% [Chiralpak® IG-3; 1500 psi, 30 °C, flow: 1.5 mL/min; 1.0% to 30.0% MeOH in 5 min; λ = 218 nm; major enantiomer (*1R,2S*), t_R = 5.55 min; minor enantiomer (*1S,2R*), t_R = 6.64 min].

1-((*1S,2S*)-2-(4-phenylbutyl)cyclohexyl)ethan-1-one (4g)

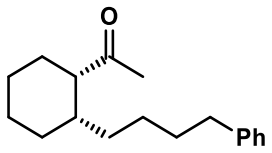

The title compound was obtained following General procedure B using 1-(cyclohex-1-en-1-yl)ethan-1-one (50 μL, 0.4 mmol, 1.0 eq.) and but-3-en-1-ylbenzene (150 μL, 1.0 mmol, 2.5 eq.).

The crude was treated following General procedure D and purified by flash column chromatography (hexane:EtOAc, 97:3, SiO_2) to afford 1-((*1S,2S*)-2-(4-phenylbutyl)cyclohexyl)ethan-1-one (78.6 mg, 0.304 mmol, 76%, 1:4 dr) as a mixture of diastereoisomers. The product was obtained as a pale-yellow oil.

^{1}H NMR (400 MHz, $CDCl_3$) δ 7.32 – 7.24 (m, 2H), 7.23 – 7.14 (m, 3H), 2.62 – 2.54 (m, 2H), 2.10 (s, 3H), 1.99 – 1.95 (m, 1H), 1.82 – 1.78 (m, 2H), 1.70 – 1.52 (m, 5H), 1.49 – 1.33 (m, 4H), 1.32 – 1.16 (m, 3H), 1.12 – 1.00 (m, 1H).

^{13}C NMR (101 MHz, $CDCl_3$) δ 211.8, 142.6, 128.4 (2C), 128.3 (2C), 125.6, 53.9, 36.6, 35.9, 31.5, 28.9, 28.6, 28.1, 27.4, 24.5, 23.6, 21.6.

$[\alpha]_D^{25}$: +5.7 (*c* 1.0, $CHCl_3$).

IR: 3021, 2932, 1702, 1454 cm^{-1}.

MS: *m/z* calculated for $C_{18}H_{25}O^-$ $[M-H]^-$ = 257.1911; found = 257.1910.

SFC analysis indicated an enantiomeric excess of 97% [Chiralpak® IG-3; 1500 psi, 30 °C, flow: 1.5 mL/min; 1.0% to 30.0% MeOH in 5 min; λ = 218 nm; major enantiomer (*1S,2S*), t_R = 3.05 min; minor enantiomer (*1R,2R*), t_R = 3.87 min].

1-((*1S,2S*)-2-(4-methylphenethyl)cyclohexyl)ethan-1-one (4h)

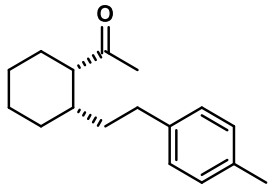

The title compound was obtained following General procedure B using 1-(cyclohex-1-en-1-yl)ethan-1-one (50 μL, 0.4 mmol, 1.0 eq.) and 1-methylstyrene (132 μL, 1.0 mmol, 2.5 eq.).

The crude was treated following General procedure D and purified by flash column chromatography (hexane:EtOAc, 97:3, SiO_2) to afford 1-((*1S,2S*)-2-(4-methylphenethyl)cyclohexyl)ethan-1-one (59.6 mg, 0.244 mmol, 61%, 1:4 dr) as a mixture of diastereoisomers. The product was obtained as a pale-yellow oil.

^{1}H NMR (500 MHz, $CDCl_3$) δ 7.14 – 7.05 (m, 2H), 7.02 – 6.95 (m, 2H), 3.57 – 3.45 (m, 1H), 2.83 – 2.79 (m, 1H), 2.39 – 2.28 (m, 5H), 1.95 – 1.92 (m, 2H), 1.88 – 1.82 (m, 2H), 1.77 (s, 3H), 1.58 – 1.40 (m, 3H), 1.30 – 1.08 (m, 3H).

^{13}C NMR (101 MHz, $CDCl_3$) δ 212.2, 144.3, 135.5, 129.2 (2C), 127.5 (2C), 48.9, 46.9, 41.9, 30.0, 28.9, 26.6, 26.2, 21.9, 21.2 (2C).

$[\alpha]_D^{25}$: +11.9 (*c* 1.0, $CHCl_3$).

IR: 3018, 2932, 1703, 1515 cm^{-1}.

MS: *m/z* calculated for $C_{17}H_{25}O^+$ $[M+H]^+$ = 245.1900; found = 245.1918.

SFC analysis indicated an enantiomeric excess of 97% [Chiralpak® IG-3; 1500 psi, 30 °C, flow: 1.5 mL/min; 1.0% to 30.0% MeOH in 5 min; λ = 218 nm; major enantiomer (*1S,2S*), t_R = 2.91 min; minor enantiomer (*1R,2R*), t_R = 3.05 min].

1-((*1S,2S*)-2-(4-(benzyloxy)butyl)cyclohexyl)ethan-1-one (4i)

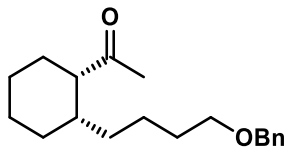

The title compound was obtained following General procedure B using 1-(cyclohex-1-en-1-yl)ethan-1-one (50 µL, 0.4 mmol, 1.0 eq.) and ((but-3-en-1-yloxy)methyl)benzene (162 µL, 1.0 mmol, 2.5 eq.).

The crude was treated following General procedure D and purified by flash column chromatography (hexane:EtOAc, 97:3, SiO_2) to afford afford 1-((*1S,2S*)-2-(4-(benzyloxy)butyl)cyclohexyl)ethan-1-one (105.0 mg, 0.364 mmol, 91%, 1:5 dr) as a mixture of diastereoisomers. The product was obtained as a pale-yellow oil.

^{1}H NMR (500 MHz, $CDCl_3$) δ 7.33 – 7.30 (m, 4H), 7.28 – 7.24 (m, 1H), 4.48 (s, 2H), 3.44 (t, *J* = 6.5 Hz, 2H), 2.57 – 2.54 (m, 1H), 2.09 (s, 3H), 1.99 – 1.96 (m, 1H), 1.83 – 1.79 (m, 1H), 1.69 – 1.47 (m, 5H), 1.46 – 1.33 (m, 4H), 1.32 – 1.15 (m, 3H), 1.04 – 0.98 (m, 1H).

^{13}C NMR (126 MHz, $CDCl_3$) δ 211.8, 138.7, 128.4(2C), 127.7(2C), 127.5, 73.0, 70.3, 53.9, 36.6, 29.9, 28.9, 28.6, 28.1, 24.5, 24.5, 23.6, 21.7.

$[\alpha]_D^{25}$: +8.7 (*c* 1.0, $CHCl_3$).

IR: 3018, 2936, 1703, 1454 cm^{-1}.

MS: *m/z* calculated for $C_{19}H_{27}O_2^-$ $[M-H]^-$ = 287.2016; found = 287.2012.

SFC analysis indicated an enantiomeric excess of 97% [Chiralpak® IG-3; 1500 psi, 30 °C, flow: 1.5 mL/min; 1.0% to 30.0% MeOH in 5 min; λ = 218 nm; major enantiomer (*1S,2S*), t_R = 3.16 min; minor enantiomer (*1R,2R*), t_R = 3.28 min].

1-((*1S,2S*)-2-(5-bromopentyl)cyclohexyl)ethan-1-one (4j)

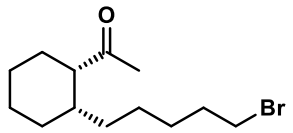

The title compound was obtained following General procedure B using 1-(cyclohex-1-en-1-yl)ethan-1-one (50 μL, 0.4 mmol, 1.0 eq.) and 5-bromoheptene (118.5 μL, 1.0 mmol, 2.5 eq.).

The crude was treated following General procedure D and purified by flash column chromatography (hexane:EtOAc, 97:3, SiO_2) to afford afford 1-((*1S,2S*)-2-(5-bromopentyl)cyclohexyl)ethan-1-one (81.5 mg, 0.296 mmol, 74%, 1:2.5 dr) as a mixture of diastereoisomers. The product was obtained as a pale-yellow oil.

^{1}H NMR (500 MHz, $CDCl_3$) δ 3.36 (t, *J* = 6.8 Hz, 2H), 2.55 – 2.53 (m, 1H), 2.09 (s, 3H), 1.96 – 1.94 (m, 1H), 1.85 – 1.70 (m, 4H), 1.67 – 1.51 (m, 2H), 1.47 – 1.31 (m, 6H), 1.27 – 1.12 (m, 3H), 1.07 – 0.94 (m, 1H).

^{13}C NMR (126 MHz, $CDCl_3$) δ 211.8, 53.9, 36.6, 34.0, 32.8, 29.0, 28.6, 28.4, 28.2, 27.0, 24.5, 23.7, 21.7.

$[\alpha]_D^{25}$: +1.7 (*c* 1.0, $CHCl_3$).

IR: 3017, 2932, 1703, 1216 cm^{-1}.

MS: *m/z* calculated for $C_{13}H_{24}O[^{79}Br]^+$ $[M+H]^+$ = 275.1005; found = 275.1011.

SFC analysis indicated an enantiomeric excess of 97% [Chiralpak® IG-3; 1500 psi, 30 °C, flow: 1.5 mL/min; 1.0% to 30.0% MeOH in 5 min; λ = 218 nm; major enantiomer (*1S,2S*), t_R = 2.97 min; minor enantiomer (*1R,2R*), t_R = 3.48 min].

1-((*1R,2R*)-2-methylcyclohexyl)ethan-1-one (4k)

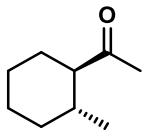

The title compound was obtained following a modified version of General procedure B using 1-(cyclohex-1-en-1-yl)ethan-1-one (50 μL, 0.4 mmol, 1.0 eq.) and $Cp_2ZrMeCl$ (271.9 mg, 1.0 mmol, 2.5 eq.) as the direct nucleophile (see page 210).

The crude was treated following General procedure C and purified by flash column chromatography (hexane:EtOAc, 97:3, SiO_2) to afford 1-((*1R,2R*)-2-methylcyclohexyl)ethan-1-one (29.7 mg, 0.212 mmol, 53%, 18:1 dr) as a mixture of diastereoisomers. The product was obtained as a pale-yellow oil.

^{1}H NMR (400 MHz, $CDCl_3$) δ 2.12 (s, 3H), 2.11 – 2.02 (m, 1H), 1.82 – 1.54 (m, 5H), 1.33 – 1.16 (m, 3H), 0.98 – 0.92 (m, 1H), 0.83 (d, *J* = 6.4 Hz, 3H).

^{13}C NMR (101 MHz, $CDCl_3$) δ 213.3, 59.4, 34.6, 33.9, 29.7, 29.2, 26.1, 25.8, 20.7.

$[\alpha]_D^{25}$: –10.8 (*c* 1.0, $CHCl_3$).

GC analysis indicated an enantiomeric excess of 98% [HYDRODEX β -3P; initial temperature 60 °C, progress rate 1.0 °C/min, final temperature 90 °C, 10 psi, flow: 2.02 mL/min; minor enantiomer (*1S,2S*), t_R = 16.89 min; major enantiomer (*1R,2R*), t_R = 17.11 min].

Analytical data are in agreement with the literature.[4]

1-((*1S,2R*)-2-methylcyclohexyl)ethan-1-one (4l)

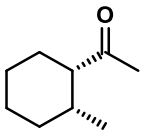

The title compound was obtained following a modified version of General procedure B using 1-(cyclohex-1-en-1-yl)ethan-1-one (50 μL, 0.4 mmol, 1.0 eq.) and $Cp_2ZrMeCl$ (271.9 mg, 1.0 mmol, 2.5 eq.) as the direct nucleophile.

The crude was treated following General procedure D and purified by flash column chromatography (hexane:EtOAc, 97:3, SiO_2) to afford 1-((*1S,2R*)-2-methylcyclohexyl)ethan-1-one (24.7 mg, 0.176 mmol, 44%, 1:2.5 dr) as a mixture of diastereoisomers. The product was obtained as a pale-yellow oil.

^{1}H NMR (400 MHz, $CDCl_3$) δ 2.54 – 2.47 (m, 1H), 2.34 – 2.26 (m, 1H), 2.12 (s, 3H), 1.82 – 1.51 (m, 5H), 1.46 – 1.38 (m, 1H), 1.31 – 1.13 (m, 2H), 0.83 (d, *J* = 7.2 Hz, 3H).

^{13}C NMR (101 MHz, $CDCl_3$) δ 211.9, 54.2, 32.8, 30.6, 28.6, 25.1, 22.2, 20.9, 14.2.

$[\alpha]_D^{25}$: +4.7 (*c* 1.0, $CHCl_3$).

GC analysis indicated an enantiomeric excess of 97% [HYDRODEX β -3P; initial temperature 60 °C, progress rate 1.0 °C/min, final temperature 90 °C, 10 psi, flow: 2.02 mL/min; minor enantiomer (*1R,2S*), t_R = 16.89 min; major enantiomer (*1S,2R*), t_R = 17.11 min].

Analytical data are in agreement with the literature.[4]

1-((*1R,2R*)-2-(4-phenylbutyl)cyclopentyl)ethan-1-one (4m)

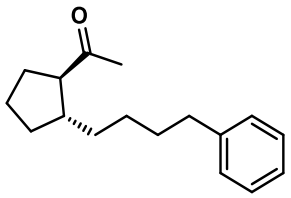

The title compound was obtained following General procedure B using 1-(cyclopent-1-en-1-yl)ethan-1-one (46 μL, 0.4 mmol, 1.0 eq.) and but-3-en-1-ylbenzene (150 μL, 1.0 mmol, 2.5 eq.).

The crude was treated following General procedure C and purified by flash column chromatography (hexane:EtOAc, 97:3, SiO_2) to afford 1-((*1R,2R*)-2-(4-phenylbutyl)cyclopentyl)ethan-1-one (67.5 mg, 0.276 mmol, 69%, >20:1 dr) as a mixture of diastereoisomers. The product was obtained as a pale-yellow oil.

^{1}H NMR (400 MHz, $CDCl_3$) δ 7.34 – 7.27 (m, 2H), 7.23 – 7.16 (m, 3H), 2.67 – 2.61 (m, 2H), 2.52 – 2.46 (m, 1H), 2.20 – 2.11 (m, 4H), 1.99 – 1.83 (m, 2H), 1.79 – 1.58 (m, 5H), 1.56 – 1.43 (m, 1H), 1.41 – 1.28 (m, 3H), 1.28 – 1.19 (m, 1H).

^{13}C NMR (101 MHz, $CDCl_3$) δ 211.6, 142.8, 128.5(2C), 128.3(2C), 125.7, 59.0, 42.6, 36.0, 35.6, 32.7, 31.7, 29.9, 29.2, 28.1, 25.0.

$[\alpha]_D^{25}$: –43.5 (*c* 1.0, $CHCl_3$).

IR: 3021, 2932, 1702, 1496 cm^{-1}.

MS: *m/z* calculated for $C_{17}H_{28}ON^+$ $[M+NH_4]^+$ = 262.2165; found = 262.2187.

SFC analysis indicated an enantiomeric excess of 97% [Chiralpak® IG-3; 1500 psi, 30 °C, flow: 1.5 mL/min; 1.0% to 30.0% MeOH in 5 min; λ = 218 nm; major enantiomer (*1R,2R*), t_R = 3.66 min; minor enantiomer (*1S,2S*), t_R = 4.14 min].

phenyl((*1R,2S*)-2-(4-phenylbutyl)cyclohexyl)methanone (4n)

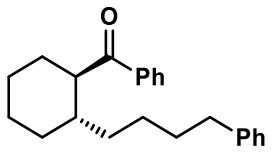

The title compound was obtained following General procedure B using cyclohex-1-en-1-yl(phenyl)methanone (74.5 μL, 0.4 mmol, 1.0 eq.) and but-3-en-1-ylbenzene (150 μL, 1.0 mmol, 2.5 eq.).

The crude was treated following General procedure C and purified by flash column chromatography (hexane:EtOAc, 97:3, SiO_2) to afford phenyl((*1R,2S*)-2-(4-phenylbutyl)cyclohexyl)methanone (112.8 mg, 0.352 mmol, 88%, 1.8:1 dr) as a mixture of diastereoisomers. The product was obtained as a pale-yellow oil.

^{1}H NMR (500 MHz, $CDCl_3$) (**major — *1R,2S***) δ 7.98 (d, *J* = 7.1 Hz, 2H), 7.60 – 7.52 (m, 1H), 7.50 – 7.45 (m, 2H), 7.26 – 7.22 (m, 3H), 7.19 – 7.10 (m, 2H), 3.21 – 3.08 (m, 1H), 2.54 – 2.50 (m, 2H), 2.05 – 1.76 (m, 5H), 1.62 – 1.20 (m, 8H), 1.18 – 0.95 (m, 2H).

^{1}H NMR (500 MHz, $CDCl_3$) (**minor — *1S,2R***) δ 7.94 – 7.89 (m, 2H), 7.50 – 7.45 (m, 2H), 7.26 – 7.22 (m, 2H), 7.19 – 7.10 (m, 2H), 7.09 – 7.04 (m, 2H), 3.57 – 3.48 (m, 1H), 2.48 (t, *J* = 7.8 Hz, 2H), 2.05 – 1.76 (m, 5H), 1.62 – 1.20 (m, 8H), 1.18 – 0.95 (m, 2H).

^{13}C NMR (126 MHz, $CDCl_3$) (**major — *1R,2S***): δ 204.9, 142.8, 137.7, 132.9, 128.7(2C), 128.5(2C), 128.2(4C), 125.6, 51.1, 38.7, 35.9, 35.0, 31.6, 31.3, 31.3, 26.4, 26.2, 26.0.

^{13}C NMR (126 MHz, $CDCl_3$) (**minor — *1S,2R***): δ 203.7, 142.7, 137.2, 132.6, 128.7(2C), 128.4(2C), 128.3(4C), 125.6, 47.9, 37.6, 35.7, 31.3, 28.9, 28.2, 27.1, 24.5, 24.5, 22.1.

$[\alpha]_D^{25}$: –23.8 (*c* 1.0, $CHCl_3$).

IR: 3025, 2937, 1678, 1217 cm^{-1}.

MS: *m/z* calculated for $C_{23}H_{29}O^+$ $[M+H]^+$ = 321.2213; found = 321.2234.

SFC analysis indicated an enantiomeric excess of 95% [Chiralpak® IG-3; 1500 psi, 30 °C, flow: 1.5 mL/min; 1.0% to 30.0% MeOH in 5 min; λ = 218 nm; minor enantiomer (*1S,2R*), t_R = 3.34 min; major enantiomer (*1R,2S*), t_R = 4.07 min].

1-((*1R,2S*)-2-(4-phenylbutyl)cyclohexyl)pentan-1-one (4o)

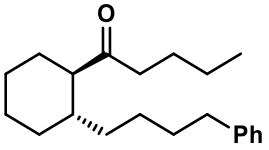

The title compound was obtained following General procedure B using 1-(cyclohex-1-en-1-yl)pentan-1-one (66.5 μL, 0.4 mmol, 1.0 eq.) and but-3-en-1-ylbenzene (150 μL, 1.0 mmol, 2.5 eq.).

The crude was treated following General procedure C and purified by flash column chromatography (hexane:EtOAc, 97:3, SiO_2) to afford 1-((*1R,2S*)-2-(4-phenylbutyl)cyclohexyl)pentan-1-one (84.1 mg, 0.280 mmol, 70%, 5:1 dr) as a mixture of diastereoisomers. The product was obtained as a pale-yellow oil.

^{1}H NMR (400 MHz, $CDCl_3$) δ 7.33 – 7.25 (m, 2H), 7.23 – 7.15 (m, 3H), 2.65 – 2.56 (m, 2H), 2.53 – 2.31 (m, 2H), 2.22 – 2.10 (m, 1H), 1.94 – 1.69 (m, 3H), 1.68 – 1.49 (m, 5H), 1.48 – 1.17 (m, 9H), 1.05 – 0.98 (m, 1H), 0.96 – 0.85 (m, 4H).

^{13}C NMR (101 MHz, $CDCl_3$) δ 215.4, 142.8, 128.5(2C), 128.4 (2C), 125.7, 57.2, 42.4, 38.4, 36.0, 34.8, 31.7, 31.0, 30.1, 26.3, 26.1, 25.9, 25.7, 22.6, 14.1.

$[\alpha]_D^{25}$: –20.7 (*c* 1.0, $CHCl_3$).

IR: 2981, 1704, 1454, 1217 cm^{-1}.

MS: *m/z* calculated for $C_{21}H_{32}ONa^+$ $[M+Na]^+$ = 323.2345; found = 323.2332.

SFC analysis indicated an enantiomeric excess of 80% [Chiralpak® IG-3; 1500 psi, 30 °C, flow: 1.5 mL/min; 1.0% to 30.0% MeOH in 5 min; λ = 218 nm; major enantiomer (*1R,2S*), t_R = 2.29 min; minor enantiomer (*1S,2R*), t_R = 2.36 min].

2-phenyl-1-((*1R,2S*)-2-(4-phenylbutyl)cyclohexyl)ethan-1-one (4p)

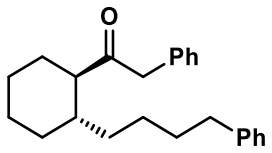

The title compound was obtained following General procedure B using 1-(cyclohex-1-en-1-yl)-2-phenylethan-1-one (80 μL, 0.4 mmol, 1.0 eq.) and but-3-en-1-ylbenzene (150 μL, 1.0 mmol, 2.5 eq.).

The crude was treated following General procedure C and purified by flash column chromatography (hexane:EtOAc, 97:3, SiO_2) to afford 2-phenyl-1-((*1R,2S*)-2-(4-phenylbutyl)cyclohexyl)ethan-1-one (53.5 mg, 0.160 mmol, 40%, 5:1 dr) as a mixture of diastereoisomers. The product was obtained as a pale-yellow oil.

^{1}H NMR (400 MHz, $CDCl_3$): δ 7.37 – 7.22 (m, 5H), 7.22 – 7.11 (m, 5H), 3.69 (s, 2H), 2.55 – 2.48 (m, 2H), 2.37 – 2.26 (m, 1H), 1.89 – 1.63 (m, 5H), 1.54 – 1.41 (m, 3H), 1.34 – 1.07 (m, 5H), 0.94 – 0.73 (m, 2H).

^{13}C NMR (101 MHz, $CDCl_3$): 212.0, 142.9, 134.1, 129.8 (2C), 128.7 (2C), 128.5 (2C), 128.4 (2C), 127.0, 125.7, 56.2, 49.9, 38.3, 35.9, 34.7, 31.7, 30.8, 30.3, 26.1, 26.0, 25.9.

$[\alpha]_D^{25}$: +3.6 (*c* 1.0, $CHCl_3$).

IR: 3020, 2934, 1708, 1217 cm^{-1}.

MS: *m/z* calculated for $C_{24}H_{31}O^+$ $[M+H]^+$ = 335.2369; found = 335.2386.

SFC analysis indicated an enantiomeric excess of 90% [Chiralpak® IG-3; 1500 psi, 30 °C, flow: 1.5 mL/min; 1.0% to 30.0% MeOH in 5 min; λ = 218 nm; major enantiomer (*1R,2S*), t_R = 2.97 min; minor enantiomer (*1S,2R*), t_R = 3.48 min].

1-((*3S,4R*)-3-(4-phenylbutyl)tetrahydro-*2H*-pyran-4-yl)ethan-1-one (4q)

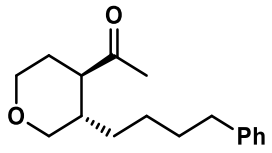

The title compound was obtained following General procedure B using 1-(3,6-dihydro-2*H*-pyran-4-yl)ethan-1-one (50.5 μL, 0.4 mmol, 1.0 eq.) and but-3-en-1-ylbenzene (150 μL, 1.0 mmol, 2.5 eq.).

The crude was treated following General procedure C and purified by flash column chromatography (hexane:EtOAc, 97:3, SiO_2) to afford 1-((*3S,4R*)-3-(4-phenylbutyl)tetrahydro-*2H*-pyran-4-yl)ethan-1-one (88.5 mg, 0.340 mmol, 85%, 6.4:1 dr) as a mixture of diastereoisomers. The product was obtained as a pale-yellow oil.

^{1}H NMR (400 MHz, $CDCl_3$) δ 7.30 – 7.23 (m, 2H), 7.19 – 7.10 (m, 3H), 4.02 – 3.95 (m, 2H), 3.37 – 3.35 (m, 1H), 3.07 – 2.99 (m, 1H), 2.63 – 2.51 (m, 2H), 2.36 – 2.28 (m, 1H), 2.14 (s, 3H), 1.92 – 1.80 (m, 1H), 1.75 – 1.49 (m, 4H), 1.37 – 1.21 (m, 2H), 1.08 – 0.75 (m, 2H).

^{13}C NMR (101 MHz, $CDCl_3$): δ 210.8, 142.5, 128.5 (2C), 128.4 (2C), 125.8, 71.5, 67.4, 54.9, 36.8, 35.8, 31.6, 30.8, 29.1, 28.9, 26.4.

$[\alpha]_D^{25}$: –14.1 (*c* 1.0, $CHCl_3$).

IR: 3019, 2934, 1711, 1217 cm^{-1}.

MS: *m/z* calculated for $C_{17}H_{25}O_2Na^+$ $[M+Na]^+$ = 283.1669; found =283.1662.

SFC analysis indicated an enantiomeric excess of 94% [Chiralpak® IG-3; 1500 psi, 30 °C, flow: 1.5 mL/min; 1.0% to 30.0% MeOH in 5 min; λ = 218 nm; major enantiomer (*3R,4S*), t_R = 4.96 min; minor enantiomer (*3S,4R*), t_R = 6.34 min].

1-((*3S,4R*)-3-(4-phenylbutyl)tetrahydro-*2H*-thiopyran-4-yl)ethan-1-one (4r)

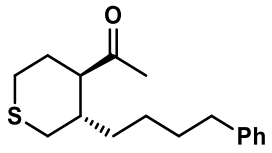

The title compound was obtained following General procedure B using 1-(3,6-dihydro-2*H*-thiopyran-4-yl)ethan-1-one (57 µL, 0.4 mmol, 1.0 eq.) and but-3-en-1-ylbenzene (150 µL, 1.0 mmol, 2.5 eq.).

The crude was treated following General procedure C and purified by flash column chromatography (hexane:EtOAc, 97:3, SiO_2) to afford 1-((*3S,4R*)-3-(4-phenylbutyl)tetrahydro-*2H*-thiopyran-4-yl)ethan-1-one (58.6 mg, 0.212 mmol, 53%, 5:1 dr) as a mixture of diastereoisomers. The product was obtained as a pale-yellow oil.

^{1}H NMR (400 MHz, $CDCl_3$) (major): δ 7.31 – 7.24 (m, 2H), 7.21 – 7.13 (m, 3H), 2.80 – 2.67 (m, 1H), 2.64 – 2.50 (m, 4H), 2.34 – 2.21 (m, 2H), 2.14 – 2.05 (m, 4H), 2.01 – 1.85 (m, 1H), 1.77 – 1.69 (m, 1H), 1.67 – 1.49 (m, 2H), 1.45 – 1.11 (m, 4H).

^{13}C NMR (101 MHz, $CDCl_3$) δ 211.3, 142.5, 128.5 (2C), 128.4 (2C), 125.8, 57.2, 38.7, 35.8, 34.1, 31.9, 31.5, 30.5, 28.9, 27.7, 26.0.

$[\alpha]_D^{25}$: –30.5 (*c* 1.0, $CHCl_3$).

IR: 3023, 2936, 1708, 1218 cm^{-1}.

MS: *m/z* calculated for $C_{17}H_{25}OSNa^+$ $[M+Na]^+$ = 299.1440; found = 299.1441.

SFC analysis indicated an enantiomeric excess of 99% [Chiralpak® IG-3; 1500 psi, 30 °C, flow: 1.5 mL/min; 1.0% to 30.0% MeOH in 5 min; λ = 218 nm; minor enantiomer (*3S*,*4R*), t_R = 5.18 min; major enantiomer (*3R*,*4S*), t_R = 5.69 min].

1-((*1S,2S*)-2-(4-phenylbutyl)cycloheptyl)ethan-1-one (4t)

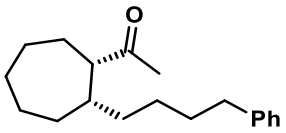

The title compound was obtained following General procedure B using 1-(cyclohept-1-en-1-yl)ethan-1-one (55.3 μL, 0.4 mmol, 1.0 eq.) and but-3-en-1-ylbenzene (150 μL, 1.0 mmol, 2.5 eq.).

The crude was treated following General procedure D and purified by flash column chromatography (hexane:EtOAc, 97:3, SiO_2) to afford 1-((*1S,2S*)-2-(4-phenylbutyl)cycloheptyl)ethan-1-one (88.3 mg, 0.324 mmol, 81%, 9:1 dr) as a mixture of diastereoisomers. The product was obtained as a pale-yellow oil.

^{1}H NMR (400 MHz, $CDCl_3$) δ 7.34 – 7.25 (m, 2H), 7.22 – 7.15 (m, 3H), 2.67 – 2.55 (m, 2H), 2.42 – 2.32 (m, 1H), 2.15 (s, 3H), 1.97 – 1.90 (m, 1H), 1.77 – 1.52 (m, 9H), 1.51 – 1.33 (m, 4H), 1.32 – 1.15 (m, 3H).

^{13}C NMR (101 MHz, $CDCl_3$) δ 212.5, 142.8, 128.5 (2C), 128.3 (2C) 125.7, 59.4, 39.3, 36.2, 35.9, 31.7, 31.0, 29.8, 29.2, 28.9, 26.9, 26.7, 26.1.

$[\alpha]_D^{25}$: +23.2 (*c* 1.0, $CHCl_3$).

IR: 2981, 2933, 1704, 1216 cm^{-1}.

MS: *m/z* calculated for $C_{19}H_{28}ONa^+$ $[M+Na]^+$ = 295.2032; found = 295.2036.

SFC analysis indicated an enantiomeric excess of 95% [Chiralpak® IG-3; 1500 psi, 30 °C, flow: 1.5 mL/min; 1.0% to 30.0% MeOH in 5 min; λ = 218 nm; major enantiomer (*1S,2S*), t_R = 3.51 min; minor enantiomer (*1R,2R*), t_R = 4.21 min].

1-((*1S,2S*)-2-(4-phenylbutyl)cyclooctyl)ethan-1-one (4u)

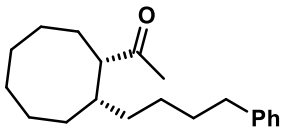

The title compound was obtained following General procedure B using 1-(cyclooct-1-en-1-yl)ethan-1-one (55.3 μL, 0.4 mmol, 1.0 eq.) and but-3-en-1-ylbenzene (150 μL, 1.0 mmol, 2.5 eq.).

The crude was treated following General procedure D and purified by flash column chromatography (hexane:EtOAc, 97:3, SiO_2) to afford 1-((*1S,2S*)-2-(4-phenylbutyl)cyclooctyl)ethan-1-one (91.7 mg, 0.320 mmol, 80%, 9:1 dr) as a mixture of diastereoisomers. The product was obtained as a pale-yellow oil.

^{1}H NMR (400 MHz, $CDCl_3$) δ 7.34 – 7.25 (m, 2H), 7.24 – 7.13 (m, 3H), 2.70 – 2.53 (m, 2H), 2.41 – 2.34 (m, 1H), 2.14 (s, 3H), 2.05 – 1.91 (m, 1H), 1.86 – 1.56 (m, 9H), 1.55 – 1.34 (m, 6H), 1.33 – 1.09 (m, 3H).

^{13}C NMR (101 MHz, $CDCl_3$) δ 212.4, 142.7, 128.5 (2C), 128.3 (2C), 125.6, 58.2, 37.3, 35.9, 35.2, 31.7, 29.3, 27.9, 27.0 (2C), 26.9, 26.5, 26.1, 25.7.

$[\alpha]_D^{25}$: +34.2 (*c* 1.0, $CHCl_3$).

IR: 3020, 2930, 1704, 1216 cm^{-1}.

MS: *m/z* calculated for $C_{20}H_{31}O^+$ $[M+H]^+$ = 287.2369; found = 287.2395.

SFC analysis indicated an enantiomeric excess of 98% [Chiralpak® IG-3; 1500 psi, 30 °C, flow: 1.5 mL/min; 1.0% to 30.0% MeOH in 5 min; λ = 218 nm; major enantiomer (*1S,2S*), t_R = 2.80 min; minor enantiomer (*1R,2R*), t_R = 2.87 min].

Phenyl((*1S,2S*)-2-(4-phenylbutyl)cyclohexyl)methanone (4v)

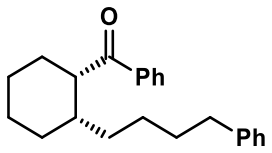

The title compound was obtained following General procedure B using cyclohex-1-en-1-yl(phenyl)methanone (74.5 μL, 0.4 mmol, 1.0 eq.) and but-3-en-1-ylbenzene (150 μL, 1.0 mmol, 2.5 eq.).

The crude was treated following General procedure D and purified by flash column chromatography (hexane:EtOAc, 97:3, SiO_2) to afford phenyl((*1S,2S*)-2-(4-phenylbutyl)cyclohexyl)methanone (102.6 mg, 0.32 mmol, 80%, 1:1.5 dr) as a mixture of diastereoisomers. The product was obtained as a pale-yellow oil.

^{1}H NMR (400 MHz, $CDCl_3$) (**major — *1S,2S***) δ 7.93 – 7.88 (m, 2H), 7.59 – 7.51 (m, 1H), 7.50 – 7.41 (m, 2H), 7.24 – 7.20 (m, 2H), 7.18 – 7.10 (m, 1H), 7.07 – 7.04 (m, 2H), 3.51 – 3.44 (m, 1H), 2.47 (t, *J* = 7.7 Hz, 2H), 2.03 – 1.62 (m, 5H), 1.60 – 1.22 (m, 8H), 1.16 – 0.97 (m, 2H).

^{1}H NMR (400 MHz, $CDCl_3$) (**minor — *1R,2S***) δ 8.00 – 7.94 (m, 2H), 7.59 – 7.51 (m, 1H), 7.50 – 7.41 (m, 2H), 7.24 – 7.20 (m, 2H), 7.18 – 7.10 (m, 3H), 3.21 – 3.08 (m, 1H), 2.52 – 2.49 (m, 2H), 2.03 – 1.62 (m, 5H), 1.60 – 1.22 (m, 8H), 1.16 – 0.97 (m, 2H).

^{13}C NMR (101 MHz, $CDCl_3$) (**major — *1S,2S***) δ 203.7, 142.7, 137.2, 132.6, 128.7 (2C), 128.5 (2C), 128.3 (4C), 125.6, 47.9, 37.6, 35.7, 31.3, 28.9, 28.2, 27.2, 24.5 (2C), 22.1.

^{13}C NMR (126 MHz, $CDCl_3$) (**minor — *1R,2S***): δ 204.9, 142.8, 137.7, 132.9, 128.7(2C), 128.5(2C), 128.2(4C), 125.6, 51.1, 38.7, 35.9, 35.0, 31.6, 31.3 (2C), 26.4, 26.2, 26.0.

$[\alpha]_D^{25}$: –18.7 (*c* 1.0, $CHCl_3$).

IR: 3025, 2937, 1678, 1217 cm^{-1}.

MS: *m/z* calculated for $C_{23}H_{29}O^+$ $[M+H]^+$ = 321.2213; found = 321.2234.

SFC analysis indicated an enantiomeric excess of 95% [Chiralpak® IG-3; 1500 psi, 30 °C, flow: 1.5 mL/min; 1.0% to 30.0% MeOH in 5 min; λ = 218 nm; major enantiomer (*1S,2S*), t_R = 3.63 min; minor enantiomer (*1R,2R*), t_R = 3.77 min].

(*3S,4S*)-3,4-dimethyl-8-phenyloctan-2-one (5a)

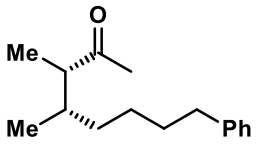

The title compound was obtained following General procedure B using 3-methyl-3-penten-2-one (45.0 µL, 0.4 mmol, 1.0 eq.) and but-3-en-1-ylbenzene (150 µL, 1.0 mmol, 2.5 eq.).

The crude was treated following General procedure C and purified by flash column chromatography (hexane:EtOAc, 97:3, SiO_2) to afford (*3S,4S*)-3,4-dimethyl-8-phenyloctan-2-one (86.2 mg, 0.37 mmol, 93%, 1:1.5 dr) as a mixture of diastereoisomers. The product was obtained as a pale-yellow oil.

^{1}H NMR (400 MHz, $CDCl_3$): δ 7.32 – 7.24 (m, 2H), 7.22 – 7.12 (m, 3H), 2.65 – 2.56 (m, 2H), 2.40 – 2.33 (m, 1H), 2.12 (s, 3H), 1.84 – 1.74 (m, 1H), 1.69 – 1.51 (m, 2H), 1.47 – 1.16 (m, 4H), 1.02 (d, *J* = 7.0 Hz, 3H), 0.89 (d, *J* = 6.7 Hz, 3H).

^{13}C NMR (101 MHz, $CDCl_3$) δ 213.0, 142.8, 128.4 (4C), 125.8, 52.9, 36.0, 35.3, 35.1, 31.8, 29.0, 26.7, 18.0, 12.8.

HRMS (ESI): *m/z* calculated for $C_{16}H_{25}O^+$ $[M+H]^+$ = 233.1900. Found = 233.1893.

IR: 3025, 2934, 1709, 1497, 1218 cm^{-1}.

$[\alpha]^{22}_D$ = -26.4 (*c* 1.0, $CHCl_3$).

SFC Analysis indicated an enantiomeric excess of 93% [Chiralpak® IG-3; 1500 psi, 30 °C, flow: 1.5 mL/min; 1.0% to 30.0% MeOH in 5 min; λ = 218 nm; major enantiomer (*3S,4S*), t_R = 2.285 min; minor enantiomer (*3R,4R*), t_R = 2.686 min].

(3*R*,4*S*)-3,4-dimethyl-8-phenyloctan-2-one (5b)

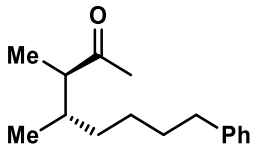

The title compound was obtained following General procedure B using 3-methyl-3-penten-2-one (45.0 μL, 0.4 mmol, 1.0 eq.) and but-3-en-1-ylbenzene (150 μL, 1.0 mmol, 2.5 eq.).

The crude was treated following General procedure D and purified by flash column chromatography (hexane:EtOAc, 97:3, SiO_2) to afford (3*R*,4*S*)-3,4-dimethyl-8-phenyloctan-2-one (86.0 mg, 0.37 mmol, 1.9:1 dr) as a mixture of diastereoisomers. The product was obtained as a pale-yellow oil.

^{1}H NMR (400 MHz, $CDCl_3$) δ 7.31 – 7.24 (m, 2H), 7.21 – 7.14 (m, 3H), 2.66 – 2.55 (m, 2H), 2.48 – 2.41 (m, 1H), 2.12 (s, 3H), 1.88 – 1.80 (m, 1H), 1.69 – 1.52 (m, 2H), 1.46 – 1.07 (m, 4H), 0.97 (d, *J* = 6.9 Hz, 3H), 0.78 (d, *J* = 6.8 Hz, 3H).

^{13}C NMR (101 MHz, $CDCl_3$) δ 212.9, 142.8, 128.5 (4C), 125.8, 51.8, 36.0, 35.3, 34.4, 31.7, 28.7, 27.1, 15.4, 11.1.

5.4.2 Enones and precursors:

1-ethynylcyclopentan-1-ol

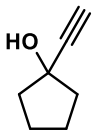

The title compound was obtained following General procedure E using cyclopentanone (442 µL, 8.0 mmol, 1.0 eq.) and ethynyltrimethylsilane (1.1 mL, 8.0 mmol, 1.6 eq.). The crude mixture was purified via flash column chromatography (hexane:EtOAc 90:10, SiO_2), 1-ethynylcyclopentan-1-ol was obtained as a pale yellow oil (531 mg, 97%).

^{1}H NMR (400 MHz, $CDCl_3$) δ 2.73 (s, 1H), 2.44 (s, 1H), 1.92 – 1.87 (m, 4H), 1.83 – 1.73 (m, 2H), 1.71 – 1.63 (m, 2H).

^{13}C NMR (101 MHz, $CDCl_3$) δ 87.9, 74.2, 71.1, 42.3 (2C), 23.4 (2C).

Analytical data are in agreement with the literature.[5]

1-ethynylcycloheptan-1-ol

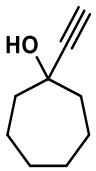

The title compound was obtained following General procedure E using cycloheptanone (535 µL, 8.0 mmol, 1.0 eq.) and ethynyltrimethylsilane (1.1 mL, 8.0 mmol, 1.6 eq.). The crude mixture was purified via flash column chromatography (hexane:EtOAc 90:10, SiO_2), 1-ethynylcycloheptan-1-ol was obtained as a pale yellow oil (636.2 mg, 92%).

^{1}H NMR (400 MHz, $CDCl_3$) δ 3.10 (s, 1H), 2.36 (s, 1H), 1.95 – 1.84 (m, 2H), 1.80 – 1.64 (m, 2H), 1.56 – 1.38 (m, 8H).

^{13}C NMR (101 MHz, $CDCl_3$) δ 88.9, 71.3, 71.2, 42.7 (2C), 27.9 (2C), 21.9 (2C).

Analytical data are in agreement with the literature.[5]

1-ethynylcyclooctan-1-ol

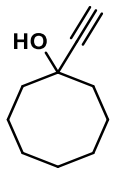

The title compound was obtained following General procedure E using cyclooctanone (605 µL, 8.0 mmol, 1.0 eq.) and ethynyltrimethylsilane (1.1 mL, 8.0 mmol, 1.6 eq.). The crude mixture was purified via flash column chromatography (hexane:EtOAc 90:10, SiO_2), 1-ethynylcyclooctan-1-ol was obtained as a pale yellow oil (722.7 mg, 95%).

^{1}H NMR (400 MHz, $CDCl_3$) δ 2.41 (s, 1H), 2.26 (s, 1H), 2.00 – 1.79 (m, 4H), 1.68 – 1.50 (m, 7H), 1.44 (m, 3H).

^{13}C NMR (101 MHz, $CDCl_3$) δ 88.8, 71.2, 71.2, 38.0 (2C), 27.9 (2C), 24.5, 22.0 (2C).

Analytical data are in agreement with the literature.[5]

1-(phenylethynyl)cyclohexan-1-ol

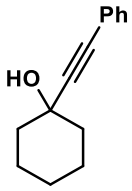

(Deprotection with K_2CO_3 in MeOH is not required for this example)

The title compound was obtained following General procedure E using cyclohexanone (520 µL, 8.0 mmol, 1.0 eq.) and phenylacetylene (880 µL, 8.0 mmol, 1.6 eq.). The crude mixture was purified via flash column chromatography (hexane:EtOAc 90:10, SiO_2), 1-(phenylethynyl)cyclohexan-1-ol was obtained as a pale yellow oil (978 mg, 98%).

^{1}H NMR (400 MHz, $CDCl_3$) δ 7.49 – 7.38 (m, 2H), 7.32 – 7.20 (m, 3H), 3.62 (s, 1H), 2.10 – 2.04 (m, 2H), 1.77 – 1.52 (m, 7H), 1.35 – 1.18 (m, 1H).

^{13}C NMR (101 MHz, $CDCl_3$) δ 131.5 (2C), 128.0 (2C), 127.9, 122.9, 93.0, 84.2, 68.9, 39.8 (2C), 25.1, 23.3 (2C).

Analytical data are in agreement with the literature.[6]

1-(pent-1-yn-1-yl)cyclohexan-1-ol

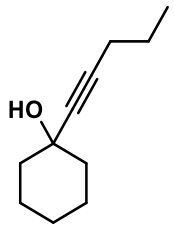

(Deprotection with K_2CO_3 in MeOH is not required for this example)

The title compound was obtained following General procedure E using cyclohexanone (520 µL, 8.0 mmol, 1.0 eq.) and pentyne (790 µL, 8.0 mmol, 1.6 eq.). The crude mixture was purified via flash column chromatography (hexane:EtOAc 90:10, SiO_2), 1-(phenylethynyl)cyclohexan-1-ol was obtained as a pale yellow oil (978 mg, 98%).

^{1}H NMR (400 MHz, $CDCl_3$) δ 2.61 (s, 1H), 2.09 (t, *J* = 7.0 Hz, 2H), 1.80 – 1.73 (m, 2H), 1.63 – 1.52 (m, 2H), 1.50 – 1.37 (m, 7H), 1.20 – 1.07 (m, 1H), 0.89 (t, *J* = 7.4 Hz, 3H).

^{13}C NMR (101 MHz, $CDCl_3$) δ 84.3, 84.2, 68.6, 40.2 (2C), 25.2, 23.4 (2C), 22.2, 20.6, 13.3.

Analytical data are in agreement with the literature.[7]

1-ethynyl-2-methylcyclohexan-1-ol

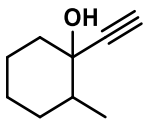

The title compound was obtained following General procedure E using 2-Methylcyclohexanone (970 µL, 8.0 mmol, 1.0 eq.) and ethynyltrimethylsilane (1.1 mL, 8.0 mmol, 1.6 eq.). The crude mixture was purified via flash column chromatography (hexane:EtOAc 90:10, SiO_2), 1-ethynyl-2-methylcyclohexan-1-ol was obtained as a pale yellow oil (993.2 mg, 90%).

^{1}H NMR (400MHz, $CDCl_3$) δ 2.47 (s, 1H), 2.07 – 1.95 (m, 1H), 1.77 – 1.40 (m, 6H), 1.31 – 1.16 (m, 2H), 1.01 (d, *J* = 3.4, 3H).

^{13}C NMR (101MHz, $CDCl_3$) δ 85.7, 74.9, 72.6, 42.0, 40.9, 33.0, 25.6, 24.5, 16.8.

Analytical data are in agreement with the literature.[6]

1-ethynylcyclopentan-1-ol

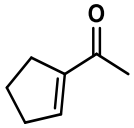

The title compound was obtained following general procedure F using ethynylcyclopentan-1-ol (531 mg, 4.82 mmol). The crude mixture was purified via flash column chromatography (hexane:EtOAc 95:5, SiO_2), 1-(cyclopent-1-en-1-yl)ethan-1-one was obtained as a pale yellow oil (475 mg, 4.33 mmol, 90%).

^{1}H NMR (400 MHz, $CDCl_3$) δ 6.74 – 6.70 (m, 1H), 2.61 – 2.47 (m, 4H), 2.30 (s, 3H), 1.97 – 1.87 (m, 2H).

^{13}C NMR (101 MHz, $CDCl_3$) δ 196.9, 146.3, 144.6, 34.1, 30.6, 26.8, 23.0.

Analytical data are in agreement with the literature.[5]

1-(cyclohept-1-en-1-yl)ethan-1-one

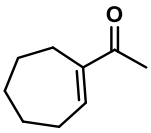

The title compound was obtained following general procedure F using ethynylcycloheptan-1-ol (636.2 mg, 4.60 mmol). The crude mixture was purified via flash column chromatography (hexane:EtOAc 95:5, SiO_2), 1-(cyclohept-1-en-1-yl)ethan-1-one was obtained as a pale yellow oil (569.4 mg, 4.12 mmol, 90%).

^{1}H NMR (400 MHz, $CDCl_3$) δ 7.08 (t, *J* = 6.7 Hz, 1H), 2.52 – 2.46 (m, 2H), 2.37 – 2.32 (m, 2H), 2.30 (s, 3H), 1.83 – 1.74 (m, 2H), 1.60 – 1.52 (m, 2H), 1.50 – 1.41 (m, 2H).

^{13}C NMR (101 MHz, $CDCl_3$) δ 199.1, 146.5, 145.6, 32.3, 29.1, 26.1, 25.8, 25.3, 25.2.

Analytical data are in agreement with the literature.[6]

(E)-1-(cyclooct-1-en-1-yl)ethan-1-one

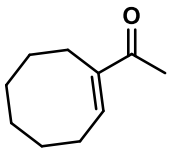

The title compound was obtained following general procedure F using ethynylcycloheptan-1-ol (636.2 mg, 4.60 mmol). The crude mixture was purified via flash column chromatography (hexane:EtOAc 95:5, SiO_2), 1-(cyclohept-1-en-1-yl)ethan-1-one was obtained as a pale yellow oil (658.1 mg, 4.31 mmol, 91%).

^{1}H NMR (400 MHz, $CDCl_3$) δ 6.87 (t, *J* = 8.3 Hz, 1H), 2.48 – 2.39 (m, 2H), 2.38 – 2.32 (m, 2H), 2.31 (s, 3H), 1.69 – 1.59 (m, 2H), 1.57 – 1.50 (m, 2H), 1.49 – 1.39 (m, 4H).

^{13}C NMR (101 MHz, $CDCl_3$) δ 199.3, 143.7, 143.3, 29.3, 29.2, 27.7, 26.7, 26.2, 25.6, 23.5.

Analytical data are in agreement with the literature.[5]

1-(cyclohex-1-en-1-yl)-2-phenylethan-1-one

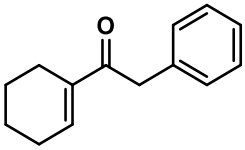

According to a modified procedure,[6] 1-(phenylethynyl)cyclohexan-1-ol (978 mg, 4.88 mmol) was dissolved in CH_3OH (5 mL) and water (0.5 mL) and the mixture was heated to 90 °C for 16 h. The mixture was cooled down to room temperature, filtered and quenched by small additions of $NaHCO_3$ until effervescence stops. The mixture was extracted with EtOAc three times. The organic fractions were combined, washed with water, brine, dried with Na_2SO_4 and concentrated under vacuum. After flash column chromatography (hexane:EtOAc 95:5, SiO_2), 1-(cyclohex-1-en-1-yl)-2-phenylethan-1-one was obtained as a pale yellow oil (478.9 mg, 49%).

^{1}H NMR (400 MHz, $CDCl_3$) δ 7.33 – 7.28 (m, 2H), 7.26 – 7.19 (m, 3H), 7.03 (tt, *J* = 3.8, 1.6 Hz, 1H), 3.95 (s, 2H), 2.31 – 2.19 (m, 4H), 1.70 – 1.54 (m, 4H).

^{13}C NMR (101 MHz, $CDCl_3$) δ 198.8, 141.3, 139.2, 135.6, 129.4(2C), 128.6(2C), 126.7, 44.1, 26.3, 23.4, 22.0, 21.6.

Analytical data are in agreement with the literature.[6]

1-(cyclohex-1-en-1-yl)pentan-1-one

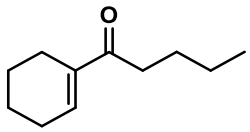

The title compound was obtained following General procedure F using ethynylcycloheptan-1-ol (636.2 mg, 4.60 mmol). The crude mixture was purified via flash column chromatography (hexane:EtOAc 95:5, SiO_2), 1-(cyclohex-1-en-1-yl)pentan-1-one was obtained as a pale yellow oil (753.9 mg, 4.18 mmol 88%).

^{1}H NMR (400 MHz, $CDCl_3$) δ 6.90 – 6.87 (m, 1H), 2.67 – 2.53 (m, 2H), 2.22 (ttt, *J* = 9.1, 4.4, 2.6 Hz, 4H), 1.68 – 1.51 (m, 6H), 1.39 – 1.26 (m, 2H), 0.90 (t, *J* = 7.4 Hz, 3H).

^{13}C NMR (101 MHz, $CDCl_3$) δ 201.8, 141.2, 139.4, 36.8, 27.1, 26.1, 23.2, 22.6, 21.7 (2C), 14.0.

Analytical data are in agreement with the literature.[8]

1-(2-methylcyclohex-1-en-1-yl)ethan-1-one

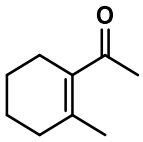

The title compound was obtained following General procedure F using 1-ethynyl-2-methylcyclohexan-1-ol (993.2 mg, 7.18 mmol). The crude mixture was purified via flash column chromatography (hexane:EtOAc 95:5, SiO_2), 1-(2-methylcyclohex-1-en-1-yl)ethan-1-one was obtained as a pale yellow oil (757.7 mg, 5.49 mmol 76%).

^{1}H NMR ($CDCl_3$, 500 MHz): *δ* 2.32–2.25 (m, 5H), 2.10–2.04 (m, 2H), 1.93–1.86 (m, 3H), 1.62–1.49(m, 4H);

^{13}C NMR (101 MHz, $CDCl_3$) δ 201.8, 139.4, 133.9, 36.3, 29.5, 26.1, 23.2, 22.6, 21.6

Analytical data are in agreement with the literature.[6]

Cyclohex-1-en-1-yl(phenyl)methanone

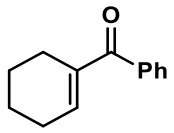

From a modified procedure,[9] Magnesium turnings (1.2 g, 49.37 mmol, 5.1 eq.) were suspended in anhydrous DMF (40 mL) and cooled at -20°C under a nitrogen atmosphere. On a separate flask, a mixture containing α,α,α-benzotrichloride (1.7 mL, 12.0 mmol, 1.24 eq.) and cyclohexanone (1 mL, 9.65 mmol, 1 eq.) in anhydrous DMF (5 mL) was formed. Half of this mixture was added quickly to the cooled solution. After the mixture turned yellow, the rest of the cyclohexanone solution was added dropwise and the mixture was stirred for 5 hours. The reaction was filtered to remove the excess magnesium grits and the clear solution was heated at 60 °C for 1 hour. The mixture was let to cool down and quenched with HCl (6 M) and extracted with EtOAc three times. The organic fractions were combined, washed with water, brine, dried with Na_2SO_4 and concentrated under vacuum. After flash column chromatography (hexane:EtOAc 95:5, SiO_2), cyclohex-1-en-1-yl(phenyl)methanone was obtained as a pale yellow oil (1.2 g, 6.44 mmol, 67%).

^{1}H NMR (500 MHz, $CDCl_3$) δ 7.56 – 7.49 (m, 2H), 7.40 – 7.33 (m, 1H), 7.31 – 7.27 (m, 2H), 6.46 (tt, *J* = 3.8, 1.7 Hz, 1H), 2.35 – 2.31 (m, 2H), 2.17 – 2.09 (m, 2H), 1.64 – 1.60 (m, 2H), 1.57 – 1.53 (m, 2H).

^{13}C NMR (126 MHz, $CDCl_3$) δ 197.5, 143.5, 138.4, 138.3, 130.9, 128.7, 127.7, 25.7, 23.6, 21.7, 21.3.

Analytical data are in agreement with the literature.[9]

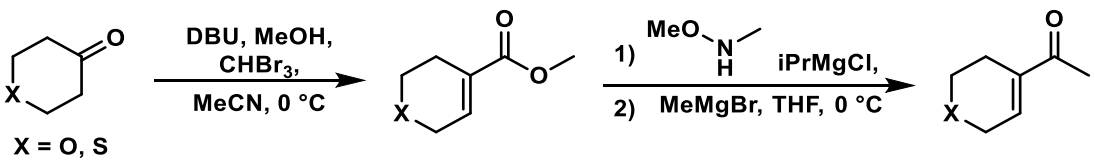

Methyl 3,6-dihydro-*2H*-pyran-4-carboxylate

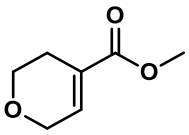

Following a modified procedure,[10] bromoform (440 µL, 5 mmol, 1.0 eq.) was slowly added to a solution of tetrahydro-*4H*-pyran-4-one (0.6 mL, 6 mmol, 1.2 eq.), DBU (2.5 mL, 16.5 mmol, 3.3 eq.), and methanol (500 µL, 12.5 mmol, 2.5 eq.) in acetonitrile (2.5 mL) at 0 °C. After 5 minutes, the mixture was allowed to reach room temperature and stirred for 16 hours. The mixture was quenched with NH_4Cl and extracted with EtOAc three times. The organic fractions were combined, washed with water, brine, dried with Na_2SO_4 and concentrated under vacuum. After flash column chromatography (hexane:EtOAc 95:5, SiO_2), methyl 3,6-dihydro-*2H*-pyran-4-carboxylate was obtained as a pale yellow oil (473 mg, 3.33 mmol, 67%).

^{1}H NMR (400 MHz, $CDCl_3$) δ 6.93 – 6.89 (m, 1H), 4.21 – 4.19 (m, 2H), 3.72 (t, *J* = 5.4 Hz, 2H), 3.69 (s, 3H), 2.32 – 2.29 (m, 2H).

^{13}C NMR (126 MHz, $CDCl_3$) δ 166.5, 137.4, 127.8, 65.1, 63.9, 51.7, 24.4.

Analytical data are in agreement with the literature.[11]

1-(3,6-dihydro-*2H*-pyran-4-yl)ethan-1-one (3b)

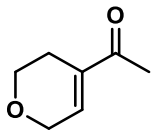

According to a modified procedure,[12] a solution of methyl 3,6-dihydro-*2H*-pyran-4-carboxylate (473 mg, 3.33 mmol, 1.0 eq.) and N,O-dimethylhydroxylamine hydrochloride (1.63 g, 16.71 mmol, 5 eq.) in THF (15 mL) was cooled to –20 °C. Isopropylmagnesium chloride (16.5 mL, 33 mmol, 2 M, 10 eq.) was added dropwise and the reaction was stirred for 5 h. The mixture was quenched with NH_4Cl_{sat}, extracted three times with Et_2O, dried over Na_2SO_4, filtered, and concentrated under reduced pressure. The crude was then redissolved in THF (5 mL) and the solution was cooled to 0 °C. A solution of MeMgBr (1.7 mL, 3 M, 5.1 mmol, 1.53 eq.) was added dropwise and the reaction was stirred for 3 h. The mixture was diluted with Et_2O and quenched with NH_4Cl_{sat}. The mixture was extracted three times with Et_2O, dried over Na_2SO_4, filtered, and concentrated under reduced pressure. The crude was purified by flash chromatography (SiO_2, hexane/EtOAc, 90:10) to afford 1-(3,6-dihydro-*2H*-pyran-4-yl)ethan-1-one (202.6 mg, 1.61 mmol, 48%) as a colourless oil.

^{1}H NMR (400 MHz, $CDCl_3$) δ 6.88 – 6.79 (m, 1H), 4.37 – 4.29 (m, 2H), 3.80 (t, *J* = 5.4 Hz, 2H), 2.39 – 2.34 (m, 2H), 2.32 (s, 3H).

^{13}C NMR (101 MHz, $CDCl_3$) δ 197.7, 138.1, 136.9, 65.0, 64.3, 25.0, 23.4.

Analytical data are in agreement with the literature.[13]

Methyl 3,6-dihydro-*2H*-thiopyran-4-carboxylate

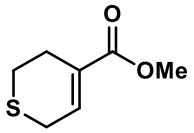

Following a modified procedure,[10] bromoform (440 µL, 5 mmol, 1.0 eq.) was slowly added to a solution of tetrahydro-*4H*-thiopyran-4-one (697.1, 6 mmol, 1.2 eq.), DBU (2.5 mL, 16.5 mmol, 3.3 eq.), and methanol (500 µL, 12.5 mmol, 2.5 eq.) in acetonitrile (2.5 mL) at 0 °C. After 5 minutes, the mixture was allowed to reach room temperature and stirred for 16 hours. The mixture was quenched with NH_4Cl and extracted with EtOAc three times. The organic fractions were combined, washed with water, brine, dried with Na_2SO_4 and concentrated under vacuum. After flash column chromatography (hexane:EtOAc 95:5, SiO_2), methyl 3,6-dihydro-*2H*-thiopyran-4-carboxylate was obtained as a pale yellow oil (573.5 mg, 3.62 mmol, 72%).

^{1}H NMR (400 MHz, $CDCl_3$) δ 7.12 (tt, *J* = 4.2, 1.9 Hz, 1H), 3.75 (s, 3H), 3.31 (dt, *J* = 4.3, 2.6 Hz, 2H), 2.80 – 2.68 (m, 2H), 2.62 – 2.47 (m, 2H).

^{13}C NMR (101 MHz, $CDCl_3$) δ 167.7, 135.6, 131.0, 52.0, 26.2, 25.2, 24.9.

1-(3,6-dihydro-2H-thiopyran-4-yl)ethan-1-one (3c)

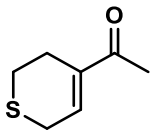

According to a modified procedure,[12] a solution of methyl 3,6-dihydro-*2H*-thiopyran-4-carboxylate (573.5 mg, 3.62 mmol, 1.0 eq.) and N,O-dimethylhydroxylamine hydrochloride (1.77 g, 18.1 mmol, 5 eq.) in THF (15 mL) was cooled to –20 °C. Isopropylmagnesium chloride (18.0 mL, 36 mmol, 2 M, 10 eq.) was added dropwise and the reaction was stirred for 5 h. The mixture was quenched with NH_4Cl_{sat}, extracted three times with Et_2O, dried over Na_2SO_4, filtered, and concentrated under reduced pressure. The crude was then redissolved in THF (5 mL) and the solution was cooled to 0 °C. A solution of MeMgBr (1.8 mL, 3 M, 5.0 mmol, 1.5 eq.) was added dropwise and the reaction was stirred for 3 h. The mixture was diluted with Et_2O and quenched with NH_4Cl_{sat}. The mixture was extracted three times with Et_2O, dried over Na_2SO_4, filtered, and concentrated under reduced pressure. The crude was purified by flash chromatography (SiO_2, hexane/EtOAc, 90:10) to afford 1-(3,6-dihydro-*2H*-pyran-4-yl)ethan-1-one (263.6 mg, 1.85 mmol, 51%) as a colourless oil.

^{1}H NMR (400 MHz, $CDCl_3$) δ 7.08 – 6.96 (m, 1H), 3.40 – 3.29 (m, 2H), 2.72 (t, *J* = 5.8 Hz, 2H), 2.56 – 2.48 (m, 2H), 2.29 (s, 3H).

^{13}C NMR (101 MHz, $CDCl_3$) δ 198.9, 140.0, 136.5, 26.3, 25.3, 24.9, 23.9.

Synthesis of *N*-Heterocycle exocyclic enones

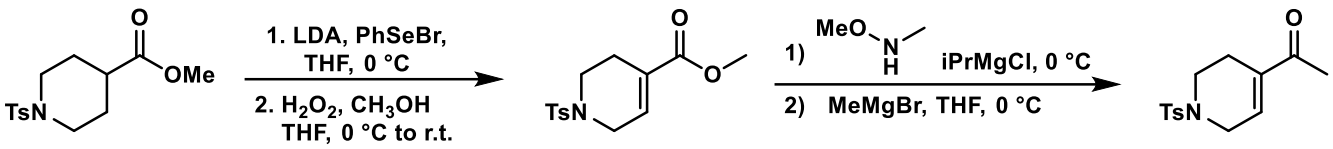

Methyl 1-tosyl-1,2,3,6-tetrahydropyridine-4-carboxylate

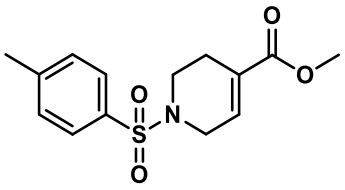

To a stirring solution of LDA (6.72 mmol, 1.4 eq.) in THF (10 mL) under nitrogen at –78 °C was added dropwise a solution of methyl 1-tosylpiperidine-4-carboxylate (1.43 g, 4.8 mmol, 1.0 eq.) in THF (5 mL). After 5 min, PhSeCl (1.38 g, 7.2 mmol. 1.5 eq.) was added and the reaction was warmed to r.t. The reaction was stirred for 2 h before quenching with NH_4Cl_{sat}. The mixture was extracted three times with Et_2O, dried over Na_2SO_4, filtered, and concentrated under reduced pressure. The crude was then redissolved in THF (5 mL) and acidified with glacial acetic acid (0.9 mL). To the solution was added H_2O (3.6 mL) and H_2O_2 (30%, 3.0 mL). After stirring for 1 h, the mixture was diluted with Et_2O and quenched with $NaHCO_{3sat}$. The mixture was extracted three times with Et_2O, dried over Na_2SO_4, filtered, and concentrated under reduced pressure. The crude was purified by flash chromatography (SiO_2, hexane/EtOAc, 85:15) to afford Methyl 1-tosyl-1,2,3,6-tetrahydropyridine-4-carboxylate (968.2 mg, 3.28 mmol, 68%) as a colourless solid.

^{1}H NMR (400 MHz, $CDCl_3$) δ 7.64 – 7.57 (m, 2H), 7.30 – 7.23 (m, 2H), 6.75 (tt, *J* = 3.5, 1.7 Hz, 1H), 3.73 – 3.61 (m, 2H), 3.65 (s, 3H), 3.16 – 3.09 (m, 2H), 2.43 – 2.37 (m, 2H), 2.35 (s, 3H).

^{13}C NMR (101 MHz, $CDCl_3$) δ 166.0, 143.8, 133.5, 132.8, 129.7 (2C), 128.6, 127.5 (2C), 51.8, 44.9, 42.4, 24.5, 21.4.

Analytical data are in agreement with the literature.[14]

1-(1-tosyl-1,2,3,6-tetrahydropyridin-4-yl)ethan-1-one (3d)

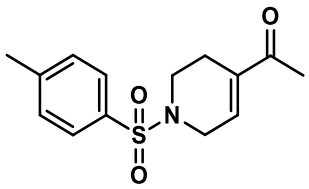

According to a modified procedure,[12] a solution of methyl-1-tosyl-1,2,3,6-tetrahydropyridine-4-carboxylate (968.2 mg, 3.28 mmol, 1.0 eq.) and N,O-dimethylhydroxylamine hydrochloride (1.6 g, 16.4 mmol, 5 eq.) in THF (15 mL) was cooled to –20 °C. Isopropylmagnesium chloride (16.4 mL, 32.8 mmol, 2 M, 10 eq.) was added dropwise and the reaction was stirred for 5 h. The mixture was quenched with NH_4Cl_{sat}, extracted three times with Et_2O, dried over Na_2SO_4, filtered, and concentrated under reduced pressure. The crude was then redissolved in THF (5 mL) and the solution was cooled to 0 °C. A solution of MeMgBr (1.65 mL, 3 M, 4.9 mmol, 1.5 eq.) was added dropwise and the reaction was stirred for 3 h. The mixture was diluted with Et_2O and quenched with NH_4Cl_{sat}. The mixture was extracted three times with Et_2O, dried over Na_2SO_4, filtered, and concentrated under reduced pressure. The crude was purified by flash chromatography (SiO_2, hexane/EtOAc, 90:10) to afford 1-(1-tosyl-1,2,3,6-tetrahydropyridin-4-yl)ethan-1-one (353.4 mg, 1.27 mmol, 39%) as a colourless solid.

^{1}H NMR (400 MHz, $CDCl_3$) δ 7.61 – 7.50 (m, 2H), 7.28 – 7.18 (m, 2H), 6.65 – 6.63 (m, 1H), 3.69 – (m, 2H), 3.06 (t, *J* = 5.7 Hz, 2H), 2.39 – 2.26 (m, 5H), 2.16 (s, 3H).

^{13}C NMR (101 MHz, $CDCl_3$) δ 197.1, 143.8, 137.0, 134.2, 132.6, 129.7 (2C), 127.4 (2C), 44.7, 42.4, 24.9, 23.2, 21.3.

Analytical data are in agreement with the literature.[15]

5.4.3 Phosphoramidites:

(11bR)-N-((*R*)-2,3-dihydro-*1H*-inden-1-yl)-N-(pentan-3-yl)dinaphtho[2,1-d:1',2'-f][1,3,2]dioxaphosphepin-4-amine (L_1)

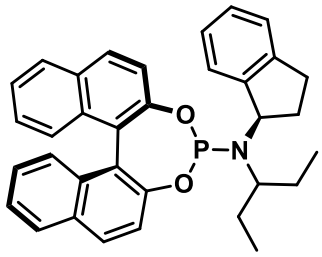

The title compound was obtained following General procedure G using (*(S)*-3,3'-diphenyl-[1,1'-binaphthalene]-2,2'-diol (715.8 g, 2.5 mmol, 1.0 eq.) and dibenzo[b,f]azepine (483.1 mg, 2.5 mmol, 1.0 eq.).

The phosphoramidite was purified by prompt flash column chromatography (hexane:CH_2Cl_2:triethylamine, 80:19:1, SiO_2). The fractions were concentrated under reduced pressure and diluted with CH_2Cl_2. The process was repeated five times (always under N_2 atmosphere) in order to remove triethylamine. The ligand **L_1** was obtained as a foamy colourless solid and used as attained.

^{1}H NMR (400 MHz, $CDCl_3$) δ 7.82 (d, *J* = 8.8 Hz, 1H), 7.77 (dd, *J* = 8.5, 2.6 Hz, 3H), 7.59 (d, *J* = 7.6 Hz, 1H), 7.49 (d, *J* = 8.8 Hz, 1H), 7.37 (d, *J* = 8.8 Hz, 1H), 7.30 – 7.24 (m, 3H), 7.23 – 7.14 (m, 2H), 7.14 – 7.05 (m, 4H), 4.69 – 4.57 (m, 1H), 2.88 – 2.81 (m, 1H), 2.75 – 2.52 (m, 2H), 2.37 – 2.24 (m, 1H), 2.15 – 2.01 (m, 1H), 1.78 – 1.73 (m, 1H), 1.64 – 1.55 (m, 1H), 1.53 – 1.33 (m, 2H), 0.84 (t, *J* = 7.4 Hz, 3H), 0.62 (t, *J* = 7.4 Hz, 3H).

^{13}C NMR (101 MHz, $CDCl_3$) δ 150.4, 150.3, 150.1, 143.5, 131.4, 130.5, 130.3, 129.7, 128.4, 128.3, 127.5, 127.3, 127.2, 126.5, 126.0, 125.9, 125.3, 124.9, 124.7, 124.4, 124.1, 122.5, 122.4, 121.8, 60.0, 58.0, 30.4, 29.6, 29.5, 27.3, 11.6, 11.5.

^{31}P NMR (162 MHz, $CDCl_3$) δ 149.31.

Analytical data are in agreement with the literature.[16]

5-((11b*S*)-2,6-diphenyldinaphtho[2,1-d:1',2'-f][1,3,2]dioxaphosphepin-4-yl)-*5H*-dibenzo[b,f]azepine (L_{21})

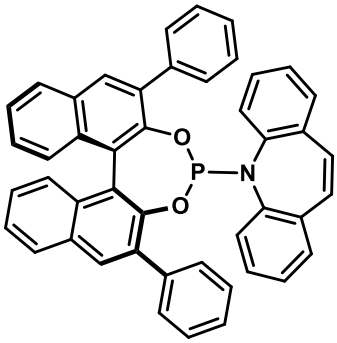

The title compound was obtained following General procedure G using (*(S)*-3,3'-diphenyl-[1,1'-binaphthalene]-2,2'-diol (1.1 g, 2.5 mmol, 1.0 eq.) and dibenzo[b,f]azepine (483.1 mg, 2.5 mmol, 1.0 eq.).

The phosphoramidite was purified by prompt flash column chromatography (hexane:CH_2Cl_2:triethylamine, 80:19:1, SiO_2). The fractions were concentrated under reduced pressure and diluted with CH_2Cl_2. The process was repeated five times (always under N_2 atmosphere) in order to remove triethylamine. The ligand **L_{21}** was obtained as a foamy colourless solid and used as attained (1.23 g, 1.86 mmol, 74%).

^{1}H NMR (400 MHz, $CDCl_3$) δ 8.14 (s, 1H), 8.02 (d, *J* = 9.0 Hz, 2H), 7.96 – 7.88 (m, 3H), 7.63 – 7.41 (m, 10H), 7.32 – 7.21 (m, 4H), 7.15 – 6.95 (m, 3H), 6.89 – 6.82 (m, 1H), 6.71 (ddd, *J* = 8.6, 5.8, 3.2 Hz, 1H), 6.61 (d, *J* = 11.6 Hz, 1H), 6.51 – 6.34 (m, 2H), 6.00 – 5.89 (m, 1H), 5.78 (d, *J* = 7.6 Hz, 1H).

^{13}C NMR (101 MHz, $CDCl_3$) δ 146.8, 142.7, 142.5, 142.3, 138.4, 137.6, 136.3, 135.4, 134.6, 132.8, 132.7, 131.4 (2C), 130.9 (2C), 130.8, 130.5 (2C), 130.3 (3C), 130.2, 129.1, 128.7 (4C), 128.6 (3C), 128.5, 128.3 (2C), 128.2, 128.1, 128.0, 127.6, 127.4, 127.1, 127.0, 126.5, 126.2 (2C), 125.9, 125.3, 125.1.

^{31}P NMR (162 MHz, $CDCl_3$) δ 136.0.

Analytical data are in agreement with the literature.[16]

5-((11cS)-2-phenyldinaphtho[2,1-d:1',2'-f][1,3,2]dioxaphosphepin-4-yl)-*5H*-dibenzo[b,f]azepine (L_{22})

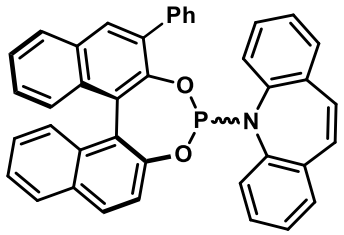

The title compound was obtained following General procedure G using *(S)*-3-(phenyl)-[1,1'-binaphthalene]-2,2'-diol (906.1 mg, 2.5 mmol, 1.0 eq.) and dibenzo[b,f]azepine (483.1 mg, 2.5 mmol, 1.0 eq.).

The phosphoramidite was purified by prompt flash column chromatography (hexane:CH_2Cl_2:triethylamine, 80:19:1, SiO_2). The fractions were concentrated under reduced pressure and diluted with CH_2Cl_2. The process was repeated five times (always under N_2 atmosphere) in order to remove triethylamine. The ligand was obtained as a foamy colourless solid and used as attained (1.04 g, 1.78 mmol, 71%). **L_{22}** was obtained as a mixture of diastereomers (1:1.86 dr). Extra carbon signals

^{1}H NMR (500 MHz, $CDCl_3$) δ 8.20 (s, 1H), 8.06 (d, *J* = 19.4 Hz, 2H), 8.01 – 7.89 (m, 4H), 7.89 – 7.84 (m, 2H), 7.82 – 7.79 (m, 1H), 7.68 – 7.54 (m, 6H), 7.52 – 7.36 (m, 8H), 7.32 – 7.18 (m, 10H), 7.18 – 6.92 (m, 9H), 6.91 – 6.76 (m, 3H), 6.65 (d, *J* = 8.8 Hz, 1H), 6.58 – 6.43 (m, 2H), 6.40 (t, *J* = 7.7 Hz, 1H), 5.99 (d, *J* = 8.1 Hz, 1H), 5.71 (d, *J* = 7.9 Hz, 1H).

^{13}C NMR (126 MHz, $CDCl_3$) δ 150.5 (2C), 149.2, 146.7, 146.5, 143.4, 143.1, 142.7 (2C), 142.4, 142.2, 138.6, 138.3, 136.6, 136.3 (2C), 135.3, 135.2 (2C), 134.8, 133.1, 132.7, 132.6, 132.4, 131.7, 131.5 (2C), 131.4, 131.0 (2C), 130.8, 130.6 (2C), 130.5, 130.4 (2C), 130.3, 130.2, 129.2, 129.1 (2C), 128.9 (3C), 128.8 (4C), 128.7, 128.5 (2C), 128.4, 128.2 (2C), 128.1 (2C), 127.9, 127.8, 127.6, 127.2, 127.1 (2C), 127.0, 126.8, 126.7, 126.3, 126.2 (2C), 126.1, 125.8 (2C), 125.4, 125.3, 125.2, 125.0, 124.4, 124.3, 122.1, 121.4, 121.2.

^{31}P NMR (162 MHz, $CDCl_3$): 137.1, 135.7 (major) (1:1.86).

IR υ_{max} (film): 2981, 1486, 1215, 956, 800, 752 cm^{-1}.

HRMS (ESI^+): *m/z* calcd for $C_{40}H_{26}NO_2P$ $[M+H]^+$: 584.17740, found 584.1774.

$[\alpha]^{25}_D$= +347.3 (*c* 1.0, $CHCl_3$).

5-((4R,11bS)-2-phenyldinaphtho[2,1-d:1',2'-f][1,3,2]dioxaphosphepin-4-yl)-*5H*-dibenzo[b,f]azepine (L_{22R})

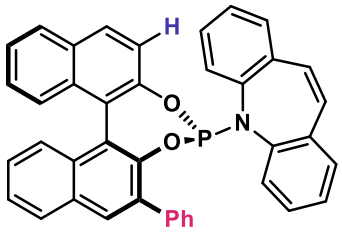

Purification to yield L_{22R} (Initial mixture of diastereoisomers, 35:65): The crude mixture of **L_{22}** was concentrated, re-dissolved with MeCN (30 mL) stirred for 30 mins and filtered under vacuum. The measured diastereomeric ratio of the filtrate is (3:1). The filter cake is then transferred to a RBF and the phosphoramidite was purified by prompt flash column chromatography (hexane:CH_2Cl_2:triethylamine, 80:19:1, SiO_2). The fractions were concentrated under reduced pressure and diluted with CH_2Cl_2. The process was repeated five times (under N_2 atmosphere) in order to remove triethylamine. The ligand was obtained as a foamy colourless solid and used as attained. **L_{22R} (S, R_P)** was obtained as a single diastereomer (416 mg, 0.71 mmol, 40%).

^{1}H NMR (400 MHz, $CDCl_3$) δ 8.05 (s, 1H), 7.97 – 7.92 (m, 1H), 7.86 – 7.79 (m, 2H), 7.79 – 7.75 (m, 1H), 7.65 – 7.52 (m, 3H), 7.45 – 7.40 (m, 1H), 7.40 – 7.34 (m, 3H), 7.28 – 7.21 (m, 3H), 7.20 – 7.15 (m, 2H), 7.15 – 7.10 (m, 1H), 7.10 – 7.04 (m, 1H), 7.04 – 6.97 (m, 1H), 6.97 – 6.92 (m, 2H), 6.92 – 6.81 (m, 1H), 6.67 – 6.57 (m, 1H), 6.53 – 6.47 (m, 1H), 6.47 – 6.42 (m, 1H).

^{13}C NMR (101 MHz, $CDCl_3$) δ 150.5 (2C), 146.5, 143.4, 143.1, 142.6, 138.3, 136.3 (2C), 135.3, 135.1, 132.6, 132.4, 131.5, 131.4, 130.6 (2C), 130.4, 130.2, 129.2, 129.1, 128.9 (2C), 128.7, 128.5, 128.4, 128.2, 128.1, 127.6, 127.2, 127.1, 126.7, 126.2, 126.1, 125.8, 125.4, 125.3, 124.4, 121.4, 121.2.

^{31}P NMR (162 MHz, $CDCl_3$) δ 135.6.

IR υ_{max} (film): 2981, 1486, 1215, 956, 800, 752 cm^{-1}.

$[\alpha]^{25}_D$= +346.1 (*c* 1.0, $CHCl_3$).

5-((4S,11c*S*)-2-phenyldinaphtho[2,1-d:1',2'-f][1,3,2]dioxaphosphepin-4-yl)-*5H*-dibenzo[b,f]azepine (L_{22S})

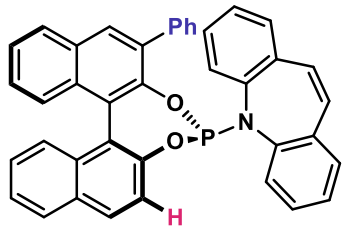

Crystallization of L_{22} (Mixture of diastereoisomers, 35:65): The crude (L_{22}) was concentrated, re-dissolved with MeCN (30 mL) stirred for 30 mins and filtered under vacuum. The measured diastereomeric ratio of the filtrate is (3:1). The filtrate was concentrated and a purified via interface recrystallisation (DCM:hexane ~ 7:93). It is important to utilize very low amounts of DCM as the ligand is highly soluble in it. The initial crystals were analysed and utilized as a nucleation site for further crystallisations, which are often required to push the crystallisation. After finishing the crystallisation process, ensuring a progressive increase in the dr of the ligand L_{22S}, the crystals were washed with hexane and dried. The ligand was obtained as a crystalline colourless solid and used as attained. **L_{22S} (S, S_P)** was obtained as a single diastereomer. (244 mg, 0.42 mmol, 23%)

^{1}H NMR (400 MHz, $CDCl_3$) δ 8.20 (s, 1H), 8.05 (d, *J* = 8.2 Hz, 1H), 8.00 – 7.88 (m, 4H), 7.65 – 7.56 (m, 3H), 7.50 m, 1H), 7.47 – 7.40 (m, 2H), 7.38 – 7.32 (m, 1H), 7.32 – 7.23 (m, 3H), 7.19 – 7.03 (m, 3H), 6.91 – 6.75 (m, 3H), 6.71 (d, *J* = 11.7 Hz, 1H), 6.44 – 6.36 (m, 1H), 5.99 (d, *J* = 8.1 Hz, 1H), 5.71 (d, *J* = 7.9 Hz, 1H).

^{13}C NMR (101 MHz, $CDCl_3$) δ 149.2, 146.6, 142.6, 142.3, 142.2, 138.6, 136.6, 135.1, 134.8, 133.1, 132.7, 131.7, 131.5, 131.0 (2C), 130.8, 130.5, 130.4, 130.3, 129.1, 128.9, 128.8 (4C), 128.5, 128.2, 128.1, 127.9, 127.8, 127.1, 127.0, 126.8, 126.3, 126.2, 125.8, 125.2, 125.0, 124.3, 122.1.

^{31}P NMR (162 MHz, $CDCl_3$) δ 137.1.

IR υ_{max} (film): 2981, 1486, 1215 cm^{-1}.

$[\alpha]^{25}_D$= +333.6 (*c* 1.0, $CHCl_3$).

5-((11c*S*)-2-(naphthalen-2-yl)dinaphtho[2,1-d:1',2'-f][1,3,2]dioxaphosphepin-4-yl)-*5H*-dibenzo[b,f]azepine (L_{24})

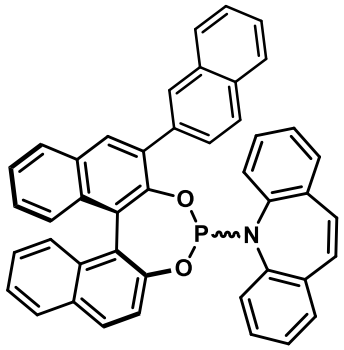

The title compound was obtained following General procedure G using *(S)*-3-(2-naphthyl)-[1,1'-binaphthalene]-2,2'-diol (1.03 g, 2.5 mmol, 1.0 eq.) and dibenzo[b,f]azepine (483.1 mg, 2.5 mmol, 1.0 eq.).

The phosphoramidite was purified by prompt flash column chromatography (hexane:CH_2Cl_2:triethylamine, 80:19:1, SiO_2). The fractions were concentrated under reduced pressure and diluted with CH_2Cl_2. The process was repeated five times (always under N_2 atmosphere) in order to remove triethylamine. The ligand was obtained as a foamy colourless solid and used as attained (811, 1.27 mmol, 51%). **L_{24}** was obtained as a mixture of diastereomers (1:1.1 dr).

^{1}H NMR (500 MHz, $CDCl_3$) δ 8.38 (s, 1H), 8.17 (d, *J* = 2.4 Hz, 1H), 8.11 – 7.86 (m, 8H), 7.86 – 7.72 (m, 3H), 7.63 – 6.54 (m, 38H), 6.53 – 6.20 (m, 3H), 6.06 – 5.89 (m, 1H), 5.41 – 5.30 (m, 1H).

^{13}C NMR (126 MHz, $CDCl_3$) δ 149.2, 143.4, 138.6, 138.3, 136.3, 135.7, 135.2, 134.8, 132.7, 132.4, 131.7, 131.5, 131.5, 131.4, 131.1, 131.0, 130.9, 130.6, 130.6, 130.5, 130.4, 130.3, 130.3, 129.2, 129.1, 128.9, 128.9, 128.8, 128.8, 128.6, 128.5, 128.5, 128.4, 128.2, 128.1, 128.1, 128.0, 127.9, 127.8, 127.6, 127.2, 127.1, 127.0, 126.8, 126.7, 126.4, 126.3, 126.2, 126.2, 126.1, 125.8, 125.8, 125.4, 125.3, 125.2, 125.0, 124.4, 122.2, 121.4, 121.2.

^{31}P NMR (162 MHz, $CDCl_3$) δ 137.1, 135.7 (major) (1:1.1).

IR υ_{max} (film): 1215, 958, 753 cm^{-1}.

HRMS (ESI^+): *m/z* calcd for $C_{44}H_{28}NO_2P$ $[M+H]^+$: 634.19300, found 634.1927.

$[\alpha]^{25}_D$= +223.8 (*c* 1.0, $CHCl_3$).

5-((11cS)-2-bromodinaphtho[2,1-d:1',2'-f][1,3,2]dioxaphosphepin-4-yl)-*5H*-dibenzo[b,f]azepine (L_{25})

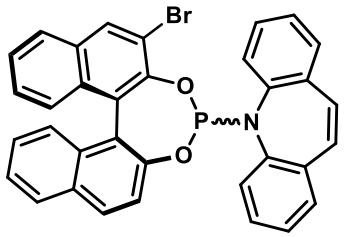

The title compound was obtained following General procedure G using *(S)*-3-bromo-[1,1'-binaphthalene]-2,2'-diol (913.1 mg, 2.5 mmol, 1.0 eq.) and dibenzo[b,f]azepine (483.1 mg, 2.5 mmol, 1.0 eq.). The phosphoramidite was purified by prompt flash column chromatography (hexane:CH_2Cl_2:triethylamine, 80:19:1, SiO_2). The fractions were concentrated under reduced pressure and diluted with CH_2Cl_2. The process was repeated five times (always under N_2 atmosphere) in order to remove triethylamine. The ligand was obtained as a foamy colourless solid and used as attained (933 mg, 1.59 mmol, 64%). **L_{25}** was obtained as a mixture of diastereomers (1:1.2 dr).

^{1}H NMR (500 MHz, $CDCl_3$) δ 8.36 (s, 1H), 8.16 (s, 1H), 8.00 (d, *J* = 8.8 Hz, 1H), 7.93 (d, *J* = 8.2 Hz, 1H), 7.87 (d, *J* = 8.3 Hz, 1H), 7.82 (dd, *J* = 15.1, 8.2 Hz, 2H), 7.73 (d, *J* = 8.0 Hz, 1H), 7.58 (d, *J* = 8.8 Hz, 1H), 7.52 – 7.14 (m, 22H), 7.10 – 6.84 (m, 9H), 6.79 (d, *J* = 8.8 Hz, 1H), 6.48 (td, *J* = 7.7, 1.6 Hz, 1H).

^{13}C NMR (126 MHz, $CDCl_3$) δ 150.5, 149.1, 146.2, 145.4, 143.0, 142.6, 142.4, 142.1, 136.5, 136.2, 135.8, 135.1, 132.8, 132.7, 132.2, 132.0 (3C), 131.7, 131.5 (3C), 131.2, 130.9, 130.2, 129.4 (2C), 129.3 (2C), 129.1, 129.0, 128.9 (2C), 128.7, 128.6 (3C), 128.5 (3C), 128.0, 127.7, 127.5, 127.4, 127.2, 127.0 (2C), 126.7 (3C), 126.4 (3C), 126.3 (2C), 125.9 (2C), 125.6 (2C), 125.0, 124.5, 123.8, 123.5, 121.9, 121.3, 120.5, 116.9, 116.4.

^{31}P NMR (162 MHz, $CDCl_3$) δ 139.0, 136.6 (major), (1:1.2).

IRυ_{max} (film): 3019, 1486, 1238, 1211 cm^{-1}.

HRMS (ESI^+): *m/z* calcd for $C_{34}H_{21}NO_2P[^{79}Br/^{80}Br]$ $[M+H]^+$: 586.0566 and 588.0549, found 586.0566 and 588.0541.

$[\alpha]^{25}_D$= +392.7 (*c* 1.0, $CHCl_3$).

5-((11cS)-2-iododinaphtho[2,1-d:1',2'-f][1,3,2]dioxaphosphepin-4-yl)-*5H*-dibenzo[b,f]azepine (L_{26})

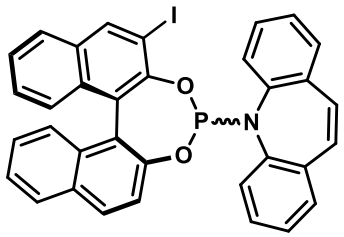

The title compound was obtained following General procedure G using *(S)*-3-iodo-[1,1'-binaphthalene]-2,2'-diol (1.03 g, 2.5 mmol, 1.0 eq.) and dibenzo[b,f]azepine (483.1 mg, 2.5 mmol, 1.0 eq.). The phosphoramidite was purified by prompt flash column chromatography (hexane:CH_2Cl_2:triethylamine, 80:19:1, SiO_2). The fractions were concentrated under reduced pressure and diluted with CH_2Cl_2. The process was repeated five times (always under N_2 atmosphere) in order to remove triethylamine. The ligand was obtained as a foamy colourless solid and used as attained (857 mg, 1.35 mmol, 54%). **L_{26}** was obtained as a mixture of diastereomers (1:1.2 dr).

^{1}H NMR (500 MHz, $CDCl_3$) δ 8.55 (s, 1H), 8.39 (s, 1H), 7.95 (d, *J* = 8.8 Hz, 1H), 7.89 – 7.86 (m, 1H), 7.83 – 7.72 (m, 4H), 7.53 – 7.50 (m, 2H), 7.44 – 7.06 (m, 22H), 7.06 – 6.80 (m, 8H), 6.75 (d, *J* = 8.8 Hz, 1H), 6.45 (td, *J* = 7.6, 1.6 Hz, 1H).

^{13}C NMR (126 MHz, $CDCl_3$) δ 150.6, 149.1, 148.3, 147.5, 143.2, 142.8, 142.4, 142.1, 139.5, 139.1, 136.6, 136.2, 135.8, 135.2, 132.8 (4C), 132.0, 131.8, 131.6 (3C), 131.4, 131.2, 130.8, 130.2, 129.5, 129.4, 129.3 (2C), 129.2, 129.0, 128.9 (2C), 128.8, 128.7 (2C), 128.6, 128.5, 128.0, 127.6, 127.4 (2C), 127.2, 127.0, 126.9, 126.7 (2C), 126.6 (2C), 126.5, 126.4, 126.3, 125.9, 125.7, 125.4, 125.2, 125.0, 124.5, 123.6, 122.5, 121.9, 121.3, 120.5, 92.3, 91.5

^{31}P NMR (162 MHz, $CDCl_3$) δ 138.6, 136.3. (major),

IR υ_{max} (film): 3019, 1486, 1214 cm^{-1}.

HRMS (ESI^+): *m/z* calcd for $C_{34}H_{21}INO_2P$ $[M+H]^+$: 634.0427, found 634.0421.

$[\alpha]^{25}_D$= +333.2 (*c* 1.0, $CHCl_3$).

5-((11cS)-2-(trimethylsilyl)dinaphtho[2,1-d:1',2'-f][1,3,2]dioxaphosphepin-4-yl)-*5H*-dibenzo[b,f]azepine (L_{28S})

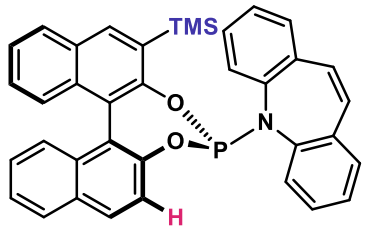

The title compound was obtained following General procedure G using *(S)*-3-trimethylsilyl-1,1'-binaphthyl-2,2'-diol (89.6 mg, 0.25 mmol, 1.0 eq.) and dibenzo[b,f]azepine (48.3 mg, 0.25 mmol, 1.0 eq.).

The phosphoramidite was purified by prompt flash column chromatography (hexane:CH_2Cl_2:triethylamine, 80:19:1, SiO_2). The fractions were concentrated under reduced pressure and diluted with CH_2Cl_2. The process was repeated five times (always under N_2 atmosphere) in order to remove triethylamine. The ligand was obtained as a foamy colourless solid and used as attained (107.9 mg, 0.19 mmol, 74%). **L_{28S}** was obtained as a single diastereomer.

^{1}H NMR (400 MHz, $CDCl_3$) δ 7.83 (s, 1H), 7.77 (d, *J* = 8.8 Hz, 1H), 7.75 – 7.66 (m, 2H), 7.38 (d, *J* = 8.8 Hz, 1H), 7.33 (d, *J* = 8.0 Hz, 1H), 7.28 – 7.18 (m, 2H), 7.07 – 6.90 (m, 6H), 6.86 (t, J = 7.5 Hz, 1H), 6.80 – 6.75 (m, 1H), 6.73 – 6.63 (m, 4H), 6.59 (t, *J* = 7.6 Hz, 1H), 0.42 (s, 9H).

^{13}C NMR (101 MHz, $CDCl_3$) δ 153.4, 148.9, 143.3, 142.4, 136.5, 135.6, 133.9, 133.2, 132.1, 131.6, 131.5, 131.4, 130.3 (2C), 129.6, 129.2, 128.7, 128.5 (2C), 128.4, 127.9, 127.8 (2C), 126.9, 126.8, 126.2, 126.1 (3C), 124.8, 124.5, 124.1, 122.0, 120.7, 1.2 (3C).

^{31}P NMR (162 MHz, $CDCl_3$) δ 138.8.

IR υ_{max} (film): 3019, 1486, 1216, 1203 cm^{-1}.

HRMS (ESI^+): *m/z* calcd for $C_{37}H_{30}NO_2PSi$ $[M+H]^+$: 580.1856, found 580.1850.

$[\alpha]^{25}_D$= +445.0 (*c* 1.0, $CHCl_3$).

5-((11cS)-2-(triisopropylsilyl)dinaphtho[2,1-d:1',2'-f][1,3,2]dioxaphosphepin-4-yl)-*5H*-dibenzo[b,f]azepine (L_{29S})

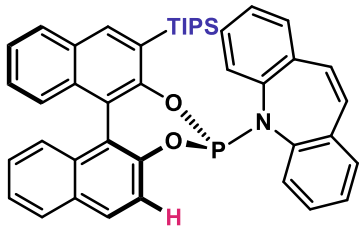

The title compound was obtained following General procedure G using *(S)*-3-triisopropylsilyl-1,1'-binaphthyl-2,2'-diol (110.7 mg, 0.25 mmol, 1.0 eq.) and dibenzo[b,f]azepine (48.3 mg, 0.25 mmol, 1.0 eq.).

The phosphoramidite was purified by prompt flash column chromatography (hexane:CH_2Cl_2: triethylamine, 80:19:1, SiO_2). The fractions were concentrated under reduced pressure and diluted with CH_2Cl_2. The process was repeated five times (always under N_2 atmosphere) in order to remove triethylamine. The ligand was obtained as a foamy colourless solid and used as attained (91.6 mg, 0.14 mmol, 56%). **L_{29S}** was obtained as a single diastereomer.

^{1}H NMR (500 MHz, $CDCl_3$) δ 8.06 (s, 1H), 7.81 (d, *J* = 8.1 Hz, 1H), 7.79 – 7.71 (m, 2H), 7.37 (d, *J* = 7.6 Hz, 1H), 7.33 – 7.19 (m, 3H), 7.17 – 7.05 (m, 3H), 7.02 (t, *J* = 7.6 Hz, 2H), 6.93 – 6.87 (m, 2H), 6.84 (d, *J* = 8.6 Hz, 1H), 6.72 – 6.59 (m, 3H), 6.34 (d, *J* = 8.0 Hz, 1H), 6.25 (d, *J* = 7.8 Hz, 1H), 1.83 (hept, *J* = 7.5 Hz, 3H), 1.20 (d, *J* = 7.5 Hz, 9H), 1.16 (d, *J* = 7.5 Hz, 9H).

^{13}C NMR (126 MHz, $CDCl_3$) δ 153.9, 148.7, 143.8, 142.1, 138.1, 136.5, 135.2, 134.0, 133.3, 132.1, 131.4, 130.6, 130.2, 129.9, 129.1, 128.8, 128.6, 128.3 (2C), 128.1, 127.8 (2C), 126.8 (2C), 126.7, 126.3, 126.2, 125.8, 124.7, 124.3, 124.2, 121.9, 120.6, 120.5, 19.8 (3C), 19.4 (3C), 13.0 (3C).

^{31}P NMR (162 MHz, $CDCl_3$) δ 133.9.

IR υ_{max} (film): 2866, 1487, 1462, 1215 cm^{-1}.

HRMS (ESI^+): *m/z* calcd for $C_{43}H_{42}NO_2PSi$ $[M+H]^+$: 664.2795, found 664.2793.

$[\alpha]^{25}_D$= +327.3 (*c* 1.0, $CHCl_3$).

5-((11cS)-2-(p-tolyl)dinaphtho[2,1-d:1',2'-f][1,3,2]dioxaphosphepin-4-yl)-*5H*-dibenzo[b,f]azepine (L_{30})

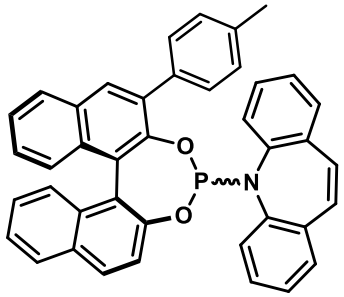

The title compound was obtained following General procedure G using *(S)*-3-(*p*-tolyl)-[1,1'-binaphthalene]-2,2'-diol (941 mg, 2.5 mmol, 1.0 eq.) and dibenzo[b,f]azepine (483.1 mg, 2.5 mmol, 1.0 eq.). The phosphoramidite was purified by prompt flash column chromatography (hexane:CH_2Cl_2:triethylamine, 80:19:1, SiO_2). The fractions were concentrated under reduced pressure and diluted with CH_2Cl_2. The process was repeated five times (always under N_2 atmosphere) in order to remove triethylamine. The ligand was obtained as a foamy colourless solid and used as attained (1.09 g, 1.82 mmol, 73%). **L_{30}** was obtained as a mixture of diastereomers (1:1 dr).

^{1}H NMR (500 MHz, $CDCl_3$) δ 8.20 (s, 1H), 8.06 (d, *J* = 15.8 Hz, 2H), 7.97 (d, *J* = 8.2 Hz, 1H), 7.91 (dd, *J* = 8.5, 6.0 Hz, 2H), 7.86 (d, *J* = 8.1 Hz, 2H), 7.78 (dd, *J* = 15.5, 8.0 Hz, 4H), 7.53 – 7.33 (m, 10H), 7.33 – 6.71 (m, 22H), 6.64 (d, *J* = 8.8 Hz, 1H), 6.59 (d, *J* = 7.8 Hz, 1H), 6.47 (td, *J* = 7.7, 1.6 Hz, 1H), 6.40 – 6.33 (m, 1H), 5.94 (d, *J* = 8.1 Hz, 1H), 5.70 (d, *J* = 7.9 Hz, 1H), 2.59 (s, 6H).

^{13}C NMR (126 MHz, $CDCl_3$) δ 150.6, 149.2, 146.8, 146.6, 143.4, 142.7, 142.6, 142.2, 137.6, 137.3, 136.7, 136.3, 135.7, 135.3 (2C), 135.1, 135.0, 134.8, 133.1, 132.6, 132.5, 132.4, 131.8, 131.5 (3C), 131.4 (2C), 130.9 (3C), 130.5 (3C), 130.4, 130.3 (3C), 130.2, 130.1, 129.5 (3C), 129.2, 129.1 (5C), 128.9 (3C), 128.8 (2C), 128.5 (3C), 128.3, 128.2, 128.1 (2C), 128.0, 127.2, 127.1 (2C), 127.0, 126.8, 126.7, 126.3, 126.2, 126.0, 125.8 (2C), 125.3, 125.1, 124.9, 124.4, 122.1, 121.4, 121.3, 21.5 (2C).

^{31}P NMR (162 MHz, $CDCl_3$) δ 137.1, 135.5.

IR υ_{max} (film): 3019, 1486, 1238, 1211 cm^{-1}.

HRMS (ESI^+): *m/z* calcd for $C_{41}H_{29}NO_2P$ $[M+H]^+$: 598.1930, found 598.1927.

[α]$^{25}_{D}$= +334.2 (*c* 1.0, $CHCl_3$).

5-((11cS)-2-(4-(trimethylsilyl)phenyl)dinaphtho[2,1-d:1',2'-f][1,3,2]dioxaphosphepin-4-yl)-*5H*-dibenzo[b,f]azepine (L_{31})

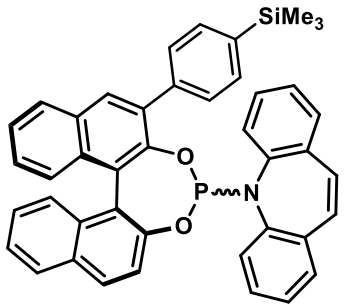

The title compound was obtained following General procedure G using *(S)*-3-(4-(trimethylsilyl)phenyl)-[1,1'-binaphthalene]-2,2'-diol (1.09 mg, 2.5 mmol, 1.0 eq.) and dibenzo[b,f]azepine (483.1 mg, 2.5 mmol, 1.0 eq.). The phosphoramidite was purified by prompt flash column chromatography (hexane:CH_2Cl_2:triethylamine, 80:19:1, SiO_2). The fractions were concentrated under reduced pressure and diluted with CH_2Cl_2. The process was repeated five times (always under N_2 atmosphere) in order to remove triethylamine. The ligand was obtained as a foamy colourless solid and used as attained (1.04 g, 1.59 mmol, 64%). **L_{31}** was obtained as a mixture of diastereomers (1:1 dr).

^{1}H NMR (500 MHz, $CDCl_3$) δ 8.16 (s, 1H), 8.05 (s, 1H), 8.01 (d, *J* = 8.2 Hz, 1H), 7.97 – 7.83 (m, 6H), 7.79 – 7.71 (m, 5H), 7.51 – 7.29 (m, 7H), 7.29 – 6.72 (m, 23H), 6.69 – 6.61 (m, 1H), 6.56 (dd, *J* = 7.9, 1.2 Hz, 1H), 6.45 (td, *J* = 7.7, 1.6 Hz, 1H), 6.38 (t, *J* = 7.6 Hz, 1H), 6.00 (d, *J* = 8.0 Hz, 1H), 5.75 (d, *J* = 8.0 Hz, 1H), 0.42 (s, 18H).

^{13}C NMR (126 MHz, $CDCl_3$) δ 150.5, 149.2, 146.5, 143.4, 143.2, 142.7, 139.9, 139.6, 138.9, 138.6, 136.4, 135.2 (2C), 133.8 (2C), 133.4 (4C), 133.1, 132.6, 132.4, 131.7, 131.5 (5C), 131.4, 130.9, 130.5, 130.4 (5C), 130.2 (3C), 129.8 (3C), 129.2 (3C), 129.1 (3C), 129.0, 128.9, 128.8 (4C), 128.7, 128.5, 128.2, 128.1, 127.9, 127.2, 127.1 (2C), 127.0, 126.7, 126.3 (2C), 126.2, 126.1, 125.9, 125.8, 125.3, 125.2, 125.0, 124.4, 124.2, 122.1, 121.4, 121.2, 119.6, 118.1, -0.7 (6C)

^{31}P NMR (162 MHz, $CDCl_3$) δ 137.3, 135.6 (major), (1:1.1).

IR υ_{max} (film): 2956, 1486, 1247, 1215 cm^{-1}.

HRMS (ESI^+): *m/z* calcd for $C_{43}H_{34}NO_2PSi$ $[M+H]^+$: 656.2169, found 656.2160.

[α]$^{25}_{D}$= +197.8 (*c* 1.0, $CHCl_3$).

5-((11cS)-2-(3,5-dimethylphenyl)dinaphtho[2,1-d:1',2'-f][1,3,2]dioxaphosphepin-4-yl)-*5H*-dibenzo[b,f]azepine (L$_{33}$)

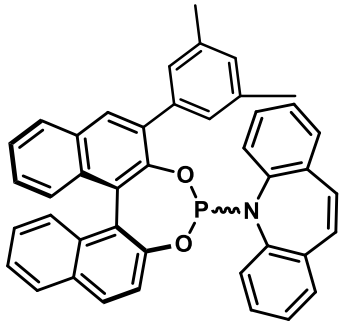

The title compound was obtained following General procedure G using *(S)*-3-(3,5-dimethylphenyl)-1,1'-bi-2-naphthol (976 mg, 2.5 mmol, 1.0 eq.) and dibenzo[b,f]azepine (483.1 mg, 2.5 mmol, 1.0 eq.). The phosphoramidite was purified by prompt flash column chromatography (hexane:CH_2Cl_2:triethylamine, 80:19:1, SiO_2). The fractions were concentrated under reduced pressure and diluted with CH_2Cl_2. The process was repeated five times (always under N_2 atmosphere) in order to remove triethylamine. The ligand was obtained as a foamy colourless solid and used as attained (1.15 g, 1.88 mmol, 75%). **L$_{33}$** was obtained as a mixture of diastereomers (1.2:1 dr).

^{1}H NMR (500 MHz, $CDCl_3$) δ 8.18 (s, 1H), 8.06 – 8.00 (m, 2H), 7.95 (d, *J* = 8.2 Hz, 1H), 7.89 (dd, *J* = 8.7, 7.0 Hz, 2H), 7.77 (dd, *J* = 7.6, 1.7 Hz, 1H), 7.56 (d, *J* = 1.7 Hz, 2H), 7.50 – 7.46 (m, 2H), 7.44 – 7.30 (m, 7H), 7.28 – 7.13 (m, 13H), 7.12 – 7.09 (m, 2H), 7.10 – 7.04 (m, 2H), 6.97 – 6.90 (m, 2H), 6.89 – 6.69 (m, 5H), 6.62 (d, *J* = 8.8 Hz, 1H), 6.58 (dd, *J* = 7.8, 1.2 Hz, 1H), 6.42 (td, *J* = 7.7, 1.6 Hz, 1H), 6.38 – 6.31 (m, 1H), 5.90 (d, *J* = 8.1 Hz, 1H), 5.76 (d, *J* = 7.9 Hz, 1H), 2.49 (s, 6H), 2.43 (s, 6H).

^{13}C NMR (126 MHz, $CDCl_3$) δ 150.5, 149.2, 146.7, 146.6, 143.4, 142.7, 142.4, 142.2, 138.3 (2C), 138.1, 137.8, 136.7, 136.4, 135.5, 135.1 (2C), 133.1, 132.6, 132.5, 132.4, 131.8, 131.6 (2C), 131.4 (2C), 130.8, 130.4 (2C), 130.3, 130.2 (2C), 129.3, 129.2 (2C), 129.0 (3C), 128.9 (3C), 128.8 (4C), 128.7 (3C), 128.5 (2C), 128.3 (2C), 128.2, 128.1 (2C), 128.0, 127.9, 127.2, 127.1 (2C), 127.0, 126.8, 126.7, 126.3, 126.1 (2C), 126.0, 125.8 (2C), 125.3, 125.1 (2C), 124.9, 124.4, 124.3, 122.1, 121.4, 121.3, 119.6, 118.1, 21.7 (2C), 21.6 (2C).

^{31}P NMR (162 MHz, $CDCl_3$) δ 137.1 (major), 135.61 (1.2:1).

IR υ_{max} (film): 3022, 1486, 1215 cm^{-1}.

HRMS (ESI^+): *m/z* calcd for $C_{42}H_{30}NO_2P$ $[M+H]^+$: 612.2087, found 612.2081.

$[\alpha]^{25}_D$= +305.1 (*c* 1.0, $CHCl_3$).

5-((11cS)-2-(3,5-di-*tert*-butylphenyl)dinaphtho[2,1-d:1',2'-f][1,3,2]dioxaphosphepin-4-yl)-*5H*-dibenzo[b,f]azepine (L_{34})

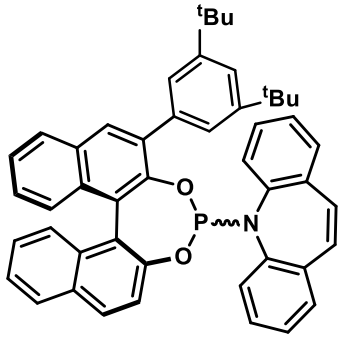

The title compound was obtained following General procedure G using *(S)*-3-(3,5-di-*tert*-butylphenyl)-1,1'-bi-2-naphthol (118.7 mg, 0.25 mmol, 1.0 eq.) and dibenzo[b,f]azepine (48.3 mg, 0.25 mmol, 1.0 eq.). The phosphoramidite was purified by prompt flash column chromatography (hexane:CH_2Cl_2:triethylamine, 80:19:1, SiO_2). The fractions were concentrated under reduced pressure and diluted with CH_2Cl_2. The process was repeated five times (always under N_2 atmosphere) in order to remove triethylamine. The ligand was obtained as a foamy colourless solid and used as attained (121.3, 0.17 mmol, 68%). **L_{34}** was obtained as a mixture of diastereomers (2.5:1 dr). ^{1}H and ^{13}C NMR describing only major diastereomer.

^{1}H NMR (500 MHz, $CDCl_3$) δ 8.25 (s, 1H), 8.09 (d, *J* = 8.3 Hz, 1H), 7.93 – 7.87 (m, 2H), 7.83 (d, *J* = 1.9 Hz, 2H), 7.71 – 7.65 (m, 1H), 7.55 – 7.03 (m, 9H), 7.01 – 6.89 (m, 1H), 6.87 – 6.73 (m, 3H), 6.56 – 6.46 (m, 1H), 6.38 – 6.31 (m, 1H), 5.92 (d, *J* = 8.0 Hz, 1H), 5.37 (d, *J* = 7.8 Hz, 1H), 1.40 (s, 18H).

^{13}C NMR (126 MHz, $CDCl_3$) δ 151.2, 149.4, 146.7, 142.6, 142.3, 137.7, 136.9, 136.0, 135.1, 131.9, 131.5, 130.3 (2C), 130.0, 129.3, 129.0, 128.9 (3C), 128.7, 128.5, 128.3, 128.1, 128.0, 127.2, 127.0, 126.8, 126.5, 126.2, 126.0, 125.7, 125.5 (2C), 125.1, 124.9 (2C), 124.3, 122.2, 121.7, 121.6, 35.2 (2C), 31.8 (6C).

^{31}P NMR (162 MHz, $CDCl_3$) δ 138.0 (major), 133.9 (2.5:1 dr).

IR υ_{max} (film): 2964, 1486, 1215 cm^{-1}.

HRMS (ESI^+): *m/z* calcd for $C_{48}H_{42}NO_2P$ $[M+H]^+$: 696.3026, found 696.302.

$[\alpha]^{25}_D$= +308.3 (*c* 1.0, $CHCl_3$).

5-((11cS)-2-mesityldinaphtho[2,1-d:1',2'-f][1,3,2]dioxaphosphepin-4-yl)-*5H*-dibenzo[b,f]azepine (L_{35})

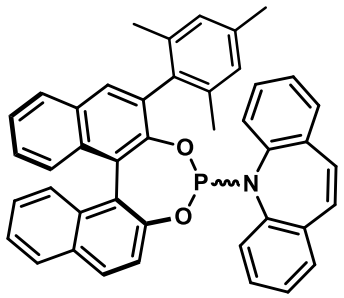

The title compound was obtained following General procedure G using *(S)*-3-mesityl-2,2'-dihydroxy-1,1'-binaphthyl (101.1 mg, 0.25 mmol, 1.0 eq.) and dibenzo[b,f]azepine (48.3 mg, 0.25 mmol, 1.0 eq.). The phosphoramidite was purified by prompt flash column chromatography (hexane:CH_2Cl_2:triethylamine, 80:19:1, SiO_2). The fractions were concentrated under reduced pressure and diluted with CH_2Cl_2. The process was repeated five times (always under N_2 atmosphere) in order to remove triethylamine. The ligand was obtained as a foamy colourless solid and used as attained (120.1 mg, 0.19 mmol, 76%). **L_{35}** was obtained as a mixture of diastereomers (9:1 dr). ^{1}H and ^{13}C NMR describing only major diastereomer.

^{1}H NMR (500 MHz, $CDCl_3$) δ 8.05 – 7.98 (m, 1H), 7.93 (d, *J* = 8.2 Hz, 1H), 7.87 (d, *J* = 8.6 Hz, 2H), 7.52 – 7.36 (m, 3H), 7.29 – 7.00 (m, 9H), 6.83 – 6.77 (m, 2H), 6.77 – 6.68 (m, 2H), 6.20 – 6.13 (m, 1H), 6.07 (d, *J* = 7.8 Hz, 1H), 5.67 – 5.63 (m, 1H), 2.47 (s, 3H), 2.38 (s, 3H), 2.15 (s, 3H).

^{13}C NMR (126 MHz, $CDCl_3$) δ 149.1, 147.7, 143.1, 142.9, 142.0 (2C), 139.0, 137.3, 136.7, 136.6, 136.5, 134.4, 133.2, 132.8, 132.7, 132.1, 132.0, 131.5, 130.7, 130.3 (2C), 129.5, 129.4, 129.3, 129.0, 128.7, 128.5, 128.1, 127.6, 127.1, 126.9, 126.8, 126.3 (2C), 125.5, 125.1, 124.9, 124.2, 123.9, 122.2, 21.8, 21.3, 20.8.

^{31}P NMR (162 MHz, $CDCl_3$) δ 134.6, 131.8 (major), (9:1).

IR υ_{max} (film): 2981, 1486, 1215 cm^{-1}.

HRMS (ESI^+): *m/z* calcd for $C_{43}H_{32}NO_2P$ $[M+H]^+$: 626.2243, found 626.2234.

$[\alpha]^{25}_D$= +151.3 (*c* 1.0, $CHCl_3$).

5-((11cS)-2-(2,4,6-triisopropylphenyl)dinaphtho[2,1-d:1',2'-f][1,3,2]dioxaphosphepin-4-yl)-*5H*-dibenzo[b,f]azepine (L_{36})

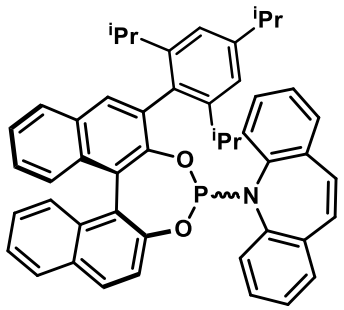

The title compound was obtained following General procedure G using *(S)*-3-(2,4,6-triisopropylphenyl)-[1,1'-binaphthalene]-2,2'-diol (122.2 mg, 0.25 mmol, 1.0 eq.) and dibenzo[b,f]azepine (48.3 mg, 0.25 mmol, 1.0 eq.).

The phosphoramidite was purified by prompt flash column chromatography (hexane:CH_2Cl_2:triethylamine, 80:19:1, SiO_2). The fractions were concentrated under reduced pressure and diluted with CH_2Cl_2. The process was repeated five times (always under N_2 atmosphere) in order to remove triethylamine. The ligand was obtained as a foamy colourless solid and used as attained (99.9 mg, 0.14 mmol, 56%). **L_{36}** was obtained as a single diastereomer. ^1H and ^{13}C NMR describing only major diastereomer.

^{1}H NMR (500 MHz, $CDCl_3$) δ 8.05 (s, 1H), 8.00 (d, *J* = 8.1 Hz, 1H), 7.91 (d, *J* = 8.7 Hz, 2H), 7.52 – 7.47 (m, 1H), 7.46 – 7.35 (m, 2H), 7.31 – 7.21 (m, 4H), 7.21 – 7.17 (m, 2H), 7.17 – 7.05 (m, 3H), 6.88 – 6.83 (m, 1H), 6.82 – 6.76 (m, 1H), 6.76 – 6.70 (m, 2H), 6.42 – 6.33 (m, 1H) 5.99 – 5.96 (m, 1H), 5.92 (d, *J* = 7.8 Hz, 1H), 3.36 (hept, *J* = 6.7 Hz, 1H), 3.18 – 3.03 (m, 2H), 1.48 – 1.36 (m, 9H), 1.27 (d, *J* = 6.7 Hz, 3H), 0.92 (d, *J* = 6.8 Hz, 3H), 0.63 (d, J = 6.7 Hz, 3H).

^{13}C NMR (126 MHz, $CDCl_3$) δ 149.2, 149.0, 148.5, 148.4, 147.4, 142.7, 142.5, 142.1, 136.7, 134.0, 133.3, 132.9, 132.8, 132.3, 132.1, 132.0, 131.6, 130.7, 130.4, 129.9, 129.5, 129.3, 129.2, 128.8, 128.5, 128.1, 127.3 (2C), 127.1, 126.7, 126.2, 126.0, 125.3, 125.0, 124.9, 124.5, 123.1, 122.4 (2C), 121.3, 34.4, 31.2, 30.6, 27.2, 25.6, 24.7, 24.4 (2C), 23.3.

^{31}P NMR (162 MHz, $CDCl_3$) δ 128.3.

IR υ_{max} (film): 2965, 1460, 1215 cm^{-1}.

HRMS (ESI^+): *m/z* calcd for $C_{49}H_{44}NO_2P$ $[M+H]^+$: 710.3182, found 710.3183.

[α]$^{25}_{D}$= +173.8 (*c* 1.0, $CHCl_3$).

(4*S*,11c*S*)-*N*,*N*-dimethyl-2-phenyldinaphtho[2,1-d:1',2'-f][1,3,2]dioxaphosphepin-4-amine (L$_{37}$)

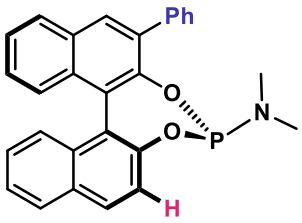

The title compound was obtained following General procedure G using *(S)*-(−)-1,1′-bi(2-naphthol) (143.2 mg, 0.5 mmol, 1.0 eq.) and Dimethylamine in THF (0.25 mL, 2 M, 0.5 mmol, 1.0 eq.).

The phosphoramidite was purified by prompt flash column chromatography (hexane:CH_2Cl_2: triethylamine, 80:19:1, SiO_2). The fractions were concentrated under reduced pressure and diluted with CH_2Cl_2. The process was repeated five times (always under N_2 atmosphere) in order to remove triethylamine. The ligand was obtained as a foamy colourless solid and used as attained (43.3 mg, 0.10 mmol, 20%). **L$_{37}$** was obtained as a mixture of diastereomers (1:1.5). ^{1}H and ^{13}C NMR describing only major diastereomer.

^{1}H NMR (400 MHz, $CDCl_3$): δ 7.99 (s, 1H), 7.92 – 7.72 (m, 4H), 7.47 – 7.36 (m, 1H), 7.37 – 7.29 (m, 4H), 7.28 – 7.21 (m, 2H), 7.24 – 7.07 (m, 4H), 2.07 (s 6H).

^{13}C NMR (101 MHz, $CDCl_3$) δ 150.8, 147.8, 138.0, 134.3, 133.6, 132.8, 131.0, 130.8 (3C), 130.0, 129.9(2C), 128.2, 128.1, 127.9(2C), 127.7, 127.6 (2C), 127.4, 126.2, 125.1, 124.7, 123.7, 122.5, 44.8 (2C).

^{31}P NMR (162 MHz, $CDCl_3$) δ 151.9, 148.8 (major). (1:1.5)

IR υ_{max} (film): 3005, 1457, 1210 cm^{-1}.

4-((4*S*,11c*S*)-2-phenyldinaphtho[2,1-d:1',2'-f][1,3,2]dioxaphosphepin-4-yl)morpholine (L$_{38}$)

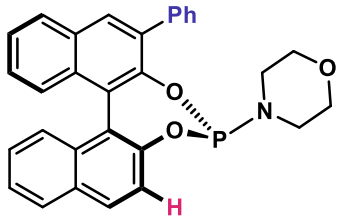

The title compound was obtained following General procedure G using (*S*)-(−)-1,1′-bi(2-naphthol) (143.2 mg, 0.5 mmol, 1.0 eq.) and morpholine (0.45 µL, 0.5 mmol, 1.0 eq.).

The phosphoramidite was purified by prompt flash column chromatography (hexane:CH_2Cl_2: triethylamine, 80:19:1, SiO_2). The fractions were concentrated under reduced pressure and diluted with CH_2Cl_2. The process was repeated five times (always under N_2 atmosphere) in order to remove triethylamine. The ligand was obtained as a foamy colourless solid and used as attained (77.1 mg, 0.16 mmol, 32%). **L$_{38}$** was obtained as a mixture of diastereomers (1:1.1). ^{1}H and ^{13}C NMR describing only major diastereomer.

^{1}H NMR (400 MHz, $CDCl_3$) δ 7.95 (s, 1H), 7.90 – 7.78 (m, 2H), 7.76 – 7.69 (m, 2H), 7.46 – 7.34 (m, 3H), 7.34 (s, 5H), 7.21 – 6.93 (m, 3H), 3.23 – 3.12 (m, 4H), 2.53 – 2.40 (m, 2H), 2.38 – 2.26 (m, 2H).

^{13}C NMR (101 MHz, $CDCl_3$) δ 149.5, 147.2,138.0, 134.1, 133.1, 132.2, 131.5, 131.0, 130.5, 130.2 (3C), 128.6, 128.5, 128.4 (2C), 128.2, 127.6, 127.1, 126.8, 126.3, 126.2, 125.2, 125.0, 124.2, 122.0, 67.6 (2C), 43.3 (2C).

^{31}P NMR (162 MHz, $CDCl_3$) δ 143.3 (major), 143.0. (1.6:1)

IR υ_{max} (film): 2966, 1469, 1213 cm^{-1}.

(4S,11cS)-*N*,*N*-diisopropyl-2-phenyldinaphtho[2,1-d:1',2'-f][1,3,2]dioxaphosphepin-4-amine (L_{39})

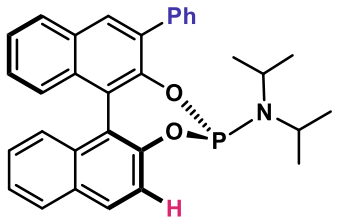

The title compound was obtained following General procedure G using *(S)*-(−)-1,1′-bi(2-naphthol) (143.2 mg, 0.5 mmol, 1.0 eq.) and diisopropylamine (70 µL, 0.5 mmol, 1.0 eq.).

The phosphoramidite was purified by prompt flash column chromatography (hexane:CH_2Cl_2: triethylamine, 80:19:1, SiO_2). The fractions were concentrated under reduced pressure and diluted with CH_2Cl_2. The process was repeated five times (always under N_2 atmosphere) in order to remove triethylamine. The ligand was obtained as a foamy colourless solid and used as attained (159.5 mg, 0.32 mmol, 64%). **L_{39}** was obtained as a mixture of diastereomers (4:1). ^{1}H and ^{13}C NMR describing only major diastereomer.

^{1}H NMR (400 MHz, $CDCl_3$): δ 7.97 (s, 1H), 7.90 – 7.75 (m, 4H), 7.45 – 7.38 (m, 1H), 7.35 – 7.31 (m, 4H), 7.27 – 7.23 (m, 2H), 7.22 – 7.09 (m, 4H), 3.13 (m, 2H), 0.95 (d, *J* = 6.7 Hz, 6H), 0.54 (d, *J* = 6.8 Hz, 6H).

^{13}C NMR (101 MHz, $CDCl_3$) δ 150.4, 148.0, 138.2, 134.3, 133.2, 132.5, 131.4, 130.6 (3C), 130.3, 129.9, 128.4 (2C), 128.1(2C), 127.4, 127.2, 127.1, 126.1, 125.9, 124.7(2C), 124.4, 123.4, 122.4, 45.0, 44.8, 24.8, 24.7, 23.5 (2C).

^{31}P NMR (162 MHz, $CDCl_3$) δ 151.7 (major), 148.9. (4:1).

IR υ_{max} (film): 2965, 1486, 1215, 1211 cm^{-1}.

(4S,11cS)-*N*-benzhydryl-*N*-methyl-2-phenyldinaphtho[2,1-d:1',2'-f][1,3,2]dioxaphosphepin-4-amine (L_{40})

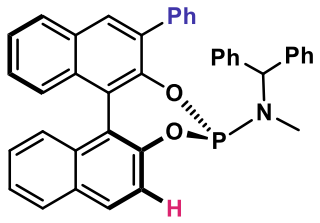

The title compound was obtained following General procedure G using *(S)*-(−)-1,1′-bi(2-naphthol) (143.2 mg, 0.5 mmol, 1.0 eq.) and *N*-(Diphenylmethyl)methylamine (98.6 mg, 0.5 mmol, 1.0 eq.).

The phosphoramidite was purified by prompt flash column chromatography (hexane:CH_2Cl_2: triethylamine, 80:19:1, SiO_2). The fractions were concentrated under reduced pressure and diluted with CH_2Cl_2. The process was repeated five times (always under N_2 atmosphere) in order to remove triethylamine. The ligand was obtained as a foamy colourless solid and used as attained (122.0 mg, 0.21 mmol, 42%). **L_{40}** was obtained as as a mixture of diastereomers (10:1). ^{1}H and ^{13}C NMR describing only major diastereomer.

^{1}H NMR (400 MHz, $CDCl_3$) δ 7.88 – 7.75 (m, 4H), 7.69 – 7.63 (m, 2H), 7.42 – 7.35 (m, 3H), 7.32 – 7.20 (m, 5H), 7.18 – 7.09 (m, 5H), 7.09 – 7.04 (m, 3H), 6.93 – 6.82 (m, 2H), 6.61 (dd, *J* = 6.6, 2.9 Hz, 2H), 5.21 (d, *J* = 9.1 Hz, 1H), 1.96 (d, *J* = 3.0 Hz, 3H).

^{13}C NMR (101 MHz, $CDCl_3$) 149.7, 147.7, 140.4, 140.0, 138.7, 134.9, 133.1, 132.3, 131.5 (2C), 130.7, 130.6, 130.3 (3C), 129.6(2C), 128.5 (4C), 128.4, 128.3, 128.2 (4C), 127.7, 127.4, 127.1(2C), 127.0, 126.2, 126.1, 125.0, 124.9, 123.5, 122.3, 67.6, 31.3.

^{31}P NMR (162 MHz, $CDCl_3$) δ 147.7 (major), 146.8. (dr 10:1)

IR υ_{max} (film): 3019, 1486, 1215, 1247 cm^{-1}.

(4S,11cS)-*N*-isopropyl-2-phenyl-*N*-((*R*)-1-phenylethyl)dinaphtho[2,1-d:1',2'-f][1,3,2]dioxaphosphepin-4-amine (L_{41})

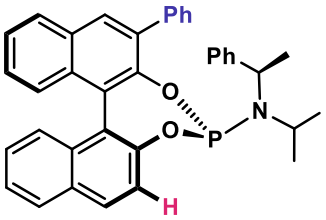

The title compound was obtained following General procedure G using *(S)*-(−)-1,1′-bi(2-naphthol) (143.2 mg, 0.5 mmol, 1.0 eq.) and *(R)*-*N*-(1-phenylethyl)propan-2-amine (81.6 mg, 0.5 mmol, 1.0 eq.).

The phosphoramidite was purified by prompt flash column chromatography (hexane:CH_2Cl_2: triethylamine, 80:19:1, SiO_2). The fractions were concentrated under reduced pressure and diluted with CH_2Cl_2. The process was repeated five times (always under N_2 atmosphere) in order to remove triethylamine. The ligand was obtained as a foamy colourless solid and used as attained (163.9 mg, 0.30 mmol, 60%). **L_{41}** was obtained as essentially a single diastereomer, traces of the other epimer could be detected by ^{31}P NMR spectroscopy.

^{1}H NMR (400 MHz, $CDCl_3$): δ 7.99 (s, 1H), 7.89 (d, *J* = 8.7 Hz, 1H), 7.87 – 7.80 (m, 4H), 7.48 (d, *J* = 8.8 Hz, 1H), 7.44 – 7.34 (m, 2H), 7.34 – 7.28 (m, 2H), 7.27 – 7.21 (m, 4H), 7.20 – 7.11 (m, 5H), 7.06 (t, *J* = 7.2 Hz, 1H), 4.34 (t, *J* = 7.6 Hz, 1H), 3.06 – 2.93 (m, 1H), 0.97 (d, *J* = 7.1 Hz, 3H), 0.73 (d, *J* = 6.7 Hz, 3H), 0.55 (d, *J* = 6.8 Hz, 3H).

^{13}C NMR (101 MHz, $CDCl_3$) δ 150.1, 147.6, 144.3, 138.1, 134.2, 133.1, 132.5, 131.4, 130.6 (2C), 130.5, 130.3, 130.0, 128.4, 128.3, 128.1 (2C), 127.9 (2C), 127.5 (2C), 127.4, 127.1, 127.0, 126.5, 126.1, 125.9, 124.7 (2C), 124.3, 123.4, 122.3, 51.1, 46.0, 24.5, 24.0, 20.4.

^{31}P NMR (162 MHz, $CDCl_3$) δ 148.2 (major), 145.3. (dr >20:1)

IR υ_{max} (film): 2981, 1486, 1215 cm^{-1}.

(4S,11cS)-2-phenyl-*N*,*N*-*bis*((*R*)-1-phenylethyl)dinaphtho[2,1-d:1',2'-f][1,3,2]dioxaphosphepin-4-amine (L42)

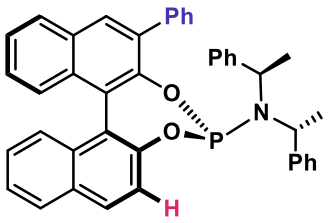

The title compound was obtained following General procedure G using *(S)*-(−)-1,1′-bi(2-naphthol) (143.2 mg, 0.5 mmol, 1.0 eq.) and *(R)-bis((R)*-1-phenylethyl)amine (112.7 mg, 0.5 mmol, 1.0 eq.).

The phosphoramidite was purified by prompt flash column chromatography (hexane:CH_2Cl_2: triethylamine, 80:19:1, SiO_2). The fractions were concentrated under reduced pressure and diluted with CH_2Cl_2. The process was repeated five times (always under N_2 atmosphere) in order to remove triethylamine. The ligand was obtained as a foamy colourless solid and used as attained (164.8 mg, 0.27 mmol, 54%). **L42** was obtained as essentially a single diastereomer, traces of the other epimer could be detected by ^{31}P NMR spectroscopy.

^{1}H NMR (400 MHz, $CDCl_3$) δ 8.22 (s, 1H), 8.10 (dd, *J* = 8.3, 1.3 Hz, 2H), 8.07 – 7.96 (m, 3H), 7.66 – 7.54 (m, 3H), 7.53 – 7.43 (m, 4H), 7.39 (dd, *J* = 8.6, 1.2 Hz, 1H), 7.33 – 7.26 (m, 2H), 7.16 (dd, *J* = 5.0, 1.9 Hz, 6H), 7.09 (d, *J* = 5.4 Hz, 4H), 4.54 (s, 2H), 1.23 (d, *J* = 7.2 Hz, 6H).

^{13}C NMR (101 MHz, $CDCl_3$) δ 150.1, 147.6, 144.3, 138.1, 134.2, 133.1, 132.5, 131.4, 130.6 (2C), 130.5, 130.3, 130.0, 128.4, 128.3, 128.1 (2C), 127.9 (2C), 127.5 (2C), 127.4, 127.1, 127.0, 126.5, 126.1, 125.9, 124.7 (2C), 124.3, 123.4, 122.3, 51.1, 46.0, 24.5, 24.0, 20.4.

^{31}P NMR (162 MHz, $CDCl_3$) δ 150.9 (major), 147.7 (dr >20:1).

IR υ_{max} (film): 2981, 1486, 1215 cm^{-1}.

(11c*S*)-2-phenyl-*N*,*N*-*bis*((*S*)-1-phenylethyl)dinaphtho[2,1-d:1',2'-f][1,3,2]dioxaphosphepin-4-amine (L_{43})

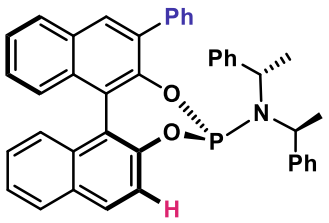

The title compound was obtained following General procedure G using *(S)*-(−)-1,1′-bi(2-naphthol) (143.2 mg, 0.5 mmol, 1.0 eq.) and *(S)-bis((S)*-1-phenylethyl)amine (112.7 mg, 0.5 mmol, 1.0 eq.).

The phosphoramidite was purified by prompt flash column chromatography (hexane:CH_2Cl_2: triethylamine, 80:19:1, SiO_2). The fractions were concentrated under reduced pressure and diluted with CH_2Cl_2. The process was repeated five times (always under N_2 atmosphere) in order to remove triethylamine. The ligand was obtained as a foamy colourless solid and used as attained (199.8 mg, 0.32 mmol, 64%). **L_{43}** was obtained as essentially a single diastereomer, traces of the other epimer could be detected by ^{31}P NMR spectroscopy.

^{1}H NMR (400 MHz, $CDCl_3$) δ 8.28 (s, 1H), 8.20 – 8.12 (m, 2H), 8.11 – 8.02 (m, 3H), 7.72 – 7.60 (m, 3H), 7.61 – 7.49 (m, 4H), 7.47 – 7.32 (m, 3H), 7.23 (dd, *J* = 5.2, 1.9 Hz, 6H), 7.17 – 7.08 (m, 4H), 4.64 – 4.49 (m, 2H), 1.26 (d, *J* = 7.2 Hz, 6H).

^{13}C NMR (101 MHz, $CDCl_3$) δ 149.9, 147.5, 143.3 (2C), 138.3, 134.3, 133.1, 132.6, 131.5, 130.8 (2C), 130.5, 130.4, 130.2, 128.5, 128.4, 128.3 (2C), 128.0 (3C), 127.8 (4C), 127.6, 127.2, 127.0, 126.6 (2C), 126.2 (2C), 124.9, 124.8, 124.4, 123.6, 122.4 (2C), 51.9, 51.8, 20.7 (2C).

^{31}P NMR (162 MHz, $CDCl_3$) δ 146.1, 144.8 (dr >20:1).

IR υ_{max} (film): 2993, 1485, 1213 cm^{-1}.

(4S,11cS)-*N*,*N*-*bis*((*S*)-1-(naphthalen-2-yl)ethyl)-2-phenyldinaphtho[2,1-d:1',2'-f][1,3,2]dioxaphosphepin-4-amine (L44)

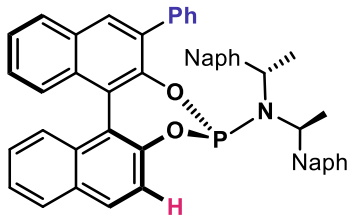

The title compound was obtained following General procedure G using *(S)*-(−)-1,1′-bi(2-naphthol) (143.2 mg, 0.5 mmol, 1.0 eq.) and *(S)-bis((S)*-1-(naphthalen-2-yl)ethyl)amine (162.6 mg, 0.5 mmol, 1.0 eq.).

The phosphoramidite was purified by prompt flash column chromatography (hexane:CH_2Cl_2: triethylamine, 80:19:1, SiO_2). The fractions were concentrated under reduced pressure and diluted with CH_2Cl_2. The process was repeated five times (always under N_2 atmosphere) in order to remove triethylamine. The ligand was obtained as a foamy colourless solid and used as attained (239.8 mg, 0.34 mmol, 68%). **L44** was obtained as a single diastereomer.

^{1}H NMR (400 MHz, $CDCl_3$) δ 8.20 (s, 1H), 8.10 – 8.05 (m, 2H), 8.04 – 7.94 (m, 3H), 7.70 (dd, *J* = 7.6, 1.7 Hz, 2H), 7.65 – 7.58 (m, 2H), 7.55 – 7.09 (m, 20H), 4.62 (s, 2H), 1.27 (d, *J* = 7.0 Hz, 6H).

^{13}C NMR (101 MHz, $CDCl_3$) δ 149.9, 147.5, 140.7(2C), 138.4, 134.4, 133.1, 133.0 (2C), 132.7, 132.4 (2C), 131.5, 130.9 (2C), 130.6, 130.4, 130.3, 128.5, 128.4 (3C), 128.0 (2C), 127.7, 127.4 (2C), 127.3 (2C), 127.2 (2C), 127.1, 126.2 (3C), 126.1, 125.7 (2C), 125.6 (2C), 125.0, 124.8, 124.4, 123.6, 122.4 (2C), 52.1, 51.9, 22.8 (2C).

^{31}P NMR (162 MHz, $CDCl_3$) δ 145.6 (major), 144.1 (dr >20:1).

IR υ_{max} (film): 2981, 1471 1215 cm^{-1}.

(4S,11cS)-*N*-cyclohexyl-*N*-((*S*)-2,3-dihydro-*1H*-inden-1-yl)-2-phenyldinaphtho[2,1-d:1',2'-f][1,3,2]dioxaphosphepin-4-amine (L45)

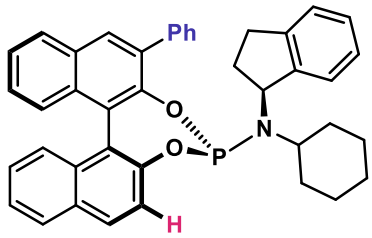

The title compound was obtained following General procedure G using *(S)*-(−)-1,1′-bi(2-naphthol) (143.2 mg, 0.5 mmol, 1.0 eq.) and *(S)*-*N*-cyclohexyl-2,3-dihydro-*1H*-inden-1-amine (107.7 mg, 0.5 mmol, 1.0 eq.).

The phosphoramidite was purified by prompt flash column chromatography (hexane:CH_2Cl_2: triethylamine, 80:19:1, SiO_2). The fractions were concentrated under reduced pressure and diluted with CH_2Cl_2. The process was repeated five times (always under N_2 atmosphere) in order to remove triethylamine. The ligand was obtained as a foamy colourless solid and used as attained (175.1 mg, 0.29 mmol, 58%). **L45** was obtained as a single diastereomer (dr >20:1).

^{1}H NMR (400 MHz, $CDCl_3$) δ 7.97 (s, 1H), 7.87 – 7.75 (m, 5H), 7.52 – 7.23 (m, 7H), 7.20 – 7.08 (m, 3H), 6.99 (d, *J* = 4.2 Hz, 2H), 6.83 (dt, *J* = 8.1, 4.2 Hz, 1H), 6.05 (d, *J* = 7.5 Hz, 1H), 4.53 – 4.30 (m, 1H), 2.86 – 2.75 (m, 1H), 2.63 – 2.49 (m, 2H), 2.40 – 2.28 (m, 1H), 2.02 – 1.88 (m, 1H), 1.66 (d, *J* = 12.2 Hz, 1H), 1.50 (d, *J* = 3.0 Hz, 1H), 1.42 – 1.33 (m, 2H), 1.27 – 1.07 (m, 3H), 0.84 – 0.68 (m, 1H), 0.66 – 0.41 (m, 2H).

^{13}C NMR (101 MHz, $CDCl_3$) δ 150.2, 147.9, 144.9, 142.4, 138.4, 134.2, 133.2, 132.5, 131.3, 130.5 (3C), 130.3, 130.2, 128.4 (3C), 128.3, 127.6, 127.0 (2C), 126.9, 126.7, 126.1, 126.0, 124.9 (2C), 124.7, 124.4, 124.3, 123.2, 122.3, 59.7, 55.5, 38.5, 35.4, 32.9, 30.2, 26.4 (2C), 25.6.

^{31}P NMR (162 MHz, $CDCl_3$) δ 152.4 (major), 148.9 (dr >20:1).

IR υ_{max} (film): 3019, 1486, 1203 cm^{-1}.

(4*S*,11c*S*)-*N*-cyclohexyl-2-phenyl-*N*-((*S*)-1,2,3,4-tetrahydronaphthalen-1-yl)dinaphtho[2,1-d:1',2'-f][1,3,2]dioxaphosphepin-4-amine (L_{46})

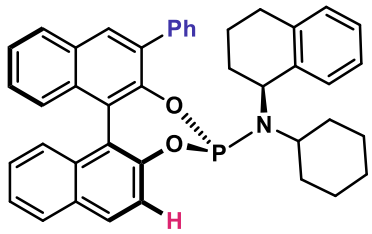

The title compound was obtained following General procedure G using *(S)*-(−)-1,1′-bi(2-naphthol) (143.2 mg, 0.5 mmol, 1.0 eq.) and *(S)*-*N*-cyclohexyl-1,2,3,4-tetrahydronaphthalen-1-amine (114.7 mg, 0.5 mmol, 1.0 eq.).

The phosphoramidite was purified by prompt flash column chromatography (hexane:CH_2Cl_2: triethylamine, 80:19:1, SiO_2). The fractions were concentrated under reduced pressure and diluted with CH_2Cl_2. The process was repeated five times (always under N_2 atmosphere) in order to remove triethylamine. The ligand was obtained as a foamy colourless solid and used as attained (169.3 mg, 0.27 mmol, 54%). **L_{46}** was obtained as a single diastereomer (dr >20:1).

^{1}H NMR (400 MHz, $CDCl_3$) δ 7.97 (s, 1H), 7.86 – 7.77 (m, 5H), 7.49 – 7.26 (m, 6H), 7.23 (d, *J* = 8.5 Hz, 1H), 7.19 – 7.08 (m, 3H), 6.93 (t, *J* = 7.3 Hz, 1H), 6.86 (d, *J* = 7.5 Hz, 1H), 6.76 (t, *J* = 7.5 Hz, 1H), 6.51 (d, *J* = 7.8 Hz, 1H), 4.27 – 3.79 (m, 1H), 2.86 – 2.43 (m, 2H), 2.05 (d, *J* = 11.7 Hz, 1H), 1.96 – 1.78 (m, 2H), 1.72 (d, *J* = 12.1 Hz, 1H), 1.55 (t, *J* = 15.2 Hz, 2H), 1.39 – 0.96 (m, 6H), 0.88 – 0.24 (m, 3H).

^{13}C NMR (101 MHz, $CDCl_3$) δ 150.0, 148.3, 139.6, 138.3, 137.5, 134.2, 133.1, 132.4, 131.2, 130.2 (5C), 128.6 (2C), 128.3 (4C) 128.1, 127.5, 127.0 (2C), 126.1, 126.0 (2C), 125.9, 124.7, 124.5, 124.3, 122.6, 122.3, 56.1, 53.4, 35.4 (2C), 32.0, 29.6, 26.4 (2C), 25.5, 22.1.

^{31}P NMR (162 MHz, $CDCl_3$) δ 153.1 (major), 150.1 (dr >20:1).

IR υ_{max} (film): 3018, 1463, 1207 cm^{-1}.

(4S,11cS)-*N*-((*S*)-2,3-dihydro-*1H*-inden-1-yl)-*N*-(pentan-3-yl)-2-phenyldinaphtho[2,1-d:1',2'-f][1,3,2]dioxaphosphepin-4-amine (L_{47})

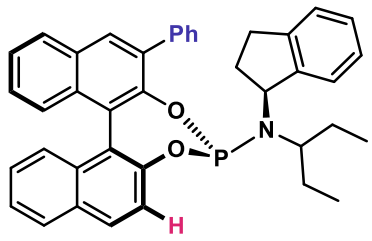

The title compound was obtained following General procedure G using *(S)*-(−)-1,1′-bi(2-naphthol) (286.4 mg, 1 mmol, 1.0 eq.) and *(S)*-*N*-(pentan-3-yl)-2,3-dihydro-*1H*-inden-1-amine (203.4 mg, 1 mmol, 1.0 eq.).

The phosphoramidite was purified by prompt flash column chromatography (hexane:CH_2Cl_2: triethylamine, 80:19:1, SiO_2). The fractions were concentrated under reduced pressure and diluted with CH_2Cl_2. The process was repeated five times (always under N_2 atmosphere) in order to remove triethylamine. The ligand was obtained as a foamy colourless solid and used as attained (261 mg, 0.44 mmol, 44%). **L_{47}** was obtained as a single diastereomer (>20:1 dr).

^{1}H NMR (400 MHz, $CDCl_3$): δ 7.93 (s, 1H), 7.84 – 7.74 (m, 5H), 7.49 – 7.43 (m, 2H), 7.42 – 7.33 (m, 2H), 7.32 – 7.25 (m, 2H), 7.25 – 7.21 (m, 1H), 7.16 – 7.07 (m, 3H), 6.97 (d, J = 3.9 Hz, 2H), 6.84 – 6.79 (m, 1H), 6.09 (d, J = 7.6 Hz, 1H), 4.42 – 4.30 (m, 1H), 2.85 – 2.77 (m, 1H), 2.62 – 2.50 (m, 2H), 2.33 – 2.25 (m, 1H), 2.06 – 1.94 (m, 1H), 1.38 – 1.26 (m, 2H), 1.26 – 1.09 (m, 2H), 0.76 (t, J = 7.4 Hz, 3H), 0.42 (t, J = 7.4 Hz, 3H).

^{13}C NMR (101 MHz, $CDCl_3$) δ:150.0, 147.9, 147.8, 144.6, 142.6, 138.7, 134.3, 133.1, 132.6, 131.3, 130.5, 130.3 (3C), 128.5 (2C), 128.4, 128.2, 127.6, 127.1, 127.0 (2C), 126.7, 126.1, 126.0, 125.2, 124.8, 124.7, 124.4, 124.3, 123.2, 122.3, 59.9, 59.6, 58.4, 30.3, 28.9, 26.7, 11.9, 11.7.

^{31}P NMR (162 MHz, $CDCl_3$) δ 148.0 (major), 147.3 (dr >20:1).

HRMS (ESI): *m/z* calculated for $C_{40}H_{37}NO_2P^+[M+H]^+$ = 594.2556. Found = 594.2546.

IR: 3012, 1508, 1462, 1408, 1328, 1217 cm^{-1}.

$[\alpha]^{22}_D$ = +216.9 (*c* 1.0, $CHCl_3$).

(4S,11cS)-*N*-((*R*)-2,3-dihydro-*1H*-inden-1-yl)-*N*-(pentan-3-yl)-2-phenyldinaphtho[2,1-d:1',2'-f][1,3,2]dioxaphosphepin-4-amine (L48)

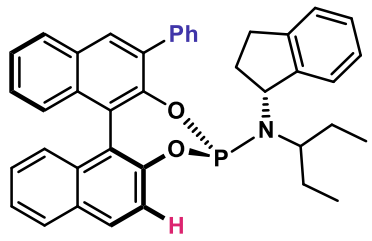

The title compound was obtained following General procedure G using *(S)*-(−)-1,1′-bi(2-naphthol) (286.4 mg, 1 mmol, 1.0 eq.) and (*R*)-*N*-(pentan-3-yl)-2,3-dihydro-*1H*-inden-1-amine (203.4 mg, 1 mmol, 1.0 eq.).

The phosphoramidite was purified by prompt flash column chromatography (hexane:CH_2Cl_2: triethylamine, 80:19:1, SiO_2). The fractions were concentrated under reduced pressure and diluted with CH_2Cl_2. The process was repeated five times (always under N_2 atmosphere) in order to remove triethylamine. The ligand was obtained as a foamy colourless solid and used as attained (349 mg, 0.59 mmol, 59%). **L48** was obtained as a single diastereomer (>20:1 dr).

^{1}H NMR (400 MHz, $CDCl_3$): δ 7.97 (s, 1H), 7.87 (d, J = 8.8 Hz, 1H), 7.83 – 7.78 (m, 4H), 7.46 (d, J = 8.7 Hz, 1H), 7.39 – 7.31 (m, 3H), 7.31 – 7.23 (m, 3H), 7.22 – 7.16 (m, 2H), 7.14 – 7.06 (m, 2H), 7.04 – 6.89 (m, 3H), 4.65 – 4.47 (m, 1H), 2.66 – 2.53 (m, 1H), 2.39 – 2.34 (m, 1H), 2.24 (s, 1H), 1.56 – 1.50 (m, 1H), 1.47 – 1.36 (m, 1H), 1.29 (pent, J = 7.3 Hz, 2H), 1.02 – 0.86 (m, 2H), 0.49 (t, J = 7.3 Hz, 3H), 0.33 (t, J = 7.4 Hz, 3H).

^{13}C NMR (101 MHz, $CDCl_3$) δ 150.2, 147.5, 147.5, 144.0, 143.5, 138.3, 134.4, 133.2, 132.5, 131.4, 130.6 (2C), 130.5, 130.3, 130.0, 128.5, 128.3, 128.2 (2C), 127.4, 127.4, 127.2, 127.1, 126.3, 126.1, 126.0, 124.9, 124.7, 124.4, 124.3, 123.7, 122.4, 59.8, 58.5, 58.3, 30.9, 30.1, 27.5, 11.7, 11.4.

^{31}P NMR (162 MHz, $CDCl_3$) δ 146.0 (major), 145.5. (>20:1)

HRMS (ESI): *m/z* calculated for $C_{40}H_{37}NO_2P^+[M+H]^+$ = 594.2556. Found = 594.2580.

IR: 2971, 2360, 1461, 1410, 1217 cm^{-1}.

$[\alpha]^{22}_D$ = +425.5 (*c* 1.0, $CHCl_3$).

(4*S*,11c*S*)-*N*-isopropyl-2-phenyl-*N*-((*S*)-1,2,3,4-tetrahydronaphthalen-1-yl)dinaphtho[2,1-d:1',2'-f][1,3,2]dioxaphosphepin-4-amine (L_{49})

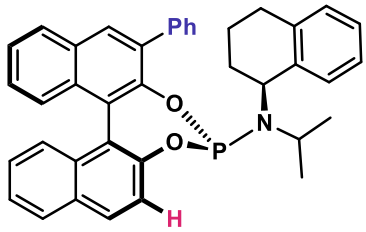

The title compound was obtained following General procedure G using *(S)*-(−)-1,1′-bi(2-naphthol) (143.2 mg, 0.5 mmol, 1.0 eq.) and *(S)*-*N*-isopropyl-1,2,3,4-tetrahydronaphthalen-1-amine (94.7 mg, 0.5 mmol, 1.0 eq.).

The phosphoramidite was purified by prompt flash column chromatography (hexane:CH_2Cl_2: triethylamine, 80:19:1, SiO_2). The fractions were concentrated under reduced pressure and diluted with CH_2Cl_2. The process was repeated five times (always under N_2 atmosphere) in order to remove triethylamine. The ligand was obtained as a foamy colourless solid and used as attained (155.4 mg, 0.27 mmol, 54%). **L_{49}** was obtained as a single diastereomer.

^{1}H NMR (400 MHz, $CDCl_3$) δ 7.95 (s, 1H), 7.90 – 7.75 (m, 5H), 7.53 – 7.43 (m, 2H), 7.43 – 7.28 (m, 4H), 7.25 – 7.21 (m, 1H), 7.19 – 7.10 (m, 3H), 6.99 – 6.92 (m, 1H), 6.90 – 6.78 (m, 2H), 6.57 (d, *J* = 7.8 Hz, 1H), 4.15 – 4.02 (m, 1H), 3.26 – 3.17 (m, 1H), 2.80 – 2.67 (m, 1H), 2.64 – 2.54 (m, 1H), 2.07 – 1.96 (m, 1H), 1.92 – 1.80 (m, 2H), 1.67 – 1.53 (m, 1H), 0.93 (d, *J* = 6.6 Hz, 3H), 0.74 (d, *J* = 6.7 Hz, 3H).

^{13}C NMR (101 MHz, $CDCl_3$) δ 150.1, 138.5, 137.8, 134.6, 132.6, 131.4, 130.7 (2C), 130.6, 130.4, 130.3 (2C), 128.7, 128.7, 128.4 (3C), 128.3, 127.6, 127.3, 127.2, 126.2, 126.2, 126.1, 125.9, 124.7 (2C), 124.5, 122.5, 47.2, 29.8, 25.0, 22.4, 22.2, 35.2, 52.9, 148.6, 139.5, 133.1.

^{31}P NMR (162 MHz, $CDCl_3$) δ 152.5 (major), 150.0 (dr >20:1).

IR υ_{max} (film): 3012, 2360, 1508, 1461 cm^{-1}.

HRMS (ESI^+): *m/z* calcd for $C_{39}H_{35}NO_2P$ $[M+H]^+$: 580.2405, found 580.2407.

(4S,11cS)-*N*-((*S*)-2,3-dihydro-*1H*-inden-1-yl)-*N*-(heptan-4-yl)-2-phenyldinaphtho[2,1-d:1',2'-f][1,3,2]dioxaphosphepin-4-amine (L_{50})

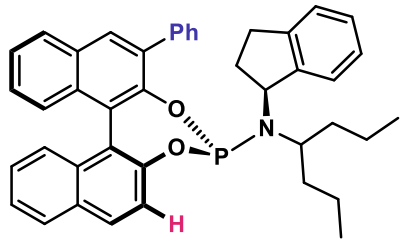

The title compound was obtained following General procedure G using *(S)*-(−)-1,1′-bi(2-naphthol) (143.2 mg, 0.5 mmol, 1.0 eq.) and *(S)*-*N*-(heptan-4-yl)-2,3-dihydro-*1H*-inden-1-amine (115.7 mg, 0.5 mmol, 1.0 eq.).

The phosphoramidite was purified by prompt flash column chromatography (hexane:CH_2Cl_2: triethylamine, 80:19:1, SiO_2). The fractions were concentrated under reduced pressure and diluted with CH_2Cl_2. The process was repeated five times (always under N_2 atmosphere) in order to remove triethylamine. The ligand was obtained as a foamy colourless solid and used as attained (158.5 mg, 0.25 mmol, 50%). **L_{50}** was obtained as a single diastereomer.

^{1}H NMR (400 MHz, $CDCl_3$) δ 7.94 (s, 1H), 7.88 – 7.76 (m, 6H), 7.51 – 7.44 (m, 2H), 7.43 – 7.22 (m, 6H), 7.18 – 7.15 (m, 1H), 7.14 – 7.10 (m, 2H), 6.99 (d, *J* = 4.2 Hz, 2H), 6.86 – 6.80 (m, 1H), 6.10 (d, *J* = 7.6 Hz, 1H), 4.50 – 4.27 (m, 1H), 2.87 – 2.75 (m, 1H), 2.64 – 2.47 (m, 2H), 2.37 – 2.26 (m, 1H), 2.10 – 1.95 (m, 1H), 1.40 – 1.27 (m, 2H), 1.28 – 1.13 (m, 3H), 0.83 – 0.71 (m, 4H), 0.43 (t, *J* = 7.4 Hz, 3H).

^{13}C NMR (101 MHz, $CDCl_3$) δ 150.0, 147.8, 144.6, 142.6, 138.7, 134.3, 133.1, 132.6, 131.4, 130.5, 130.3 (4C), 128.5 (2C), 128.4, 128.3, 127.6, 127.1 (2C), 127.0, 126.7, 126.1, 126.0, 125.2, 124.8, 124.7, 124.4, 124.3, 123.1, 122.3, 59.9, 58.4, 38.0, 30.3 (2C), 28.9 (2C), 26.7, 11.9, 11.7.

^{31}P NMR (162 MHz, $CDCl_3$) δ 148.0 (major), 147.3 (dr >20:1).

IR υ_{max} (film): 2971, 1462, 1408, 1328 cm^{-1}.

HRMS (ESI^+): *m/z* calcd for $C_{42}H_{41}NO_2P$ $[M+H]^+$: 622.2875, found 622.2888.

5-((11bS)-2,6-diiododinaphtho[2,1-d:1',2'-f][1,3,2]dioxaphosphepin-4-yl)-*5H*-dibenzo[b,f]azepine (L_{51})

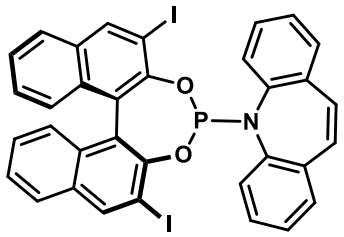

The title compound was obtained following General procedure G using *(S)*-3,3'-diiodo-[1,1'-binaphthalene]-2,2'-diol (1.16 g, 2.0 mmol, 1.0 eq.) and dibenzo[b,f]azepine (386.4 mg, 2.0 mmol, 1.0 eq.).

The phosphoramidite was purified by prompt flash column chromatography (hexane:CH_2Cl_2:triethylamine, 80:19:1, SiO_2). The fractions were concentrated under reduced pressure and diluted with CH_2Cl_2. The process was repeated five times (always under N_2 atmosphere) in order to remove triethylamine. The ligand **L_{51}** was obtained as a foamy colourless solid and used as attained (1.17 g, 1.54 mmol, 77%).

^{1}H NMR (400 MHz, $CDCl_3$) δ 8.36 (d, *J* = 9.1 Hz, 1 H), 8.11 (d, *J* = 8.0 Hz, 1 H), 7.76 (d, *J* = 8.0 Hz, 2 H), 7.60 (d, *J* = 9.0 Hz, 1 H), 7.48 (m, 2 H), 7.24 – 6.85 (m, 12 H) 6.53 (m, 1 H).

^{13}C NMR (101 MHz, $CDCl_3$) δ 152.5, 149.1, 146.6, 145.9, 143.0, 133.3, 132.7, 132.4 (4C), 130.5, 131.1, 130.0 (4C), 129.5, 129.7, 129.0, 129.4, 128.6 (4C), 128.7, 127.6, 127.6, 127.3, 126.8, 126.4, 125.3, 122.3, 122.6.

^{31}P NMR (162 MHz, $CDCl_3$) δ 137.7.

5.4.4 Binols

_(S)_-2,2'-_bis_(methoxymethoxy)-1,1'-binaphthalene

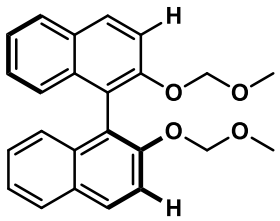

_(S)_-binaphthol (5.60 g, 19.6 mmol, 1.0 eq.) was dissolved in THF (80 mL) and stirred at 0 °C for 10 min. NaH (60% in mineral oil, 2.0 g, 50.0 mmol, 2.55 eq.) was then slowly added in small portions. After stirring for 1 h at 0 °C, a chloromethyl methyl ether solution (0.5 M in acetonitrile, 11.0 mL, 68.3 mmol, 3.5 eq) was added. The reaction was stirred for 16 h at rt. The reaction was slowly quenched with sat. NH_4Cl_{aq} (10 mL). The organic and aqueous layers were partitioned, and the aqueous phase was extracted with Et_2O (3 × 20 mL). The combined organic phases were dried over Na_2SO_4, filtered, and concentrated under reduced pressure. After column chromatography (hexane:EtOAc, 80:20, SiO_2), _(S)_-2,2'-_bis_(methoxymethoxy)-1,1'- binaphthalene (6.90 g, 18.4 mmol, 94 %) was obtained as a colourless solid.

^{1}H NMR (400 MHz, $CDCl_3$): δ 7.98 – 7.93 (m, 2H), 7.88 (ddt, _J_ = 8.2, 1.2, 0.5 Hz, 2H), 7.58 (d, _J_ = 9.0 Hz, 2H), 7.35 (ddd, _J_ = 8.1, 6.6, 1.3 Hz, 2H), 7.23 (ddd, _J_ = 8.0, 6.6, 1.3 Hz, 2H), 7.16 (ddt, _J_ = 8.5, 1.5, 0.8 Hz, 2H), 5.08 (d, _J_ = 6.7 Hz, 2H), 4.98 (d, _J_ = 6.7 Hz, 2H), 3.15 (s, 6H).

Analytical data are in agreement with the literature.[17]

***(S)*-3-iodo-2,2'-*bis*(methoxymethoxy)-1,1'-binaphthalene**

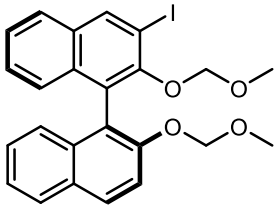

(S)-2,2'-*bis*(methoxymethoxy)-1,1'-binaphthalene (3.0 g, 8.0 mmol, 1.0 eq.) was dissolved in dry THF (40 mL). The reaction was cooled at -78 °C and *n*-BuLi (2.5 M in hexane, 4.0 mL, 10.0 mmol, 1.25 eq.) was added dropwise. The light-yellow solution turned brown. After 30 min, the reaction was allowed to warm up at 0 °C and stirred for 1 h. Iodine (2.64 g, 10.4 mmol, 1.3 eq.) was added at -78 °C and the reaction was stirred at rt over 16 h. After addition, the solution turned pale yellow. After completion, the reaction was poured in a saturated solution of NH_4Cl (10 mL). The organic and aqueous layers were partitioned, and the aqueous phase was extracted with Et_2O (3 × 20 mL). The combined organic phases were dried over Na_2SO_4, filtered, and concentrated under reduced pressure. After column chromatography (hexane:EtOAc, 90:10, SiO_2), *(S)*-3-iodo-2,2'-*bis*(methoxymethoxy)-1,1'-binaphthalene (2.28 g, 5.0 mmol, 63%) was obtained as a colourless solid.

^{1}H NMR (400 MHz, $CDCl_3$) δ 8.24 (s, 1H), 7.97 (d, *J* = 9.1 Hz, 1H), 7.88 – 7.84 (m, 1H), 7.81 – 7.75 (m, 1H), 7.58 (d, *J* = 9.1 Hz, 1H), 7.45 – 7.33 (m, 2H), 7.31 – 7.27 (m, 2H), 7.24 – 7.10 (m, 2H), 5.14 (d, *J* = 7.0 Hz, 1H), 5.04 (d, *J* = 7.0 Hz, 1H), 4.77 (d, *J* = 5.4 Hz, 1H), 4.73 (d, *J* = 5.4 Hz, 1H), 3.19 (s, 3H), 2.70 (s, 3H).

^{13}C NMR (101 MHz, $CDCl_3$) δ 152.9, 151.7, 139.4, 133.9, 132.5, 130.1, 129.5, 127.9, 126.9 (2C), 126.8, 126.4, 126.1, 125.7, 125.5, 124.2, 120.1, 116.2, 99.2, 94.8, 93.0, 56.8 (2C), 56.0 (2C).

Analytical data are in agreement with the literature.[18]

***(S)*-3,3'-diiodo-2,2'-*bis*(methoxymethoxy)-1,1'-binaphthalene**

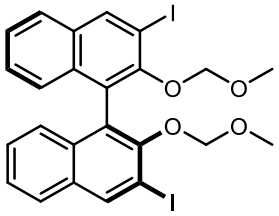

(S)-2,2'-*bis*(methoxymethoxy)-1,1'-binaphthalene (3.0 g, 8.0 mmol, 1.0 eq.) was dissolved in dry THF (40 mL). The reaction was cooled at -78 °C and *n*-BuLi (2.5 M in hexane, 8.0 mL, 20.0 mmol, 2.5 eq.) was added dropwise. The light-yellow solution turned brown. After 30 min, the reaction was allowed to warm up at 0 °C and stirred for 1 h. Iodine (5.28 g, 20.8 mmol, 2.6 eq.) was added at -78 °C and the reaction was stirred at rt over 16 h. After addition, the solution turned pale yellow. After completion, the reaction was poured in a saturated solution of NH_4Cl (10 mL). The organic and aqueous layers were partitioned, and the aqueous phase was extracted with Et_2O (3 × 20 mL). The combined organic phases were dried over Na_2SO_4, filtered, and concentrated under reduced pressure. After column chromatography (hexane:EtOAc, 90:10, SiO_2), *(S)*-3,3'-diiodo-2,2'-*bis*(methoxymethoxy)-1,1'-binaphthalene (2.65 g, 4.2 mmol, 53%) was obtained as a colourless solid.

^{1}H NMR (400 MHz, $CDCl_3$) δ 8.57 (s, 2H), 7.79 (d, *J* = 8.2 Hz, 2H), 7.45 – 7.41 (m, 2H), 7.32 – 7.28 (m, 2H), 7.22 – 7.19 (m, 2H), 4.84 (d, *J* = 5.7 Hz, 2H), 4.72 (d, *J* = 5.7 Hz, 2H), 2.62 (s, 6H).

^{13}C NMR (101 MHz, $CDCl_3$) δ 152.2 (2C), 140.0 (2C), 133.8 (2C), 132.2 (2C), 127.2 (2C), 126.8 (2C), 126.6 (2C), 126.3 (2C), 125.9 (2C), 99.4 (2C), 92.6 (2C), 56.5 (2C).

Analytical data are in agreement with the literature.[19]

***(S)*-3-phenyl-[1,1'-binaphthalene]-2,2'-diol**

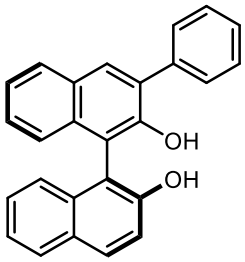

(S)-3-iodo-2,2'-*bis*(methoxymethoxy)-1,1'- binaphthalene (1.0 eq.), phenylboronic acid (2.2 eq.), K_3PO_4 (2.0 eq.), $Pd(OAc)_2$ (5 mol%) and PPh_3 (11 mol %) were dissolved in dry THF (0.1 M). The reaction was refluxed for 18 h and was then quenched with $NH_4Cl_{sat.}$ (5 mL). The aqueous phase was extracted with Et_2O (3 x 15 mL), and the combined organic phases were dried over Na_2SO_4, filtered and concentrated under reduced pressure. The crude obtained was often a viscous bright red oil. An HCl solution (4 M in 1,4-dioxane, 8.0 eq.) was then added to the crude. The reaction was stirred at 60 °C for 2 h and the resulting mixture was concentrated under reduced pressure. The substituted BINOL was purified via flash column chromatography flash chromatography (hexane:Et_2O, 90:10, SiO_2) to afford *(S)*-3-(phenyl)-[1,1'-binaphthalene]-2,2'-diol (305 mg, 0.84 mmol, 84 %) as a colourless foamy solid.

^{1}H NMR (400 MHz, $CDCl_3$) δ 8.03 (s, 1H), 7.99 (d, *J* = 8.9 Hz, 1H), 7.95 – 7.88 (m, 2H), 7.77 – 7.70 (m, 2H), 7.50 (t, *J* = 7.5 Hz, 2H), 7.46 – 7.36 (m, 4H), 7.36 – 7.30 (m, 2H), 7.26 – 7.22 (m, 1H), 7.18 – 7.13 (m, 1H), 5.30 (s, 1H), 5.12 (s, 1H).

^{13}C NMR (101 MHz, $CDCl_3$) δ 152.8, 150.4, 137.5, 133.6, 133.1, 131.6, 131.5, 130.8, 129.7, 129.6 (2C), 128.6 (4C), 128.0 (2C), 127.6 (2C), 124.5, 124.4, 124.3, 124.1, 117.9, 111.9, 111.6.

$[\alpha]^{25}_D$= –115.3 (*c* 1.0, $CHCl_3$).

Analytical data are in agreement with the literature.[17]

***(S)*-[1,1':3',2''-ternaphthalene]-2,2'-diol**

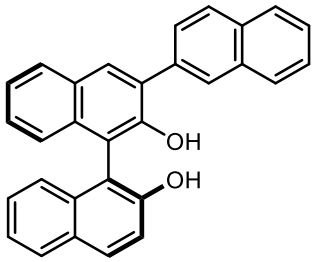

Procedure

(S)-3-bromo-2,2'-*bis*(methoxymethoxy)-1,1'- binaphthalene (453.3 mg, 1.00 mmol, 1.0 eq.), 2-naphthylboronic acid (378.4 mg, 2.20 mmol, 2.2 eq.), K_3PO_4 (424.5 mg, 2.00 mmol, 2.0 eq.), $Pd(OAc)_2$ (11.2 mg, 0.05 mmol, 5 mol%) and PPh_3 (28.8 mg, 0.11 mmol, 11 mol %) were dissolved in dry THF (24 mL). The reaction was refluxed for 18 h and was then quenched with $NH_4Cl_{sat.}$ (5 mL). The aqueous phase was extracted with Et_2O (3 x 15 mL), and the combined organic phases were dried over Na_2SO_4, filtered and concentrated under reduced pressure. The crude obtained was often a viscous bright red oil. An HCl solution (1.33 M in 1,4-dioxane, 6 mL, 8 mmol, 8.0 eq) was then added to the crude. The reaction was stirred at 60 °C for 2 h and the resulting mixture was concentrated under reduced pressure. After column chromatography (hexane:Et_2O, 90:10, SiO_2), *(S)*-3-(2-naphthyl)-[1,1'-binaphthalene]-2,2'-diol (268 mg, 0.65 mmol, 65 %) was obtained as a colourless foamy solid.

^{1}H NMR (400 MHz, $CDCl_3$): δ 8.23 (d, *J* = 1.7 Hz, 1H), 8.15 (s, 1H), 8.02 – 7.87 (m, 7H), 7.57 – 7.53 (m, 2H), 7.46 – 7.28 (m, 6H), 7.23 – 7.19 (m, 1H), 5.40 (s, 1H), 5.17 (s, 1H).

^{13}C NMR (101 MHz, $CDCl_3$): δ152.8, 150.6, 135.1, 133.6 (2C), 133.2, 132.9, 131.9, 131.5, 130.8, 129.7, 129.6, 128.7, 128.6 (2C), 128.4, 128.1, 127.8 (2C), 127.6 (2C), 126.4 (2C), 124.6, 124.5, 124.4, 124.2, 117.9, 112.0, 111.6.

IR υ_{max} (film): 3504, 3058, 1620, 1595, 1507, 1384, 1215, 1176, 1138, 820, 748 cm^{-1}.

HRMS (ESI^-): *m/z* calcd for $C_{30}H_{19}O_2$ $[M-H]^-$: 411.13910, found 411.1392

$[\alpha]^{25}_D$= -132.5 (*c* 1.0, $CHCl_3$).

***(S)*-3-bromo-[1,1'-binaphthalene]-2,2'-diol**

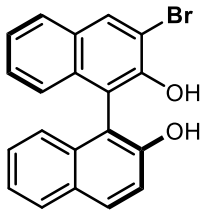

An HCl solution (1.33 M in 1,4-dioxane, 6 mL, 8 mmol, 8.0 eq) was added to *(S)*-3-bromo-2,2'-*bis*(methoxymethoxy)-1,1'-binaphthalene (453.3 mg, 1.00 mmol, 1.0 eq.). The reaction was stirred at 60 °C for 2 h and the resulting mixture was concentrated under reduced pressure. After column chromatography (hexane: Et_2O, 80:20, SiO_2), *(S)*-3-bromo-[1,1'-binaphthalene]-2,2'-diol (365.2 mg, 0.9 mmol, 90 %) was obtained as a colourless solid.

^{1}H NMR (400 MHz, $CDCl_3$): δ 8.28 (s, 1H), 7.97 (d, J = 8.9 Hz, 1H), 7.93 – 7.86 (d, J = 8.2, 1H), 7.85 – 7.80 (d, J = 8.2, 1H), 7.45 – 7.27 (m, 5H), 7.17 – 7.13 (d, J = 8.4, 1H), 7.15-7.03 (m, 1H), 5.56 (s, 1H), 4.91 (s, 1H).

^{13}C NMR (101 MHz, $CDCl_3$): δ 152.3, 149.0, 133.5, 133.3, 133.0, 131.5, 130.1, 129.5, 128.6, 128.0, 127.6 (2C), 125.2, 124.8, 124.3, 124.1, 117.9, 113.4, 112.2, 111.9.

$[\alpha]^{25}_D$= -65.3 (*c* 1.0, $CHCl_3$).

Analytical data are in agreement with the literature.[20]

***(S)*-3-iodo-[1,1'-binaphthalene]-2,2'-diol**

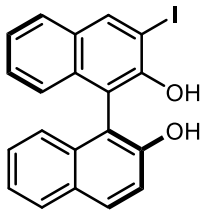

(S)-2,2'-*bis*(methoxymethoxy)-1,1'-binaphthalene (748.9 mg, 2.0 mmol, 1.0 eq.) was dissolved in dry THF (10 mL). The reaction was cooled at -78 °C and *n*-BuLi (2.5 M in hexane, 1.0 mL, 2.5 mmol, 1.25 eq.) was added dropwise. The light-yellow solution turned brown. After 30 min, the reaction was allowed to warm to 0 °C and stirred for 1 h at this temperature. Iodine (659.9 mg, 2.6 mmol, 1.3 eq.) was dissolved in dry THF (2 mL) forming a dark red solution and was added dropwise at -78 °C. The reaction was stirred while it rose to rt over 16 h. After addition of iodine the solution turned pale yellow.

After completion, the reaction was quenched with a saturated solution of NH_4Cl (10 mL). The organic and aqueous layers were partitioned, and the aqueous phase was extracted with Et_2O (3 × 20 mL). The combined organic phases were dried over Na_2SO_4, filtered, and concentrated under reduced pressure. An HCl solution (1.33 M in 1,4-dioxane, 12 mL, 16 mmol, 8.0 eq) was then added to the crude product. The reaction was stirred at 60 °C for 2 h and the resulting mixture was concentrated under reduced pressure. After column chromatography (hexane: Et_2O, 80:20, SiO_2), *(S)*-3-iodo-[1,1'-binaphthalene]-2,2'-diol (410 mg, 1.0 mmol, 50 %) was obtained as a pale yellow solid.

^{1}H NMR (400 MHz, $CDCl_3$): δ 8.54 (s, 1H), 7.98 (d, *J* = 9.0 Hz, 1H), 7.90 (dt, *J* = 8.2, 0.9 Hz, 1H), 7.84 – 7.77 (m, 1H), 7.43 – 7.34 (m, 3H), 7.32 (dddd, *J* = 8.3, 6.9, 2.2, 1.4 Hz, 2H), 7.16 – 7.06 (m, 2H), 5.50 (s, 1H), 4.93 (s, 1H).

^{13}C NMR (101 MHz, $CDCl_3$): δ152.4, 150.9, 140.6, 133.5, 133.2, 131.6, 130.8, 129.5, 128.5, 128.1, 127.6, 127.4, 124.9, 124.6, 124.2 (2C), 117.9, 111.8, 111.6, 86.3.

$[\alpha]^{25}_D$= -92.8 (*c* 1.0, $CHCl_3$).

Analytical data are in agreement with the literature.[21]

***(S)*-3-(trimethylsilyl)-[1,1'-binaphthalene]-2,2'-diol**

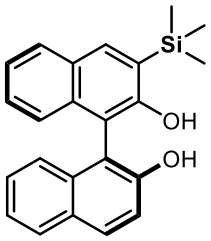

According to a modified procedure[22] *(S)*-2,2'-*bis*(methoxymethoxy)-1,1'-binaphthalene (748.9 mg, 2.0 mmol, 1.0 eq.) was dissolved in dry THF (10 mL). The reaction was cooled at -78 °C and *n*-BuLi (2.5 M in hexane, 1.0 mL, 2.5 mmol, 1.25 eq.) was added dropwise. The light-yellow solution turned brown. After 30 min, the reaction was let to warm up at 0 °C and stirred for 1 h. Chlorotrimethylsilane (330 µL, 2.6 mmol, 1.3 eq.) was added dropwise at -78 °C and the reaction was stirred while its temperature slowly rose to rt over 16 h. After addition the solution turned pale yellow.

After completion, the reaction was quenched with a sat. solution of NH_4Cl (5 mL). The organic and aqueous layers were partitioned, and the aqueous phase was extracted with Et_2O (3 × 10 mL). The combined organic phases were dried over Na_2SO_4, filtered, and concentrated under reduced pressure. An HCl solution (1.33 M in 1,4-dioxane, 12 mL, 16 mmol, 8.0 eq.) was then added to the crude. The reaction was stirred at 60 °C for 2 h and the resulting mixture was concentrated under reduced pressure. After column chromatography (hexane: Et_2O, 80:20, SiO_2), *(S)*-3-trimethylsilyl-1,1'-binaphthyl-2,2'-diol (553 mg, 1.54 mmol, 77 %) was obtained as a colourless solid.

^{1}H NMR (400 MHz, $CDCl_3$) δ 8.01 (s, 1H), 7.85 (d, *J* = 8.9 Hz, 1H), 7.82 – 7.77 (m, 2H), 7.32 – 7.12 (m, 5H), 7.07 (d, *J* = 8.7 Hz, 1H), 7.01 (d, *J* = 8.3 Hz, 1H), 5.11 (s, 1H), 4.97 (s, 1H), 0.33 (s, 9H).

^{13}C NMR (101 MHz, $CDCl_3$) δ 157.0, 152.9, 138.1, 134.3, 133.6, 131.5, 129.6, 129.4, 129.2, 128.7, 128.5, 127.8, 127.6, 124.4, 124.1, 124.1, 123.9, 117.8, 111.3, 109.3, –1.0 (3C).

$[\alpha]^{25}_D$= –104.7 (*c* 1.0, $CHCl_3$).

Analytical data are in agreement with the literature.[23]

***(S)*-3-(triisopropylsilyl)-[1,1'-binaphthalene]-2,2'-diol**

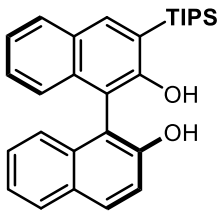

According to a modified procedure[22] *(S)*-2,2'-*bis*(methoxymethoxy)-1,1'-binaphthalene (748.9 mg, 2.0 mmol, 1.0 eq.) was dissolved in dry THF (10 mL). The reaction was cooled at -78 °C and *n*-BuLi (2.5 M in hexane, 1.0 mL, 2.5 mmol, 1.25 eq.) was added dropwise. The light-yellow solution turned brown. After 30 min, the reaction was let to warm up at 0 °C and stirred for 1 h. Triisopropylsilane chloride (560 µL, 2.62 mmol, 1.31 eq.) was added dropwise at -78 °C and the reaction was stirred while its temperature slowly rose to rt over 16 h. After addition the solution turned pale yellow.

After completion, the reaction was quenched with a sat. solution of NH_4Cl (5 mL). The organic and aqueous layers were partitioned, and the aqueous phase was extracted with Et_2O (3 × 10 mL). The combined organic phases were dried over Na_2SO_4, filtered, and concentrated under reduced pressure. An HCl solution (1.33 M in 1,4-dioxane, 12 mL, 16 mmol, 8.0 eq.) was then slowly added to the crude. The reaction was stirred at 60 °C for 2 h and the resulting mixture was concentrated under reduced pressure. After column chromatography (hexane: Et_2O, 80:20, SiO_2), *(S)*-3-triisopropylsilyl-1,1'-binaphthyl-2,2'-diol (597 mg, 1.34 mmol, 67 %) was obtained as a colourless solid.

^{1}H NMR (400 MHz, $CDCl_3$) δ 8.08 (s, 1H), 7.83 (d, *J* = 8.9 Hz, 1H), 7.80 (d, *J* = 7.4 Hz, 1H), 7.76 (d, *J* = 7.3 Hz, 1H), 7.25 – 7.20 (m, 3H), 7.20 – 7.14 (m, 2H), 7.09 – 7.04 (m, 1H), 7.03 – 6.98 (m, 1H), 5.13 (s, 1H), 4.95 (s, 1H), 1.52 (hept, *J* = 7.5 Hz, 3H), 1.08 (dd, *J* = 7.5, 2.3 Hz, 18H).

^{13}C NMR (101 MHz, $CDCl_3$) δ 157.2, 152.9, 140.1, 134.1, 133.6, 131.4, 129.6, 129.3, 128.7, 128.5, 127.7, 127.5, 124.8, 124.2, 124.1, 123.9, 123.8, 117.8, 111.3, 109.4, 19.2 (6C), 11.6 (3C).

HRMS (ESI^-): *m/z* calcd for $C_{29}H_{33}O_2Si$ $[M-H]^-$: 441.2255, found 441.2253.

$[\alpha]^{25}_D$= –80.51 (*c* 1.0, $CHCl_3$).

***(S)*-3-(*p*-tolyl)-[1,1'-binaphthalene]-2,2'-diol**

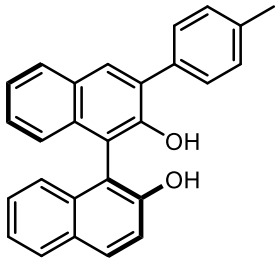

(S)-3-bromo-2,2'-*bis*(methoxymethoxy)-1,1'-binaphthalene (453.3 mg, 1.00 mmol, 1.0 eq.), *p*-tolylboronic acid (299.1 mg, 2.20 mmol, 2.2 eq.), K_3PO_4 (424.5 mg, 2.00 mmol, 2.0 eq.), $Pd(OAc)_2$ (11.2 mg, 0.05 mmol, 5 mol%) and PPh_3 (28.8 mg, 0.11 mmol, 11 mol %) were dissolved in dry THF (24 mL). The reaction was refluxed for 18 h and was then quenched with $NH_4Cl_{sat.}$ (5 mL). The aqueous phase was extracted with Et_2O (3 x 15 mL), and the combined organic phases were dried over Na_2SO_4, filtered and concentrated under reduced pressure. The crude obtained was often a viscous bright red oil. An HCl solution (1.33 M in 1,4-dioxane, 6 mL, 8 mmol, 8.0 eq) was then added to the crude. The reaction was stirred at 60 °C for 2 h and the resulting mixture was concentrated under reduced pressure. After column chromatography (hexane:Et_2O, 90:10, SiO_2), *(S)*-3-(*p*-tolyl)-[1,1'-binaphthalene]-2,2'-diol (295 mg, 0.78 mmol, 78 %) was obtained as a colourless foamy solid.

^{1}H NMR (400 MHz, $CDCl_3$): δ 7.87 (s, 1H), 7.83 – 7.79 (m, 1H), 7.79 – 7.72 (m, 2H), 7.54 – 7.46 (m, 2H), 7.29 – 7.06 (m, 8H), 7.02 (dd, *J* = 8.3, 1.1 Hz, 1H), 5.19 (s, 1H), 4.97 (s, 1H), 2.30 (s, 3H).

^{13}C NMR (101 MHz, $CDCl_3$): δ 152.7, 150.5, 137.8, 134.5, 133.6, 133.0, 131.3 (2C), 130.8, 129.6 (4C), 129.4 (2C), 128.5 (2C), 127.5, 127.4, 124.5, 124.4, 124.3, 124.1, 117.9, 111.8 (2C), 21.4.

IR υ_{max} (film): 3505 (br), 3056, 1620, 1596, 1438, 1382, 1263, 1214, 1177 cm^{-1}.

HRMS (ESI^-): *m/z* calcd for $C_{27}H_{19}O_2$ $[M-H]^-$: 375.1391, found 375.1388.

$[\alpha]^{25}_D$= -114.3 (*c* 1.0, $CHCl_3$).

***(S)*-3-(4-(trimethylsilyl)phenyl)-[1,1'-binaphthalene]-2,2'-diol**

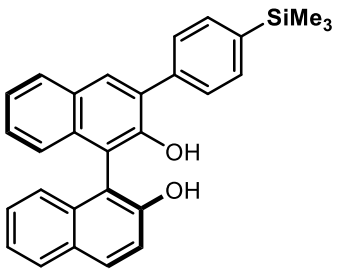

(S)-3-bromo-2,2'-*bis*(methoxymethoxy)-1,1'-binaphthalene (453.3 mg, 1.00 mmol, 1.0 eq.), 4-(trimethylsilyl) phenylboronic acid (427.0 mg, 2.20 mmol, 2.2 eq.), K_3PO_4 (424.5 mg, 2.00 mmol, 2.0 eq.), $Pd(OAc)_2$ (11.2 mg, 0.05 mmol, 5 mol%) and PPh_3 (28.8 mg, 0.11 mmol, 11 mol %) were dissolved in dry THF (24 mL). The reaction was refluxed for 18 h and was then quenched with $NH_4Cl_{sat.}$ (5 mL). The aqueous phase was extracted with Et_2O (3 x 15 mL), and the combined organic phases were dried over Na_2SO_4, filtered and concentrated under reduced pressure. The crude obtained was often a viscous bright red oil. An HCl solution (1.33 M in 1,4-dioxane, 6 mL, 8 mmol, 8.0 eq) was then added to the crude. The reaction was stirred at 60 °C for 2 h and the resulting mixture was concentrated under reduced pressure. After column chromatography (hexane:Et_2O, 90:10, SiO_2), *(S)*-3-(4-(trimethylsilyl)phenyl)-[1,1'-binaphthalene]-2,2'-diol (347 mg, 0.8 mmol, 80 %) was obtained as a colourless foamy solid.

^{1}H NMR (400 MHz, $CDCl_3$): δ 8.03 (s, 1H), 7.99 (dd, *J* = 9.1, 0.7 Hz, 1H), 7.94 – 7.88 (m, 2H), 7.75 – 7.71 (m, 2H), 7.69 – 7.64 (m, 2H), 7.43 – 7.36 (m, 3H), 7.34 – 7.28 (m, 2H), 7.25 – 7.22 (m, 1H), 7.16 – 7.04 (m, 1H), 5.30 (s, 1H), 5.13 (s, 1H), 0.32 (s, 9H).

^{13}C NMR (101 MHz, $CDCl_3$): δ 153.8, 151.4, 141.1, 138.8, 134.6 (2C), 134.5, 134.0, 132.6, 132.5, 131.7, 130.6, 130.5, 129.9(2C), 129.6, 129.5, 128.5(2C), 125.5, 125.4, 125.3, 125.1, 118.8, 112.8, 112.5, 0.0 (3C).

IR υ_{max} (film): 3517, 2954, 1620, 1597, 1437, 1385, 1248 cm^{-1}.

HRMS (ESI^-): *m/z* calcd for $C_{29}H_{25}O_2$ $[M-H]^-$: 433.1629, found 433.1623.

$[\alpha]^{25}_D$= -80.6 (*c* 1.0, $CHCl_3$).

***(S)*-3-(3,5-dimethylphenyl)-[1,1'-binaphthalene]-2,2'-diol**

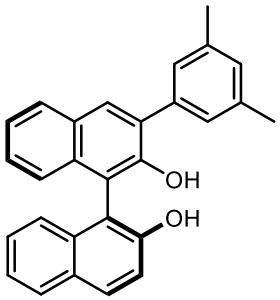

(S)-3-bromo-2,2'-*bis*(methoxymethoxy)-1,1'-binaphthalene (453.3 mg, 1.00 mmol, 1.0 eq.), 3,5-dimethylphenylboronic acid (330.0 mg, 2.2 mmol, 2.2 eq.), K_3PO_4 (424.5 mg, 2.0 mmol, 2.0 eq.), $Pd(OAc)_2$ (11.2 mg, 0.05 mmol, 5 mol%) and PPh_3 (28.8 mg, 0.11 mmol, 11 mol %) were dissolved in dry THF (24 mL). The reaction was refluxed for 18 h and was then quenched with $NH_4Cl_{sat.}$ (5 mL). The aqueous phase was extracted with Et_2O (3 x 15 mL), and the combined organic phases were dried over Na_2SO_4, filtered, and concentrated under reduced pressure. The crude obtained was often a viscous bright red oil. An HCl solution (1.33 M in 1,4-dioxane, 6 mL, 8 mmol, 8.0 eq) was then added to the crude. The reaction was stirred at 60 °C for 2 h and the resulting mixture was concentrated under reduced pressure. After column chromatography (hexane:Et_2O, 90:10, SiO_2), *(S)*-3-(3,5-dimethylphenyl)-1,1'-bi-2-naphthol (289 mg, 0.74 mmol, 74 %) was obtained as a colourless foamy solid.

^{1}H NMR (400 MHz, $CDCl_3$): δ 7.90 (s, 1H), 7.86 (d, *J* = 8.9 Hz, 1H), 7.87 – 7.73 (m, 2H), 7.31 – 7.18 (m, 7H), 7.16 – 7.11 (m, 1H), 7.07 – 6.98 (m, 1H), 6.98 (dt, *J* = 1.7, 0.9 Hz, 1H), 5.27 (s, 1H), 5.00 (s, 1H), 2.31 (s, 6H).

^{13}C NMR (101 MHz, $CDCl_3$): δ 152.5, 150.3, 138.3 (2C), 137.1, 133.5, 133.0, 131.3, 131.2, 130.9, 129.7, 129.5 (2C), 128.4 (2C), 127.3 (4C), 124.4 (2C), 124.3, 123.9, 117.7, 112.0, 111.8, 21.5 (2C).

$[\alpha]^{25}_D$= -110.4 (*c* 1.0, $CHCl_3$).

Analytical data are in agreement with the literature.[18]

***(S)*-3-(3,5-di-*tert*-butylphenyl)-[1,1'-binaphthalene]-2,2'-diol**

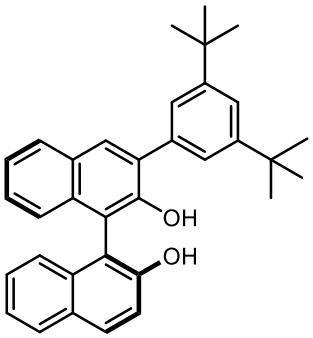

Modifying an existing procedure,[24] to a solution of activated magnesium turnings (164.1 mg, 6.75 mmol, 4.5 eq.) in dry THF (10 mL) at rt under Ar atmosphere 1-bromo-3,5-di-*tert*-butylbenzene (1.21 g, 4.5 mmol, 3.0 eq.) was added followed by a catalytic amount of iodine. The Grignard reagent mixture was heated up to 65 °C, refluxed for 1 h and then cooled down to 30 °C. In a separate flask a suspension of *(S)*-3-iodo-2,2'-*bis*(methoxymethoxy)-1,1'-binaphthalene (678.0, 1.5 mmol, 1.00 eq.) and $Ni(PPh_3)_2Cl_2$ (98.1 mg, 0.15 mmol, 0.1 eq.) in dry THF (5 mL) was stirred at rt under an argon atmosphere. The Grignard reagent (formed *in situ*) was added dropwise to the reaction mixture at rt over 15 min. The reaction was refluxed for 16 h and then quenched by pouring it on to 1 M $HCl_{(aq)}$ (20 mL). The organic layer was separated, and aqueous layer extracted with Et_2O (2 × 10 mL). The combined organic layers were dried over Na_2SO_4 and concentrated under reduced pressure to obtain a white/yellow solid. An HCl solution (1.33 M in 1,4-dioxane, 9 mL, 12 mmol, 8.0 eq.) was then added to the crude. The reaction was stirred at 60 °C for 2 h and the resulting mixture was concentrated under reduced pressure. After column chromatography (hexane: Et_2O, 90:10, SiO_2), *(S)*-3-(3,5-di-*tert*-butylphenyl)-1,1'-bi-2-naphthol (229 mg, 0.48 mmol, 32 %) was obtained as a colourless solid.

^{1}H NMR (500 MHz, $CDCl_3$) δ 8.08 (s, 1H), 8.04 – 7.97 (m, 2H), 7.95 – 7.90 (m, 1H), 7.59 (d, *J* = 1.9 Hz, 2H), 7.56 (t, *J* = 1.8 Hz, 1H), 7.48 – 7.26 (m, 6H), 7.24 – 7.20 (m, 1H), 5.49 (s, 1H), 5.19 (s, 1H), 1.44 (s, 18H).

^{13}C NMR (126 MHz, $CDCl_3$) δ 155.0, 152.7, 152.5, 151.3, 150.5, 136.4, 133.6, 133.1, 131.8, 131.4, 131.2, 129.6, 129.6, 128.5, 127.4, 127.4, 124.7, 124.4, 124.0 (2C), 122.2, 117.8, 115.1, 112.4, 111.9, 109.8, 35.2 (2C), 31.7 (6C).

IR υ_{max} (film): 3524, 2965, 1596, 1216 cm^{-1}.

HRMS (ESI$^+$): *m/z* calcd for $C_{34}H_{35}O_2$ [M+H]$^+$: 475.2632, found 475.2632.

[α]$^{25}_D$= –87.7 (*c* 1.0, $CHCl_3$).

***(S)*-3-mesityl-[1,1'-binaphthalene]-2,2'-diol**

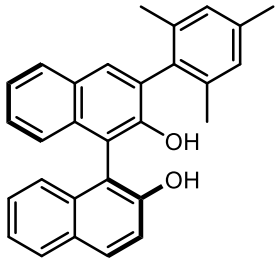

Modifying an existing procedure,[24] to a solution of activated magnesium turnings (164.1 mg, 6.75 mmol, 4.5 eq.) in dry THF (10 mL), at rt under an argon atmosphere, 2-bromomesitylene (688 µL, 4.5 mmol, 3.0 eq.) was added followed by a catalytic amount of iodine. The Grignard reagent mixture was heated up to 65 °C, refluxed for 1 h and then cooled down to 30 °C.

In a separate flask a suspension of *(S)*-3-iodo-2,2'-*bis*(methoxymethoxy)-1,1'-binaphthalene (678.0, 1.5 mmol, 1.00 eq.) and $Ni(PPh_3)_2Cl_2$ (98.1 mg, 0.15 mmol, 0.1 eq.) in dry THF (5 mL) was stirred at rt under an argon atmosphere. The Grignard reagent (formed *in situ*) was added dropwise to the reaction mixture at rt over 15 min. The reaction was refluxed for 16 h and then quenched by pouring it over 1 M $HCl_{(aq)}$ (20 mL). The organic layer was separated, and aqueous layer extracted with Et_2O (2 × 10 mL). The combined organic layers were dried over Na_2SO_4 and concentrated under reduced pressure to obtain a white/yellow solid. An HCl solution (1.33 M in 1,4-dioxane, 9 mL, 12 mmol, 8.0 eq.) was then added to the crude. The reaction was stirred at 60 °C for 2 h and the resulting mixture was concentrated under reduced pressure. After column chromatography (hexane: Et_2O, 90:10, SiO_2), *(S)*-3-mesityl-2,2'-dihydroxy-1,1'-binaphthyl (307 mg, 0.76 mmol, 51 %) was obtained as a colourless solid.

^{1}H NMR (400 MHz, $CDCl_3$) δ 7.85 (d, *J* = 8.9 Hz, 1H), 7.78 – 7.74 (m, 2H), 7.68 (s, 1H), 7.32 – 7.17 (m, 5H), 7.15 – 7.09 (m, 2H), 6.92 (s, 2H), 4.96 (s, 1H), 4.89 (s, 1H), 2.24 (s, 3H), 2.03 (s, 3H), 2.02 (s, 3H).

^{13}C NMR (101 MHz, $CDCl_3$) δ 152.3, 150.7, 138.0, 137.3, 137.1, 133.5, 133.4, 132.7, 131.4, 131.0, 129.8, 129.7, 129.6, 128.7 (2C), 128.6, 128.4, 127.3 (2C), 124.5, 124.4, 124.3, 123.9, 117.8, 112.7, 111.6, 21.3, 20.7, 20.6.

$[\alpha]^{25}_D$= –116.6 (*c* 1.0, $CHCl_3$).

Analytical data are in agreement with the literature.[25]

(S)-3-(2,4,6-triisopropylphenyl)-[1,1'-binaphthalene]-2,2'-diol

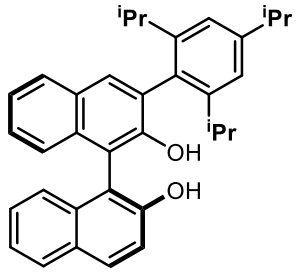

Modifying an existing procedure,[24] to a solution of activated magnesium turnings (164.1 mg, 6.75 mmol, 4.5 eq.) in dry THF (10 mL), at rt under an argon atmosphere, 1-bromo-2,4,6-tri-isopropylbenzene (1.14 mL, 4.5 mmol, 3.0 eq.) was added followed by a catalytic amount of iodine. The Grignard reagent mixture was heated up to 65 °C, refluxed for 1 h and then cooled down to 30 °C.

In a separate flask of *(S)*-3-iodo-2,2'-*bis*(methoxymethoxy)-1,1'- binaphthalene (678.0 mg, 1.5 mmol, 1.00 eq.) and $Ni(PPh_3)_2Cl_2$ (98.1 mg, 0.15 mmol, 0.1 eq.) in dry THF (5 mL) was stirred at rt under an argon atmosphere. The Grignard reagent (formed *in situ*) was added dropwise to the reaction mixture at rt over 15 min. The reaction was refluxed for 16 h and then quenched by pouring it on to 1 M $HCl_{(aq)}$ (20 mL). The organic layer was separated, and aqueous layer extracted with Et_2O (2 × 10 mL). The combined organic layers were dried over Na_2SO_4 and concentrated under reduced pressure to obtain a white/yellow solid. An HCl solution (1.33 M in 1,4-dioxane, 9 mL, 12 mmol, 8.0 eq.) was then added to the crude. The reaction was stirred at 60 °C for 2 h and the resulting mixture was concentrated under reduced pressure. After column chromatography (hexane: Et_2O, 90:10, SiO_2), *(S)*-3-(2,4,6-triisopropylphenyl)-[1,1'-binaphthalene]-2,2'-diol (291 mg, 0.6 mmol, 40 %) was obtained as a colourless solid.

^{1}H NMR (400 MHz, $CDCl_3$) δ 7.83 (d, *J* = 8.9 Hz, 1H), 7.79 – 7.75 (m, 2H), 7.70 (s, 1H), 7.34 – 7.26 (m, 2H), 7.22 (m, 2H), 7.19 – 7.08 (m, 3H), 7.04 (s, 2H), 4.97 (s, 1H), 4.86 (s, 1H), 2.91 – 2.81 (m, 1H), 2.69 – 2.56 (m, 2H), 1.21 (d, *J* = 6.9 Hz, 6H), 1.07 (d, *J* = 6.8 Hz, 6H), 1.01 (d, *J* = 6.9 Hz, 6H).

^{13}C NMR (101 MHz, $CDCl_3$) δ 152.2, 151.4, 149.6, 148.0, 147.8, 133.5, 133.4, 131.6, 130.9, 130.0, 129.5 (2C), 129.3, 128.5 (2C), 127.3, 127.1, 124.6, 124.5, 124.3, 123.8, 121.5, 121.4, 117.8, 113.0, 111.4, 34.5, 31.2, 31.1, 24.6, 24.5, 24.2 (2C), 24.1, 24.0.

IR υ_{max} (film): 3522, 2961, 1383, 1216 cm^{-1}.

$[\alpha]^{25}_{D}$= –118.3 (*c* 1.0, $CHCl_3$).

5.4.5 Organometallic nucelophiles:

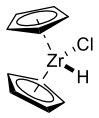

Cp_2ZrClH

Schwartz reagent was prepared according to a literature procedure from Cp_2ZrCl_2, which gives more reliable and consistent results than commercially available material.[26]

The lithium aluminum hydride ($LiAlH_4$) reduction of zirconocene dichloride (Cp_2ZrCl_2) leads to over-reduction and give zirconocene dihydride (Cp_2ZrH_2). Washing Cp_2ZrH_2 with dichloromethane (CH_2Cl_2) yields the Schwartz reagent.

Zirconocene dichloride (10.0 g, 0.0343 mol) was added to a flame-dry 100 mL Schlenk flask wrapped with aluminium foil under argon. Dry THF (65 mL) was added and the suspension was stirred at 35 °C for 30 minutes. $LiAlH_4$ in Et_2O (1 M, 9.4 mmol) was added dropwise to the mixture over about 30 minutes. The resulting suspension was stirred for 1.5 hours. The red mixture was Schlenk-filtered under argon and washed with dry tetrahydrofuran (4 × 10 mL), dichloromethane (2 × 20 mL), and diethyl ether (4 × 10 mL). The precipitate was dried under high vacuum to give an off-white/light pink powder (7.38 g, 83%). The solid was stored under argon in a small flame-dried aluminium foiled two-neck flask.

Material obtained this way has an average purity better than 95% (zirconocene dihydride being the impurity). The Schwartz reagent can be kept and remain pure for months under these storage conditions if flushed with vacuum/Ar (3 times) after each use.

$Cp_2ZrClCH_3$

Following a reported procedure,[27] a 250 mL Schlenk flask was loaded with zirconocene dichloride (10.0 g, 34.2 mmol, 1.0 eq.), CH_2Cl_2 (80 mL), and then aniline (3.4 mL, 37.2 mmol, 1.1 eq.). After stirring for 5 minutes, distilled water (0.43 mL, 23.8 mmol, 0.7 eq.) was added, immediately forming a colourless solid of aniline hydrochloride salt. The mixture was stirred for approximately 3 hours at room temperature, after which the flask was placed in a refrigerator (+3 °C to +7 °C) for 15 hours. The resulting mixture was subjected to cold filtration under argon, yielding a clear yellowish filtrate. The filtered solid was rinsed once with cold (0 °C) CH_2Cl_2 (10 mL), and the CH_2Cl_2 filtrate was concentrated, resulting in a yellowish solid. Dry pentane (10 mL) was added, and the mixture was stirred for 30 minutes. The suspension was filtered, the colourless solid was washed once with dry pentane (10 mL), and it was then dried under high vacuum for 1 hour, producing the zirconium bridged oxide $(Cp_2ZrCl)_2(\mu - O)$ (7.66 g, 14.5 mmol, 85%) as a light pink solid.

The above solid was transferred to a 100 mL Schlenk flask and dry CH_2Cl_2 (70 mL) was added. The flask was then carefully charged with trimethylaluminium solution (2 M in hexane, 18.1 mL, 36.1 mmol, 2.5 eq.) at room temperature. Special care needs to be taken when handling $AlMe_3$ due to it being highly pyrophoric. Within seconds, the mixture turned into a homogeneous yellowish solution. After 1.5 h, dry Et_2O (30 mL) was added, and stirring was stopped after 2 minutes. The flask was then transferred to a rotary evaporator, where the solution was slowly concentrated (30 °C, 450 mbar) until the first yellow solids started to precipitate (leaving about 3 – 5 mL of solution in the flask). The flask was then removed, stirring was resumed, and dry pentane (30 mL) was added. After 10 minutes of stirring, the colourless solid formed was filtered under argon and washed twice with dry pentane (20 mL each). Note: the reactive pentane solutions containing excess $AlMe_3$ were carefully quenched at 0 °C under N_2 with isopropanol, ethanol, water, and finally 1 M HCl(aq). The solid was then dried under high vacuum for 3 hours, yielding $Cp_2ZrMeCl$ 1 (5.47 g, 20.0 mmol, 69%) as a white to off-white solid. Product stored under an argon atmosphere and flushed with vacuum/Ar (3 times) after each use.

5.5 SFC traces

SFC Traces for compound **4a**

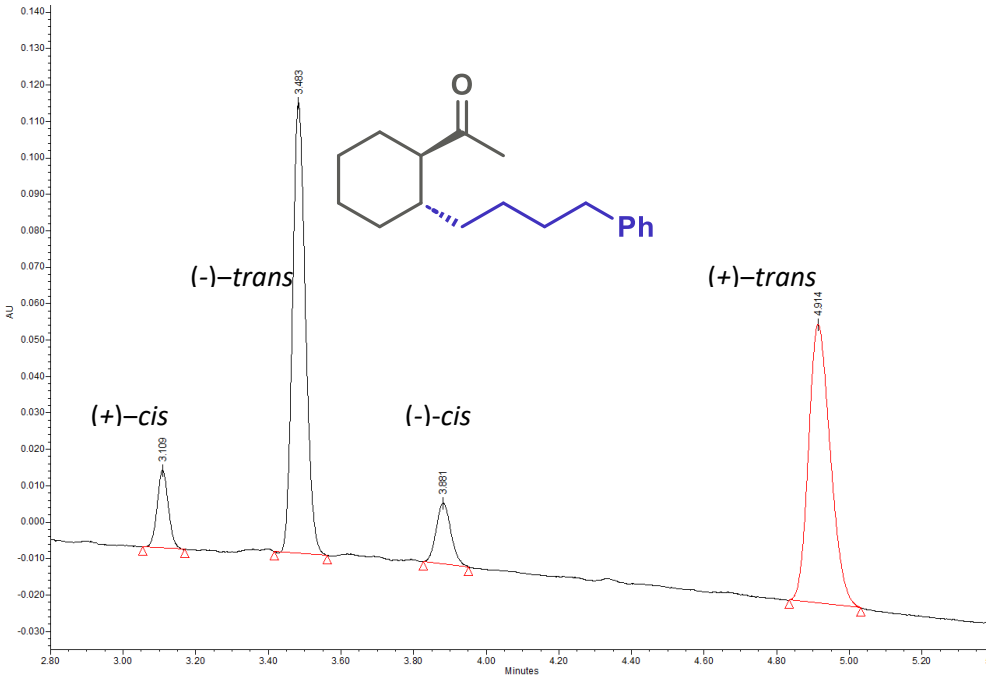

	Name	Retention Time (min)	PDA/FLR Match1 Lib. Name	Area (µV*sec)	% Area
1		3.483		306221	48.98
2		4.914		319028	51.02

	Name	Retention Time (min)	PDA/FLR Match1 Lib. Name	Area (µV*sec)	% Area
1		3.109		45123	49.11
2		3.881		46764	50.89

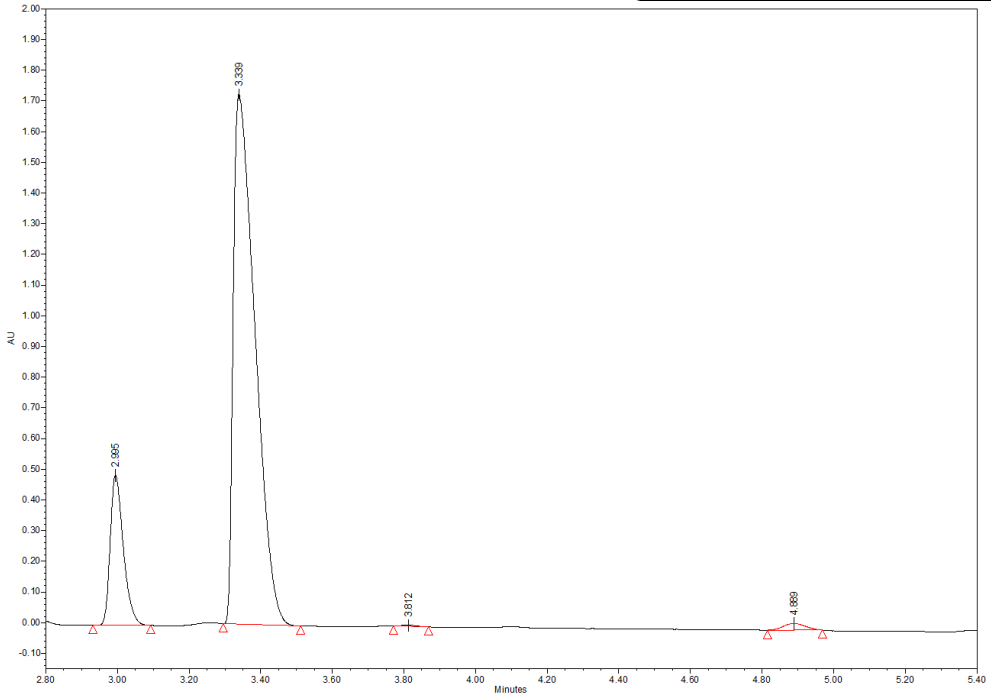

	Name	Retention Time (min)	PDA/FLR Match1 Lib. Name	Area (µV*sec)	% Area
1		3.339		7258780	98.66
2		4.889		98926	1.34

	Name	Retention Time (min)	PDA/FLR Match1 Lib. Name	Area (µV*sec)	% Area
1		2.995		1251745	98.93
2		3.812		13499	1.07

Figure 5.1: SFC traces for compound (±)-**4a** (top) and enantioenriched (-)-**4a** (bottom).

SFC Traces for compound **4b**

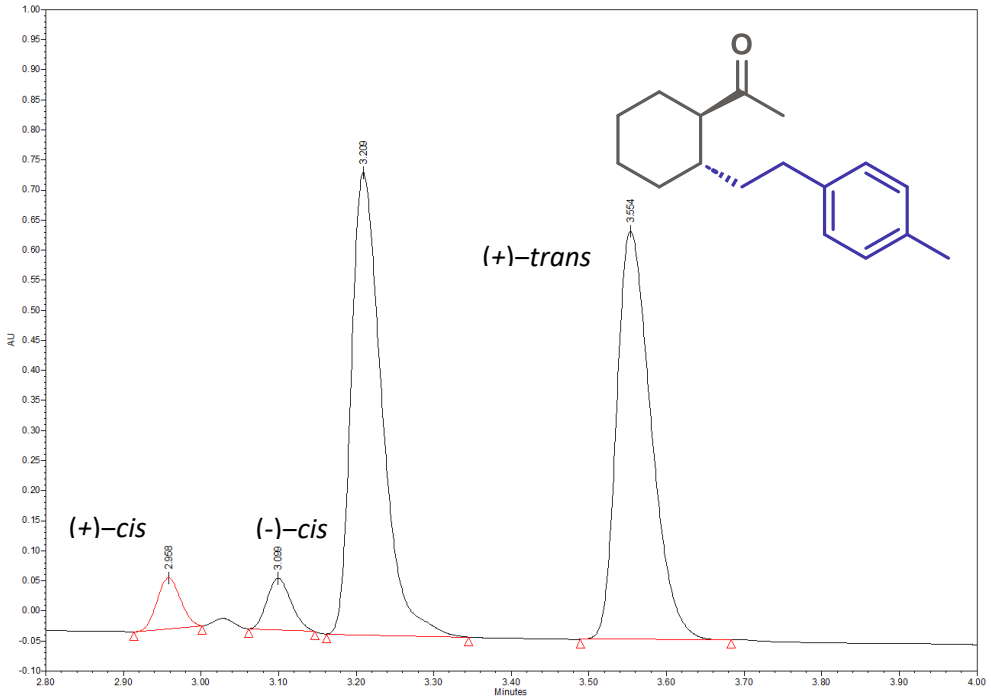

	Name	Retention Time (min)	Purity1 Angle	Purity1 Threshold	PDA/FLR Match1 Spect. Name	PDA/FLR Match1 Angle	PDA/FLR Match1 Threshold	PDA/FLR Match1 Lib. Name	Area (µV*sec)	% Area
1		3.209							2103516	50.19
2		3.554							2087332	49.81

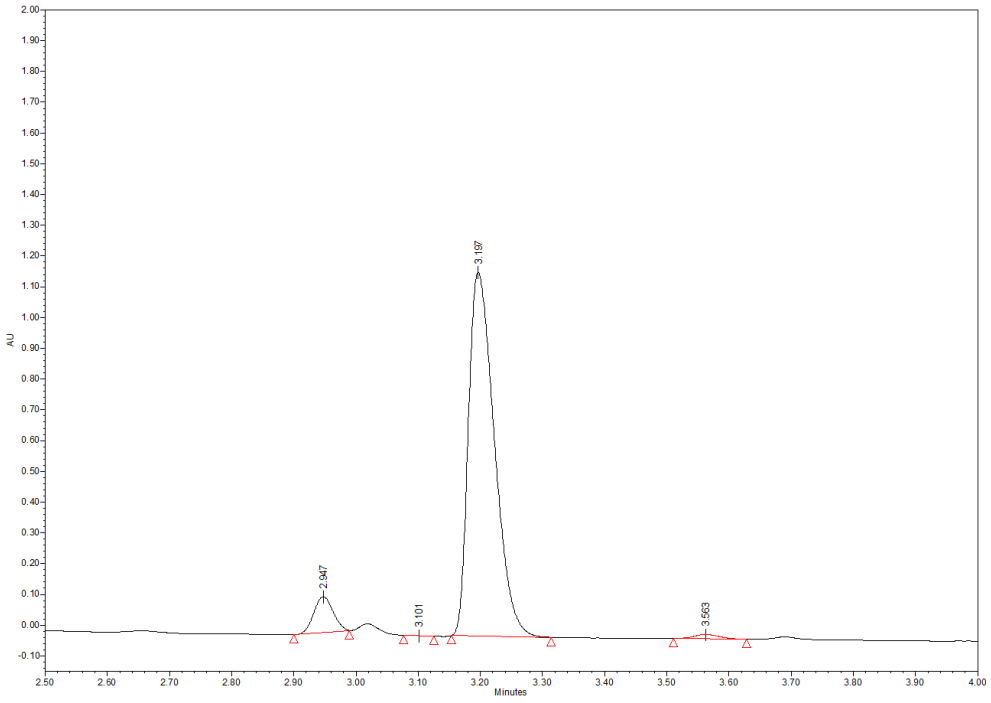

	Name	Retention Time (min)	Purity1 Angle	Purity1 Threshold	PDA/FLR Match1 Spect. Name	PDA/FLR Match1 Angle	PDA/FLR Match1 Threshold	PDA/FLR Match1 Lib. Name	Area (µV*sec)	% Area
1		3.197							3434047	98.73
2		3.563							44123	1.27

Figure 5.2: SFC traces for compound (±)-**4b** (top) and enantioenriched (-)-**4b** (bottom).

SFC Traces for compound **4c**

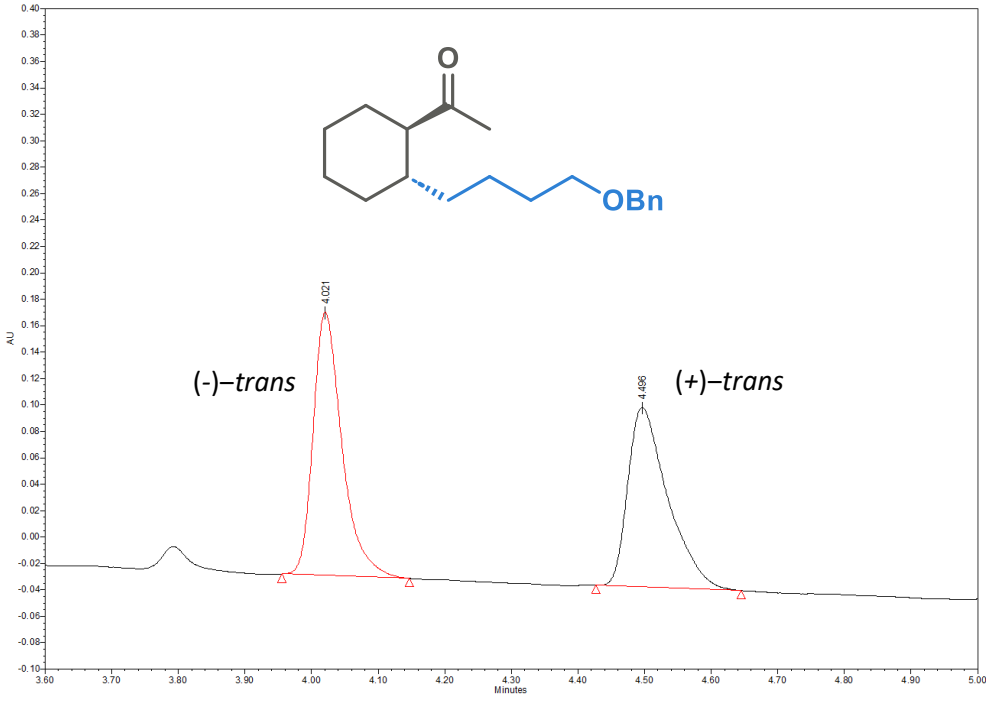

	Name	Retention Time (min)	Purity1 Angle	Purity1 Threshold	PDA/FLR Match1 Spect. Name	PDA/FLR Match1 Angle	PDA/FLR Match1 Threshold	PDA/FLR Match1 Lib. Name	Area (µV*sec)	% Area
1		4.021							600911	51.44
2		4.496							567183	48.56

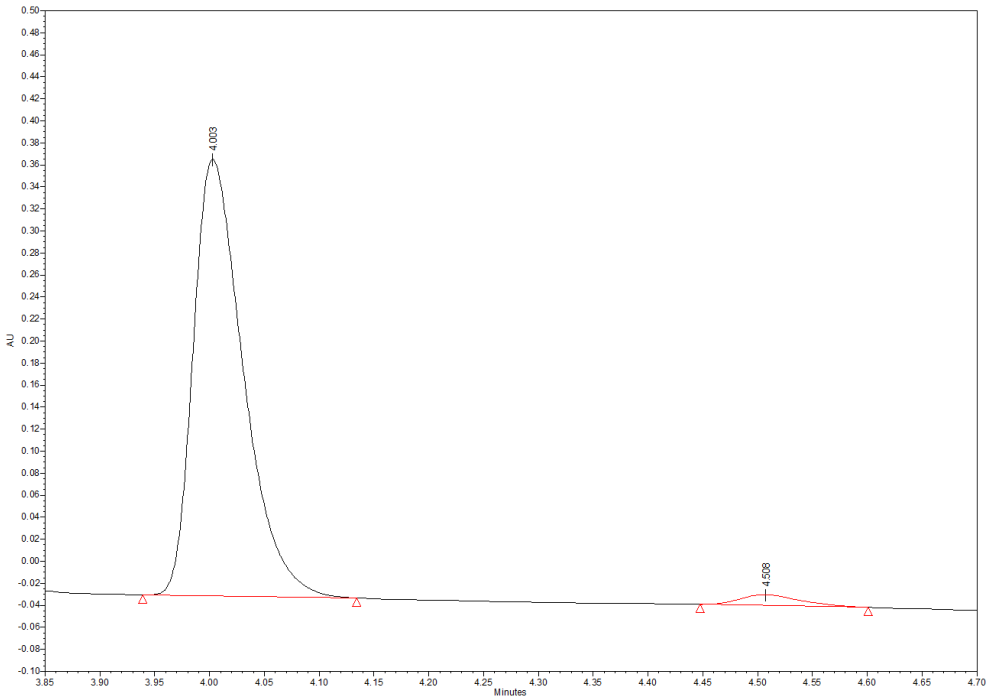

	Name	Retention Time (min)	Purity1 Angle	Purity1 Threshold	PDA/FLR Match1 Spect. Name	PDA/FLR Match1 Angle	PDA/FLR Match1 Threshold	PDA/FLR Match1 Lib. Name	Area (µV*sec)	% Area
1		4.003							1259471	97.11
2		4.508							37469	2.89

Figure 5.3: SFC traces for compound (±)-**4c** (top) and enantioenriched (-)-**4c** (bottom).

SFC Traces for compound **4d**

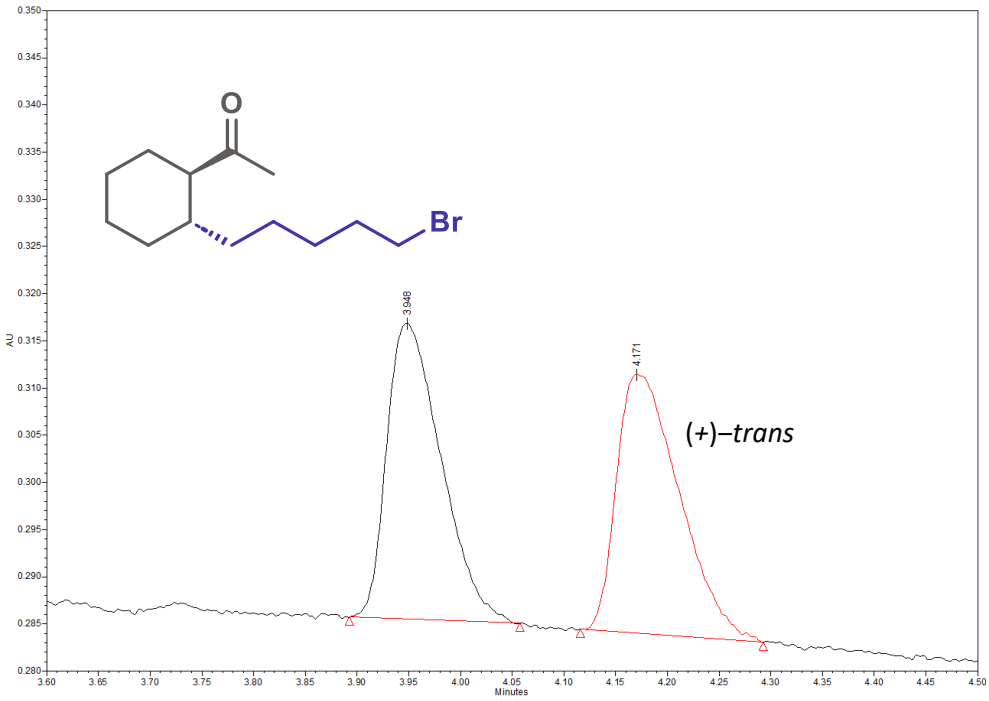

	Name	Retention Time (min)	Purity1 Angle	Purity1 Threshold	PDA/FLR Match1 Spect. Name	PDA/FLR Match1 Angle	PDA/FLR Match1 Threshold	PDA/FLR Match1 Lib. Name	Area (µV*sec)	% Area
1		3.948							114685	49.73
2		4.171							115930	50.27

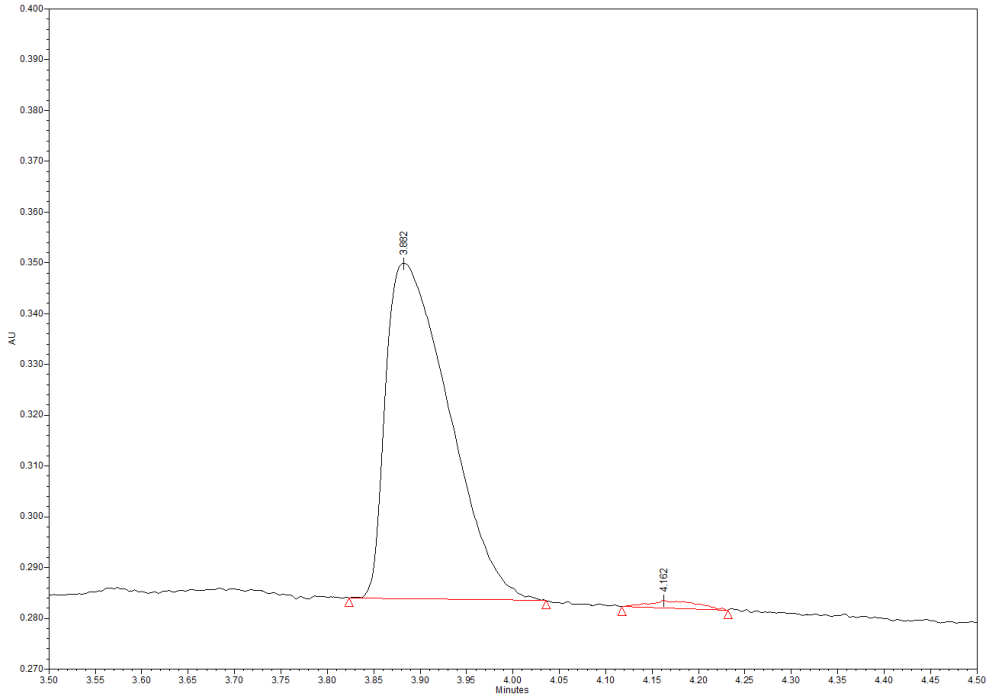

	Name	Retention Time (min)	Purity1 Angle	Purity1 Threshold	PDA/FLR Match1 Spect. Name	PDA/FLR Match1 Angle	PDA/FLR Match1 Threshold	PDA/FLR Match1 Lib. Name	Area (µV*sec)	% Area
1		3.882							313061	98.26
2		4.162							5539	1.74

Figure 5.4: SFC traces for compound (±)-**4d** (top) and enantioenriched (-)-**4d** (bottom).

SFC Traces for compound **4e**

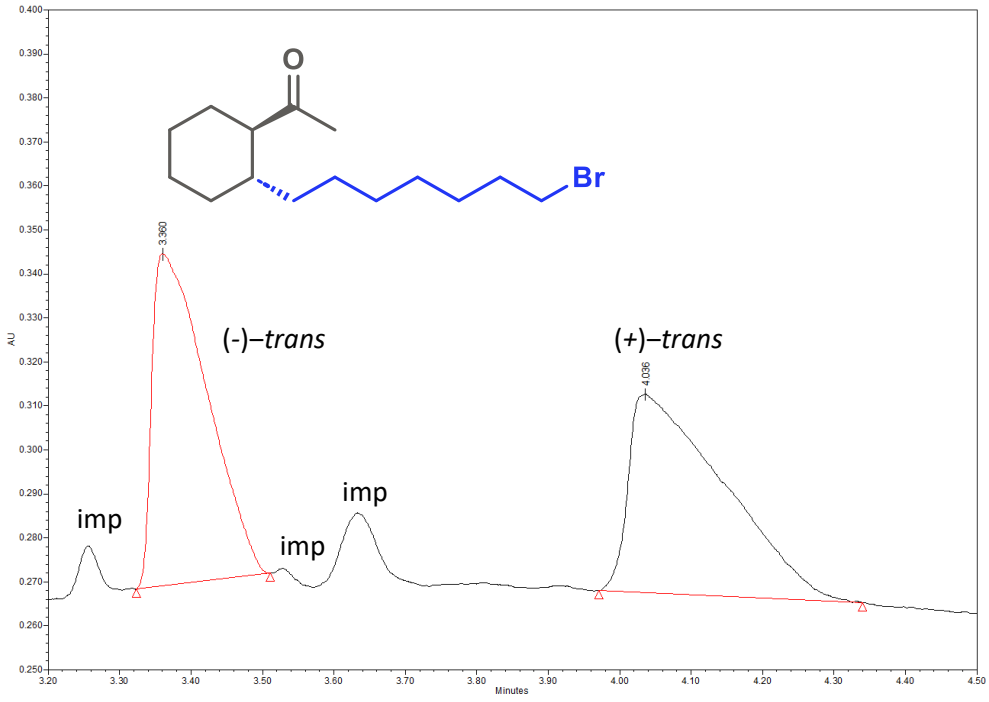

	Name	Retention Time (min)	Purity1 Angle	Purity1 Threshold	PDA/FLR Match1 Spect. Name	PDA/FLR Match1 Angle	PDA/FLR Match1 Threshold	PDA/FLR Match1 Lib. Name	Area (µV*sec)	% Area
1		3.360							401605	49.02
2		4.036							417698	50.98

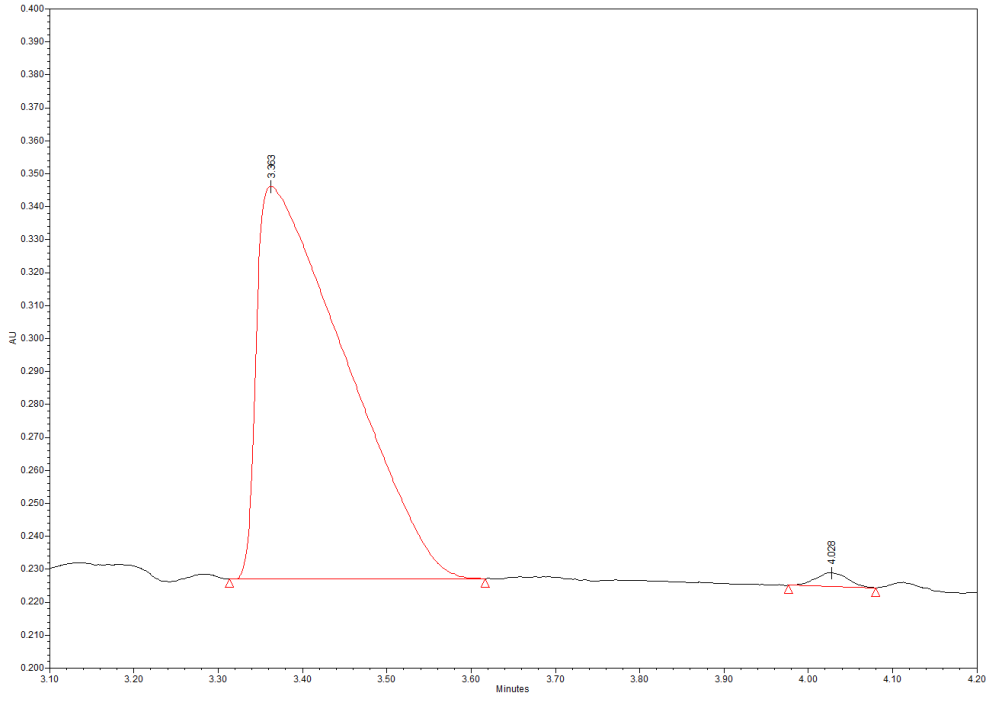

	Name	Retention Time (min)	Purity1 Angle	Purity1 Threshold	PDA/FLR Match1 Spect. Name	PDA/FLR Match1 Angle	PDA/FLR Match1 Threshold	PDA/FLR Match1 Lib. Name	Area (µV*sec)	% Area
1		3.363							866564	98.75
2		4.028							10932	1.25

Figure 5.5: SFC traces for compound (±)-**4e** (top) and enantioenriched (-)-**4e** (bottom).

SFC Traces for compound **4f**

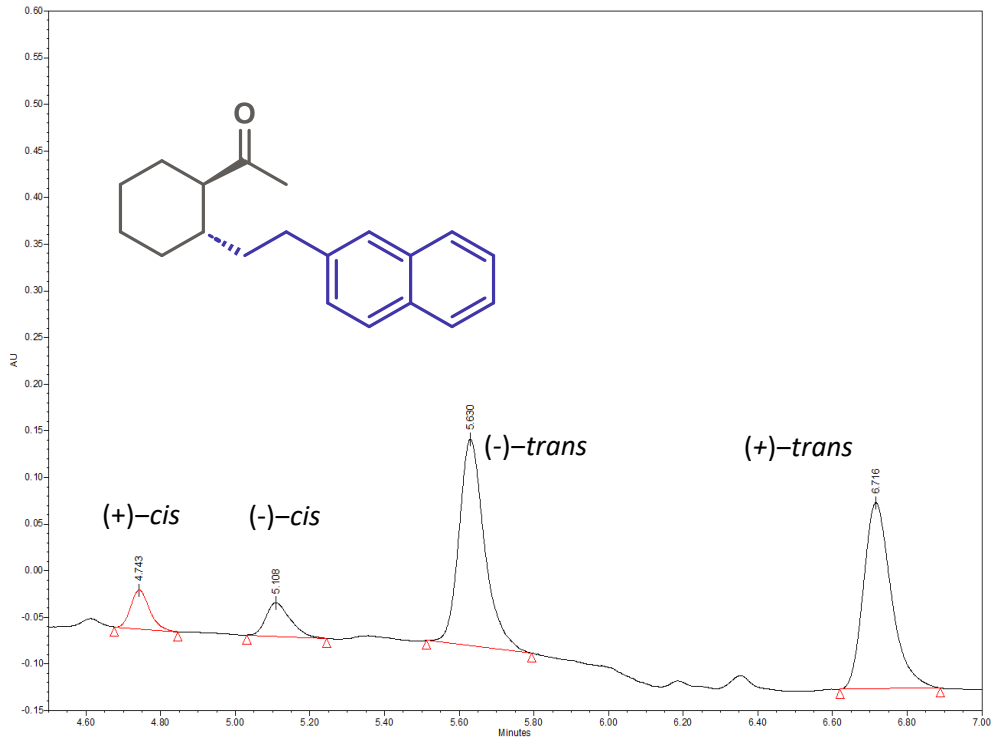

	Name	Retention Time (min)	PDA/FLR Match1 Lib. Name	Area (µV*sec)	% Area
1		5.630		1055273	50.55
2		6.716		1032427	49.45

	Name	Retention Time (min)	PDA/FLR Match1 Lib. Name	Area (µV*sec)	% Area
1		4.743		144771	47.18
2		5.108		162064	52.82

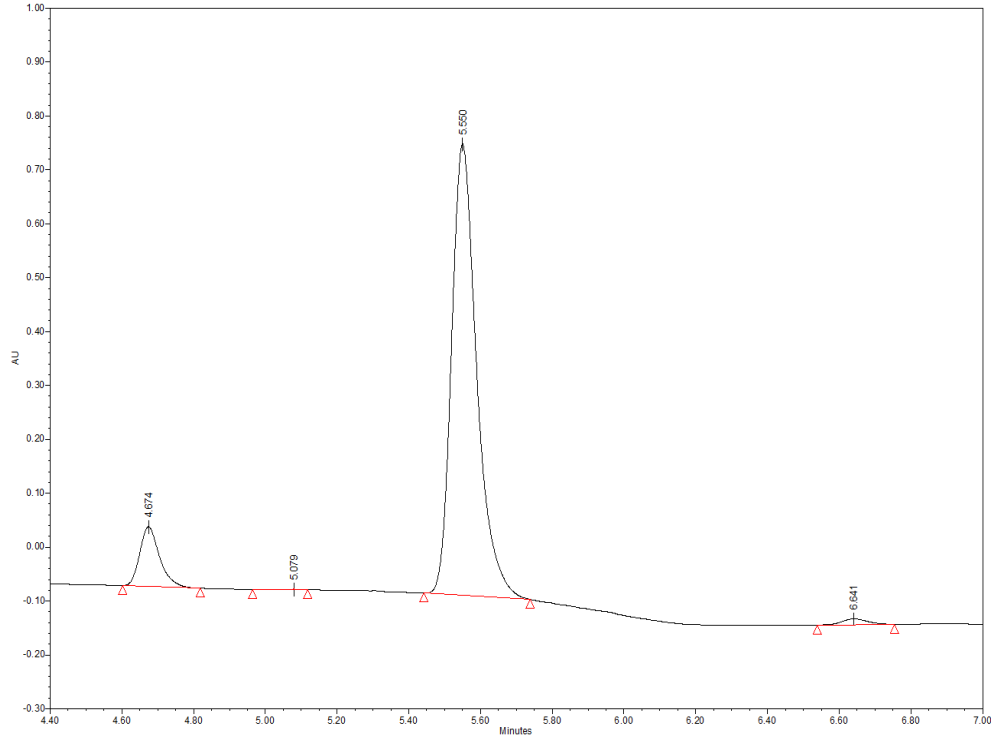

	Name	Retention Time (min)	PDA/FLR Match1 Lib. Name	Area (µV*sec)	% Area
1		4.674		426455	98.65
2		5.079		5838	1.35

	Name	Retention Time (min)	PDA/FLR Match1 Lib. Name	Area (µV*sec)	% Area
1		5.550		4078635	98.73
2		6.641		52377	1.27

Figure 5.6: SFC traces for compound (±)-**4f** (top) and enantioenriched (-)-**4f** (bottom).

SFC Traces for compound **4g**

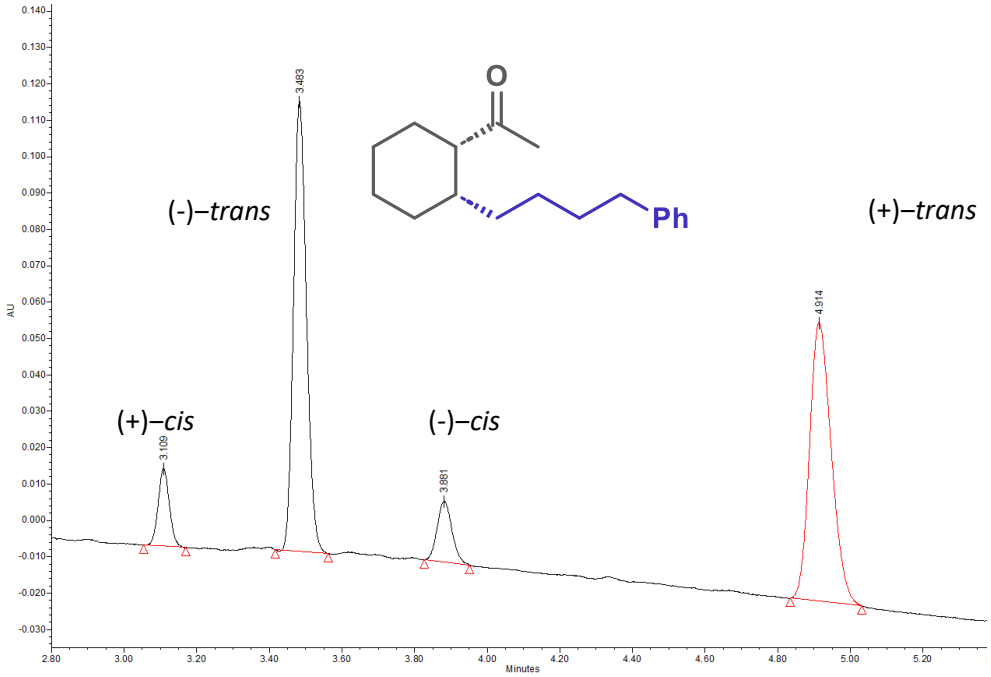

	Name	Retention Time (min)	Purity1 Angle	Purity1 Threshold	PDA/FLR Match1 Spect. Name	PDA/FLR Match1 Angle	PDA/FLR Match1 Threshold	PDA/FLR Match1 Lib. Name	Area (µV*sec)	% Area
1		3.109							45123	49.11
2		3.881							46764	50.89

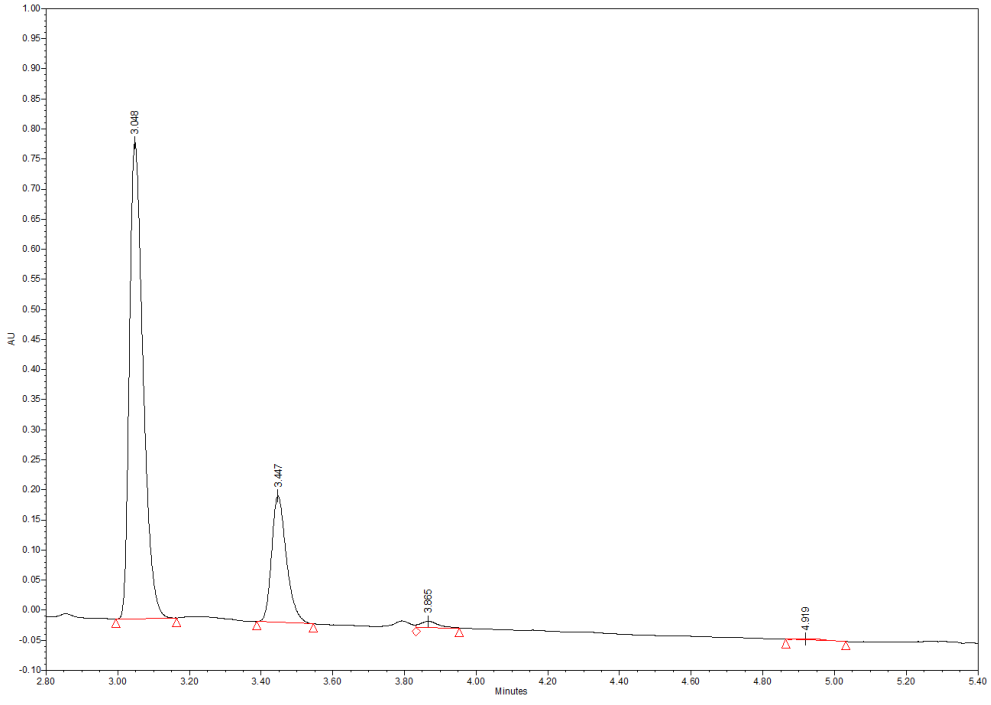

	Name	Retention Time (min)	Purity1 Angle	Purity1 Threshold	PDA/FLR Match1 Spect. Name	PDA/FLR Match1 Angle	PDA/FLR Match1 Threshold	PDA/FLR Match1 Lib. Name	Area (µV*sec)	% Area
1		3.048							2089159	98.40
2		3.865							33968	1.60

Figure 5.7: SFC traces for compound (±)-**4g** (top) and enantioenriched (+)-**4g** (bottom).

SFC Traces for compound **4h**

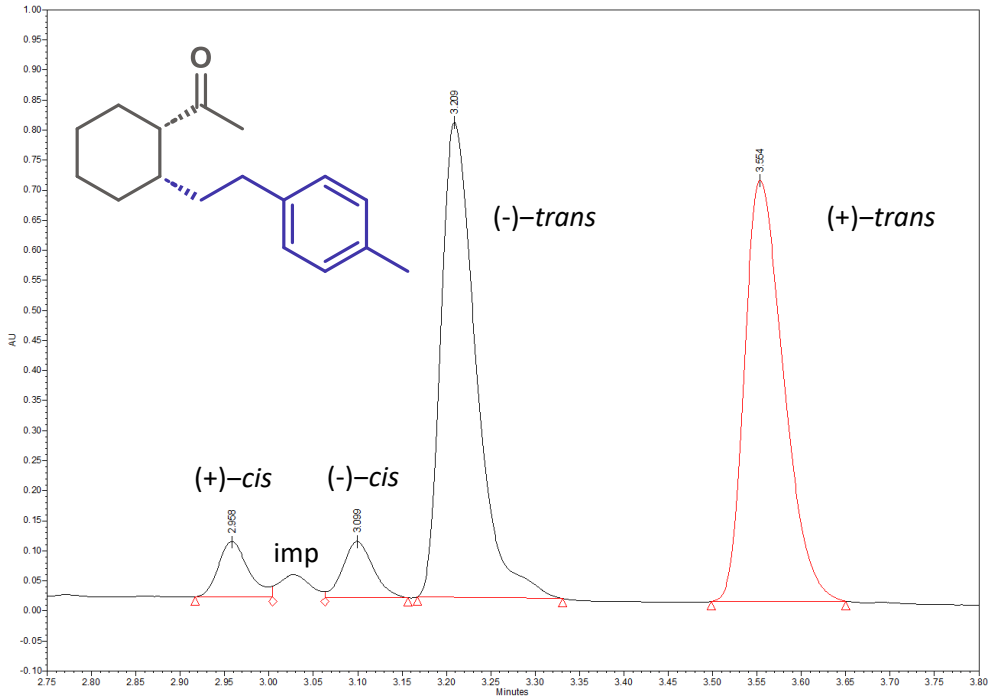

	Name	Retention Time (min)	Purity1 Angle	Purity1 Threshold	PDA/FLR Match1 Spect. Name	PDA/FLR Match1 Angle	PDA/FLR Match1 Threshold	PDA/FLR Match1 Lib. Name	Area (µV*sec)	% Area
1		2.958							217343	49.63
2		3.099							220555	50.37

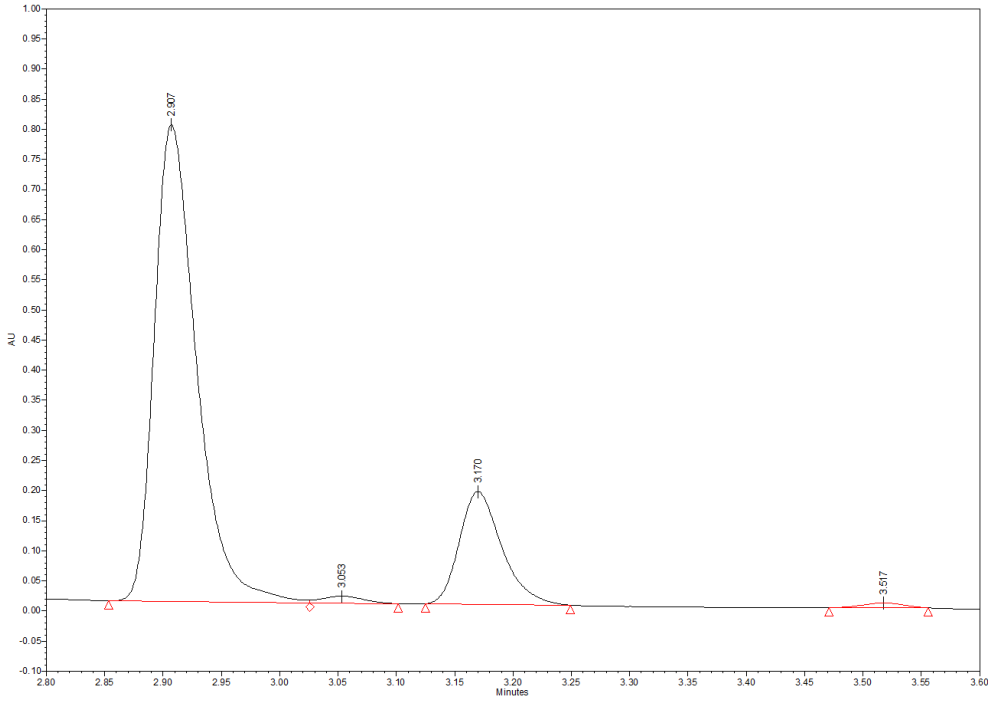

	Name	Retention Time (min)	Purity1 Angle	Purity1 Threshold	PDA/FLR Match1 Spect. Name	PDA/FLR Match1 Angle	PDA/FLR Match1 Threshold	PDA/FLR Match1 Lib. Name	Area (µV*sec)	% Area
1		2.907							1994676	98.58
2		3.053							28699	1.42

Figure 5.8: SFC traces for compound (±)-**4h** (top) and enantioenriched (+)-**4h** (bottom).

SFC Traces for compound **4i**

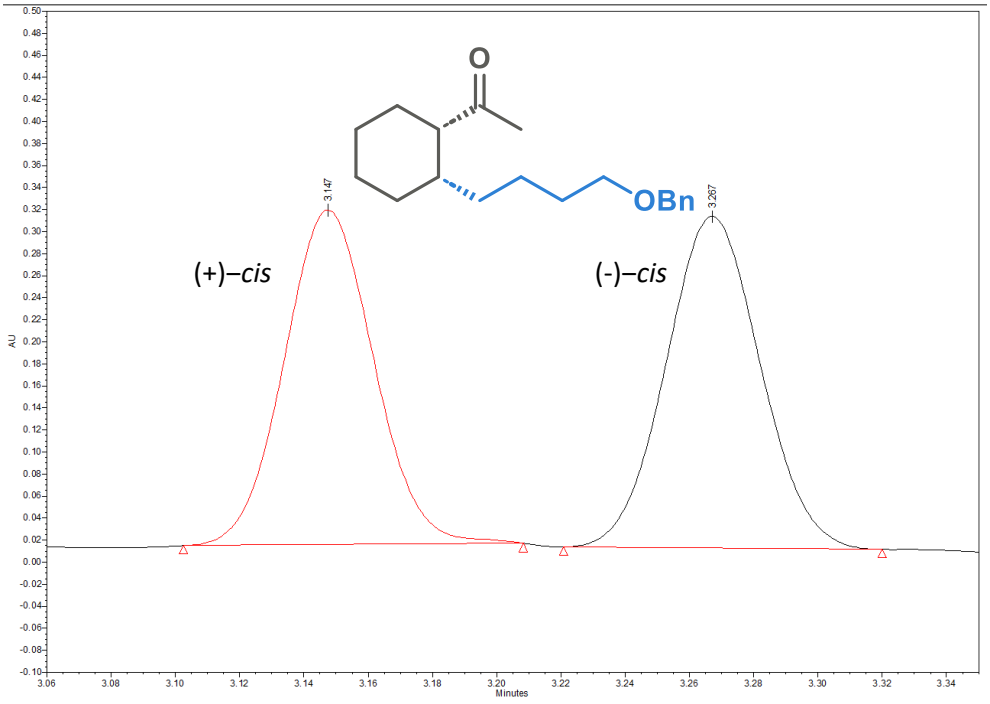

	Name	Retention Time (min)	Purity1 Angle	Purity1 Threshold	PDA/FLR Match1 Spect. Name	PDA/FLR Match1 Angle	PDA/FLR Match1 Threshold	PDA/FLR Match1 Lib. Name	Area (µV*sec)	% Area
1		3.147							589649	48.98
2		3.267							614111	51.02

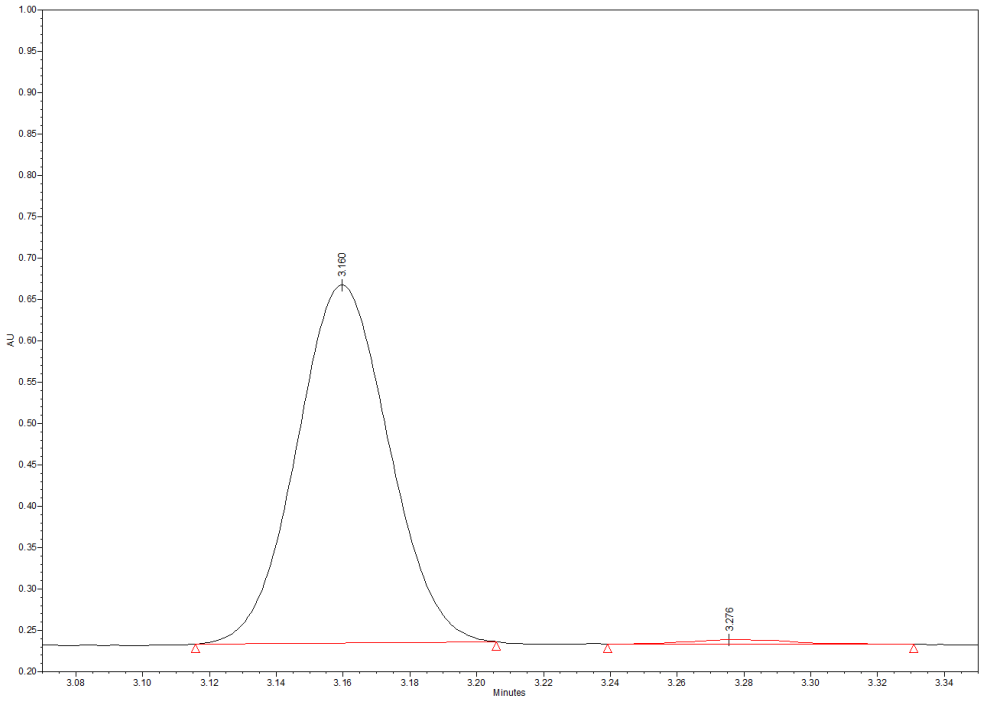

	Name	Retention Time (min)	Purity1 Angle	Purity1 Threshold	PDA/FLR Match1 Spect. Name	PDA/FLR Match1 Angle	PDA/FLR Match1 Threshold	PDA/FLR Match1 Lib. Name	Area (µV*sec)	% Area
1		3.160							829036	98.55
2		3.276							12182	1.45

Figure 5.9: SFC traces for compound (±)-**4i** (top) and enantioenriched (+)-**4i** (bottom).

SFC Traces for compound **4j**

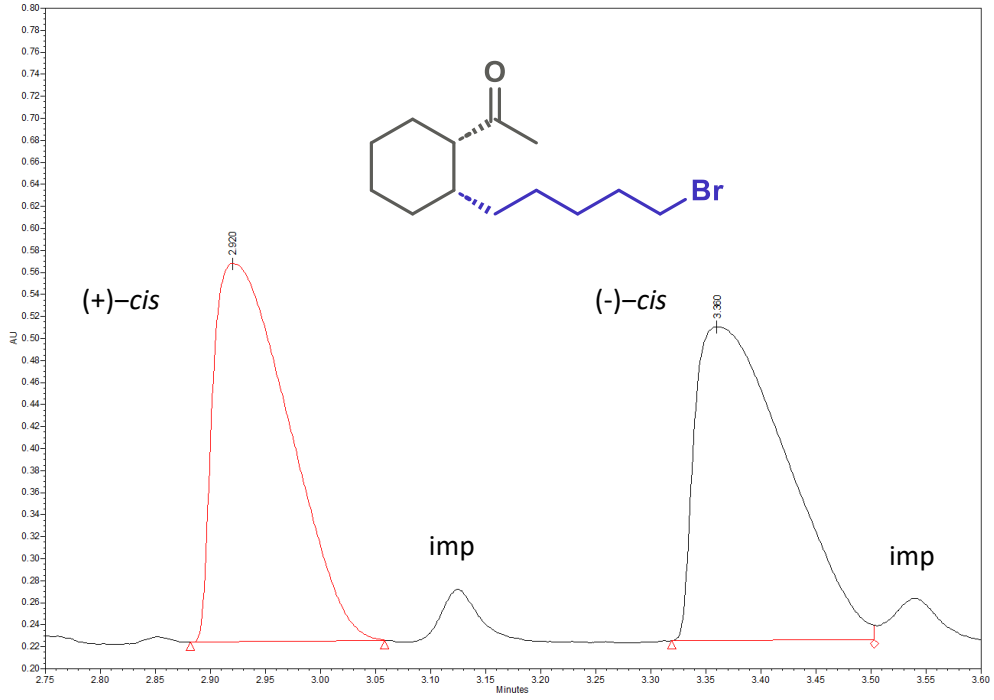

	Name	Retention Time (min)	Purity1 Angle	Purity1 Threshold	PDA/FLR Match1 Spect. Name	PDA/FLR Match1 Angle	PDA/FLR Match1 Threshold	PDA/FLR Match1 Lib. Name	Area (µV*sec)	% Area
1		2.920							1631316	49.62
2		3.360							1656319	50.38

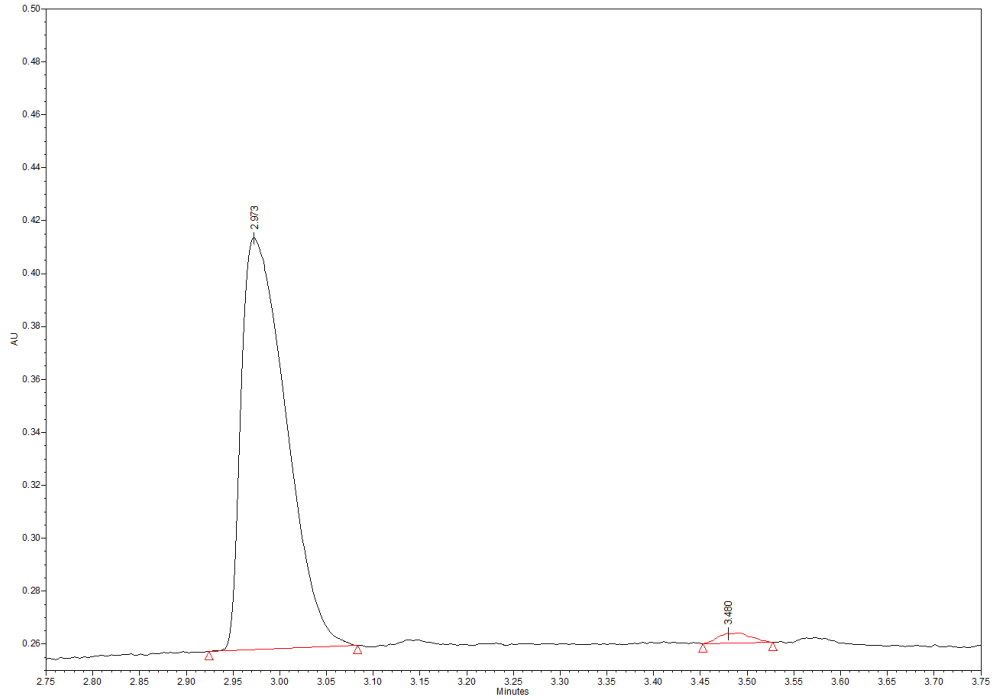

	Name	Retention Time (min)	Purity1 Angle	Purity1 Threshold	PDA/FLR Match1 Spect. Name	PDA/FLR Match1 Angle	PDA/FLR Match1 Threshold	PDA/FLR Match1 Lib. Name	Area (µV*sec)	% Area
1		2.973							517581	98.27
2		3.480							9125	1.73

Figure 5.10: SFC traces for compound (±)-**4j** (top) and enantioenriched (+)-**4j** (bottom).

GC Traces for compounds **4k** and **4l**

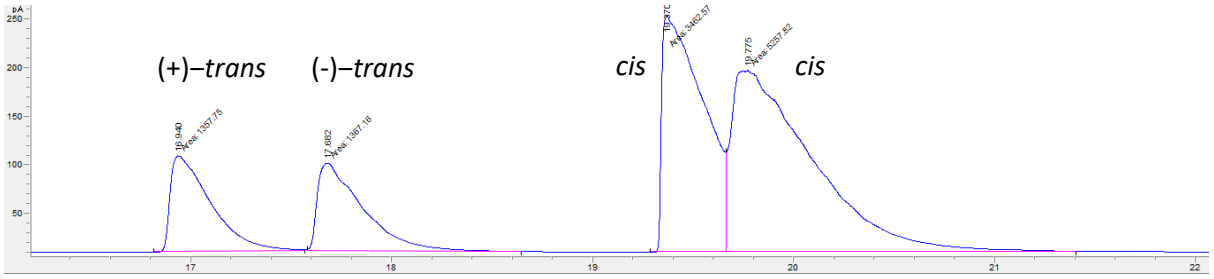

#	Time	Area	Height	Width	Area%	Symmetry
1	16.944	1354.2	98	0.2304	49.680	0.268
2	17.687	1371.7	88.8	0.2574	50.320	0.294

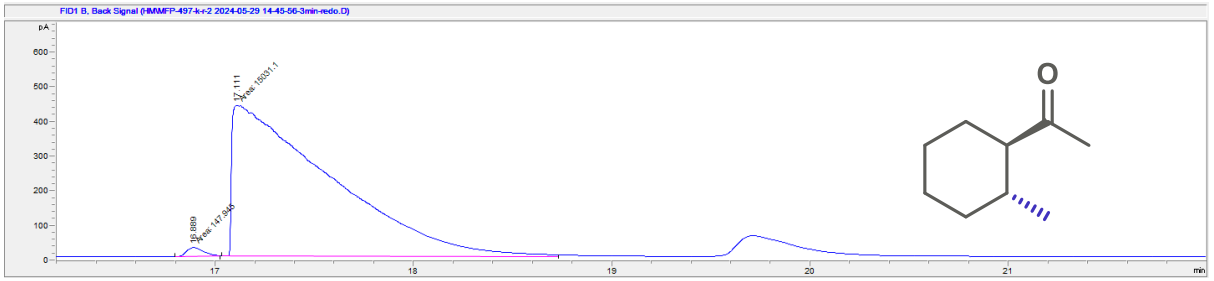

#	Time	Area	Height	Width	Area%	Symmetry
1	16.889	147.9	25.2	0.0977	0.975	0.745
2	17.111	15031.1	433.1	0.5784	99.025	6.02E-2

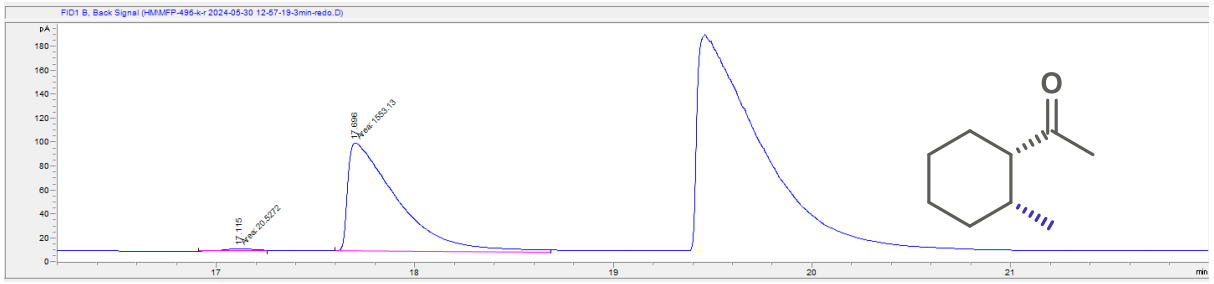

#	Time	Area	Height	Width	Area%	Symmetry
1	17.115	20.5	1.9	0.1774	1.304	0.877
2	17.696	1553.1	90.2	0.2871	98.696	0.154

Figure 5.11: GC traces for compound (±)-**4l** (top), enantioenriched (-)-**4k** (middle) and enantioenriched (+)-**4l** (bottom). Determination of ee based on the ee of the *trans*-diastereomer for either isomer.

SFC Traces for compound **4m**

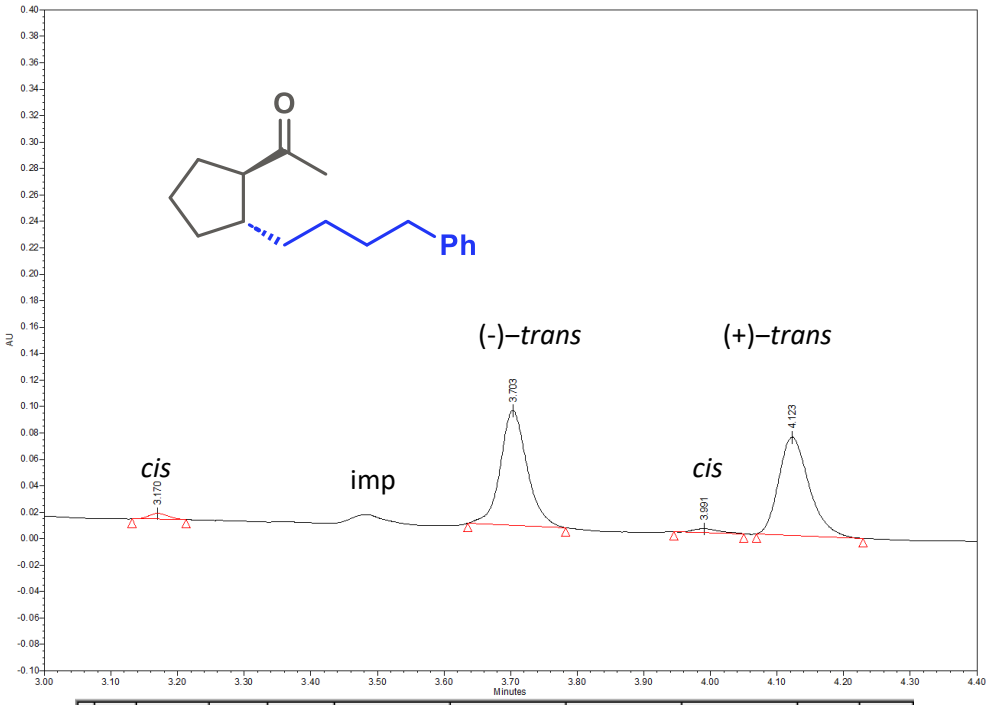

	Name	Retention Time (min)	Purity1 Angle	Purity1 Threshold	PDA/FLR Match1 Spect. Name	PDA/FLR Match1 Angle	PDA/FLR Match1 Threshold	PDA/FLR Match1 Lib. Name	Area (µV*sec)	% Area
1		3.703							237237	50.02
2		4.123							237062	49.98

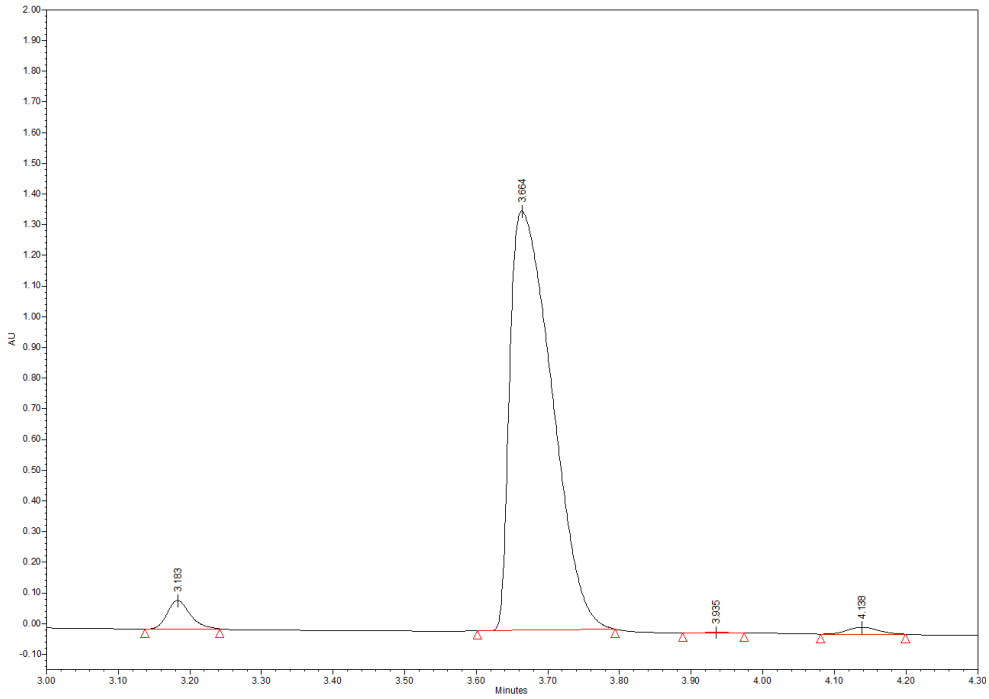

	Name	Retention Time (min)	Purity1 Angle	Purity1 Threshold	PDA/FLR Match1 Spect. Name	PDA/FLR Match1 Angle	PDA/FLR Match1 Threshold	PDA/FLR Match1 Lib. Name	Area (µV*sec)	% Area
1		3.664							5554632	98.67
2		4.138							74666	1.33

Figure 5.12: SFC traces for compound (±)-**4m** (top) and enantioenriched (-)-**4m** (bottom).

SFC Traces for compound **4n**

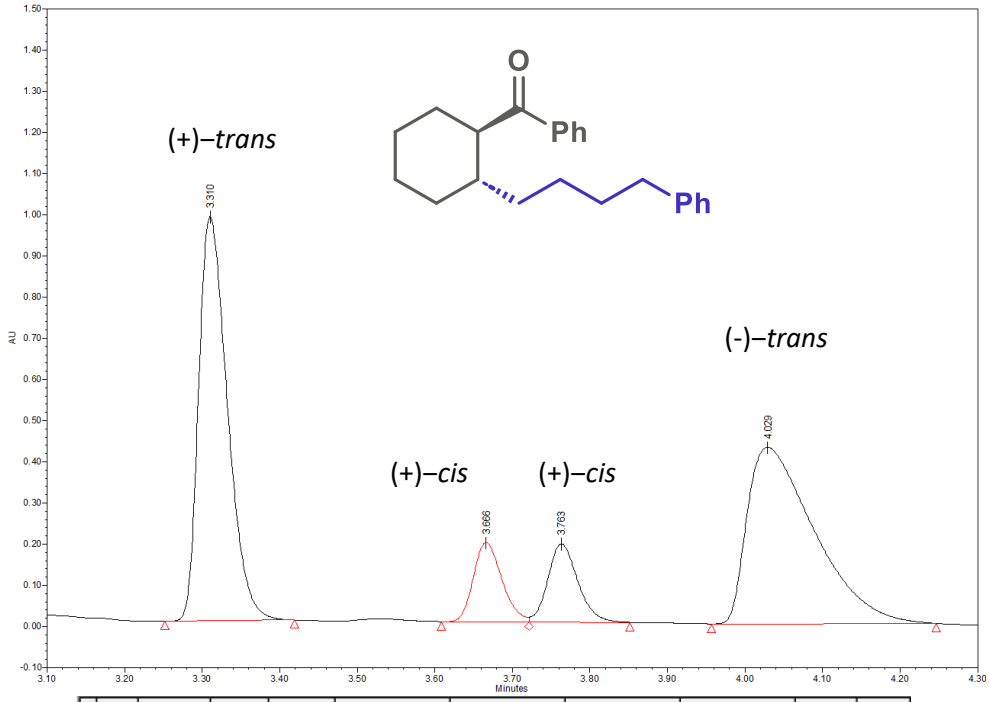

	Name	Retention Time (min)	Purity1 Angle	Purity1 Threshold	PDA/FLR Match1 Spect. Name	PDA/FLR Match1 Angle	PDA/FLR Match1 Threshold	PDA/FLR Match1 Lib. Name	Area (µV*sec)	% Area
1		3.310							2531541	49.53
2		4.029							2579494	50.47

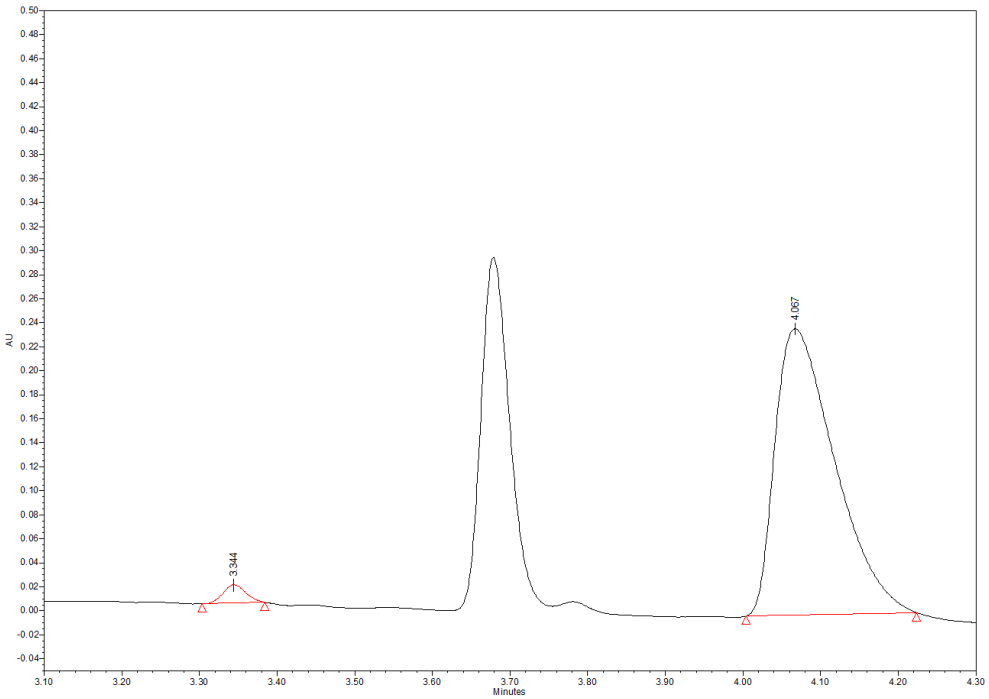

	Name	Retention Time (min)	Purity1 Angle	Purity1 Threshold	PDA/FLR Match1 Spect. Name	PDA/FLR Match1 Angle	PDA/FLR Match1 Threshold	PDA/FLR Match1 Lib. Name	Area (µV*sec)	% Area
1		3.344							27567	2.41
2		4.067							1116553	97.59

Figure 5.13: SFC traces for compound (±)-**4n** (top) and enantioenriched (-)-**4n** (bottom).

SFC Traces for compound **4o**

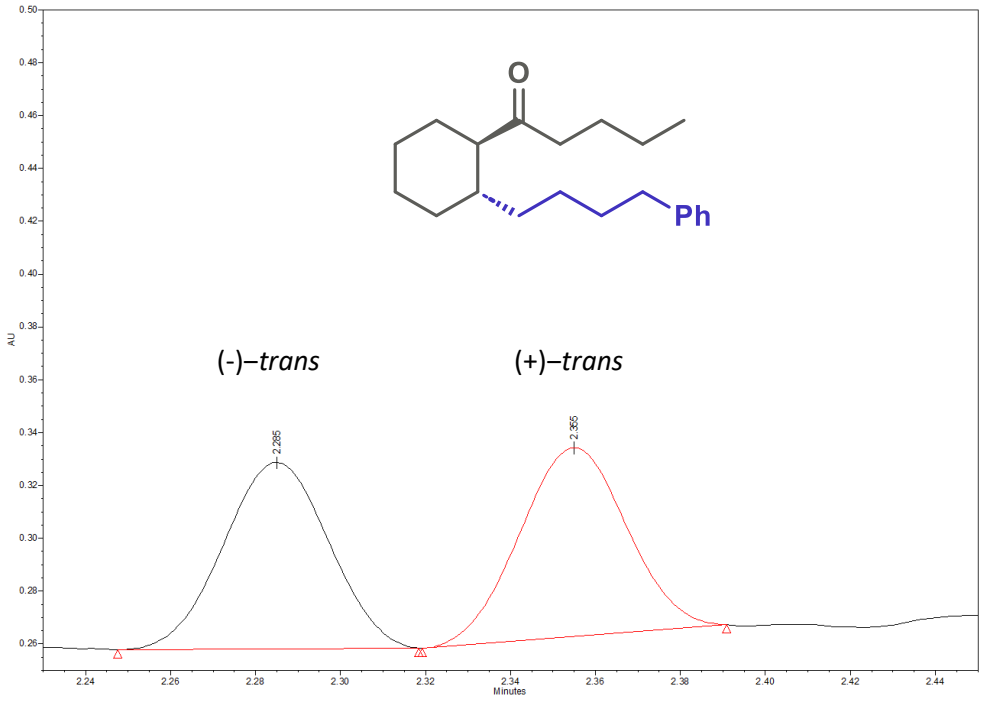

	Name	Retention Time (min)	Purity1 Angle	Purity1 Threshold	PDA/FLR Match1 Spect. Name	PDA/FLR Match1 Angle	PDA/FLR Match1 Threshold	PDA/FLR Match1 Lib. Name	Area (µV*sec)	% Area
1		2.285							121380	49.25
2		2.355							125093	50.75

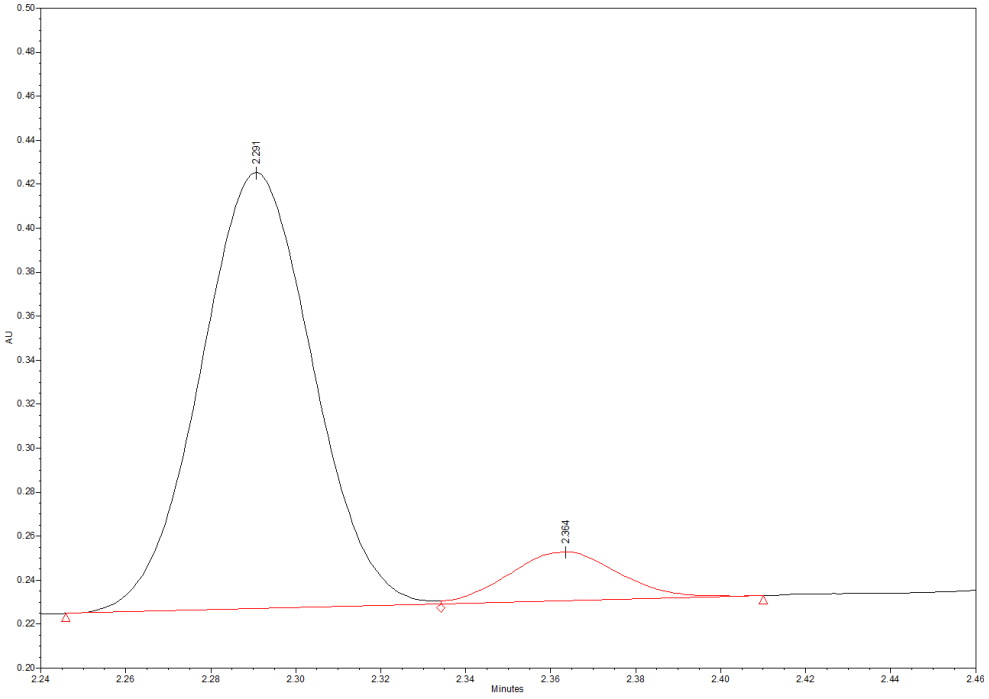

	Name	Retention Time (min)	Purity1 Angle	Purity1 Threshold	PDA/FLR Match1 Spect. Name	PDA/FLR Match1 Angle	PDA/FLR Match1 Threshold	PDA/FLR Match1 Lib. Name	Area (µV*sec)	% Area
1		2.291							362887	90.24
2		2.364							39233	9.76

Figure 5.14: SFC traces for compound (±)-**4o** (top) and enantioenriched (-)-**4o** (bottom).

SFC Traces for compound **4q**

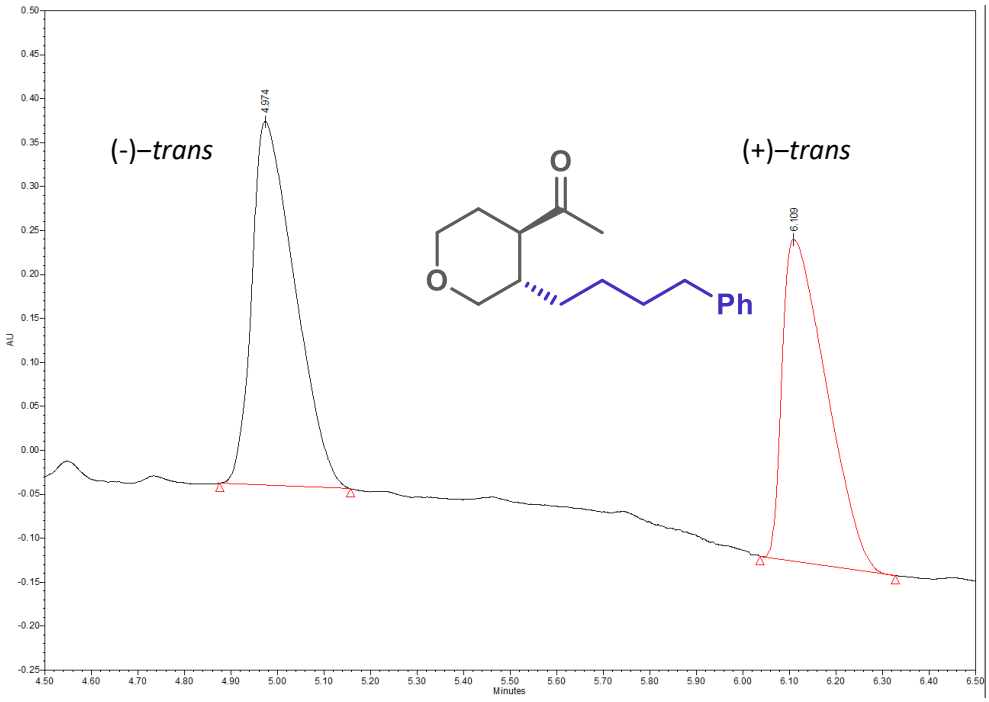

	Name	Retention Time (min)	Purity1 Angle	Purity1 Threshold	PDA/FLR Match1 Spect. Name	PDA/FLR Match1 Angle	PDA/FLR Match1 Threshold	PDA/FLR Match1 Lib. Name	Area (µV*sec)	% Area
1		4.974							2654965	52.41
2		6.109							2411194	47.59

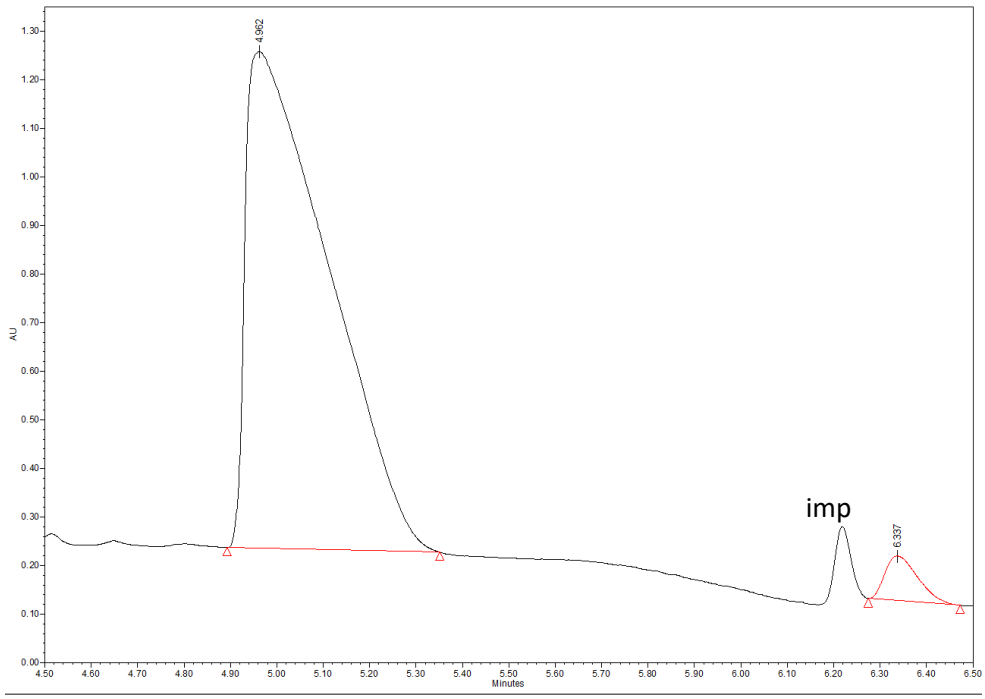

	Name	Retention Time (min)	Purity1 Angle	Purity1 Threshold	PDA/FLR Match1 Spect. Name	PDA/FLR Match1 Angle	PDA/FLR Match1 Threshold	PDA/FLR Match1 Lib. Name	Area (µV*sec)	% Area
1		4.962							12696197	96.54
2		6.337							454859	3.46

Figure 5.15: SFC traces for compound (±)-**4q** (top) and enantioenriched (-)-**4q** (bottom).

SFC Traces for compound **4r**

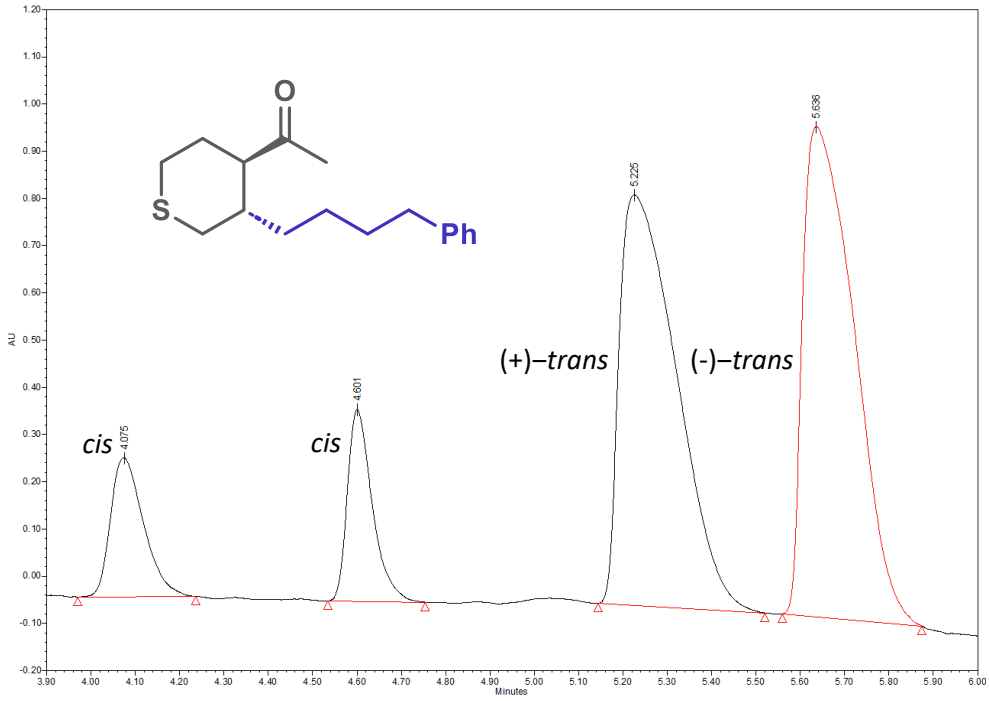

	Name	Retention Time (min)	Purity1 Angle	Purity1 Threshold	PDA/FLR Match1 Spect. Name	PDA/FLR Match1 Angle	PDA/FLR Match1 Threshold	PDA/FLR Match1 Lib. Name	Area (µV*sec)	% Area
1		5.225							7765359	48.58
2		5.636							8219483	51.42

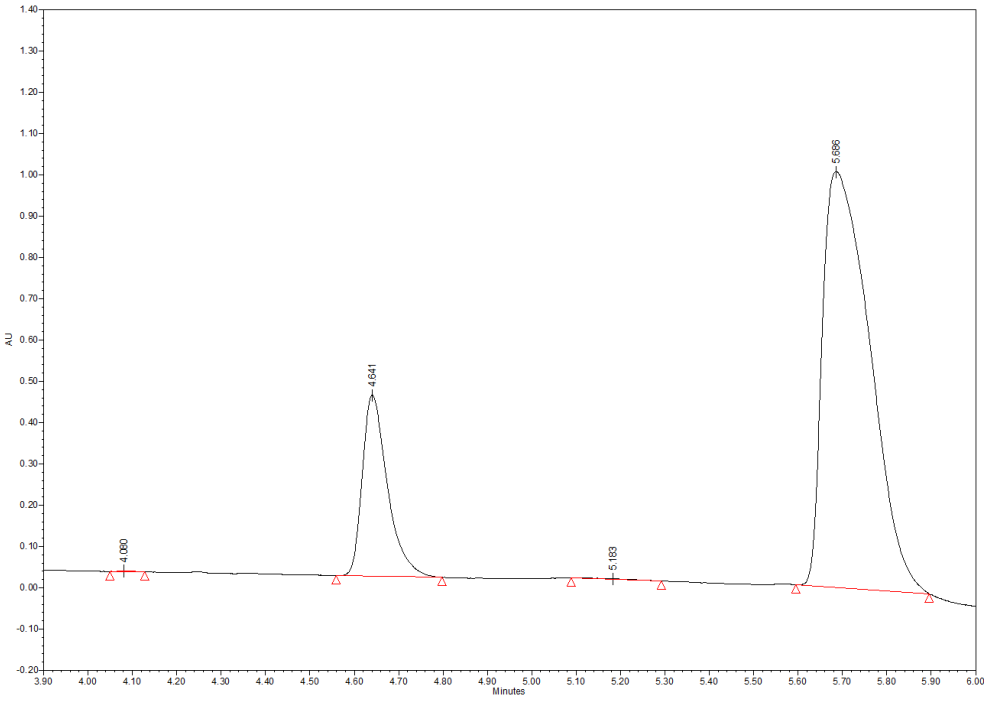

	Name	Retention Time (min)	Purity1 Angle	Purity1 Threshold	PDA/FLR Match1 Spect. Name	PDA/FLR Match1 Angle	PDA/FLR Match1 Threshold	PDA/FLR Match1 Lib. Name	Area (µV*sec)	% Area
1		5.183							21103	0.28
2		5.686							7538506	99.72

Figure 5.16: SFC traces for compound (±)-**4r** (top) and enantioenriched (-)-**4r** (bottom).

SFC Traces for compound **4t**

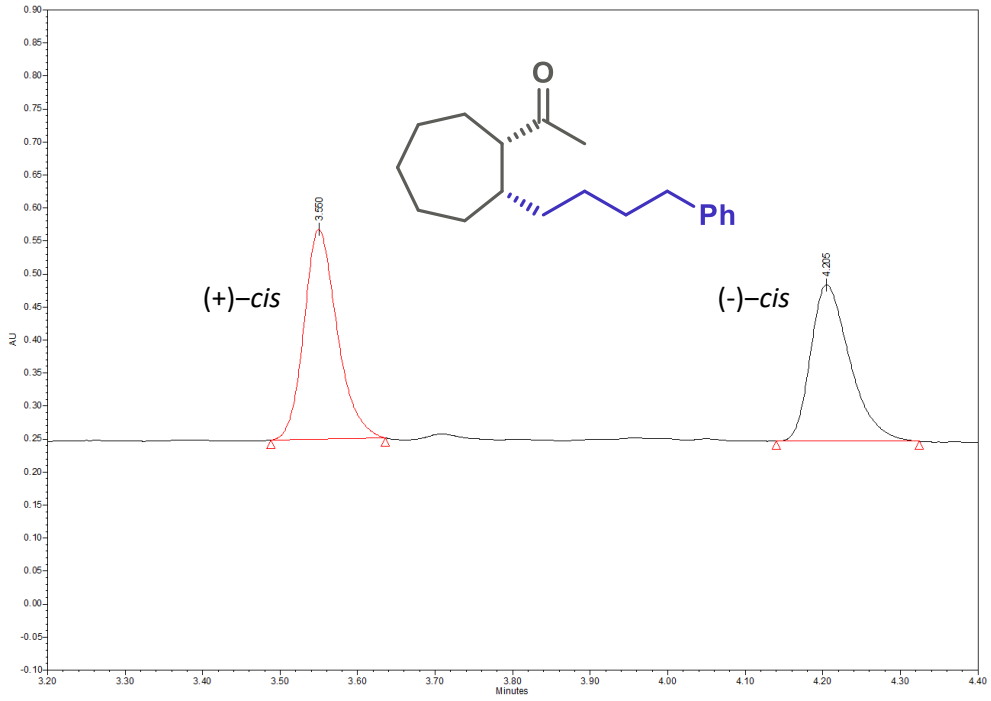

	Name	Retention Time (min)	Purity1 Angle	Purity1 Threshold	PDA/FLR Match1 Spect. Name	PDA/FLR Match1 Angle	PDA/FLR Match1 Threshold	PDA/FLR Match1 Lib. Name	Area (µV*sec)	% Area
1		3.550							945999	53.20
2		4.205							832229	46.80

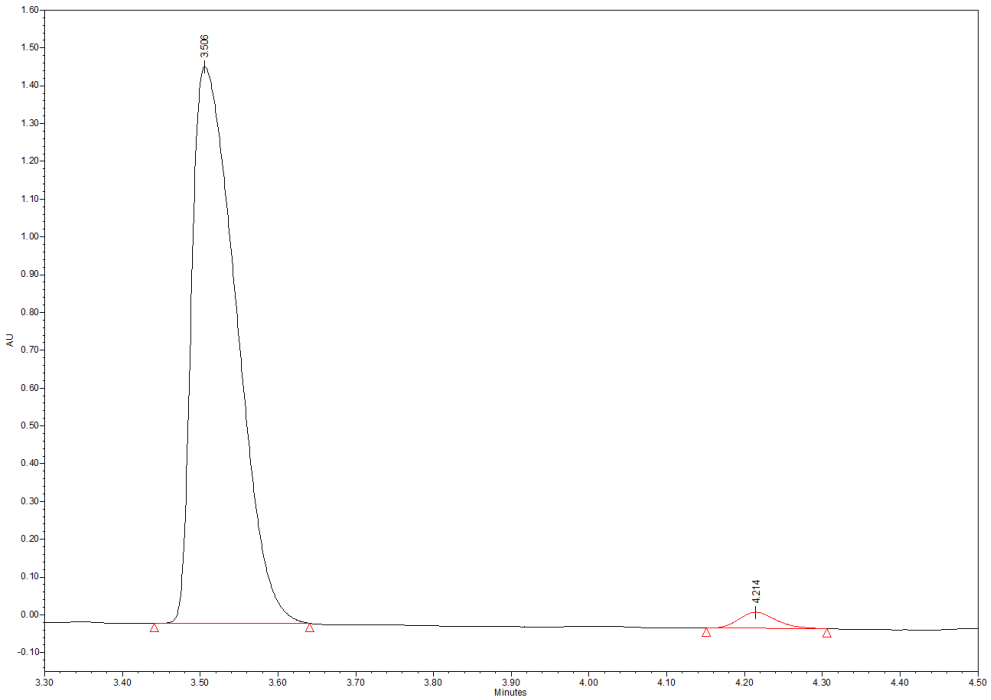

	Name	Retention Time (min)	Purity1 Angle	Purity1 Threshold	PDA/FLR Match1 Spect. Name	PDA/FLR Match1 Angle	PDA/FLR Match1 Threshold	PDA/FLR Match1 Lib. Name	Area (µV*sec)	% Area
1		3.506							5809974	97.58
2		4.214							143918	2.42

Figure 5.17: SFC traces for compound (±)-**4t** (top) and enantioenriched (+)-**4t** (bottom).

SFC Traces for compound **4u** (*trans* minor isomer)

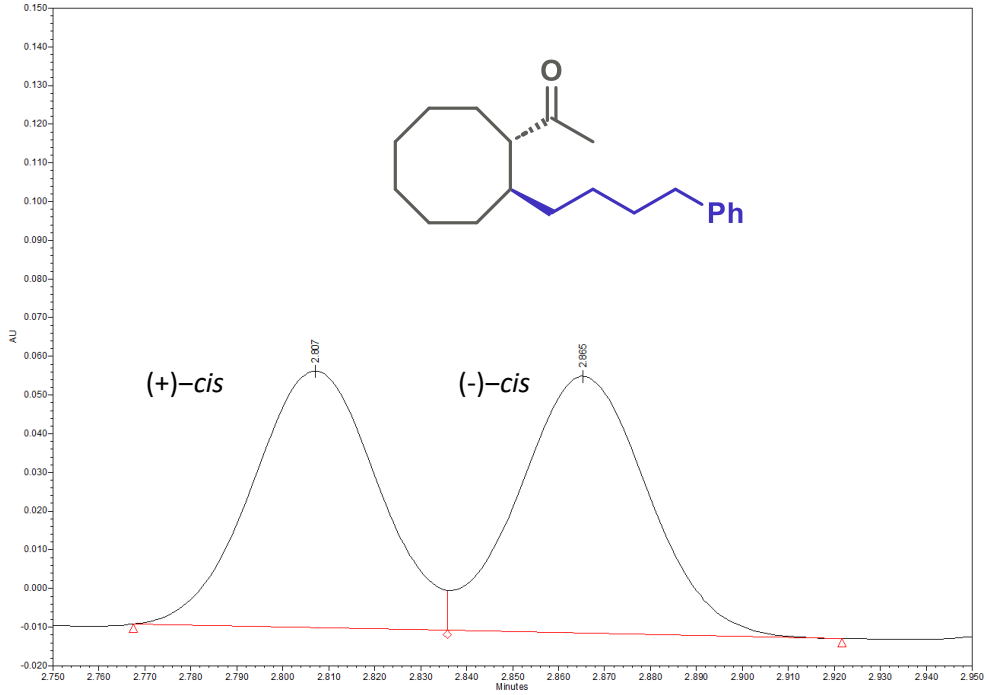

	Name	Retention Time (min)	Purity1 Angle	Purity1 Threshold	PDA/FLR Match1 Spect. Name	PDA/FLR Match1 Angle	PDA/FLR Match1 Threshold	PDA/FLR Match1 Lib. Name	Area (µV*sec)	% Area
1		2.807							126205	49.36
2		2.865							129473	50.64

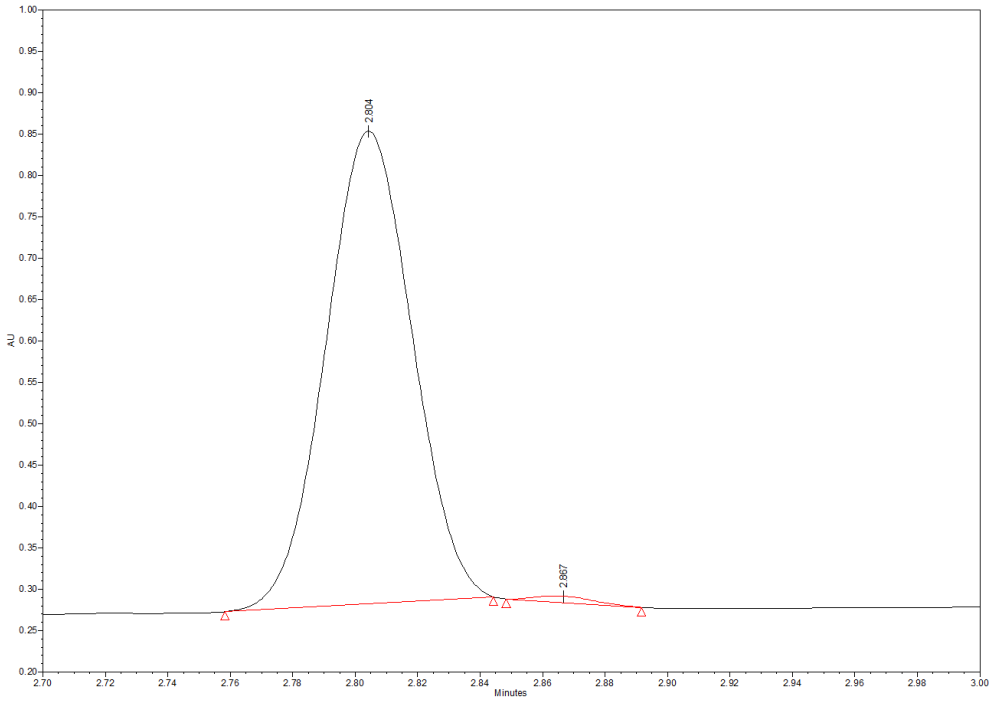

	Name	Retention Time (min)	Purity1 Angle	Purity1 Threshold	PDA/FLR Match1 Spect. Name	PDA/FLR Match1 Angle	PDA/FLR Match1 Threshold	PDA/FLR Match1 Lib. Name	Area (µV*sec)	% Area
1		2.804							1097661	99.13
2		2.867							9614	0.87

Figure 5.18: SFC traces for compound (±)-**4u** (top) and enantioenriched (+)-**4u** (bottom). ee of the *cis*-major product is based on SFC trace of *trans* isomer.

SFC Traces for compound **4v**

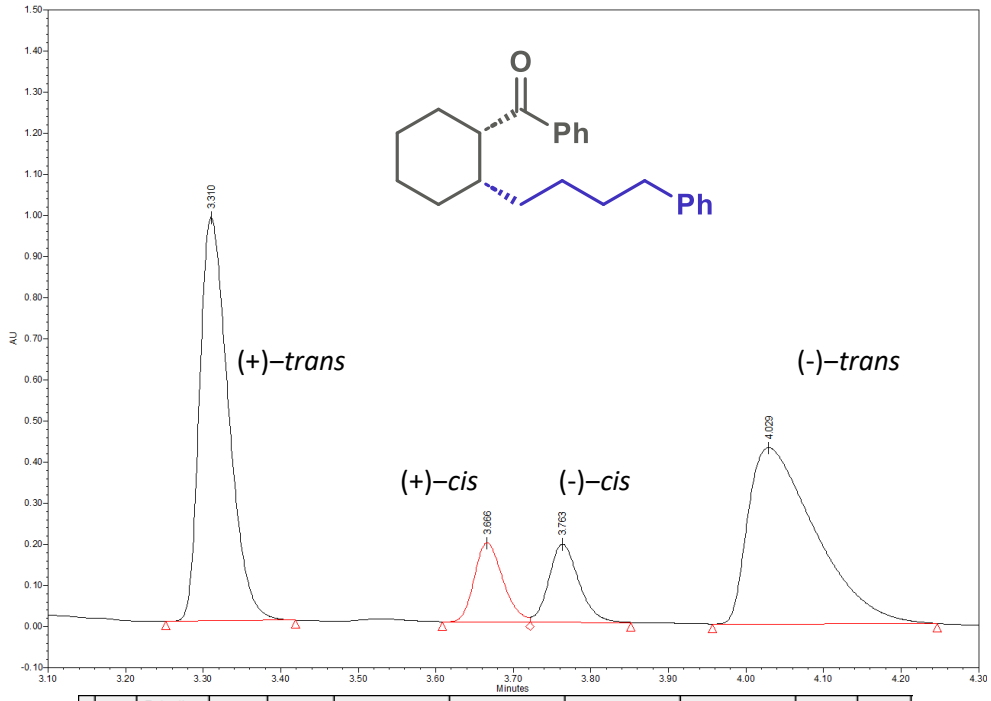

	Name	Retention Time (min)	Purity1 Angle	Purity1 Threshold	PDA/FLR Match1 Spect. Name	PDA/FLR Match1 Angle	PDA/FLR Match1 Threshold	PDA/FLR Match1 Lib. Name	Area (µV*sec)	% Area
1		3.666							490744	49.21
2		3.763							506423	50.79

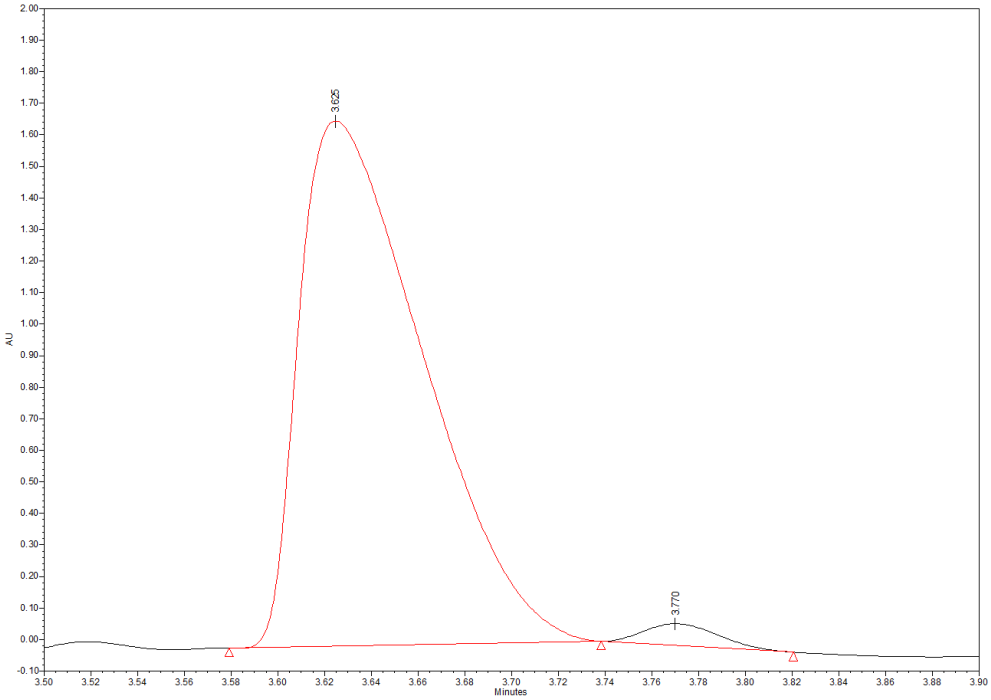

	Name	Retention Time (min)	Purity1 Angle	Purity1 Threshold	PDA/FLR Match1 Spect. Name	PDA/FLR Match1 Angle	PDA/FLR Match1 Threshold	PDA/FLR Match1 Lib. Name	Area (µV*sec)	% Area
1		3.625							6117611	97.54
2		3.770							154075	2.46

Figure 5.19: SFC traces for compound (±)-**4v** (top) and enantioenriched (+)-**4v** (bottom).

5.6 Crystal structure of Ligand L_{22S} (P,S_P)

Crystal structure available at CCDC

Name: 5-(2-phenyl-4H-dinaphtho[2,1-d:1',2'-f][1,3,2]dioxaphosphepin-4-yl)-5H-dibenzo[b,f]azepine

Deposition Number: 2386299

Chemical structure:

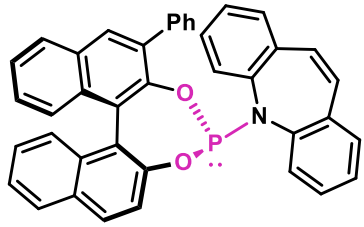

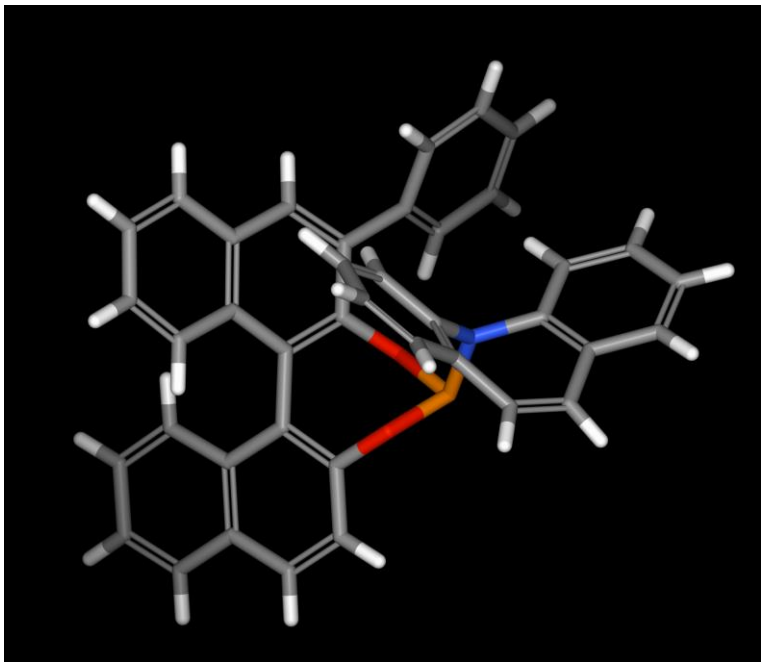

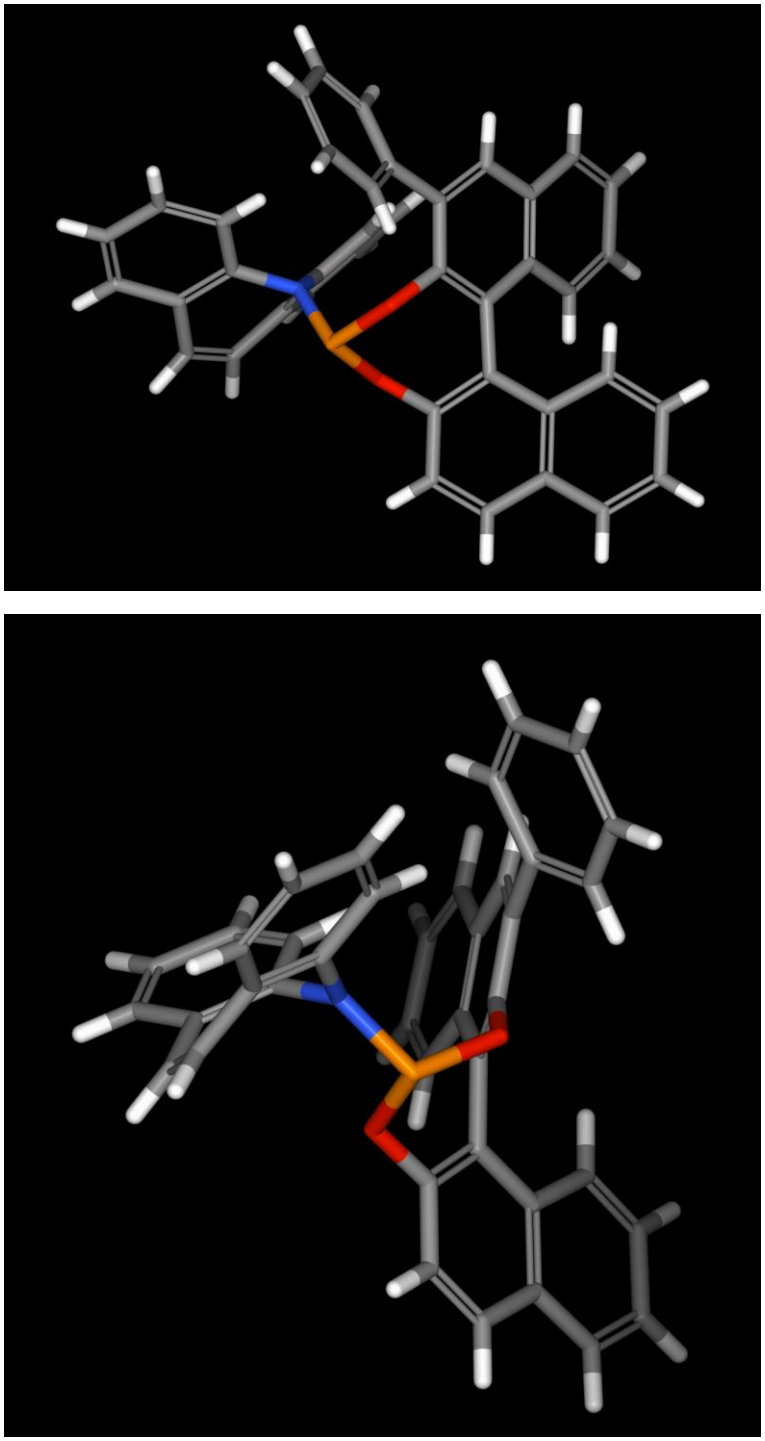

Figure 5.20: Crystal structure of L_{22S}

5.7 References:

1. M. Yoshida, M. Hayashi, K. Shishido, *Org. Lett.*, 2007, **9**, 1643–1646.
2. F. Zulfiqar, A. Malik, *Z. Naturforsch. B*, 2001, **56**, 1227–1234.
3. Z. Gao, S. P. Fletcher, *Chem. Sci.*, 2017, **8**, 641–646.
4. M. Vuagnoux-d'Augustin, A. Alexakis, *Chem. Eur. J.*, 2007, **13**, 9647–9662.
5. V. Cadierno, S. E. García-Garrido, J. Gimeno, *Adv. Synth. Catal.*, 2006, **348**, 101–110.
6. G. C. Nandi, B. M. Rathman, K. K. Laali, *Tetrahedron Lett.*, 2013, **54**, 6258–6263.
7. S. Kamijo, T. Hoshikawa, M. Inoue, *Tetrahedron Lett.*, 2010, **51**, 872–874.
8. J. R. Hermanson, M. L. Gunther, J. L. Belletire, A. R. Pinhas, *J. Org. Chem.*, 1995, **60**, 1900–1903.
9. W. Yan, J. Qing, H. Mei, J. Nong, J. Huang, J. Zhu, H. Jiang, L. Liu, L. Zhang, J. Li, *Bioorg. Med. Chem. Lett.*, 2015, **25**, 5682–5686.
10. M. Koyama, T. Kawakami, T. Okazoe, K. Nozaki, *Chem. Eur. J.*, 2019, **25**, 10913–10917.
11. V. Bordas, M. Furegati, J. Hamon, J. H.-H. Hinrichs, Z. Hong, F. Lima, F. Limam, H. Moebitz, S. Nocito, N. Schmiedeberg, J. Schoepfer, R. Strang, F. Zecri, H. Yu, Y. Zhang, X. Yang, S. Zhang, W. Li, *WO 2024/079623 A1*, Novartis AG.
12. K. Kubota, S. Osaki, M. Jin, H. Ito, *Angew. Chem. Int. Ed.*, 2017, **56**, 6646–6650.
13. M. P. Schramm, D. S. Reddy, S. A. Kozmin, *Angew. Chem. Int. Ed. Engl.*, 2001, **40**, 4274–4277.
14. D. Scarpi, C. Capanni, S. Visi, C. Faggi, E. G. Occhiato, *J. Org. Chem.*, 2024, **89**, 14108–14119.
15. S. Nagasawa, Y. Sasano, Y. Iwabuchi, *Chem. Eur. J.*, 2017, **23**, 10276–10279.
16. A. Brethomé, *A Physical-Organic Approach to Asymmetric Catalysis: Design and Synthesis of Chiral Ligands Using Multivariate Modelling*, Doctoral Thesis, University of Oxford, Wolfson College, Michaelmas 2019.
17. M. Shi, L.-H. Chen, C.-Q. Li, *J. Am. Chem. Soc.* 2005, **127**, 3790–3800.
18. T. Harada, K. Kanda, *Org. Lett.* 2006, **8**, 3817–3819.
19. D. Mosca, A. Stopin, J. Wouters, N. Demitri, D. Bonifazi, *Chem. Eur. J.* 2017, **23**, 15348–15354.
20. S. Qu, M. D. Greenhalgh, A. D. Smith, *Chem. Eur. J.* 2019, **25**, 2816–2823.

21. Y. Li, Q. Li, *Org. Lett.* 2012, **14**, 4362–4365.
22. T. Hashimoto, Y. Naganawa, K. Maruoka, *J. Am. Chem. Soc.*, 2011, **133**, 8834–8837.
23. K. N. Gavrilov, S. V. Zheglov, I. M. Novikov, I. V. Chuchelkin, V. K. Gavrilov, V. V. Lugovsky, I. A. Zamilatskov, *Russ. Chem. Bull.* 2015, **64**, 1595–1601.
24. A. R. Ankireddy, K. Paidkondala, R. Syed, R. Gundla, Ch. V. R. Reddy, T. Ganapathi, *Russ. J. Gen. Chem.*, 2020, **90**, 1507–1517.
25. K. Ishihara, H. Kurihara, M. Matsumoto, H. Yamamoto, *J. Am. Chem. Soc.* 1998, **120**, 6920–6930.
26. S. L. Buchwald, S. J. LaMaire, R. B. Nielsen, B. T. Watson, S. M. King, *Org. Synth.*, 1993, **71**, 77.
27. K. Garrec, S. P. Fletcher, *Org. Lett.*, 2016, **18**, 3814–3817.